ENDOTHELIAL TRPV4 DYSFUNCTION IN A STREPTOZOTOCIN-DIABETIC RAT MODEL

YOUSIF A. SHAMSALDEEN

A thesis submitted in partial fulfilment of the requirements of the University of Hertfordshire for the degree of Doctor of Philosophy

The programme of research was carried out in the
School of Pharmacy, Pharmacology and Postgraduate medicine,
Faculty of Life and Medical Sciences,
University of Hertfordshire

June 2016

Abstract

Diabetes mellitus is a complex disease characterised by chronic hyperglycaemia due to compromised insulin synthesis and secretion, or decreased tissue sensitivity to insulin, if not all three conditions. Endothelial dysfunction is a common complication in diabetes in which endothelium-dependent vasodilation is impaired. The aim of this study was to examine the involvement of TRPV4 in diabetes endothelial dysfunction. Male Charles River Wistar rats (350–450 g) were injected with 65mg/kg streptozotocin (STZ) intraperitoneally. STZ-injected rats were compared with naïve rats (not injected with STZ) or control rats (injected with 10ml/kg of 20mM citrate buffer, pH 4.0–4.5), if not both. Rats with blood glucose concentrations greater than 16mmol/L were considered to be diabetic. As the results revealed, STZ-diabetic rats showed significant endothelial dysfunction characterised by impaired muscarinic-induced vasodilation, as well as significant impairment in TRPV4-induced vasodilation in aortic rings and mesenteric arteries. Furthermore, STZ-diabetic primary aortic endothelial cells (ECs) showed a significant reduction in TRPV4-induced intracellular calcium ($[Ca^{2+}]i$) elevation. TRPV4, endothelial nitric oxide synthase (eNOS), and caveolin-1 (CAV-1) were also significantly downregulated in STZ-diabetic primary aortic ECs and were later significantly restored by in vitro insulin treatment. Methylglyoxal (MGO) was significantly elevated in STZ-diabetic rat serum, and nondiabetic aortic rings incubated with MGO (100μM) for 12 hours showed significant endothelial dysfunction. Moreover, nondiabetic primary aortic ECs treated with MGO (100μM) for 5 days showed significant TRPV4 downregulation and significant suppression of 4-α-PDD-induced $[Ca^{2+}]i$ elevation, which was later restored by L-arginine (100μM) co-incubation. Incubating nondiabetic aortic rings with MGO (100μM) for 2 hours induced a spontaneous loss of noradrenaline-induced contractility persistence. Moreover, MGO induced significant $[Ca^{2+}]i$ elevation in Chinese hamster ovary cells expressing rat TRPM8 channels (rTRPM8), which was significantly inhibited by AMTB (1–5μM). Taken together, TRPV4, CAV-1, and eNOS can form a functional complex that is downregulated in STZ-diabetic aortic ECs and restored by insulin treatment. MGO elevation might furthermore contribute to diabetes endothelial dysfunction and TRPV4 downregulation. By contrast, MGO induced the loss of contractility persistence, possibly due to MGO's acting as a TRPM8 agonist.

Acknowledgements

First of all, I would like to express my sincere gratitude to my supervisors, Dr. Christopher Benham and Dr. Lisa Lione for their continuous support throughout my PhD, for their patience, motivation, and immense knowledge. Their guidance supported me in all the time of research and writing of this thesis. I could not have imagined having a better supervisors for my PhD study.

Beside my supervisors, I would like to thank Professor Stuart Bevan for giving me the opportunity to conduct part of my research in his lab in Wolfson Centre for Age Related Diseases at King's College London with the support of his colleague, Dr. David Andersson for their patience and invaluable guidance.

My sincere thanks also goes to Dr. Richard Hoffman, Dr. Louise Mackenzie and Dr. Mahmoud Iravani for their insightful comments and encouragement throughout my PhD study.

I am grateful to Professor Anwar Baydoun and members in his research group, particularly Mr. Mahdi Alsugoor for their help and support for cell culture studies.

I thank my colleagues for the stimulating discussions, for the intensive work and support together, and for all the fun we have had in the last three years, namely Mr. David Clarke, Mrs. Lena Pye, Dr. Sara Pritchard and Ms. Golnaz Ranjbar. I also thank my colleagues in the Wolfson Centre for Age Related Diseases at King's College London, particularly Dr. Mateus Rossato.

This PhD study, and the rest of my qualifications and degrees would not be possible without the invaluable financial and psychological support from my family: my parents, my brothers and sister, who I cannot find any word to express my gratitude to them.

Publications:

Papers

- Shamsaldeen, Y. A., Mackenzie, L. S., Lione, L. A., & Benham, C. D. (2016). Methylglyoxal, A Metabolite Increased in Diabetes is Associated with Insulin Resistance, Vascular Dysfunction and Neuropathies. *Current Druge Metabolism, 17*(4), 359-367.

Abstracts

- TRPV4 dysfunction in endothelial cells from STZ treated rats reversed by insulin, New Therapeutics for Diabetes and Obesity (G1), 17th - 21st of April 2016, San Diego. California
- Decrease in TRPV4 Expression in Vascular Endothelium From STZ Treated Rats is Reversed by Insulin Treatment. 2015. Proceedings of the British Pharmacological Society at (https://bps.conference-services.net/resources/344/3974/pdf/PHARM15_0016.pdf)
- TRPV4 Dysfunction in Both Endothelial and Smooth Muscle Cells From Diabetic Rat Aorta. 2014. Proceedings of the British Pharmacological Society at (http://www.pa2online.org/abstract/abstract.jsp?abid=32564&kw=trpv4&author=shamsaldeen&cat=-1&period=58).
- Complex effects on rat aorta tone of acute methylglyoxal treatment. 2013. Proceedings of the British Pharmacological Society at (http://www.pa2online.org/abstract/abstract.jsp?abid=31215&kw=trpv4&author=shamsaldeen&cat=-1&period=-1).
- NADPH oxidase is the source of ROS in STZ rat aorta; use of the novel highly selective NOX inhibitor VAS2870. 2013. (http://uhra.herts.ac.uk/bitstream/handle/2299/12183/YLS2013abs.pdf;jsessionid=CF8B7757BF3F9245BD7511D8ECEF079B?sequence=2)
- Cambridge neuroscience event: ion channels in health and disease 2013. (http://www.neuroscience.cam.ac.uk/events/abstracts.php?key=e2d28c410e&pw=Submit&event_permalink=50903b958e)

Table of Contents

List of Figures

List of Tables

Abbreviations List

Abbreviation	**Definition**
$[Ca^{2+}]i$	Intracellular calcium ions concentration
4-αPDD	4α-Phorbol 12,13-didecanoate
5',6'- EET	5, 6- epoxyeicosatrienoic acid
20-HETE	20-hydroxyeicosattraenoic acid
AA	Arachidonic acid
ADA	American diabetes association
ADP	Adenine diphosphoribose
ADMA	Asymmetric di-methyl arginine
AGE	Advanced glycation end products
AKAP150	A-kinase anchoring protein
AMTB	N-(3-Aminopropyl)-2-[(3-methylphenyl)methoxy]-N-(2-thienylmethyl)benzamide hydrochloride
Ang II	Angiotensin II
AP	Action potential
APKD	Autosomal polycystic kidney disease
ASMCs	Aortic smooth muscle cells
AT1R	Angiotensin receptor-1
ATP	Adenosine 5′-triphosphate
AVP	Vasopressin
BCA assay	Bicinchoninic acid assay
BCECs	Bovine coronary endothelial cells
BH2	Dihydrobiopterin
BH4	Tetrahydrobiopterin
BKCa	Large conductance calcium-dependent potassium channels
β-NAD^+	β-nicotinamide adenine dinucleotide
BP	Blood pressure
BSA	Bovine serum albumin
CaM	Calcium calmodulin
CamK	Calmodulin kinase
CAV-1	Caveolin-1
CC	Carbachol
CEL	Nε-carboxyethyl lysine
cGMP	Cyclic guanylyl mono phosphate
CHO	Chinese hamster ovary
CML	N^6-carboxymethyllysine
COX-1	Cyclooxygenase-1
CRC	Concentration response curve
CRP	C-reactive protein
DAG	Diacyl glycerol
DDAH	Dimethylaminohydrolase
DDW	Deionised distilled water
Dil-Ac-LDL	Acetylated low density lipoprotein
DHAP	Dihydroxyacetone phosphate
DM	Diabetes mellitus
DMSO	Dimethyl slufoxide

DMEM	Dulbecco's Modified Eagle Medium
DNA	Deoxyribonucleic acid
DW	Distilled water
ECF	Extracellular fluid
ECL	Enhanced chemiluminescence
ECs	Endothelial cells
EDHF	Endothelium derived hyperpolarising factor
eIF2α	Eukaryotic initiation factor2α
ERAD	Endoplasmic reticulum-associated degradation
EDRF	Endothelium derived relaxing factor
EET	Epoxyeicosatrienoic acid
eNOS	Endothelial nitric oxide synthase
EPCs	Endothelial progenitor cells
EPO	Epoxygenase
ER	Endoplasmic reticulum
ET-1	Endothelin-1
ETA	Endothelin receptor-A
FA	Fatty acids
FAD	Flavin adenine dinucleotide
FBC	Final bath concentration
FBS	Foetal bovine serum
FCS	Foetal calf serum
FL	Fructoselysine
FMN	Flavin mononucleotide
FWC	Final well concentration
GAPDH	Glyceraldehyde 3-phosphate dehydrogenase
GC	Guanylate cyclase
GCH	GTP cyclohydrolase I
GLO	Glyoxalase
GLUT	Glucose transporters
GMP	Guanylyl mono phosphate
GPCR	G-protein coupled receptor
GPCR-IP3	G-protein coupled receptor-elaborated inositol triphosphate
GSH	Reduced glutathione
GSSG	Oxidized glutathione
HBSS	Hanks' balanced salt solution
HB	Hank's buffer
HC067047	2-Methyl-1-[3-(4-morpholinyl)propyl]-5-phenyl-*N*-[3-(trifluoromethyl)phenyl]-1*H*-pyrrole-3-carboxamide
HDL	High density lipoprotein
HEPES	4-(2-Hydroxyethyl)piperazine-1-ethanesulfonic acid, N-(2-Hydroxyethyl)piperazine-N′-(2-ethanesulfonic acid)
HMG-CoA reductase	The 3-hydroxy-3-methyl-glutaryl-coenzyme A reductase
hTRP channels	Human transient receptor potential channels

I.P	Intraperitoneal
IAA	Insulin autoantibody
IDDM	Insulin dependent diabetes mellitus
IDF	International diabetes federation
IFN-γ	Interferon-γ
IκB	Inhibitor nuclear factor of kappa light polypeptide gene enhancer in B-cells inhibitor
iNOS	Inducible nitric oxide synthase
IP	Isopropyl alcohol
IP3	Inositol 1,4,5,-triphosphate
IP3-R	Inositol 1,4,5,-triphosphate receptor
IR	Insulin receptor
IRS	Insulin receptor substrate
JNK	c-Jun N-terminal kinase
K_{ATP}	ATP-sensitive potassium channels
KB	Ketone body
Kca	Calcium-activated potassium channels
KO	Knockout
Krebs solution	Krebs-Hensileit physiological solution
Kv	Voltage-gated potassium channels
LA	L-arginine
LDL	Low density lipoprotein
LGCs	Ligand-gated cation channels
L-NAME	L-NG-Nitro-L-arginine methyl ester hydrochloride
LPS	Lipopolysaccharides
LSCM	laser scanning confocal microscope
M3	Muscarinic receptor-3
M5	Muscarinic receptor-5
MAPK	Mitogen activated protein kinase
MDCK	Madin-Darby canine kidney
MEM	Minimum Essential Medium
MEP	Myoendothelial projections
MGO	Methylglyoxal
MLC	Myosin light chain
MLCP	Myosin light chain phosphatase
MNU	N-methyl-N-nitrosurea
MODY	Maturity-onset diabetes of the young
MOLD	methylglyoxal-derived lysine-lysine dimer
MSCC	Mechanosensitive cation channels
M.wt	Molecular weight
NA	Noradrenaline
NAD^+	Nicotine adenine dinucleotide
NADPH	Nicotinamide adenine dinucleotide phosphate
ND	Neonatal diabetes
NF κB	Nuclear factor κB

nNOS	Neuronal nitric oxide synthase
Non-insulin dependent diabetes mellitus	NIDDM
NOS	Nitric oxide synthase
NSCC	Non-selective cation channel
$O^{\cdot}_2$	Peroxide anions
OAG	1-oleoyl-2-acetyl-sn-glycerol
ONOO-	Peroxynitrite
OS	Oxidative stress
OVLT	Organum vasculosum ligamentum terminals
ox-LDL	Oxidised LDL
p-Akt	Phosphorylated Akt
PERK	Protein kinase receptor-like eukaryotic initiation factor 2 kinase
PG	Prostaglandins
PGH_2	Prostaglandin H_2
PGI_2	Prostacyclin
PHD	Pleckstrin homology domain
PI3K	phosphatidylinositol 3-kinase
PI3K/Akt	phosphatidylinositol 3-kinase/Akt
PIP2	Phosphatidylinositol 4,5-bisphosphate
PK	Protein kinase
PKA	Protein kinase A
PKB	Protein kinase B
PKC	Protein kinase C
PKG	Protein kinase G
PKR	Protein kinase receptor
PLA2	Phospholipase-A2
PLC	Phospholipase-C
p-p38	Phosphorylated p38MAPK
PPAR-α	Peroxisome proliferator activated receptor-α
PPAR-γ	Peroxisome proliferator activated receptor-γ
PPOH	6-(2-propargyloxyphenyl) hexanoic acid
RAGE	Advanced glycated end products receptor
RBC	Erythrocytes
RN-1734	2,4-Dichloro-*N*-isopropyl-*N*-(2-isopropylaminoethyl)benzenesulfonamide
RN-1747	1-(4-Chloro-2-nitrophenyl)sulfonyl-4-benzylpiperazine
ROCCs	Receptor-operated cation channels
ROI	Region of interest
ROS	Reactive oxygen species
RT-PCR	Reverse transcriptase polymerase chain reaction
r-TRPM8	Chinese hamster ovary cells transfected with rat TRPM8 channel
RyR	Ryanodine receptors
SACs	Stretch activated calcium channels
SDS	Sodium dodecyl disulphate
SDW	Sterile deionised water

SEM	Standard error mean
SERCA	Sarcoplasmic/endoplasmic calcium ATPase
sGC	Soluble guanylate cyclase
SH2	Sulfhydryl
SH3	Thiol
SK3	Small conductance calcium-activated potassium channel
SNP	Sodium nitroprusside
SOCs	Store operated calcium channels
SOCCs	Store operated cation channels
SR	Sarcoplasmic reticulum
SR-BI	Scavenger receptor class B isoform I
SSAO	Semi-carbazide sensitive amine oxidase
STZ	Streptozotocin
$t_{1/2}$	half-life
T1DM	Type 1 diabetes mellitus
T2DM	Type 2 diabetes mellitus
TEMED	NNN'N'-Tetramethylethylenediamine
TK	Tyrosine kinase
TM	Transmembrane
TNF-α	Tumour necrosis factor-α
TRP channels	Transient receptor potential channels
TRPM	Melastatin transient receptor potential channel
TRPV	Vanilloid transient receptor potential channel
VCAM-1	Vascular cells' adhesion molecules
VGCC	Voltage-gated calcium channels
VSM	Vascular smooth muscle
VSMCs	Vascular smooth muscle cells

Chapter 1: General introduction

1.1. Diabetes mellitus definition

Diabetes mellitus (DM) is a complex disease characterised by chronic blood glucose elevation (hyperglycaemia) due to compromised insulin synthesis and secretion or declined tissue sensitivity to insulin, if not all three conditions (F. M. Ashcroft & Rorsman, 2012). In 2015, the International Diabetes Federation (2015) reported that approximately 415 million people worldwide have diabetes and that DM accounted for approximately 5 million deaths, or one death every 6 seconds.

1.2. Diabetes mellitus types

Of all diabetes patients, approximately 10% are diagnosed with type-1-DM—that is, insulin dependent DM (T1DM)—which is mainly attributed to autoimmune aetiological factors such as plasma islet-cells antibodies that destroy pancreatic β-cells (American Diabetes Association, 2012; F. M. Ashcroft & Rorsman, 2012). Children aged less than 12 years comprise the majority of T1DM patients who require lifelong insulin treatment for their survival. However, two types of monogenic diabetes are commonly misdiagnosed as T1DM due to early symptoms detection: neonatal diabetes (ND), which is diagnosed in the first 6 months of life, and maturity-onset diabetes of the young (MODY), which affects individuals aged less than 25 years (F. M. Ashcroft & Rorsman, 2012). Numerous therapeutic options are available to manage diabetes, including glibenclamide, which is a sulphonylurea capable of controlling 90% of cases of ND as well as MODY patients in general (F. M. Ashcroft & Rorsman, 2012).

Approximately 90% of diabetic patients have type-2-DM (T2DM), which is regarded as a complex disease whose risk factors include genetic factors, lifestyle, age, obesity, pregnancy, and gender (Chao & Henry, 2010). Unlike T1DM, T2DM does not require its patients to receive insulin injections or pumps in order to survive, since insulin secretion is partially deficient or resisted, if not both, the latter primarily attributed to increased abdominal fat and obesity (American Diabetes Association, 2012; F. M. Ashcroft & Rorsman, 2012). Reduced insulin secretion derives from an altered insulin signalling cascade or reduced β-cell mass, if not both. However, studies remain inconclusive regarding the extent of β-cell mass reduction. As a case in point, an earlier study with 91 obese patients showed that approximately 65% of β-cell deficiency was associated with T2DM (Butler et al., 2003), whereas another concluded that only 10% of β-cell mass reduction was associated with the range of altered insulin signalling components that initiate diabetes (Del Guerra et al., 2005).

1.3. Insulin secretion

Glucose-induced insulin secretion is a calcium-dependent cascade. Glucose-transporters-1 (GLUT-1) uptake plasma glucose into pancreatic β-cells to generate ATP (F. M. Ashcroft & Rorsman, 2012), which is accompanied with ADP reduction and ATP-sensitive potassium (K_{ATP}) channels closure (Arkhammar, Nilsson, Rorsman, & Berggren, 1987). Once K_{ATP} channels close, calcium ions (Ca^{2+}) flow in through corresponding channels and thereby initiate insulin exocytosis (Frances M Ashcroft, Harrison, & Ashcroft, 1984). However, glucose is not the only insulin release stimulator. As Figure 1 shows, lipids and proteins are also insulin secretagogues, as are other neurotransmitters and hormones, including incretins, which stimulate insulin secretion independently from Ca^{2+} (F. M. Ashcroft & Rorsman, 2012; Vilsbøll et al., 2008).

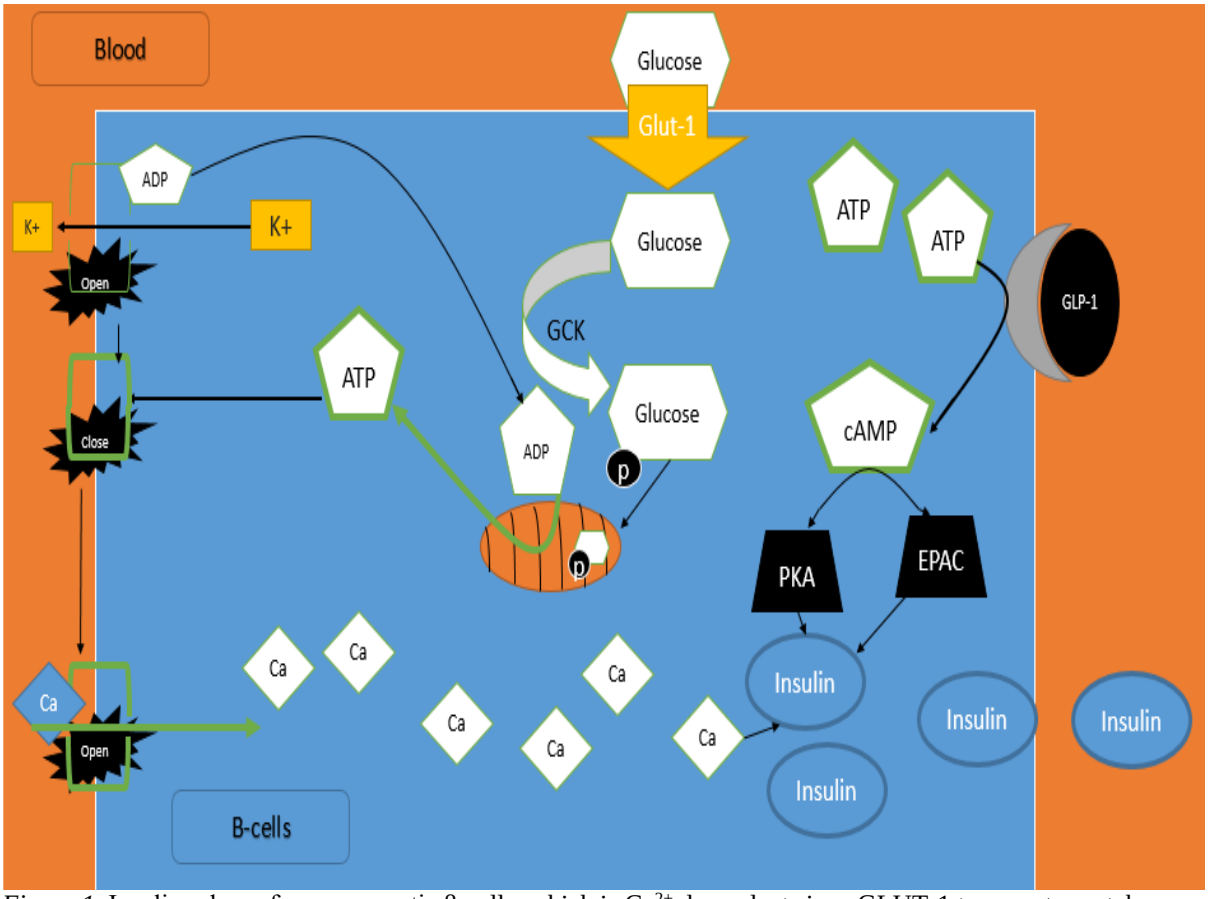

Figure 1. Insulin release from pancreatic β-cells, which is Ca^{2+} dependent since GLUT-1 transporter uptake glucose is metabolised to stimulate the closure of potassium channels that triggers Ca^{2+} influx, whereas glucagon-like peptide-1 (GLP-1) stimulates insulin secretion independent from Ca^{2+}; adapted from F. M. Ashcroft and Rorsman (2012).

1.3.1. Insulin signalling

Insulin signalling is a complicated cascade that begins when insulin binds to its corresponding tyrosine kinase (TK)-coupled receptor, an insulin receptor (IR) that is phosphorylated to provide docking sites for intracellular proteins that function as insulin receptor substrates (IRS1-4) (Taniguchi, Emanuelli, & Kahn, 2006). Since it exerts TK activity, IR phosphorylates IRS1-4 to unveil an interactive sulfhydryl (SH2) domain responsible for activating phosphatidylinositol 3-kinase/protein kinase B (PI3K/PKB), as well as Ras-mitogen-activated protein kinase (MAPK) pathways that trigger approximately 40 cellular targets for glucose uptake, protein synthesis, and vesicular trafficking (X. Jia & Wu, 2007; Krüger et al., 2007; Taniguchi et al., 2006). Although ubiquitously expressed in the body, IRs are primarily expressed in metabolically active cells such as hepatocytes and adipocytes (Desbuquois et al., 1993), as well as in the hippocampus, where they are involved in cognition and memory (Ho et al., 2012). More specifically, endothelial IRs are involved in regulating vascular tone by mediating nitric oxide (NO) release and thus vasodilation (Federici et al., 2004). Insulin binding to IRS-1 stimulates endothelial nitric oxide synthase (eNOS) phosphorylation at serine-1177 and threonine-497 and thereby induces NO generation (Nigro et al., 2014), , as figure 2 illustrates. However, in T2DM, insulin resistance correlates to diabetes complications such as endothelial dysfunction (Mustafa, Sharma, & McNeill, 2009).

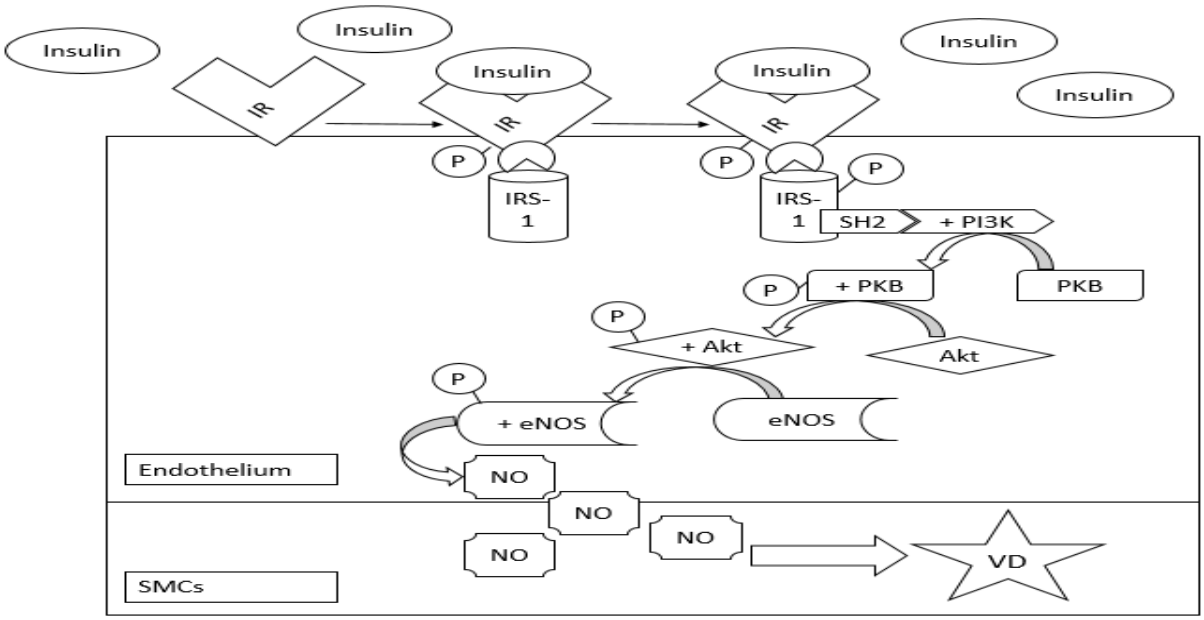

Figure 2. Insulin-induced endothelial nitric oxide (NO) signalling cascade, in which insulin binds to insulin receptors (IR) phosphorylated to be further bound with insulin receptor substrate-1 (IRS-1) in order to activate a phosphatidylinositol 3-kinase/protein kinase B (PI3K/PKB) pathway that culminates with Akt phosphorylation. Akt phosphorylation activates endothelial nitric oxide synthase (eNOS), which generates NO as a means to achieve vasodilation (Shamsaldeen, Mackenzie, Lione, & Benham, 2016).

1.4. Diabetes complications

Given its increasing prevalence, DM is forecast to affect approximately 600 million people worldwide by 2035 (DiabetesUK, 2014). Diabetes complications such as endothelial dysfunction, nephropathy, and neuropathic pain occur in both T1DM and T2DM patients, and approximately 50% of diabetics have demonstrated some of those complications at their initial diagnoses (M. Davies, Brophy, Williams, & Taylor, 2006; UK Prospective Diabetes Study Group, 1991). Diabetes complications compromise diabetic patients' quality of life and contribute to significant economic burden (M. Davies et al., 2006). In 2011, for example, the UK National Health Services spent approximately £8 billion on managing diabetes complications and burdened the national treasury with a cost of approximately £24 billion, a figure that by 2035 is expected to reach approximately £40 billion, or 17% of the total expenditure on health resources (Hex, Bartlett, Wright, Taylor, & Varley, 2012). Furthermore, currently available diabetes therapies have several contraindications and pose adverse effects, and accordingly, the aim to efficiently manage diabetes complications remains unachieved (Virally et al., 2007). As such, new therapeutic strategies are required to manage diabetes complications and should focus on understanding the precise pathophysiology and selection or development of therapeutic options accordingly (Harden & Cohen, 2003). Among the numerous complications of diabetes, endothelial dysfunction is the chief focus of this research. Clarifying the physiology of endothelium-dependent vasodilation should provide a robust foundation for understanding the pathophysiology of endothelial dysfunction in diabetes.

1.4.1. Endothelium-dependent vasodilation

Blood vessels are primarily composed of three layers: the outer layer (tunica adventitia), the medial layer (smooth muscle cells, or tunica media), and the inner layer (endothelium or tunica intima) (C. W. Chen, Corselli, Peault, & Huard, 2012). The endothelium regulates vascular tone by releasing numerous vasodilators, including NO, prostaglandins (PG), and endothelium-derived hyperpolarising factor (EDHF), in addition to vasoconstrictors such as endothelin-1 (ET-1) and angiotensin II (Ang II) (Tabit, Chung, Hamburg, & Vita, 2010).

On the whole, the endothelium mediates the transmission of electrical signals from one locus to remotely control vascular tone (Garland & Weston, 2011).

NO in endothelial cells (ECs) is generated by way of endothelial NO synthase (eNOS), which oxidises L-arginine into L-citrulline (M. I. Lin et al., 2003). eNOS or NOS-3 is a

constitutively active enzyme in the ECs that can be further stimulated by receptor-dependent agonists that increase $[Ca^{2+}]i$ and compromise plasma membrane phospholipid symmetry (Cines et al., 1998; A. Dhar, Dhar, Desai, & Wu, 2010). eNOS is attached to the membranous caveolar protein, caveolin-1 (CAV-1), from which eNOS is displaced to become active through calcium calmodulin (CaM) binding (Adak, Wang, & Stuehr, 2000; H. Wang, Wang, Liu, Chai, & Barrett, 2009). NO diffuses to the vascular smooth muscle cells (VSMCs), where it activates the soluble guanylate cyclase (sGC) that generates cyclic guanosine-3,5-monophosphate (cGMP) in order to achieve vasodilation (van den Oever, Raterman, Nurmohamed, & Simsek, 2010). cGMP inhibits the voltage-gated calcium channels (VGCC)-mediated Ca^{2+} entry into the VSMCs to inhibit the vasoconstriction. At the same time, cGMP activates potassium channels such as BKca, K_{ATP}, and voltage-gated potassium channels (Kv), which induces membrane hyperpolarisation and vasodilation (Dong, Waldron, Cole, & Triggle, 1998; Murphy & Brayden, 1995b). cGMP also activates PKG, which in turn activates myosin light-chain phosphatase (MLCP) that dephosphorylates the myosin light chain (MLC) and causes further vasodilation (Poulos, 2006). NO reduces $[Ca^{2+}]i$ in the VSMCs by activating the sarcoplasmic and endoplasmic calcium ATPase (SERCA) pumps that uptake $[Ca^{2+}]i$ in order to fill cellular calcium stores and thereby inhibit the store operated calcium channels (SOCs) from inducing vasoconstriction (Cohen et al., 1999). Another NOS isoform, inducible NO synthase (iNOS), is induced by inflammatory mediators such as cytokines to release NO independent of Ca^{2+} (Kleinert, Pautz, Linker, & Schwarz, 2004). Experimentally, iNOS expression can be induced by lipopolysaccharides (LPS), a bacterial cell wall component (Hattori, Hattori, & Kasai, 2003). A previous study showed that LPS-incubation reduces vascular contractility and thereby induces vascular relaxation in rat aortic strips denuded from the endothelium; such relaxation was mediated by the release of NO and the activation of calcium-activated potassium channels (Kca) channels in VSMCs (Hall, Turcato, & Clapp, 1996). Therefore, inducing iNOS expression might be associated with the activation of Kca that is responsible for the vasodilation associated with septic shock (Hall et al., 1996). Moreover, NO generated by iNOS was shown to inhibit cytokine-induced vasospasm in the coronary arteries of pigs (Fukumoto et al., 1997).

In addition to NO, cyclooxygenase-1 (COX-1) in ECs metabolises arachidonic acid (AA) to produce prostacyclin, which is a potent vasodilator (Mitchell, Ali, Bailey, Moreno, & Harrington, 2008). AA is then liberated from the ECs membrane through the action of phospholipase A2 (PLA2) (Lambert, Pedersen, & Poulsen, 2006). Endothelial COX-1

initially metabolises AA into prostaglandin G_2, which is then metabolised through the peroxidase activity of COX-1 into prostaglandin H_2 (PGH_2) (Mitchell et al., 2008). Afterward, PGH_2 is metabolised into the vasodilator prostacyclin (PGI_2) through prostaglandin G synthase (Mitchell et al., 2008). Prostacyclin mediates vasodilation by activating the K_{ATP} channels in VSMCs, which prompts membrane hyperpolarisation and, in turn, vasodilation (Jackson, Konig, Dambacher, & Busse, 1993). Moreover, prostacyclin binds to the prostacyclin receptor IP, a G-protein coupled receptor (GPCR) that activates the Gαs subunit that consequently activates adenylyl cyclase (AC), which converts endothelial ATP into cAMP. Otherwise, it can activate the Gαq subunit that further activates the membranous PLC to hydrolyse the membrane PIP2 into IP3 and DAG (Lawler, Miggin, & Kinsella, 2001). Accordingly, IP3 binds to the endoplasmic reticulum (ER) IP3-R to induce the release of Ca^{2+} from ER stores to mediate endothelium Ca^{2+} entry, which is a crucial step in initiating endothelium-dependent vasodilation (Murata et al., 2007). As another previous study showed, blocking BKca through iberiotoxin (25–50nM) prevented prostacyclin-induced vasodilation and thereby revealed BKca involvement in aortic vasodilation in guinea pigs (Clapp, Turcato, Hall, & Baloch, 1998).

Along with NO and prostacyclin, a third endothelial vasodilatory pathway is EDHF (G. Chen, Suzuki, & Weston, 1988). Previous studies have been conducted to identify the mechanism of action of EDHF and consequently revealed the involvement of a wide range of potassium channels. In eNOS knockout (KO) mice, acetylcholine-induced vasodilation was significantly inhibited by a physiological salt solution high in potassium (40mM) or iberiotoxin (100nM), which revealed BKca as an essential element of the EDHF pathway (A. Huang et al., 2000). Moreover, apamin (30nM), a selective SKca blocker, significantly inhibited EDHF-mediated vasodilation in rabbit mesenteric arteries treated with acetylcholine (Murphy & Brayden, 1995a). Another study revealed IKca as an additional component of EDHF-mediated vasodilation, since charybdotoxin (0.3μM) inhibited acetylcholine-induced vasodilation in rat hepatic arteries, though such did not occur when charybdotoxin was substituted with iberiotoxin (0.1μM), which thereby revealed IKca involvement in mediating EDHF (Zygmunt & Högestätt, 1996). However, the role of K_{ATP} might not be essential to the EDHF pathway. Indeed, previous studies have shown that glibenclamide (5μM), a K_{ATP} blocker, did not inhibit hyperpolarisation induced by EDHF in rabbit mesenteric arteries (Murphy & Brayden, 1995a). In addition to the involvement of Kca channels, as numerous studies have revealed, epoxyeicosatrienoic acid (EET) is another essential component in the EDHF

pathway. In one such study, the metabolism of AA through cytochrome P450 epoxygenase proved to be the primary vasodilatory pathway in small epicardial arteries (Widmann, Weintraub, Fudge, Brooks, & Dellsperger, 1998). Another study showed that applying 5, 6-EET to cultured rat ASMCs effected membrane hyperpolarisation similar to that of EDHF (Popp, Bauersachs, Hecker, Fleming, & Busse, 1996). At the same time, when the synthesis of 5, 6-EET, and 11, 12-EET and 14, 15-EET was inhibited by SKF 525a, AA-induced vasodilation became significantly inhibited in the bovine coronary artery, which highlighted EET derivatives as essential components of the EDHF pathway (Hecker, Bara, Bauersachs, & Busse, 1994; Rosolowsky & Campbell, 1993).

However, the predominant role of each of the three aforementioned vasodilatory pathways differs according to blood vessel size. In a previous study, EDHF and the metabolism of AA through cytochrome P450 epoxygenase was the chief vasodilatory pathway in small epicardial arteries (Sandow & Hill, 2000; Widmann et al., 1998). By contrast, the NO pathway was identified as the primary mediator in large epicardial arteries (Widmann et al., 1998). Such findings are consistent with the idea that the role of the EDHF pathway in mediating vasodilation is greater than that of NO in small vessels (Shimokawa et al., 1996). That dynamic might be attributed to expanded myoendothelial gap junctions in smaller arteries (e.g., mesenteric arteries), which furnish sites for electrical communication between the endothelium and vascular smooth muscle (VSM) (Sandow & Hill, 2000).

Added to the three primary vasodilation pathways, at least 21 distinct transient receptor potential (TRP) channels have been recognised in VSMCs in studies involving Western blotting, reverse transcription polymerase chain reaction (RT-PCR), and immunohistochemistry (H. Y. Kwan, Huang, & Yao, 2007). TRP channels are ion channels that differ in their permeability to sodium (Na^+), potassium (K^+), and Ca^{2+} (Watanabe, Murakami, Ohba, Takahashi, & Ito, 2008), and most moderate Ca^{2+} conductance at a conductance ratio of P Ca^{2+}/ P Na^+ = 0.3–10 (Watanabe et al., 2008). VSMCs' TRP channels include all TRPCs and TRPMs, in addition to TRPV1–TRPV4, TRPP1, and TRPP2 (H. Y. Kwan et al., 2007). Similar TRP were also found in the endothelium along with TRPA1, though not TRPM5 (Earley, Gonzales, & Garcia, 2010; H. Y. Kwan et al., 2007; Watanabe et al., 2008). As cation channels, TRP channels exert vascular tone regulation in both systemic and pulmonary circulations (Watanabe et al., 2008) and are involved in controlling VSMCs survival pathways by regulating Ca^{2+}, Mg^{2+} and Na^+ homeostasis, which is mediated by calcium-selective or -nonselective receptor-operated Ca^{2+} channels (ROCCs), if not both, that

stimulate VGCCs through Na^+-mediated cell depolarisation (Watanabe et al., 2008). Sustained endothelium Ca^{2+} entry contributes to NO and PG generation and thereby vasodilation (D. X. Zhang et al., 2009). Notably, NO is among the vasodilators released in response to shear stress and TRPV4 activation (Sena, Pereira, & Seiça, 2013; Sukumaran et al., 2013).

Numerous researchers have shown how TRP channels contribute to vascular tone regulation, as summarised in Table 1.

Table 2 TRP channels contribution in vascular tone regulation

TRP channel	**The vascular effect of TRP channel activation**
TRPC1	Endothelium independent vasodilation by BKca coupling (H.-Y. Kwan et al., 2009) and mediating ET-1-induced vasoconstriction (Bergdahl et al., 2003)
TRPC2	Pseudogene (Vannier et al., 1999)
TRPC3	Bradykinin-induced vasodilation mediated by endothelial TRPC3 (C.-l. Liu, Huang, Nga, Leung, & Yao, 2006) and pyrimidine and ET-1-induced vasoconstriction mediated by TRPC3 (Peppiatt-Wildman, Albert, Saleh, & Large, 2007; Reading, Earley, Waldron, Welsh, & Brayden, 2005)
TRPC4	Significant impairment of muscarinic-induced vasodilation by TRPC4 knockout (KO) (Marc Freichel et al., 2001) and TRPC4 downregulation prevents stretch-induced vascular offset (Lindsey, Tribe, & Songu-Mize, 2008)
TRPC5	TRPC5 is a SOC in dwarf rabbit's VSMCs (S.-Z. Xu, Boulay, Flemming, & Beech, 2006), and TRPC5 nitrosylation provides positive feedback for TRPC5-induced Ca^{2+} influx in the endothelium (T. Yoshida et al., 2006)
TRPC6	TRPC6 translocation activated by 11, 12-EET, which may contribute to vasodilation through endothelial Kca activation (Fleming et al., 2007), and increased contractility provided by TRPC6 KO VSMCs (Dietrich et al., 2005)
TRPC7	Vasopressin (AVP)-induced depolarisation in VSMCs contributed to TRPC7 and TRPC6 heteromultimeric channels (Maruyama et al., 2006), and ET-1-induced vasoconstriction mediated by TRPC7 (Peppiatt-Wildman et al., 2007)
TRPM1	Vascular effects yet to be investigated
TRPM2	Oxidative stress-induced endothelial cells' hyperpermeability and apoptosis mediated by TRPM2 (Hecquet, Ahmmed, Vogel, & Malik, 2008)
TRPM3	Vasoconstriction in murine arteries induced by TRPM3 (Naylor et al., 2010)
TRPM4	Vasoconstriction induced by TRPM4 (Gonzales, Garcia, Amberg, & Earley, 2010; Reading & Brayden, 2007)
TRPM6	Mg^{2+} influx into the VSMCs mediated by TRPM6, though the exact function of TRPM6 is unclear (Touyz et al., 2006)

TRPM7	Mg^{2+} influx into the VSMCs mediated by TRPM7 in response to Ang II (Touyz et al., 2006), and Mg^{2+} influx into the VSMCs mediated by TRPM7 to further mediate bradykinin endothelium-dependent vasodilation (Callera et al., 2009; Paravicini, Yogi, Mazur, & Touyz, 2009)
TRPM8	Vasodilation in pre-contracted mesenteric and thoracic aortic arteries induced by TRPM8 agonists (C. D. Johnson et al., 2009; Silva et al., 2015), and endothelium independent vasodilation possibly induced by TRPM8 via BKca (A. I. Bondarenko, R. Malli, & W. F. Graier, 2011a; Earley, Heppner, Nelson, & Brayden, 2005)
TRPP1	Blood shear stress-induced endothelial nitric oxide (NO) generation mediated by TRPP1 in a KO study (Nauli et al., 2008)
TRPP2	Blood shear stress-induced endothelial NO generation partially mediated by TRPP2 in a KO study (AbouAlaiwi et al., 2009)
TRPV1	Endothelium-dependent vasodilation through capsaicin ingestion (D. Yang et al., 2010), and vasoconstriction induced with TRPV1 activated in C-fibres (Scotland et al., 2004)
TRPV2	May contribute to vasoconstriction (Muraki et al., 2003)
TRPV3	Endothelium-dependent vasodilation following treatment with carvacrol, a dietary TRPV3 agonist (Earley et al., 2010)
TRPV4	Endothelium-dependent vasodilation through shear stress activation and independent vasodilation through BKca activation (Earley et al., 2005; Earley et al., 2009)
TRPA1	Significant reduction in propofol-induced vasodilation in TRPA1 KO mice and with TRPA1 antagonism (Sinha, 2013)

The variety of TRP channels expressions in ECs has been explained by two theories. First, different TRP channels are activated by different activators and hence endow ECs with different mechanisms for Ca^{2+} influx (X. Yao & Garland, 2005). For instance, TRPV4 is activated mechanically by blood flow shear stress (Köhler et al., 2006) and TRPM2 by ADP-ribose, which oxidative stress (OS) releases from mitochondria (Desai & Clapham, 2005). Second, TRP channels activation might yield different functional responses according to channel properties, including the Ca^{2+} conductance profile, in addition to the level of expression at different vascular beds (X. Yao & Garland, 2005). TRPC5 is expressed predominantly in human coronary artery ECs, whereas human pulmonary arteries express TRPC4 (Yip et al., 2004). Such variation in TRP channels expression in different vascular beds is important for understanding the physiology and pathophysiology of ECs in different vascular regions (X. Yao & Garland, 2005).

In vasodilatory pathways in general, when endothelial muscarinic receptors are activated, GPCR-bound AC converts the cytoplasmic ATP into cAMP, which in turn activates cAMP-dependent protein kinase A (PKA) that phosphorylates and activates the ER's IP3-R to

potentiate the release of Ca^{2+} from cellular stores (Bugrim, 1999). Moreover, cAMP was reported to enhance EDHF electrical signalling via the myoendothelial gap junction (Griffith, Chaytor, Taylor, Giddings, & Edwards, 2002). Endothelial muscarinic and prostacyclin GPCR activates membranous PLC to hydrolyse membrane PIP2 into IP3 and diacyl glycerol (DAG) (Everaerts, Nilius, & Owsianik, 2010; Miggin & Kinsella, 2002). The generated IP3 binds to its corresponding IP3-R on the ER to facilitate the release of Ca^{2+}, which is essential to activate IKca and SKca and thereby induce membrane hyperpolarisation, which becomes transmitted through myoendothelial projections (MEPs) and the myoendothelial gap junction to the VSM layer underneath (Bagher & Garland, 2014). Increased blood shear stress activates membrane bound PLA2, which generates AA from the membrane cholesterol, followed by a series of reactions that generate EETs, TRPV4 activators, and EDHF mediators (Earley et al., 2005; Hecker et al., 1994; Lambert et al., 2006; Rosolowsky & Campbell, 1993). A previous study showed that TRPV4 forms a functional complex with BKca and ryanodine receptors (RyR) in the smooth muscle layer (Earley et al., 2005). RyR located on the sarcoplasmic reticulum (SR)—that is, the ER muscular equivalent in the smooth muscle layer— stimulates Ca^{2+} sparks that activate BKca to induce the hyperpolarisation of smooth muscle cell membrane and thus vasodilation (Earley et al., 2005). The activation of VSM's TRPV4 elevates Ca^{2+} sparks and potentiates BKca activity to induce smooth muscle cells membrane hyperpolarisation and vasodilation (Earley et al., 2005). Moreover, the endothelial TRPV4-mediated Ca^{2+} influx activates IKca and SKca (Bagher et al., 2012; Ma et al., 2013). The activation of endothelial muscarinic receptors induces PI3K to phosphorylate Akt, which together with the CaM complex activates eNOS and ultimately generates NO (A. Dhar et al., 2010). As Figure 3 shows, TRPV4 is involved in the activation of eNOS and in mediating muscarinic-induced endothelium-dependent vasodilation (Köhler et al., 2006).

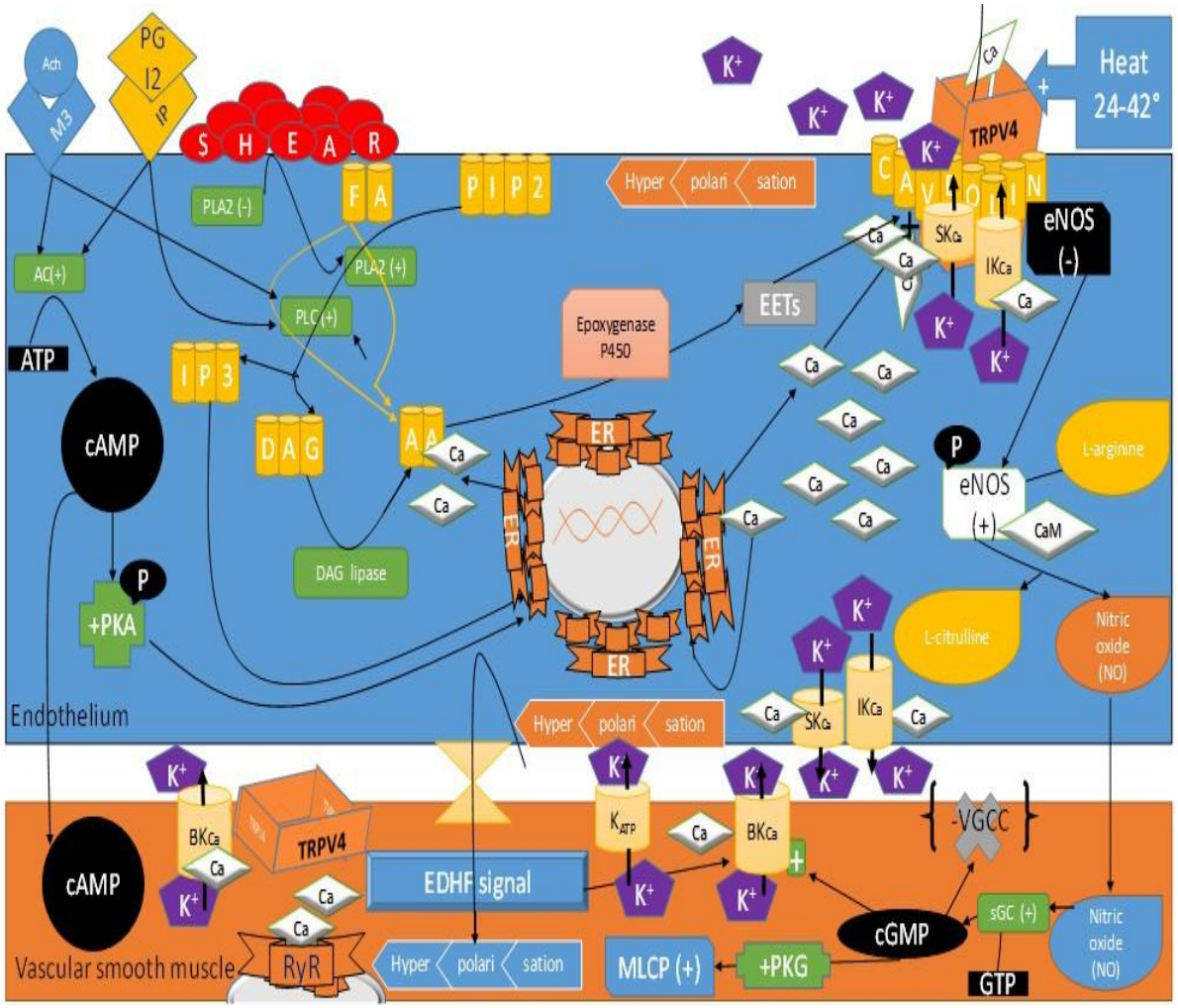

Figure 3. Endothelial-dependent vasodilation pathways: nitric oxide (NO), prostacyclin (PGI_2), and endothelium-derived hyperpolarising factor (EDHF). TRPV4-induced calcium (Ca^{2+}) influx activates endothelial NO synthase (eNOS), small conductance calcium-activated potassium channels (SKca), and intermediate conductance calcium-activated potassium channels (IKca). By facilitating the potassium efflux and inducing hyperpolarisation, which is transmitted to the vascular smooth muscle (VSM), the result is hyperpolarisation as part of EDHF. The EDHF signal is involved in the activation of epoxygenase enzymes that generate epoxyeicosatrienoic acid (EET), which activate TRPV4 in the endothelium and VSM. VSM's TRPV4-induced Ca^{2+}influx triggers large conductance calcium-activated potassium channels (BKca), while eNOS is activated to release NO, which diffuses to the VSM to activate cyclic guanylate mono phosphate (cGMP) that inhibits voltage-gated calcium channels and activates both potassium channels and myosin light chain phosphatase (MLCP) to induce vasodilation. PGI_2 binds to the G-protein coupled receptor IP to induce adenylate cyclase (AC) and phospholipase C (PLC), and AC causes cyclic adenosine monophosphate to induce the release of calcium from endoplasmic reticulum (ER) cellular stores. PLC metabolises membranous phosphatidylinositol 4, 5- bisphosphate (PIP2) into inositol 1, 4,5- triphosphate (IP3) and diacyl glycerol (DAG), after which IP3 binds to the IP3 receptors (IP3-R) of the ER to cause the release of calcium and hence activate eNOS, SKca, and IKca.

1.4.2. Endothelial dysfunction in diabetes

Cardiovascular diseases refer to numerous pathological conditions that affect the heart or blood vessels, if not both, and with 31% of deaths worldwide each year, represent the greatest factor of mortality in humans (World Health Organization, 2015).

Diabetes mellitus is considered to be a metabolic and vascular disease, with compromised circulation due to endothelial dysfunction as a common complication (Sena et al., 2013). Diabetics are therefore prone to fungal infections and ulcers, nephropathy and retinopathy as a consequence of impaired vasodilation due to endothelial dysfunction (American Diabetes Association, 2012; A. Dhar et al., 2010; Sena et al., 2013).

Endothelial dysfunction is a common diabetes complication in which endothelium-dependent vasodilation becomes impaired (Kolluru, Bir, & Kevil, 2012). The principal determinant of endothelial dysfunction is decreased NO bioavailability, with increased ET-1 biosynthesis as a close second (Bakker, Eringa, Sipkema, & van Hinsbergh, 2009). The primary factors govern the bioavailability of endothelial NO: the generation of NO from eNOS and the elimination of active NO (van den Oever et al., 2010). Numerous studies have revealed different pathways of accelerated NO elimination. As they have shown, under physiological circumstances, NO is produced from the dimeric eNOS that utilises L-arginine and molecular oxygen parallel to reducing nicotinamide adenine dinucleotide phosphate (NADPH) as a co-substrate (M. I. Lin et al., 2003). This coupled oxidation reaction occurs in the presence of other cofactors, including flavin adenine dinucleotide (FAD), flavin mononucleotide (FMN), tetrahydrobiopterin (BH4) and calmodulin (Adak et al., 2000). However, uncoupled eNOS generates superoxide anions and other ROS without producing NO owing to the addition of NADPH-derived electrons to the molecular oxygen rather than the substrate L-arginine (Guzik et al., 2002).

By inhibiting its synthesis or downregulating its synthesising enzyme, GTP cyclohydrolase I (GCH), BH4 downregulation contributes to eNOS uncoupling (Alp et al., 2003). Superoxide anions quench NO to produce peroxynitrite anions ($ONOO^-$) that compromise NO bioavailability and oxidise BH4 to dihydrobiopterin (BH2), as well as suppress GCH expression and thereby reduce BH4 expression (Alp et al., 2003; Milstien & Katusic, 1999). Elevated BH2 reduces NO production in addition to aggravating eNOS uncoupling due to BH4 reduction (Alp et al., 2003; Milstien & Katusic, 1999). In a previous clinical study, BH4 intra-arterial infusion (500μg/min) improved the endothelial function in diabetic patients, although such treatment did not significantly improve for non-diabetic volunteers (Heitzer, Krohn, Albers, & Meinertz, 2000). That study therefore concluded that endothelial dysfunction in T2DM might be attributed to the reduction in BH4 bioavailability (Heitzer et al., 2000). In another study, when human umbilical vein ECs were treated with high glucose concentration (30mM), the 26S proteasome activity significantly increased and yielded

$ONOO^-$-dependent GCH ubiquitination and degradation, which culminated with BH4 deficiency (J. Xu et al., 2007). Such GCH degradation was accompanied by BH4 reduction in streptozotocin (STZ)-mice aortic homogenates, which indicated that GCH downregulation could cause diabetic BH4 downregulation (J. Xu et al., 2007).

Asymmetric di-methyl arginine (ADMA) is an endogenous eNOS inhibitor which is metabolised to citrulline through dimethylaminohydrolase (DDAH) (Sena et al., 2013). In their clinical study with 135 T2DM patients, Krzyzanowska, Mittermayer, Wolzt, and Schernthaner (2007) found that approximately 50% of patients who experienced cardiovascular events were the same ones with plasma ADMA greater than 0.63μM. Accordingly, they postulated that ADMA could be used as a cardiovascular risk biomarker in diabetic patients (Cavusoglu et al., 2010; Krzyzanowska et al., 2007). At the same time, DDAH activity became significantly compromised in T2DM Sprague–Dawley rats and was accompanied with significant ADMA elevation and cGMP downregulation (K. Y. Lin et al., 2002). Such compromised DDAH activity and cGMP downregulation were also reproduced in human ECs (HMEC-1) treated with high glucose concentration (25mM) (K. Y. Lin et al., 2002).

As the substrate for eNOS, L-arginine is metabolised through arginase to yield ornithine which is in turn metabolised through the urea cycle (Kim et al., 2009). Arginase upregulation or hyperactivity, if not both, compromises L-arginine availability to induce eNOS uncoupling that culminates with ROS production and suppressed NO generation (Kim et al., 2009). Plasma arginase-1 (i.e., approximately 0.3 ng/ml) and arginase-2 (i.e., approximately 0.2 ng/ml) concentrations have been reported to be similar in T2DM patients and non-diabetic volunteers (Kashyap, Lara, Zhang, Park, & DeFronzo, 2008). However, plasma arginase activity was significantly higher in T2DM patients than non-diabetic individuals (Kashyap et al., 2008). Kashyap et al. (2008) also revealed that insulin infusion ($80mU/m^2$) for 4 hours significantly reduced arginase activity in T2DM patients and even reached a normal level of activity (i.e., approximately 0.2μmol/ml/hr). In another study conducted with STZ-diabetic rats, both the activity and expression of arginase significantly increased in STZ-diabetic rats' aortic rings, which showed significant endothelial dysfunction as a result (Romero et al., 2008). Furthermore, treating bovine coronary ECs (BCECs) with a high glucose concentration (25mM) induced OS, which was accompanied with arginase upregulation (Romero et al., 2008). The 3-hydroxy-3-methyl-glutaryl-coenzyme A (HMG-CoA) reductase

inhibitor, simvastatin (5mg/kg) restored endothelial function in STZ-diabetic rats by suppressing arginase expression and activity (Romero et al., 2008).

Endothelial dysfunction might also be attributed to the impairment of the eNOS signalling cascade that culminates with reduced NO production (Kolluru et al., 2012; Tabit et al., 2010). eNOS is activated via the activation of the PI3K/Akt system, from which Akt phosphorylates eNOS at serine 1177 residue and threonine 497 to induce NO generation (A. Dhar et al., 2010; M. I. Lin et al., 2003). A previous research detected the attenuation of the PI3K/Akt/eNOS cascade in diabetes (Liang et al., 2009), namely that endothelial progenitor cells (EPCs) treated with advanced glycation end products (AGE) significantly suppressed Akt and eNOS phosphorylation accompanied with compromised NO release (Liang et al., 2009). However, the peroxisome proliferator activated receptor-γ (PPAR-γ) agonist, rosiglitazone (10nM), induced Akt/eNOS upregulation, which was accompanied with improved NO release (Liang et al., 2009). Another NO pathway component is the TRPV4 channel, which is highly expressed in the endothelium. Accordingly, by focusing on TRPV4 channel involvement in diabetes endothelial dysfunction, this research seeks to clarify the physiological role of the TRPV4 channel in the endothelium in order to provide a robust foundation for explaining its pathophysiological contribution in endothelial dysfunction in diabetes.

1.4.3. TRPV4 and endothelial dysfunction in diabetes

Highly expressed in ECs, TRPV4 is a major vascular tone controller (Köhler et al., 2006). Although numerous researchers have suggested that TRPV4 is activated directly, others have demonstrated its indirect activation by way of mechanical stimulation or endothelium-derived 5',6'- EET (Christensen & Corey, 2007; Köhler et al., 2006). TRPV4 enhances Ca^{2+} influx to generate NO in addition to EDHF (Köhler et al., 2006). Moreover, TRPV1 and TRPV4 are central blood pressure (BP) regulators expressed in hypothalamic circumventricular organs such as organum vasculosum ligamentum terminals (OVLT) (Liedtke & Friedman, 2003; Naeini, Witty, Séguéla, & Bourque, 2006). TRPV4 senses blood osmolarity in the OVLT and thereby triggers the release of vasopressin (AVP) through hypertonicity-induced cation depolarisation, which induces vasoconstriction and water retention (Liedtke & Friedman, 2003; Mizuno, Matsumoto, Imai, & Suzuki, 2003). Furthermore, as KO mice studies have revealed, TRPV4 is essential in muscarinic-mediated endothelium-dependent vasodilation via a novel mechanism that involves Ca^{2+} influx by way of endothelium derived factor (11, 12

EET)-activated TRPV4 (Earley et al., 2005). Moreover, 11, 12 EET was shown to facilitate TRPV4 complex formation with RyR and BKca in VSMCs and thereby facilitate vasodilation (Earley et al., 2005). TRPV4-mediated Ca^{2+} influx involves cooperative gating through a four-channel cluster in MEPs (Bagher & Garland, 2014). Such TRPV4 cooperative gating requires A-kinase anchoring protein (AKAP150) in MEPs to induce hyperpolarisation-induced vasodilation through the activation of Kca, including BK_{Ca}, as several studies have (Bagher & Garland, 2014; Earley et al., 2005; M. Freichel et al., 2005). Pharmacological studies have shown the expression of TRPV4 channels as components of ECs in dilating mouse mesenteric arteries, rat aortic rings, and carotid arteries (Baylie & Brayden, 2011). H. Y. Kwan et al. (2007) hypothesised that dysfunction in TRPV4 contributes to endothelial dysfunction, while Köhler et al. (2006) earlier provided initial evidence of the involvement in TRPV4 dysfunction in endothelial dysfunction when flow-induced vasodilation was abolished by TRPV4 blockers, ruthenium red, and the PLA2 inhibitor, arachidonyl trifluoromethyl ketone, in rat carotid arteries. A more recent study demonstrated TRPV4 downregulation in STZ-rats' mesenteric endothelium (Ma et al., 2013), which was accompanied with suppressed SKca, contributed to endothelial dysfunction (Ma et al., 2013). Moreover, TRPV4 downregulation was found to be involved in diabetic endothelial dysfunction and retinopathy (Monaghan et al., 2015). These studies provide a very robust foundation that correlates TRPV4 alteration with diabetes endothelium dysfunction.

Taken together, all of those studies provide a very robust foundation for correlating TRPV4 alteration with endothelium dysfunction in diabetes. Accordingly, since the aim of this research is to investigate the role of TRPV4 as a member of the TRPC family in endothelial dysfunction in diabetes, it should offer a further explanation of TRPC in order provide a better understanding of their role in the body.

1.5. TRP channels

When specific gene mutation caused visual impairment in *Drosophila* by disrupting Ca^{2+} entry in specific cells, the gene was termed TRP, which bioinformatics analysis showed had 29 mammalian homologues (Pedersen, Owsianik, & Nilius, 2005; Ramsey, Delling, & Clapham, 2006).

1.5.1. TRP channels function

TRP channels are ion channels that differ in their permeability to Na^+, K^+, and Ca^{2+} (Watanabe et al., 2008). Most TRP channels possess moderate Ca^{2+} conductance with a conductance ratio of P Ca^{2+}/ P Na^+ = 0.3–10 (Watanabe et al., 2008). Ca^{2+} performs essential diverse cellular functions as its baseline concentration (100nM) increases by up to 100-fold during cell excitation (Watanabe et al., 2008). Such a wide range of Ca^{2+} elevation is shown to be involved in different cellular activities at variable durations as for instance neurotransmission (short-term) as well as cell cycle regulation (long-term) (Watanabe et al., 2008). Ca^{2+} is released from cellular storage, smooth ER, or its muscular analogue, SR, in response to G-protein coupled receptor-elaborated inositol triphosphate (GPCR-IP3). IP3 binds to the corresponding ER's IP3-receptor (IP3-R) or SR's ryanodine receptor coupled with VGCCs (Huo, Lu, & Guo, 2010). Through specific channels, Ca^{2+} influx can perform specific cellular functions such as, the generation of cardiomyocytes action potential (AP), which is partly triggered through reversed Na^+/Ca^{2+} exchanger-Ca^{2+} entry (Watanabe et al., 2008). Moreover, ligand-activated cation channels (LGCs) are considered to be extracellular Ca^{2+} sources (Watanabe et al., 2008). Similarly, receptor-activated cation channels have a slower onset of action, which involves cellular signalling and second messenger activation to yield Ca^{2+} entry (Bootman, Berridge, & Roderick, 2002). Such a mechanism of action appears in SOCs such as TRPV4/TRPC1 heteromeric channels in the endothelium (Ma, Cheng, Wong, et al., 2011). Mechanical forces also facilitate Ca^{2+} entry through stretch-activated Ca^{2+} channels (SACs) (Köhler et al., 2006).

A few TRP channels, including TRPM3α1, TRPM4, and TRPM5 are more permeable to monovalent ions (e.g., P Ca^{2+}/ P $Na^+ < 0.05$) (Pedersen et al., 2005). By contrast, other TRP channels are highly selective to Ca^{2+} (e.g., P Ca^{2+}/ P $Na^+ > 100$) such as TRPM3α2, TRPV5, and TRPV6 (Pedersen et al., 2005; Watanabe et al., 2008). However, TRPM6 and TRPM7 are permeable to Mg^{2+} and toxic heavy metals ions such as lead (Pb^{2+}) (Inoue, Jian, & Kawarabayashi, 2009; Ramsey et al., 2006). Permeability to such varied ions permeability among different TRP channels may be due to heterogeneous tetramer formation, since each subunit may provide distinct ion selectivity and permeability and thereby different channel properties (Ramsey et al., 2006). Cell response to TRP channels furthermore depends on the rate and amount of membranous TRP channels expression and the ability of cells to amplify TRP channels signals through the degree of the integrity of downstream cascade components (Winston, Toma, Shenoy, & Pasricha, 2001). TRP channels are involved in numerous

physiological and cellular functions, including sensory information transduction, visceral function modulation, cell growth, proliferation, and apoptosis (Inoue et al., 2009). Such a range of functions reflects TRP channels' involvement in different cellular stages, from initial cascade signalling to the level of gene expression (Inoue et al., 2009). TRP channels are also signal amplifiers and integrators and thus cellular sensors and detectors, in which roles they provide numerous physiological functions, including growth cone guidance (Ramsey et al., 2006).

1.5.2. TRP channels topology

Bioinformatics studies have identified TRP channels' structural features with 6-transmembrane (6-TM) domains of long cytosolic N- and C-termini (Mio et al., 2007). Those domains provide numerous protein-protein interaction motifs to yield a centralised, tetrameric ion-conducting pore, which is commonly located between the 5th and 6th TM domains (Pedersen et al., 2005). Moreover, the 6-TM domains share consensus homologous 25 aminoacid residues of 6 invariable aminoacids called TRP box, in addition to pleckstrin homology domain (PHD) (Ferguson, Lemmon, Schlessinger, & Sigler, 1995; Nilius, Mahieu, Karashima, & Voets, 2007). Each PHD requires a complementary sequence from a relevant endogenous cognate activator and hence endows the TRP channels with polymodal activation properties, meaning that different TRP channels of different PHDs require different activators (Ramsey et al., 2006). Interestingly, as Figure 4 indicates, mammalian TRP families have approximately 20% sequence homology (Clapham, 2003).

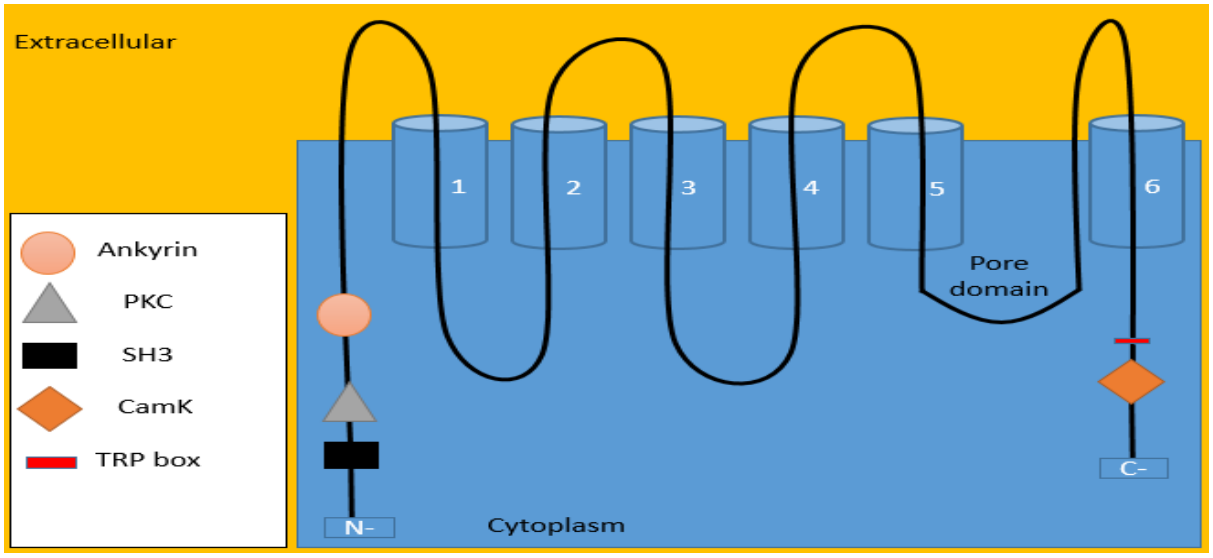

Figure 4. Transient receptor potential (TRP) channel topology of 6-TM domains, with a TRP box and other specific binding domains on N- and C-termini, protein kinase C (PKC), calmodulin kinase (CamK), and SH3 (i.e., thiol domain); adapted from Pedersen et al. (2005).

1.5.3. TRP channels family

As Figure 5 illustrates, human TRP (hTRP) channels are primarily categorised into 6 subfamilies, each with distinct activation profiles (Inoue et al., 2009).

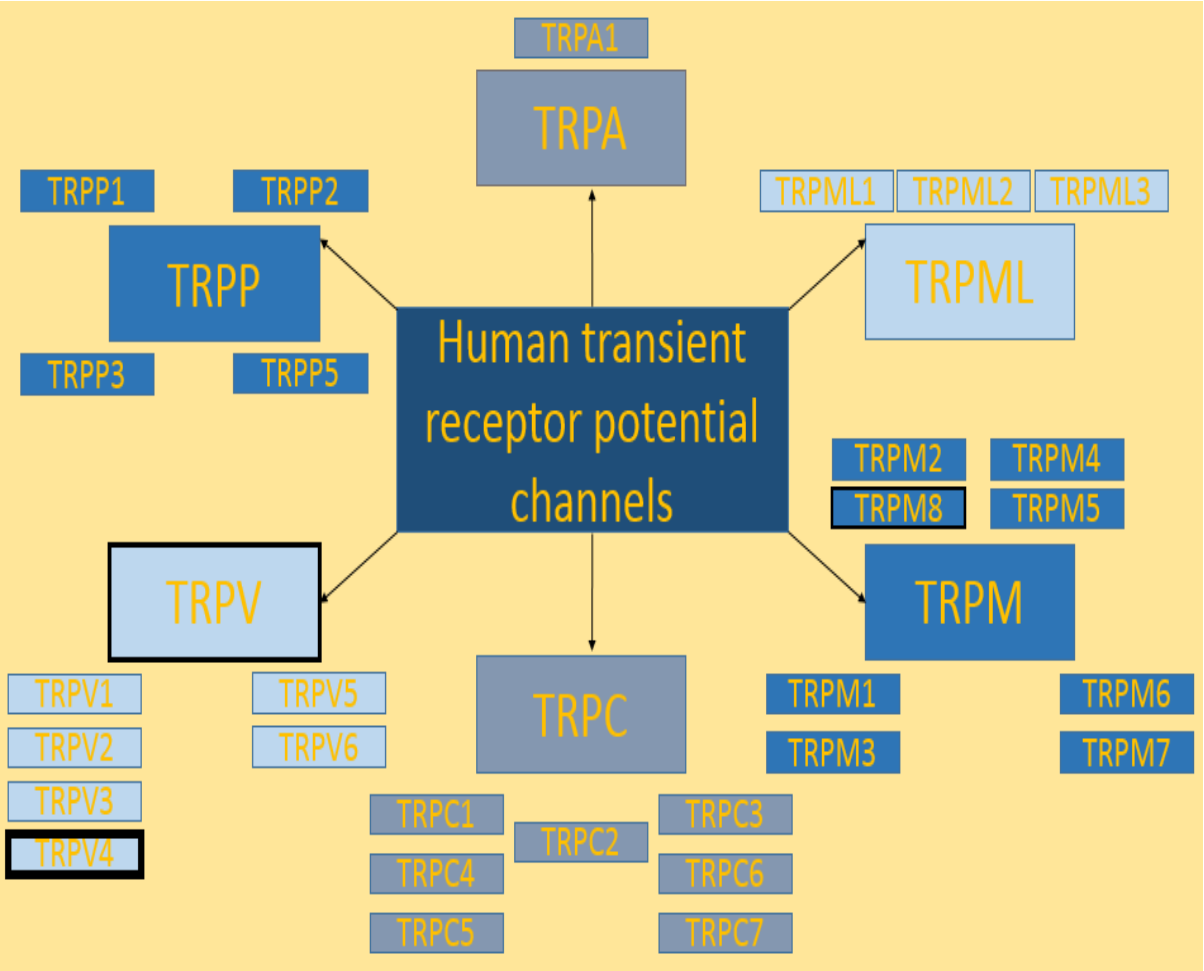

Figure 5. Human transient receptor potential (TRP) channels family of 6 subfamilies (i.e, TRPC, TRPV, TRPM, TRPML, TRPP and TRPA1) adapted from Inoue et al. (2009).

- TRPC

The first identified mammalian TRP channels subfamily, simply called TRPC, exhibited approximately 40% homology to the TRPC of *Drosophila* (Wes et al., 1995). In general, TRPCs are canonically and classically activated channels (Ramsey et al., 2006). whose mechanism involves either DAG-mediated ROCCs or PLC-mediated store-operated cation channels (SOCCs) (Tseng et al., 2004; Venkatachalam, Zheng, & Gill, 2003). TRPCs are categorised into 3 groups according to their functionality and sequence alignment (Ramsey et al., 2006) as follows.

- TRPC1, TRPC4 & TRPC5

TRPC1 forms heteromeric complexes with TRPC3, TRPC4 and TRPC5 to function as Gq/11 ROCC (Strübing, Krapivinsky, Krapivinsky, & Clapham, 2001). Complexes with TRPC4 and TRPC5commonly appear in brain tissue, where they emit minor regulated outward-rectifying current and facilitate ion conductance (Strübing et al., 2001). TRPC5 homomeric channels are essential regulators of hippocampal growth cone morphology through PI3K, PI5K, and Rac cascades in response to growth factors (Greka, Navarro, Oancea, Duggan, & Clapham, 2003; Ramsey et al., 2006). In particular, TRPC5 channel is activated by trivalent cations such as gadolinium (Gd^{3+}) or at high extracellular Ca^{2+} concentration (e.g., 1.5mM) (Jung et al., 2003; F. Zeng et al., 2004).

- TRPC3, TRPC6 and TRPC7

TRPC3, TRPC6, and TRPC7 form a three-membered subfamily with approximately 80% sequence homology (Ramsey et al., 2006). The basal activities of TRPC3 and TRPC6 are controlled by glycosylated asparagine residues of S1–S4 extracellular loop domains (Dietrich et al., 2003), and those channels are stimulated by nonreceptor TK (i.e., Src and Fyn) and inhibited by PKC and PKG (Hisatsune et al., 2004; H.-Y. Kwan, Huang, & Yao, 2004; J Shi, Ju, Saleh, Albert, & Large, 2010; Vazquez, Wedel, Kawasaki, Bird, & Putney, 2004; Venkatachalam et al., 2003). By contrast, CaM positively regulates TRPC6 and negatively controls TRPC7 activities (J. Shi et al., 2004).

- TRPC2

Although an expressed pseudogene is a nonfunctional channel in humans (Vannier et al., 1999), in rodents TRPC2 is DAG-activated and essential in pheromone signal transduction, as well as in fertilisation in both male and female mice (Liman, Corey, & Dulac, 1999; Lucas, Ukhanov, Leinders-Zufall, & Zufall, 2003).

- TRPM

TRPM is another TRP subfamily of 8 members named after TRPM1, which is activated with melastatin for what is called TRPM (Inoue et al., 2009). TRPM is classified into 3 groups as follows.

- TRPM1 and TRPM3

TRPM1 is a prognostic marker since it is downregulated in malignant localised melanoma (Duncan et al., 1998), while as a chemically activated nonselective cation channel (NSCC), TRPM3 is expressed in different splice variants known as TRPM3α1–5 (Oberwinkler, Lis, Giehl, Flockerzi, & Philipp, 2005). Among them, TRPM3α1 is a monovalent selective ion channel, whereas TRPM3α2 is a divalent selective ion channel. However, both TRPM3α1 and TRPM3α2 are constitutively active and inhibited by Mg^{2+} (Oberwinkler et al., 2005). Physiologically, TRPM3 is essential in the kidneys where it regulates Ca^{2+} homeostasis (Grimm, Kraft, Sauerbruch, Schultz, & Harteneck, 2003).

- TRPM4 and TRPM5

TRPM4 and TRPM5 channels are distinctively activated through elevated $[Ca^{2+}]_i$ and considered to be highly monovalent selective (Launay et al., 2002; Ullrich et al., 2005). Heteromeric complexes with TRPM4 and TRPM5 channels control the myogenic vasoconstriction, since both channels exhibit a voltage-dependent deactivation at negative membrane potential (Earley, Waldron, & Brayden, 2004; Nilius et al., 2003). Moreover, TRPM5 is essential in the taste signalling pathway, since TRPM5 KO mice studies have demonstrated a significant absence of the bitter and sweet taste sensations (Y. Zhang et al., 2003).

- TRPM6 and TRPM7

TRPM6 and TRPM7 are characterised by their distinct dual function as ion channels and serine and threonine protein kinase (PK) (Clark et al., 2008; Takezawa et al., 2004). The PK activity is chiefly regarded to the C-terminus of TRPM7 that is attributed to auto-phosphorylation (Takezawa et al., 2004). TRPM6 is constitutively active and implicated in Ca^{2+} and magnesium (Mg^{+2}) homeostasis, given its primary expression in the kidneys and intestine (Voets et al., 2004), TRPM7 is a mechanosensitive cation channel (MSCC) or chemically activated NSCC, if not both, that facilitates anoxia-induced brain cell death as a consequence of accumulated ROS (Aarts et al., 2003).

- TRPM2 and TRPM8

TRPM2 and TRPM8 share approximately 40% of sequence homology and both channels are MSCC and chemically activated NSCC (Inoue et al., 2009; Pedersen et al., 2005). TRPM2 is a cellular redox sensor that exists in two splice variants: the short (i.e., TRPM2S) and the

long (i.e., TRPM2L) which are co-localised in the plasma membrane (W. Zhang et al., 2003). TRPM2L is activated by ADP-ribose, which is released from mitochondria upon OS to induce cell death, while TRPM2S suppresses the OS-induced Ca^{2+} influx by way of TRPM2L (Perraud et al., 2005; W. Zhang et al., 2003). However, TRPM8 is an NSCC first discovered in prostate and represents an androgen-activated cation channel (Lei Zhang & Barritt, 2004). More recently, TRPM8 was found to be highly expressed in sensory neurons and implicated in cold-sensation (Andersson, Nash, & Bevan, 2007). In general, TRPM8 is expressed in both ECs and VSMCs in numerous vascular beds, including rat aorta, mesenteric arteries, femoral arteries, and tail artery (Earley, 2010; H. Y. Kwan et al., 2007). RT-PCR studies have shown showed that TRPM8 is the most expressed TRPM channel in VSMCs (Earley, 2010), while others have demonstrated that TRPM8-inudced vasodilation is partially endothelium-dependent (C. D. Johnson et al., 2009). Menthol and icilin, as TRPM8 agonists induced vasodilation in pre-contracted mesenteric and thoracic aortic arteries (C. D. Johnson et al., 2009; Silva et al., 2015). A previous study conducted by X. R. Liu et al. (2013) indicated showed significant impairment in menthol-induced pulmonary artery vasodilation in pulmonary hypertensive rat model. Such impaired vasodilation was associated with TRPM8 downregulation in pulmonary artery ECs. Another recent study added that topical menthol gel (0.04-8.0%) enhanced skin blood flow through EDHF (Craighead & Alexander, 2016). The co-expression of TRPM8 and TRPV4 channels in the aortic vasculature was concluded as novel Ca^{2+} entry pathways that might control the systemic circulation by way of EDHF (Garland, Plane, Kemp, & Cocks, 1995; X. R. Yang, Lin, McIntosh, & Sham, 2006).

TRPM8 can act through pathways other than TRPV4. For instance, endothelial muscarinic receptors stimulate PLC, an enzyme that hydrolyses membranous PIP2 into IP3 and DAG, from which IP3 can activate TRPV4 and bind to ER's IP3-R to induce stored Ca^{2+} release (Everaerts et al., 2010). However, since TRPM8 is activated by the TRP-domain bound PIP2, upon the activation of muscarinic pathways and TRPV4 later on, TRPM8 might be inhibited, since its cytoplasmic activator, PIP2, is metabolised via PLC activation (B. Liu & Qin, 2005; Rohács, Lopes, Michailidis, & Logothetis, 2005). Previous studies have thus identified lysophosphatidylinositol as an extracellular mediator and an intracellular messenger that affects several ion channels, including BKCa and TRPM8 (D. A. Andersson et al., 2007; Bondarenko et al., 2011a; A. I. Bondarenko, R. Malli, & W. F. Graier, 2011b). Therefore, BKca might form a signalling complex with TRPM8 by taking advantage of

lysophosphatidylinositol, which suggests that TRPM8 and TRPV4 pathways might share BKca as a vasodilatory downstream target in the vasculature (Bondarenko et al., 2011a; Earley et al., 2005).

- TRPML

TRPML is a three-membered subfamily consisting of TRPML-1, TRPML-2, and TRPML-3 and from which TRPML-1 mutation emerges to contribute to a progressive neurodegenerative disorder called mucolipidosis type IV (Pedersen et al., 2005; Sun et al., 2000). Accordingly, all these members are called mucolipins (Ramsey et al., 2006). TRPML-1 regulates endosomal and lysosomal trafficking and thus lysosomal degradation in proteins (LaPlante et al., 2002; LaPlante et al., 2004). TRPML-3 KO studies have furthermore shown the essential role of the channel in hearing and vestibulation, due to its expression in hair cells and stereocilia (H. Xu, Delling, Li, Dong, & Clapham, 2007).

- TRPP

TRPP is a four-membered subfamily consisting of TRPP1, TRPP2, TRPP3 and TRPP5 (Inoue et al., 2009). TRPP2 mutation is implicated in autosomal polycystic kidney disease (APKD), a common genetic condition characterised by the formation of numerous kidney cysts that culminates in kidney failure (Mochizuki, Wu, Hayashi, & Xenophontos, 1996). TRPP1 and TRPP2 form heteromeric complexes of calcium-permeable NSCC which is regulated by fluid flow through renal epithelial primary cilia and thus acts as a Ca^{2+} permeable ion channel (Delmas et al., 2004).

- TRPV

TRPV is a six-membered subfamily whose members are activated through vanilloid molecules such as capsaicin (Inoue et al., 2009). Accordingly, the channels are labelled with "V" and categorised into 2 groups (Inoue et al., 2009), as follows.

    - TRPV1-TRPV4

These 4 members are MSCC and chemically activated NSCC (Inoue et al., 2009; Pedersen et al., 2005). TRPV1 is broadly expressed in the body and thereby implicated in numerous functions, including control of gastrointestinal tract motility and satiety, nociception and thermos-sensation activated at approximately 43°C (Davis et al., 2000; Rosenbaum, Gordon-Shaag, Munari, & Gordon, 2004; X. Wang, Miyares, & Ahern, 2005). By contrast, TRPV2

exhibits approximately 50% homology with TRPV1 and is commonly found in the CNS, myenteric plexus, nodose ganglionm and keratinocytes where it is implicated in modulating the noxious heat sensation threshold activated at approximately 52°C (Caterina, Rosen, Tominaga, Brake, & Julius, 1999; Leffler, Linte, Nau, Reeh, & Babes, 2007). TRPV3 plays an essential role in thermosensation and thermal preferences, and its expression has been shown in keratinocytes and TRPV3 KO mice showing a lack of thermosensation activated at approximately 33°C (Moqrich et al., 2005; Peier et al., 2002). Lastly, TRPV4 initially named VR-OAC when discovered though sequence homology screening of the mammalian genome (Everaerts et al., 2010), is expressed ubiquitously and plays essential roles in endothelium-dependent vasodilation (Sukumaran et al., 2013). It is expressed in the distal convoluted tubule where it regulates the urine osmolality (Tian et al., 2004). Numerous researchers have suggested that TRPV4 is capable of direct and indirect activation through mechanical stimulation or second messengers such as endothelium-derived 5, 6-epoxyeicosatrienoic acid (5', 6'-EET) (Liedtke & Friedman, 2003; Vriens et al., 2005).

- TRPV5 and TRPV6

Both TRPV5 and TRPV6 are constitutively active and have approximately 75% sequence homology (Inoue et al., 2009; Ramsey et al., 2006). Distinguished by their inwardly rectifying current with extremely high Ca^{2+} selectivity due to the negatively charged ring aspartate residue in selectivity controller pores (Pedersen et al., 2005; Voets et al., 2001), both channels are essential in controlling renal Ca^{2+} reabsorption and vitamin D-facilitated calcium absorption in the small intestine (J. Hoenderop et al., 2003; J. G. Hoenderop et al., 2000; Nijenhuis, Hoenderop, Nilius, & Bindels, 2003).

- TRPA1

A single-membered subfamily of distinct 14 ankyrin repeats in the NH_2 terminal (Story et al., 2003), TRPA1 is a MSCC and a chemically activated NSCC which can be activated by organic TRPA1 agonist such as allicin from garlic or allyl isothiocyanate from mustard oil (Inoue et al., 2009; Macpherson et al., 2005). A recent research concluded that TRPA1 is a pivotal mediator for nociception and pain signalling in diabetic neuropathic pain (Eberhardt et al., 2012).

1.5.4. TRP channels' mechanism of action

Several researchers have classified TRP channels' mechanisms of action differently for instance, according to the mechanism of activation (Clapham, 2003; Inoue et al., 2009), and the nature of activator (Ramsey et al., 2006). Classified according to the type of activator, TRP channels are categorised into 4 groups, as follows.

- Receptor activation (i.e., GPCR and PKs)

GPCR-activated PLC hydrolyses membranous phosphatidylinositol (4,5) bisphosphate (PIP2) into DAG and IP3 (Lawler et al., 2001). Consequently, IP3 binds to its corresponding smooth ER's IP3-R to facilitate the release of Ca^{2+} from cellular stores (Murata et al., 2007). When ER Ca^{2+} stores are depleted, SOCs become activate to induce Ca^{2+} influx, as shown in TRPV4/TRPC1 heteromeric channels in the endothelium (Ma, Cheng, Wong, et al., 2011). At the same time, DAG activates PKC, which binds and activates TRPV4 to induce Ca^{2+} influx and thus endothelium-dependent vasodilation (Sonkusare et al., 2014).

- Ligand activation

TRP channels are activated by 4 primary types of agonists: exogenous small molecules, including capsaicin-activated chemosensors, such as TRPV1 (Benham, Davis, & Randall, 2002); lipid metabolites such as 11, 12- EET, which activates TRPV4 to induce vasodilation (Earley et al., 2009); purine nucleotides or their metabolites, if not both, including β-nicotinamide adenine dinucleotide (β-NAD+) and adenine diphosphoribose (ADP-ribose) which activate TRPM2 (W. Zhang et al., 2003); and inorganic ions such as Ca^{2+} (Ramsey et al., 2006), as a previous study concluded, $[Ca^{2+}]i$ directly activates TRPA1 conducted by (Zurborg, Yurgionas, Jira, Caspani, & Heppenstall, 2007).

- Direct activation

TRP channels are activated directly in polymodal fashion via, for instance, temperature variation or mechanical stress (Voets, Talavera, Owsianik, & Nilius, 2005). Such stimulators can indirectly trigger a second messenger that phosphorylates TRP channels, as shown in hypotonically-swollen TRPV4-expressing cells (Alessandri-Haber et al., 2003).

- Store operated

Excessive amplified cellular signalling depletes ER from its cellular Ca^{2+} stores, and thereby stimulates a compensatory TRP channels-induced Ca^{2+} influx through SOCs (Ramsey et al.,

2006). Since the mechanism of SOCs is intertwined with ROCCs, when cellular Ca^{2+} stores are depleted and SOCs are activated, which is in turn associated with ROCC activation in order to maintain the cellular Ca^{2+} homeostasis as shown in TRPV4/TRPC1 heteromeric channels in vascular ECs (Ma, Cheng, Wong, et al., 2011).

However, when classified according to their molecular mechanism of activation, TRP channels are divided into 3 categories as follows.

- Bilayer dependent mechanism

When the plasma membrane is stretched, its curvature increases and allosterically enhances hydrophobic molecule binding (Inoue et al., 2009). Once the plasma membrane is bound with hydrophobic molecules, the net effect of channel opening or closing depends on specific conformational changes and amphiphilic (i.e., amphipathic) molecule binding (Suchyna et al., 2004). By extension, TRP channels blockers bind to the outer region of the channel which is consistent with the inward closure of the (Spassova, Hewavitharana, Xu, Soboloff, & Gill, 2006). TRPC6 is regulated via that mechanism and thus contributes to vascular myogenic tone regulation, as Figure 6 shows (Spassova et al., 2006).

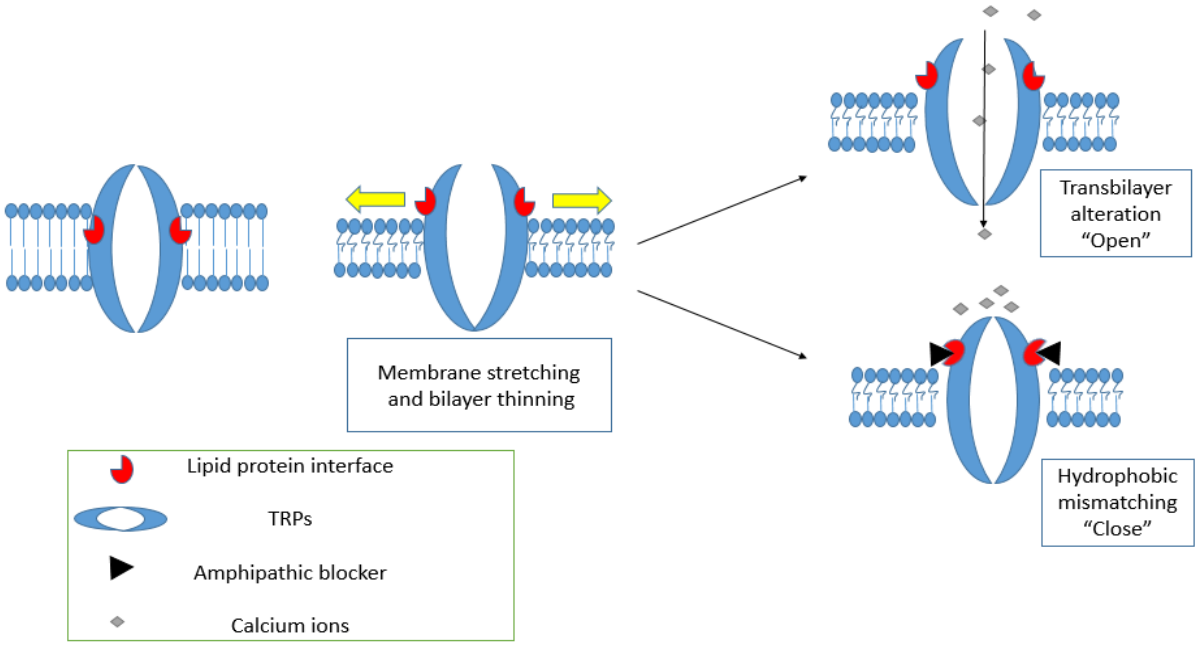

Figure 6. Bilayer-dependent mechanism in TRP channels, in which the stretched membrane affords binding sites for amphiphilic molecules (black triangle) to govern the TRP channels gating as shown when it binds to the outer site and closes the channel; adapted from Inoue et al. (2009).

- Tethered mechanism

Cytoskeletal proteins (e.g., integrin) form supportive structural scaffolds that are interconnected with intracellular components such as G-proteins that construct anchored frameworks with TM proteins (Inoue et al., 2009). Such mechanobiochemical integrity occurs in audio vestibular cells (i.e., tip-links), where head movement stimulates the steriocilia through strength-dependent deflection that culminates the activation of MSCC, as illustrated in Figure 7 (M. Andersson et al., 2007).

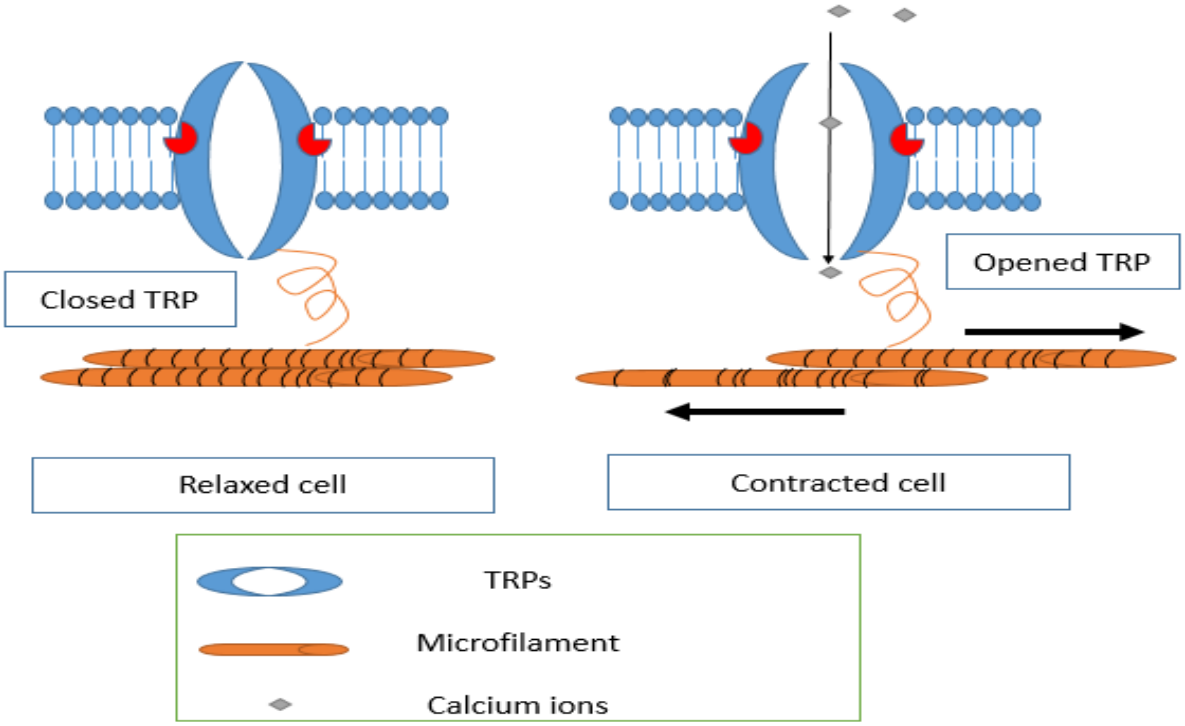

Figure 7. The tethered mechanism involves cytoskeletal modification and thus cellular response in transient receptor potential (TRP) channels; adapted from Inoue et al. (2009).

- Mechanical biochemical conversion

This category exhibits a slower mechanism of activation than the other mechanisms, since it involves the transconversion of mechanical forces into biochemical signals—for example, triggering enzymes and/or second messenger activation through membrane stretching (Inoue et al., 2009). Indeed, such a mechanism was found in TRPV4, which mediates vasodilation through NO and EDHF in response to shear stress, as shown in Figure 8 (Köhler et al., 2006).

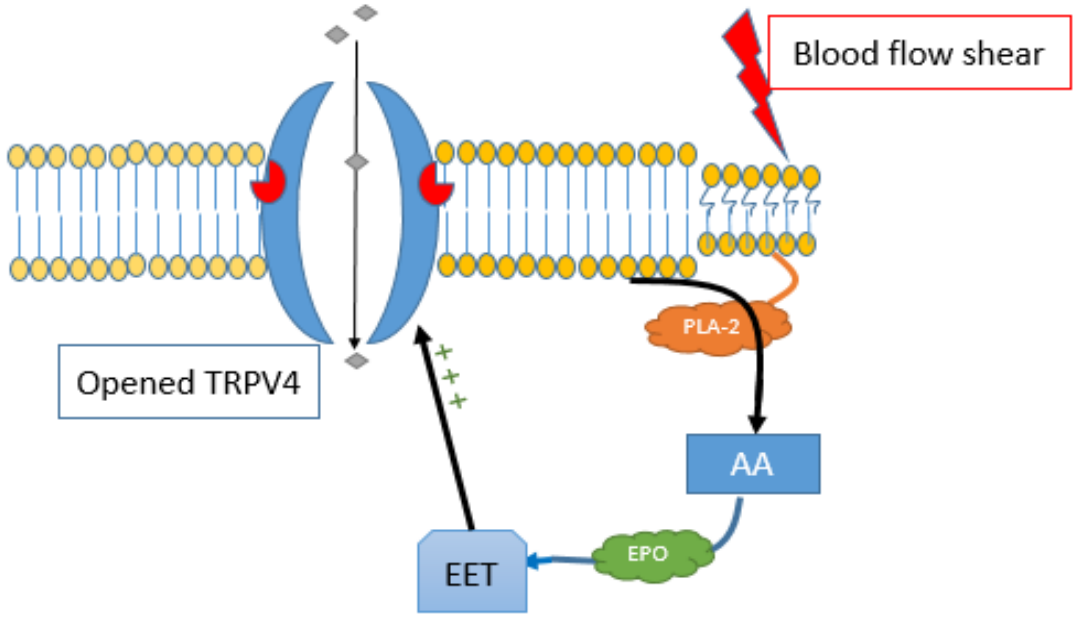

Figure 8. Mechanical biochemical conversion in transient receptor potential (TRP) channels. With mechanically generated second messengers that trigger the synergistic biochemical activation of TRP channels, blood flow shear activates membrane-bound phospholipase-A2 (PLA-2), which generates arachidonic acid (AA) from membrane cholesterol, followed by epoxygenase's (EPO) production of epoxyeicosatrienoic acid (EET), which is a direct TRPV4 activator; adapted from Inoue et al. (2009).

Recent studies have aimed to decipher the diabetes complications through investigating the molecular pathophysiology, one of which concluded that TRPA1 might play a major role in mediating diabetes neuropathic pain through methylglyoxal (MGO) (Eberhardt et al., 2012). Moreover, MGO induced significant endothelium impairment through inhibiting eNOS phosphorylation (A. Dhar et al., 2010). Since MGO effect on endothelium-dependent vasodilation and endothelial TRPV4 will be covered in this research. Therefore, introducing MGO into the next section will provide an insight toward its role in mediating diabetes complications.

1.6. MGO and diabetes

Diabetes mellitus is associated with chronic hyperglycaemia, in which fasting blood glucose concentration exceeds 7mmol/L (125mg/dl) (Sheader, Benson, & Best, 2001). Approximately 0.5% of glycolytic pathways generate electrophilic ROS such as MGO (Uchida, 2000). MGO generates AGE by reacting with various cellular and interstitial molecules such as proteins and phospholipids (Uchida, 2000). As a result of reacting with cellular molecules, MGO becomes trapped intracellularly and induces OS (Kalapos, 2013), which in turn disrupts cellular membrane integrity in order to facilitate MGO leakage into circulation (Eberhardt et al., 2012; Kalapos, 2013; Sheader et al., 2001). At the same time, glycolysis-derived MGO interacts with cellular proteins and nucleic acid and hence accelerates AGE production and β-cells cytotoxicity (Sheader et al., 2001). AGE act as ligands for their corresponding receptors, RAGE, which are multiligand receptors of the immunoglobulin superfamily expressed on different cell types, including ECs, VSMCs, and monocytes (Schmidt, Du Yan, Wautier, & Stern, 1999). Hyperglycaemia induces RAGE expression, which becomes normalised through GLO1 overexpression and thus reveals the contribution of MGO in inducing RAGE expression (D. Yao & Brownlee, 2010).

MGO-derived hydroimidazolone is an AGE specifically recognised by RAGE that causes long-term diabetic complications by enhancing numerous signalling cascades, including c-Jun N-terminal kinase (JNK) phosphorylation (p-JNK), which is associated with insulin resistance, pancreatic β-cells apoptosis, and atherosclerosis (Bennett, Satoh, & Lewis, 2003; Harja et al., 2008; Xue et al., 2014). Accordingly, MGO cytotoxicity exacerbates hyperglycaemia and DM complications (Sheader et al., 2001). Physiological human plasma MGO concentration is approximately 150nM and increases to fourfold in T2DM (Nicolay et al., 2006).

However, MGO has not been significantly correlated to blood glucose concentration for 2 technical reasons: the limited capacity to accurately measure total MGO, which is highly reactive and can damage sampled proteins or DNA, and the heterogeneity of participants' backgrounds (Kalapos, 2013).

1.6.1. MGO sources

The 4 primary sources of MGO can be summarised as $MGO_{sources} = MGO_{carbohydrates} + MGO_{lipids} + MGO_{proteins} + MGO_{exogenous}$ (Shamsaldeen et al., 2016). As shown in Figure 9, MGO is

biosynthesised from 3 main integrated metabolic pathways: carbohydrates, lipid pathways, protein metabolism, and exogenous MGO.

- Carbohydrates

Reducing sugars react with proteins' amino groups to generate Schiff's bases that are structurally rearranged to form Amadori products, which are then subjected to a series of reactions to generate AGE (Uchida, 2000). Accordingly, MGO is generated primarily via phosphorylating glycolysis, which involves triose-phosphate enzymatic metabolism, the pentose phosphate shunt, sorbitol pathways such as xylitol metabolism, and glucoxidation (Kalapos, 2013). More specifically, triose-phosphate accumulation is involved in diabetic nephropathy, which emphasises the involvement of carbohydrate-generated MGO pathways in complications in diabetes. The pathway can also be inhibited by thiamine, as Figure 9 illustrates (Hammes et al., 2003; Jadidi, Karachalias, Ahmed, Battah, & Thornalley, 2003).

- Lipid pathways

Lipid peroxidation of polyunsaturated fatty acids yields short hydrocarbon molecules of highly reactive aldehydes, such as ketoaldehydes, from which MGO is generated (Kalapos, 2013). In particular, MGO is generated from the non-enzymatic and enzymatic metabolism of acetoacetate and acetone intermediates, respectively (Kalapos, 2013; Uchida, 2000). Triose-phosphate is a common intermediate metabolite found in both lipolysis and glycolysis (Kalapos, 2013), whereas acetoacetate is a major ketone body (KB) elevated in T2DM patients' plasma (Mahendran et al., 2013) Previous studies have found that diabetes is associated with increased lipolysis, the suppression of which improves insulin sensitivity and glucose use (Arner & Langin, 2014; Lim, Hollingsworth, Smith, Thelwall, & Taylor, 2011). Moreover, plasma isopropyl alcohol (IP) is significantly increased (5mg/dl) in diabetic patients with ketoacidosis (Jones & Summers, 2000). Alcohol dehydrogenase metabolises acetone into IP via the reduction of NAD^+ reduction into NADH. Therefore, as Figure 9 shows, diabetes-accelerated lipolysis contributes to MGO elevation which can exacerbate the diabetes complications (Jones & Summers, 2000; Laffel, 1999).

- Protein metabolism

Numerous researchers revealed the susceptibility of tyrosine-, serine-, threonine- and glycine-rich proteins to oxidation (Kalapos, 2013; Uchida, 2000). Those aminoacid residues are enzymatically converted to MGO through acetone and aminoacetone intermediates (Kalapos,

2013; Uchida, 2000). In particular, aminoacetone intermediates are converted to MGO by semi-carbazide sensitive amine oxidase (SSAO), an enzyme that is elevated in diabetic patients' plasma (Kalapos, 2013). A previous study with STZ-diabetic rats showed that protein catabolism increases by approximately 50% (Mitch et al., 1999), which is attributed to insulin resistance and increased glucocorticoids production in the STZ-diabetic rats as illustrated in Figure 9 (Mitch et al., 1999).

- Exogenous MGO

Processed sugar, protein, and fat-rich food, in addition to tobacco are the main exogenous sources of MGO (Uribarri et al., 2007). According to Banning (2005), coffee and whiskeys are also MGO-containing beverages. The average daily consumption of AGE is 16000kU AGE, which becomes exaggerated through processing at high temperatures (Goldberg et al., 2004). For example, the AGE content of oven-fried chicken breast is 900kU/g, whereas that of boiled chicken breast is 100kU/g (Goldberg et al., 2004). When reduced sugars such as glucose interact with proteins' free amino groups (i.e., Maillard reaction), N-substituted glycosylamine emerges (Martins, Jongen, & van Boekel, 2001). In the presence of water, N-substituted glycosylamine undergoes Amadori rearrangement to yield the Amadori product 1-amino-1-deoxy-2-ketose (Martins et al., 2001). The rearranged Amadori product is then degraded through 2,3 enolisation to form numerous carbonyl compounds, including those of acetol, pyruvaldehyde, and diacetyl (Martins et al., 2001), which interact with cellular amino acids to form aldehydes and α-aminoketones (Martins et al., 2001). Previous studies have found that Maillard reaction products are significantly increased in diabetics' skin collagen as N^6-carboxymethyllysine (CML), fructoselysine (FL), and pentosidine all of which are associated with accelerated aging (Dyer et al., 1993). Additionally, CML is significantly elevated in diabetic plasma, which becomes exacerbated when purely prepared AGE beverages are ingested (Jones & Summers, 2000). In another study, CML elevation was associated with eNOS downregulation and dysfunction, in addition to the stimulation of the release of vascular cells' adhesion molecules (VCAM-1), which are all together contribute to vascular dysfunction (Uribarri et al., 2007).

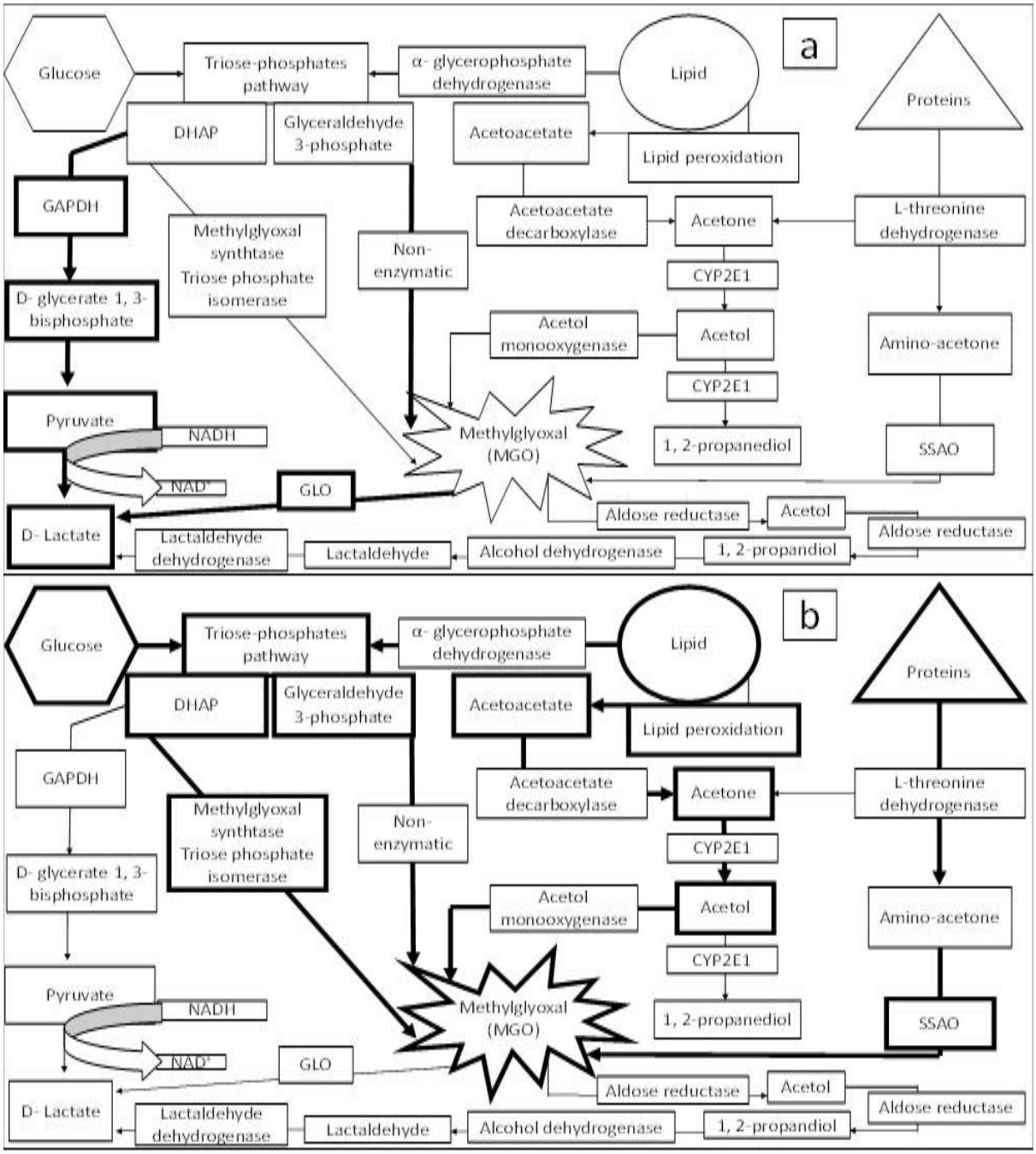

Figure 9. Endogenous sources of methylglyoxal (MGO) from glucose, lipid, and protein metabolism. (A) The normal condition shows low MGO production from glycolysis, lipolysis, or proteolysis with major sources represented in bold arrows. (B) Diabetes is associated with increased MGO production from hyperglycaemia, accelerated lipolysis, and proteolysis, represented with thick borders and bold arrows, which are accompanied by compromised glyoxalase activity; DHAP = Dihydroxyacetone phosphate, GAPDH = Glyceraldehyde 3-phosphate dehydrogenase, SSAO = Semicarbazide-sensitive amino oxidase (Shamsaldeen et al., 2016).

1.6.2. MGO metabolism

MGO is metabolised through two enzymatic systems: the glyoxalase (GLO) system consisting of glyoxalase 1 and 2 (GLO1 and GLO2, respectively) and, to a lesser extent, the aldose reductase system (Kalapos, 2013). Both systems are GSH-dependent. The GLO system is the major metabolic pathway and involves GLO-1, the most MGO-detoxifying enzyme that converts MGO to D-lactate (Bierhaus et al., 2012; Kalapos, 2013). Since the sorbitol pathway contributes to 11% of glucose metabolism, bi-modal aldose reductase acts as aldehyde reductase instead of ketone reductase and thereby preferentially produces acetol (Kalapos, 2013). Accordingly, CYP2E1-converted acetol is further converted to MGO, which catalyses a futile cycle that depletes intracellular GSH and elevates acetol in diabetic plasma (Kalapos, 2013).

1.6.3. MGO and insulin

Insulin resistance is a complex condition in which physiologically normal insulin concentration becomes insufficient to mediate glucose uptake and usage due to insulin signalling disruption, which releases more insulin to meet the demand of tissues (S. Jia, H., Ross, & Wu, 2006; X. Jia & Wu, 2007). In their study on skeletal muscle L8 cells, 3T3-L1 adipocytes, and H4-II-E hepatocytes, S. Jia et al. (2006) showed that MGO compromises insulin function by targeting insulin β-chain arginine residues through adding extra 126Da to the insulin molecule. Furthermore, another study conducted by X. Jia and Wu (2007) on 3T3-L1 adipocytes revealed that MGO suppresses IRS-1 phosphorylation and PI3K.

1.6.4. MGO and diabetes endothelial dysfunction

Several authors have correlated MGO elevation to vascular dysfunction and end organ damage, including that of nephropathy (Chang, Wang, & Wu, 2005). Vascular dysfunction is a common complication in DM that often culminates in stroke and myocardial infarction (A. Dhar et al., 2010; Ruiter, Van Golde, Schaper, Stehouwer, & Huijberts, 2012). MGO inhibits eNOS activation by inhibiting the phosphorylation of serine 1177 residue, thereby prevents NO release and inducing endothelial dysfunction (A. Dhar et al., 2010). An earlier study on rat aortic smooth muscle cells (ASMCs) showed that MGO-induced vascular dysfunction was attributed to NO and hydrogen peroxide (H_2O_2) generation and hence induced $ONOO^-$ formation, which compromises NO bioavailability (Chang et al., 2005). The overexpression of GLO-1 in STZ-diabetic rats moreover showed improved vascular function with MGO and

AGE reduction (Ruiter et al., 2012). However, treating ECs with MGO scavengers such as diacetyl cysteine restored vascular function (A. Dhar et al., 2010).

MGO preferentially targets amino acids such as lysine to form Nε-carboxyethyl lysine (CEL) and the MGO-derived lysine–lysine dimer (MOLD), arginine to form 5-methylimidazolone, tetra-hydropyrimidine, and argpyrimidine, as well as a sulfhydryl group containing cysteine, which forms stabilised S-lactyl cysteine via keto-enol tautomerism to cause both CEL and MOLD elevation in diabetic serum (Uchida, 2000). In their immunohistochemical study, Oya et al. (1999) observed significant elevation in argpyrimidine in diabetic patients' arteries, which stressed the implications of MGO in arterial injury as a complication of diabetes mellitus.

In addition to those vascular complications, the lifespan of erythrocytes (RBC) is reduced in diabetes. As Nicolay et al. (2006) have shown, MGO concentration is significantly increased in diabetics' RBC, putatively due to rapid GLO-dependent metabolism in the RBC that shifts the MGO gradient from the plasma to the RBC (Kalapos, 2013). Moreover, MGO accumulation in the RBC induces eryptosis, RBC suicidal death characterised by membrane blistering, and cell membrane phospholipid tangling accompanied with phosphatidylserine exposure that triggers cell apoptosis, which culminates in diabetic anaemia (Föller, Huber, & Lang, 2008).

1.7. Aims and objectives

Recent studies have shown that TRPV4 is downregulated in retinal microvascular endothelium (Monaghan et al., 2015) and that endothelial TRPV4 was downregulated in STZ-diabetic rats' mesenteric arteries (Ma et al., 2013). TRPV4 is coupled and functionally regulated by CAV-1 (Saliez et al., 2008), which was shown to be coupled with eNOS, and both were downregulated in STZ-diabetic rats' kidneys and bovine aortic ECs; accordingly, such downregulation was reversed by way of insulin treatment (Komers et al., 2006; H. Wang et al., 2009). In response to those findings, the aim of the present study was to investigate the influence of diabetes on the endothelium, with a chief focus on TRPV4 function, by using STZ-diabetic rats' aortic and mesenteric arteries. The experimental designs were devised according to three primary goals: 1) to investigate the effect of diabetes on muscarinic, TRPV4, and TRPM8 function in aortic ECs using appropriate agonists and antagonists, as well as to study downstream targets involved in vasodilation induced by muscarinic, TRPV4, and TRPM8 pathways; 2) to explore serum markers that might be associated with hyperglycaemia and diabetic endothelial dysfunction through enzyme-linked

immunosorbent assay (ELISA) studies; and 3) to apply a selected marker—namely, MGO—to nondiabetic aortic rings and ECs in order to test the hypothesis that MGO contributes to endothelial dysfunction in diabetes.

The objectives of this study were thus the following:

1. To examine the effect of a muscarinic agonist (i.e., carbachol), TRPV4 agonists (i.e., RN-1747 and 4-αPDD), and a TRPM8 agonist (i.e., icilin) on pre-contracted thoracic aortic rings in the presence and absence of a TRPV4 antagonist (i.e., HC067047) and TRPM8 antagonist (i.e., AMTB);
2. To investigate the involvement of NOS and BKca in the signalling cascade of muscarinic, TRPV4, and TRPM8 pathways in naïve aortic rings;
3. To investigate the endothelium dependence of muscarinic, TRPV4-, and TRPM8-induced vasodilation by removing (i.e., denuding) the endothelium in naïve aortic rings;
4. To measure blood glucose concentration, body weight, serum MGO, and oxidised low-density lipoprotein (ox-LDL) with an ELISA analysis of STZ-diabetic and control rats;
5. To investigate the influence of STZ-induced diabetes on muscarinic, TRPV4, and TRPM8-induced vasodilation in aortic rings and further examine any vascular dysfunction in mesenteric arteries (i.e., muscarinic and TRPV4), given the findings of a previous study with eNOS KO mice that revealed that NO plays a major role in mediating endothelium-dependent vasodilation in the aorta but not in mesenteric arteries (Chataigneau et al., 1999). Along similar lines, it also sought to describe TRPV4 function in primary aortic ECs through fura-2 Ca^{2+} imaging and laser scanning confocal microscopy (LSCM);
6. To investigate the effect of MGO diabetic level on nondiabetic aortic rings, primary aortic ECs, and ASMCs to provide evidence of MGO implications in endothelial dysfunction in diabetes;
7. To examine the effect of L-arginine on counteracting MGO diabetic-level effects, including (i) MGO-induced vascular dysfunction through organ bath experiments on pre-contracted naïve aortic rings treated with a carbachol concentration response curve, (ii) MGO-suppressed iNOS expression and total NO_2 production in primary ASMCs treated with IFN-γ and LPS with sodium dodecyl disulphate (SDS)–polyacrylamide gel electrophoresis (PAGE) Western blotting, and (iii) MGO-

suppressed TRPV4-mediated [Ca2+]i in naïve primary ECs treated with TRPV4 agonist (4-αPDD) with fura-2 Ca^{2+} imaging.

8. To identify the effect of insulin treatment on TRPV4 function in STZ-diabetic ECs through fura-2 Ca^{2+} imaging and on the expression of TRPV4, CAV-1, and eNOS in primary aortic ECs through LSCM; and
9. To investigate the acute effect of MGO on vascular tone through organ bath and FlexStation studies.

Chapter 2: General methodology:

2.1. Animals and environmental conditions

Male Wistar rats (Charles River) weighing 350–450g at baseline were housed in pairs in standard cages (Tecniplast 2000P) with sawdust (Datesand grade 7 substrate) and shredded paper wool bedding and provided with freely available water and food (5LF2 10% protein LabDiet). The room with the cages had a constant temperature of 22 ± 2 °C and a 12 hours light–dark cycle (lights on from 7:00 to 19:00). All tests were conducted under the light phase of that cycle.

All experiments were approved by the institutional Animal Welfare and Ethics Review Committee, conducted in accordance with guidelines established by the Animals (Scientific Procedures) Act 1986 and European directive 2010/63/EU, and carried out under project licence PPL70/7732.

2.2. Diabetes induction

Diabetes inducers (i.e., diabetogenics) are experimental toxins, including alloxan and STZ (Lenzen, 2008). Despite resembling T1DM plasma insulin and blood glucose concentrations, diabetogenics induce β-cells necrosis, which is associated with initial insulin release, whereas in T1DM, β-cells dysfunction is attributed primarily to inflammatory and apoptotic factors such as interferon-γ (IFN-γ) and tumour necrosis factor-α (TNF-α) (Lenzen, 2008; Sheader et al., 2001). Numerous differences shift favour toward STZ, since alloxan is less stable at physiological conditions (pH 7.4, 37°C), in which it decomposes into alloxanic acid with a 90- seconds half-life ($t_{1/2}$), whereas STZ is more stable with a half-life of approximately 1 hour ($t_{1/2}$) (Szkudelski, 2001). Moreover, alloxan is highly hydrophilic and therefore less stable in aqueous solutions, in which it decomposes into another lipophilic derivative, butylalloxan, which distributes throughout a wide range of tissues' cellular membranes and has been shown to accumulate in the tubular cells of kidneys, where in culminates in nephrotoxicity before inducing diabetes (Lenzen, 2008). By contrast, STZ is highly stable in aqueous media and induces diabetes according to its selective N-methyl-N-nitrosourea (MNU) moiety, which encourages STZ to act on only GLUT-2-expressing tissues such as pancreatic β-cells (Elsner, Guldbakke, Tiedge, Munday, & Lenzen, 2000). Alloxan induces diabetes by generating reactive oxygen species (ROS), which can be abolished if alloxan is kept oxidised (e.g., with dialuric acid), in which case ROS generation is omitted and thus unavailable to induce diabetes (Lenzen, 2008). Conversely, STZ induces diabetes through its MNU-coupled hexose C-2 (Lenzen, 2008). STZ is less lipophilic and hence less invasive than

alloxan and thus more dependent on GLUT-2, which facilitates STZ endocytosis into β-cells, where it alkylates O^6-guanine DNA to induce cell necrosis (Elsner et al., 2000). STZ moreover induces nephrotoxicity and hepatotoxicity, since the kidneys and liver express GLUT-2 transporters (Schnedl, Ferber, Johnson, & Newgard, 1994). In sum, STZ-induced diabetes is attributed primarily to three targeted cellular components, starting with nicotine adenine dinucleotide (NAD^+) depletion, which leads to impaired mitochondrial enzymatic function, mitochondrial genome damage, and β-cell dysfunction associated with inhibited gene expression, all to yield a net response of inhibited insulin biosynthesis and secretion, as well as impaired glucose metabolism (Akbarzadeh et al., 2007; Szkudelski, 2001).

2.2.1. STZ-induced diabetes

Male Charles River Wistar rats (approximately 350-450g) were injected with 65mg/kg STZ intraperitoneally (i.p., dose volume 10ml/kg). STZ-injected rats were compared to either naïve rats (non-injected) or controls, if not both, the latter of which were injected with 20mM of citrate buffer (pH 4.0–4.5, dose volume 10 m/kg). STZ was dissolved in pH 4.5 citrate buffer to a concentration of 6.5mg/ml (dose volume 10ml/kg for a dose of 65mg/kg i.p). The solution was kept in 4°C for 30 minutes and injected i.p. within 30–60 minutes after being prepared to enhance the efficacy and safety of dried STZ powder dissolved in sodium citrate solution. The period used (30–60 minutes) was based on the equilibrium between STZ anomers α and β, of which the highly toxic anomer, α, predominantly existed in the freshly prepared STZ. Therefore, anomer-equilibrated STZ solution was less toxic and more efficacious since the degradation rat of citrate-buffered STZ solution was 1%/day (de la Garza-Rodea, Knaän-Shanzer, den Hartigh, Verhaegen, & van Bekkum, 2010).
Once injected, all STZ rats had a choice of 2% sucrose water or unmodified drinking water in their home cages for 48 hours in order to minimise the risk of hypoglycaemia. After 48 hours all STZ rats were supplied with extra unmodified drinking water to compensate for diabetic polydipsia. Home cages were changed more frequently due to polyuria. After injection, food was also changed from 10% protein (LabDiet 5LF2, EURodent Diet 10%) to a protein-rich diet (22% protein, LabDiet 5LF5, EURodent Diet 14%) in order to compensate for possible diabetes-induced protein loss. Blood glucose was measured before i.p. injection (i.e., baseline measurement) 2–7 days after i.p. injection as a means to confirm hyperglycaemia and lastly on the day of euthanasia (i.e., terminal measurement). Blood glucose was measured from a single drop of tail vein blood, obtained by a needle prick of conscious rats, using an Accu-Chek blood glucose monitor (Roche). Rats with blood glucose concentrations greater

than 16mmol/L (≥ 300mg/dl) were considered to be diabetic (i.e., hyperglycaemic) and included in the diabetes study. All experiments were powered to take into consideration the animals' loss of 10% weight through the provision of sucrose water, a high-protein diet, and frequent home cage changes.

2.3. Tissue determination, isolation and preparation

All rats were euthanized according to the Schedule 1 procedure by CO_2 asphyxiation, followed by cervical dislocation. Their thoracic aortas or mesenteric arteries, if not both, were rapidly removed and dissected into an oxygenated Krebs–Henseleit physiological solution (i.e., Krebs solution).

2.3.1. Aortic rings and organ bath setup

Aortic rings were isolated in an organ bath to facilitate the examination of the whole tissue isometric response following numerous treatments and conditions. A freshly isolated aorta was cut into approximately 2–3mm-wide rings after the surrounding connective tissue was removed. Each aortic ring was threaded by superior and inferior loops, so that the inferior loop was attached to a fixed hook and kept suspended in a Bennett isolated tissue vessel organ bath of 95% O_2/5% CO_2 Krebs solution (pH 7.4) at 37 ± 1°C. The superior loop was attached by a long terminal thread to the FT-100 force transducer under 1 g of tension force immediately after LabScribe software (iWORKS, version 1.817) was calibrated with a standard 1 g weight (measurement scale 0.25–2 g). An FT-100 force transducer transmitted the tissue responses to an iWORKS amplifier, which generated electrical signals to be recorded with LabScribe.

For the purposes of viability, aortic rings were initially contracted with 123-mM potassium chloride Krebs solution (i.e., high-potassium Krebs) and relaxed through continuous washes with normal Krebs solution (Table 3) until reaching the baseline of approximately 1 g. Thereafter, aortic rings were left to equilibrate for 60–90 minutes with approximately 15-minutes washing intervals.

Aortic rings were rubbed with a cotton thread to mechanically remove the endothelium. Afterward, the rings were contracted with noradrenaline (NA) (300nM) followed by carbachol cumulative concentration response curve (CRC, 30nM–300μM) to ensure the removal of the endothelium, since muscarinic-induced vasodilation is endothelium dependent (Furchgott & Zawadzki, 1980).

2.3.2. Mesenteric artery and myography

Mesenteric arteries were examined in a four-channel myograph (DMT) to assess findings of aortic rings and to investigate whether pharmacological responses to the applied treatments differed. This procedure was based on a previous eNOS KO study with mice that revealed that NO plays a major role in mediating endothelium-dependent vasodilation in the aorta but not in mesenteric arteries (Chataigneau et al., 1999). Mesenteric arteries were kept in myograph wells, where they were stretched and calibrated in cooperation with LabChart 7 software. With a DMT 2000 stereomicroscope (magnification 4–40×), mesenteric arteries were gently cleaned and isolated. Mesentery was placed on a black background tray with the duodenum upward, thereby endowing the whole tissue with a C shape in order to position the vein toward the objective lens of the microscope, with the artery downward and proximal to the tray surface. Blood vessels were carefully cleaned and arteries isolated and kept in physiological solution. Mesenteric arteries were threaded with stainless steel wire 40-µm thick and stretched laterally and carefully, while the tension force was observed with LabChart software for calibration and zeroing purposes. Mesenteric arteries were treated with high-potassium Krebs solution to examine their viability by inducing VGCC-activated contraction. Once contraction plateaued, tissues were washed with normal Krebs solution to induce complete relaxation with zero contraction. Afterward, tissues were equilibrated for approximately 30 minutes before treatment.

To examine the extent of vasoconstriction, aortic rings were treated with freshly prepared NA EC_{80} (300nM) mixed with ascorbic acid, and the contraction force was measured. The extent of vasoconstriction was determined with iWORKS version 1.817. Each value of the CRC was estimated regarding the baseline value and the value of the trace before adding the vasoconstrictor, which was approximately 1 g in aortic rings and 0mN in mesenteric arteries. The maximum contraction force was calculated as 100%, and the other contraction forces were normalised to the maximum contraction force as a percentage of maximum contraction considering the baseline to be 0%.

To measure the extent of vasodilation, each value of the CRC was estimated regarding the baseline value and value of the trace before adding NA EC_{80}, which was approximately 1 g in aortic rings and 0mN in mesenteric arteries. The NA EC_{80}-induced contraction was normalised as 0% vasodilation. Each vasodilatory response was normalised as a percentage of the NA EC_{80}-induced contraction, after which estimated values were subtracted from 0. The maximum vasodilation that reached 0 g tension force was -100% (Figure 10).

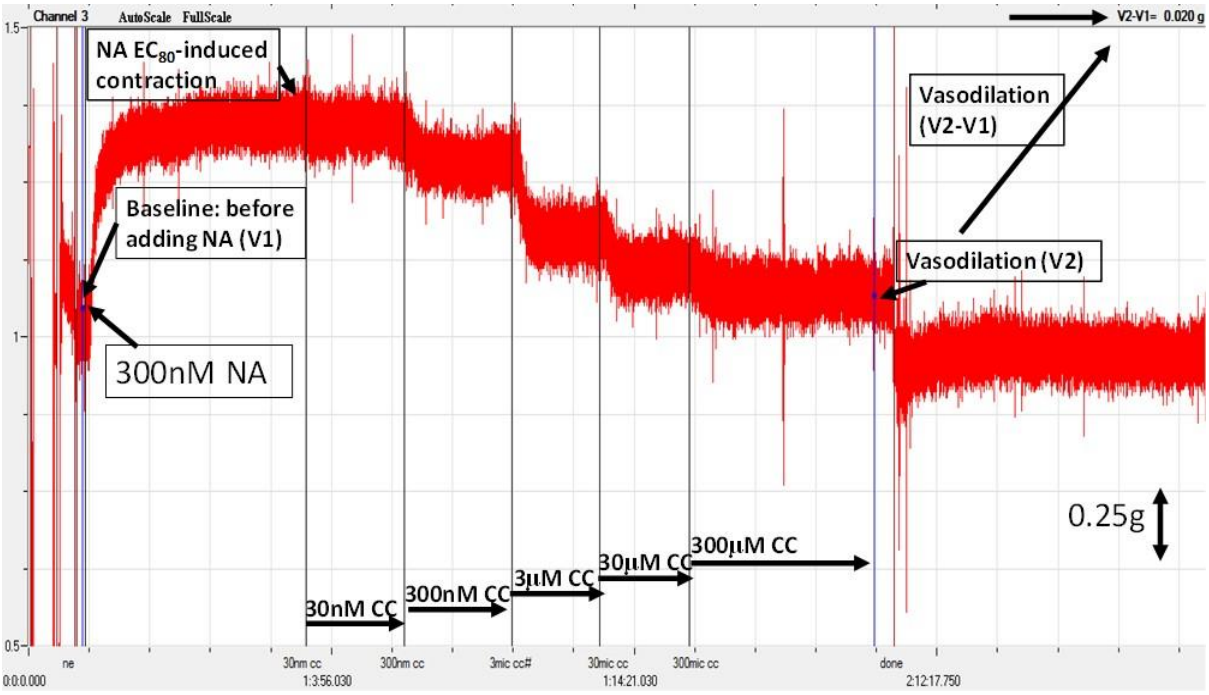

Figure 10. Representative trace of concentration response curve of carbachol (CC) after pre-contracting the aortic ring with noradrenaline (NA).

Table 2 Krebs–Henseleit and high-potassium Krebs solutions components dissolved in 1 L of distilled water

Chemical	**Supplier**	**Concentration added (g/L)**	**Molarity (M)**
Sodium chloride (NaCl) *For high K^+ Krebs*	Fisher Scientific, UK	6.9 **0**	118mM **0mM**
Potassium chloride (KCl) *For high K^+ Krebs*	Fisher Scientific, UK	0.36 **9.2**	4.8mM **123mM**
Potassium dihydrogen phosphate (KH_2PO_4)	Fisher Scientific, UK	0.16	1.2mM
Magnesium sulphate ($MgSO_4$)	Fisher Scientific, UK	0.29	2.4mM
Sodium hydrogen carbonate ($NaHCO_3$)	Fisher Scientific, UK	2.1	25mM
Calcium chloride ($CaCl_2$)	Fisher Scientific, UK	0.74	6.7mM
Glucose ($C_6H_{12}O_6$)	Fisher Scientific, UK	2	10mM

2.3.3. Estimating noradrenaline (NA) concentration required for 80% of the maximum vasoconstriction (EC_{80})

Naïve rats' arteries (i.e., aorta and mesenteric) were treated with the NA CRC to induce vasoconstriction through final bath concentrations (10nM–10µM). Accordingly, EC_{80} was determined in terms of a nonlinear regression curve for robust fit using GraphPad Prism 5.0. Tissues were washed with normal Krebs solution for approximately 30–45 minutes with 5-minutes washing intervals before the next experiment commenced.

All drugs were dissolved in a suitable vehicle and prepared according to the following equation:

$$\text{Drug weight (mg)} \;/\; (\text{M.wt})/X \qquad (1)$$

X= shift-log y of the stock's e^{-y}

For example, the NA stock solution of 100mM was prepared by dissolving 8.3mg of NA in [83mg/(337g/mol/10)] = 2.4 ml of distilled water, which was the appropriate volume for estimating the required stock solution of NA. However, MGO was prepared by dissolving 180 µl of MGO in 10 ml distilled water to yield 100mM. All stock solutions were prepared according to Equation (1) by being dissolved in the appropriate solvent (Table 3) and stored as 200 µl aliquots at -20°C, except MGO, which was stored at 2–8°C.

2.3.4. Serum isolation

Thoracic aortic blood was collected in a glass beaker, samples were left to coagulate at room temperature (25°C), and noncoagulated supernatant was collected in Eppendorf tubes. Afterward, samples were centrifuged at 13,000 rpm for 5 minutes at 25°C. Thereafter, the supernatant (i.e., serum) was collected in a new Eppendorf tube and stored immediately at -80°C to be analysed with ELISA and bicinchoninic acid (BCA) assay for total protein count (Section 2.8).

2.4. Isolation of primary aortic ECs

Primary aortic ECs were cultured to examine the expression level and localisation of TRPV4, eNOS, and CAV-1 under LSCM, while primary ECs were studied with a fura-2 Ca^{2+} imaging fluorescence microscope. All experiments were conducted to support tissue findings at the cellular level. Rat aortas were freshly isolated and plunged into sterile Hank's balanced salt solution (HBSS), per the recommendations of Battle, Arnal, Challah, and Michel (1994), and

primary cell isolation was performed in a laminar air flow cabinet. Aortas were transferred aseptically into another sterile tube containing sterile HBSS, a step which was repeated five times to ensure that all blood was washed from the aortas. Aortas were cleaned of connective tissue using autoclaved forceps and scissors and then cut into small rings 2–3mm in length (Battle et al., 1994; Ding, Gonick, & Vaziri, 2000). Afterward, aortic rings were transferred into a sterile tube containing warm medium 199 (10 ml) containing collagenase and agitated for 90 minutes at 37°C (Battle et al., 1994; Ding et al., 2000). The tube was returned to the laminar air flow cabinet and mixed with 1–2 ml new-born calf serum to halt collagenase activity (Ding et al., 2000). A wide mouth pipette was used to forcibly flush the aortic rings in order to dislodge any possible loosely hanging ECs (Ding et al., 2000). Aortic rings were then transferred to a new sterile falcon tube and mixed with sterile HBSS for ASMC isolation (Section 2.4). The medium 199 containing new-born calf serum, collagenase, and ECs was then centrifuged for 5 -minutes at 10000 rpm at 25°C (Battle et al., 1994). The supernatant was discarded, and the small pellet containing ECs was resuspended in 3 ml of collagenase-free media 199 (Ding et al., 2000). The resuspended pellet was then plated in a collagen-coated t-25 flask later left in the incubator (95% O_2, 37°C) for 25–30 minutes (Dolman, Drndarski, Abbott, & Rattray, 2004). Primary aortic ECs were expected to attach more quickly than ASMCs or fibroblasts (Battle et al., 1994). Accordingly, the flask was examined at approximately 5- minutes intervals under a light microscope to ensure ECs adherence, since the recommended initial adhering incubation is approximately 25–30 minutes (Dolman et al., 2004). The medium was then aspirated, and recently adhered cells were washed twice with HBSS to remove any possible impurities, debris, or ASMCs (Battle et al., 1994). The flask was then added with complete Dulbecco's modified Eagle's medium (DMEM, 3 ml) containing horse serum (15%) and foetal calf serum (4%), ECs growth factor 75µg/ml, and heparin powder (0.005% w/v) in addition to streptomycin-penicillin 1× (Battle et al., 1994; Ding et al., 2000). After 3 days, half of the medium (approximately 1.5 ml) was changed and left for another 3 days. Within 5 days, clusters of ECs emerged, as illustrated in Figure 11.

Cell culture flasks were next coated with collagen. Briefly, rat tail collagen (type I, 10 mg) was dissolved in glacial acetic acid (10 ml) in small autoclaved glass bottles (final volume of 0.1 g%). The solution was then gently mixed with 1.1 ml chloroform (1% v/v), which settled at the bottom, and the autoclaved glass bottle was subjected to U/V light for 25 minutes before being left in 4°C overnight. Afterward, the collagen solution was transferred to a new small autoclaved glass bottle without the chloroform, which was left at the bottom to be

discarded. The required amount of collagen coat was 4 ml for the t-25 flask; thus, 0.7 ml of collagen stock was added to the HBSS (3.3 ml). The collagen coat was then added to the t-25 flask and subjected to U/V light before being transferred to the incubator (95% O_2, 37°C) overnight. Thereafter, the collagen coat was aseptically aspirated, and the flask was washed twice with HBSS before cells were added (Sitterley, 2008a).

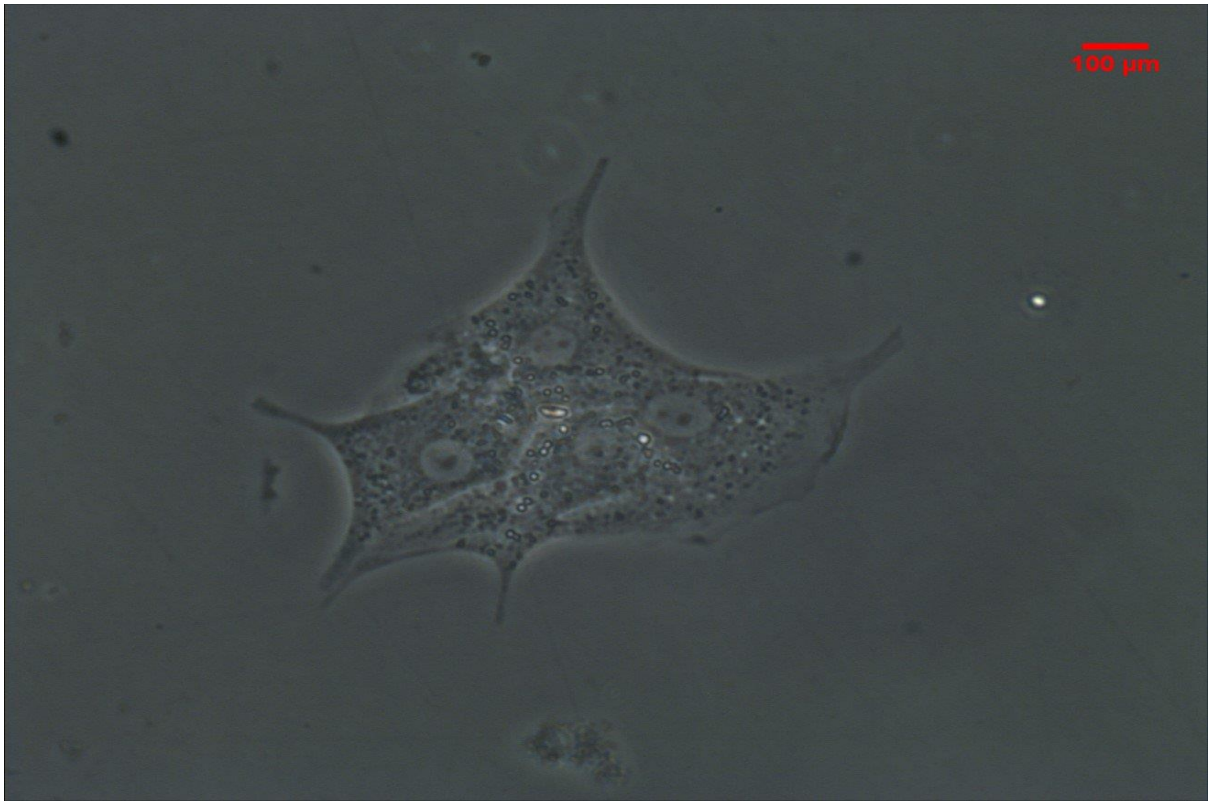

Figure 11. Primary aortic endothelial cell cluster shown in T-25 flask coated with collagen after 5 days of isolation from rat aorta through collagenase digestion (400×).

2.5. Isolation of primary ASMCs

Primary ASMCs were examined to investigate the expression level of proteins of interest, iNOS, and TRPV4 through SDS–PAGE Western blotting. During ECs isolation, aortic rings were kept in a sterile tube with HBSS, and aortic rings were cut longitudinally and flipped so that the internal layer of the explants stuck to the flask's bottom. The flask was then mounted vertically and added to the complete DMEM mixture (3 ml) with foetal calf serum (15%) and streptomycin penicillin 1×. The flask was left vertically in the incubator (5% CO_2, 37°C) for 90 minutes so that the medium was not in direct contact with the explants. Thereafter, the flask was gently placed horizontally so that the explants were not detached from the flask surface. The medium was kept unchanged, and after 3 days, half of it (approximately 1.5 ml)

was changed and left for another 3 days. Within 5 days, clusters of smooth muscle cells were observed, as Figure 13 shows (Kenagy, Hart, Stetler-Stevenson, & Clowes, 1997).

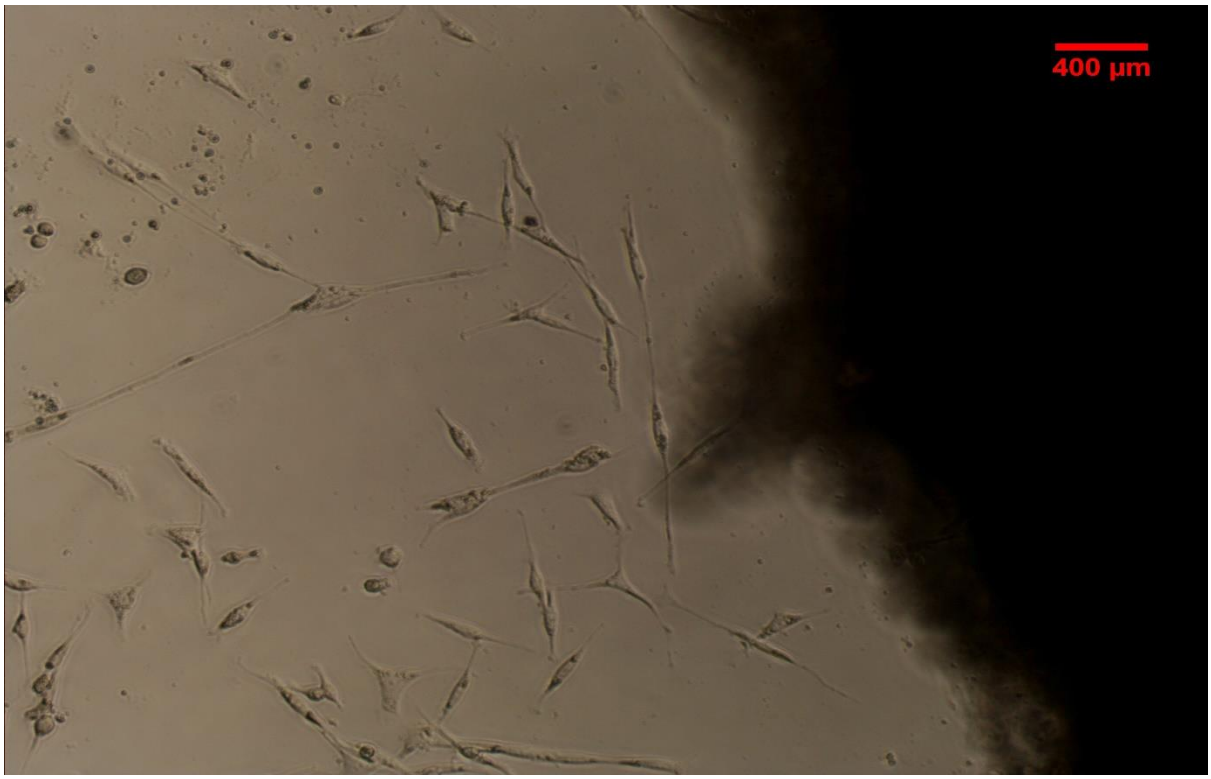

Figure 12. Primary aortic smooth muscle cells (ASMCs); an aortic explant denuded from endothelium and adventitia (the dark side of the picture) was plated in t-25, and spindle-shaped ASMC growth started at day 4 (400×).

2.6. Calcium imaging with fura-2

Measuring the Ca^{2+} influx in primary ECs was an elegant method for examining the viability of the isolation technique and to correlate the findings with other in vitro and in vivo studies. The method used calcium-sensitive fluorescent probes such as fura-2, a dye that shows changes in its fluorescent properties when it binds to Ca^{2+} (Morgan & Thomas, 1999). Fura-2 is applied as acetoxymethyl (AM) ester that enhances the dye's membrane permeability. Once the dye crosses the cellular membrane, intracellular esterase enzymes remove the ester moiety to yield the hydrophilic fura-2 that has become trapped intracellularly. Therefore, the process can concentrate the dye to approximately 100-fold the initial extracellular concentration of the AM ester (Morgan & Thomas, 1999). Fura-2 is a dual excitation dye that emits fluorescence at a wavelength of 510nm. The intracellular fura-2 exists in two forms: the free fura-2, which is excited at 380nm to emit fluorescence, and the Ca^{2+} bound fura-2, which is excited at 340nm to emit fluorescence at 510nm (Morgan & Thomas, 1999). Accordingly, upon Ca^{2+} influx, Ca^{2+} binds to fura-2, which is excited at 340nm to emit fluorescence at 510nm by ratiometric recording (Iredale & Dickenson, 1995).

Primary ECs were digested with trypsin and seeded on autoclaved glass coverslips 0.16–0.19-mm thick coated with poly-L-lysine to enhance the adherence of ECs. Briefly, autoclaved glass coverslips were placed in a sterile 6-well plate, covered with poly-L-lysine, and left in the incubator overnight (Sitterley, 2008b). Afterward, the extra poly-L-lysine was aspirated, and the coverslips were washed with Hank's buffer (HB) containing 5.6mM of KCl, 138mM of NaCl, 4.2mM of $NaHCO_3$, 1.2mM of NaH_2PO_4, 2.6mM of $CaCl_2$, 1.2mM of $MgCl_2$, 10mM of glucose, and 10mM of HEPES with a pH of 7.4 (Smith, Proks, & Moorhouse, 1999). The autoclaved coated glass coverslips were then seeded with primary ECs (200µl) and left in the incubator (5% CO_2, 37°C) for 3–5 hours, after which the cells were observed under a light microscope to ensure their adherence. Thereafter, the wells were mixed with complete ECs media (2 ml) and left in the incubator (5% CO_2, 37°C) overnight. The ECs were washed, and the media with or without treatments were changed until the ECs become confluent (i.e., at approximately 70%). ECs were next washed three to five times with HB before being treated with fura-2AM solution, composed of HB with fura-2AM (5 µM), 2% pluronic F-127, and 2% foetal bovine serum (FBS), per the recommendations of A. J. Huang et al. (1993); (Ma, Cheng, Wonga, et al., 2011). The ECs were incubated with fura-2AM solution in the dark at room temperature for 45–60 minutes (Ma, Cheng, Wonga, et al., 2011). Afterward, the coverslips were extensively washed with HB for 5-7 times to remove the extracellular fura-2AM and incubated with HB containing 2% FBS in the dark at room temperature for 30 minutes to enhance the hydrolysis of intracellular fura-2AM. Thereafter, the coverslips were washed for 5 times with HB before starting the experiment was begun (A. J. Huang et al., 1993) and placed under the Nikon Eclipse TE200 epifluorescence microscope (40×). A drop of immersion oil (type NF, nd= 1.515, Nikon) was mounted on the lens to enhance image resolution by correcting the refraction index and collecting more diffracted orders using the scientific image-processing IPLab software version 4.04. The coverslips were subjected to an experiment lasting 600 seconds that included a frame-shot every 10 seconds for 60 frames per experiment.

2.7. Laser scanning confocal microscopy

Confocal microscopy is an optical imaging method with three-dimensional sectioning capability widely applied in biomedical sciences to study fixed or living objects with a fluorescent probe. Modern confocal microscopes are relatively easy to operate and have been integrated in many multiuser imaging facilities. Among the different types of confocal microscopes is the LSCM, which provides a better resolution than the conventional light microscope (theoretical maximum resolution of 0.2µm), but less than the transmission

electron microscope (0.1nm). LSCM imaging starts by bathing the entire specimen in laser light; sensitive photomultiplier tube detectors are used, as well as scanning mirrors controlled by a computer to improve the imaging process. Image improvement also involves confining the illumination and detection to a single point in the specimen with limited diffraction through an objective lens with scanning devices. Therefore, regions of interests (ROI) labelled with fluorescence light-emitting probes are detected by a photomultiplier behind a pinhole to construct an image with imaging software (Goy & Psaltis, 2012).

2.7.1. Primary aortic ECs imaging

Primary ECs were seeded on autoclaved poly-L-lysine coated glass coverslips 0.16–0.19-mm thick and grown to reach approximately 70% confluency. ECs were labelled with acetylated low-density lipoprotein (Dil-Ac-LDL). Briefly, the coverslips were washed five times with HBSS, and ECs were washed with serum-free DMEM and incubated with Dil-Ac-LDL (10μg/ml in serum-free media) in the incubator for 4 hours. The coverslips were then washed with HBSS five times before being incubated with paraformaldehyde (4%) in the dark at room temperature for 1 hours to fix the cells. Afterward, the ECs were permealised with Triton-X100 (0.5% in HBSS) incubation for 10 minutes in the dark at room temperature. The coverslips were again washed with HBSS three times, after which the ECs were incubated with rabbit primary antibody for TRPV4, eNOS, or CAV-1 in blocking solution composed of phosphate buffer saline (pH 7.4), bovine serum albumin (BSA, 1%), and foetal calf serum (FCS, 2%) (1:100) overnight at 4°C. Thereafter, cells were again washed five times with HBSS before being incubated with the fluorescent goat secondary anti-rabbit antibody (1:1,000) for 2 hours at room temperature. The coverslips were yet again washed five times with HBSS and mounted on a microscope glass slide with a drop of mounting media containing DAPI, which stained the nucleus blue. ECs were visualised with Nikon C1 CLSM and EZ-C1 silver version 3.9 software. Primary aortic ECs were characterised under the laser confocal microscope (488nm), characterised as ROI red fluorescence staining less than 650nm and by the presence of the DAPI-stained nucleus, and visualised under 480nm. The protein of interest—namely, TRPV4, CAV-1, or eNOS—was probed indirectly through a secondary fluorescence antibody and visualised under a 515-nm wavelength. From each coverslip, four cells were selected and analysed. The images were then uploaded to ImageJ 1.46r software for quantitative analysis with the split-channel function and with ‘Colour’ selected on the image menu. Thereafter, each cell was selected and analysed with the measure function of the analyse menu.

2.8. BCA assay and SDS-PAGE Western blotting

Western blotting, or protein blotting, is a fundamental technique in biomedical sciences that detects a protein of interest from a complex protein population extracted from cell or tissue lysates. Protein detection is based on three aspects: gel electrophoresis, which separates proteins according to their size as they travel through the resolving gel; the transfer of the separated proteins to a membrane; and protein probing with a selective antibody visualised through an imaging system such as enhanced chemiluminescence (ECL), per the recommendations of Kurien and Scofield (2006).

ASMCs were washed with ice-cold HBSS three times followed by hot lysis buffer at 95°C (lysis buffer pH 7.4, 24mg of Tris-HCl, 200mg of SDS in 20-ml deionised distilled water with protease inhibitor cocktail of 1µl/ml). Afterward, cells were scrapped with lysis buffer to form cell lysates collected in Eppendorf tubes and sonicated for 30 seconds with ultrasound water bath three times with 10-seconds intervals in between. Afterward, Eppendorf tubes were transferred in heating blocks and heated at 95°C for 5 minutes before being centrifuged at 10000 rpm for 5 minutes. The supernatant was collected for BCA assay and Western blotting. For Western blotting, cells lysates were added with bromophenol blue (5x) by ratio of 4:1 and kept in -80°C.

BCA assay is a colorimetric analytical method that is applied to determine the protein concentration in a sample (Bainor, Chang, McQuade, Webb, & Gestwicki, 2011). BCA assay is based on measuring the formation of cuprous ions (Cu^{+}) from cupric ions (Cu^{+2}) through the Biuret complex formed in alkaline solutions of proteins using BCA (Olson & Markwell, 2007). The first reaction culminates with the interaction of copper and BCA with the amino acids cysteine, cystine, tryptophan, and tyrosine in the protein (Olson & Markwell, 2007). Thereafter, the BCA reagent forms a complex with Cu^{+} that yields a purple $Cu^{+1}(BCA)_2$ chromophore of an optimum absorbance at the 562-nm wavelength (Bainor et al., 2011). The test tube protocol requires only two reagents, and the relationship between protein concentration and absorbance is nearly linear (Olson & Markwell, 2007) over a wide working range (0–40nM/100µl), as shown in Figure 13.

Accordingly, BCA assay was initially conducted on a standard curve estimated from eight standard solutions of different concentrations obtained from BSA stock solution in deionised distilled water (1% w/v).

In a nonsterile 96-well plate, samples and standards were added as 5µl triplicates. To unify the vehicle, 5µl of lysis buffer was added to the standard wells, whereas 5µl of distilled water was added to each sample's well. BCA reagents A and B were mixed in a ratio of 9.8:0.2, of which 100µl was added into each well. The plate was shaken for 45 minutes and samples were read at 620nm using an Ascent Multiskan plate reader and software, version 2.6 (Thermo Labsystems Oy).

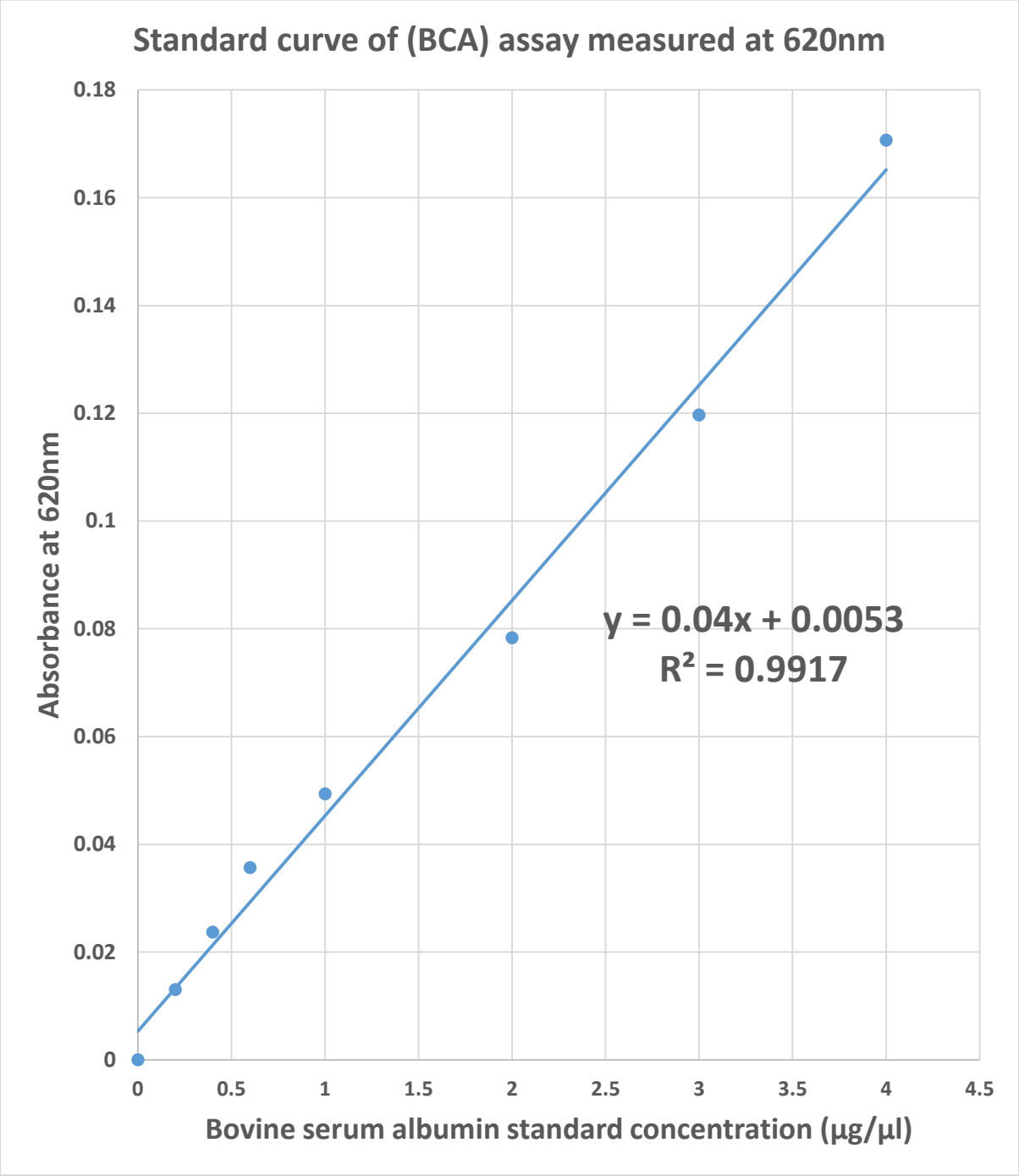

Figure 13. Bicinchoninic acid (BCA) assay standard curve, estimated from eight different BSA standard solutions (0–4µg/µl) loaded in 96-well plates treated with BCA reagents A and B mixture and shaken at room temperature before being read at the 620-nm wavelength.

2.8.1. Western blotting

The Western blotting gel chambers were prepared from 8% acrylamide resolving gel [2.66 ml of 30% acrylamide, 2.5 ml of Tris-HCl, pH 8.8 (1.5M), 100µl of SDS 10%, 100µl of ammonium persulfate 10%, and 6µl of tetramethylethylenediamine (TEMED), all in 4.64 ml deionised distilled water] and stacking gel [0.52 ml of 30% acrylamide, 1 ml of Tris-HCl, pH 6.8 (0.5M), 40µl of SDS 10%, 20µl of ammonium persulphate 10% and 4µl of TEMED, all in 2.44 ml deionised distilled water]. The Western blotting gel glass chambers were placed in a loading tank containing tank buffer [Tris-HCl (0.025M), glycine 0.192M, and SDS 0.1% in deionised distilled water]. The gels were loaded with 20-µg proteins calculated from BCA assay and run at 20m amp/gel current using a Thermo–Fisher PowerPack for approximately 60 minutes. Once samples reached the bottom of the resolving gel front, the gels were mounted on polyvinylidene difluoride immobilon-P transfer membranes of 0.45 µm pore size in a semidry transfer chamber, subjected to 25 mV for 20 minutes and added with transfer buffer [Tris-HCl (4.8mM), glycine (3.9mM) and SDS (0.00375%), pH 8.3 in deionised distilled water with freshly added methanol (20%)]. Briefly, the membrane was mounted on three Whatmann filter papers, and the gel was placed atop the membrane and topped with another three Whatmann filter papers, so that the membrane was between the gel and the positive side of the semidry chamber. Afterward, the membrane was incubated with blocking buffer for 2 hours on a shaker [blocking buffer: Tris-HCl (1mM), NaCl (10mM), Tween-20 (0.1% v/v) in deionised distilled water, pH 7.5] and added with bovine serum albumin (5% w/v). The gels were then mixed with Coomassie Blue to ensure that the proteins were transferred to the membrane, after which the blocking buffer was removed and the membrane incubated on a shaker with primary antibody in blocking buffer overnight at 4°C. Thereafter, the membrane was washed with washing buffer [Tris-HCl (1mM), NaCl (10mM) and Tween-20 (0.1% v/v)] in deionised distilled water, pH 7.5) three times for 15 minutes (net washing time: 45 minutes). The secondary antibody in blocking buffer was added to the membrane on a shaker for 2 hours the membrane was washed with washing buffer three times for 15 minutes (net first washing time: 45 minutes). Lastly, the membrane was treated with ECL detection reagents A [p-coumaric acid (25 µl, 90mM)] + luminol (50 µl, 250mM) in 5 ml of Tris-HCl (100mM), pH 8.5] and B [3 µl of 30% H_2O_2 in 5 ml of Tris-HCl (100mM), pH 8.5) and left on the shaker for 5 minutes. The protein of interest was detected using a Thermo Scientific MYECL imager. Western blotting results were quantified with densitometric

analysis, which is based on comparing the band density of the protein of interest (i.e., iNOS or TRPV4) to that of the loading control protein (i.e., β-actin).

2.9. Data analysis

All experimental data are presented as mean ± standard error mean (SEM). The number of different experiments conducted from different batches (i.e., animals or cell passages) is referred to as the group size (N), whereas the number of repeats within the same experimental batch is termed as n. Therefore, data subjected to statistical analysis have at least N= 3 and n= 6 when data showed consistency and robust reproducibility; however, most data were collected from sample sizes of N= 4 and n= 8.

Griess assay, BCA assay, and ELISA analysis were conducted by loading each sample in triplicate, except with ox-LDL ELISA, in which samples were loaded in duplicate, as recommended by the manufacturers. Technical repeats were conducted to ensure the reliability of the produced values.

Data analysis was performed with GraphPad Prism 5.0 software to determine the level of significance. When the level of probability (p) was less than 0.05 (*), 0.01 (**), or 0.001 (***), the effect of the difference was deemed significant. Two-way analysis of variance (ANOVA) was conducted to examine the effect of two independent variables in specific experiments (e.g., organ bath studies), in terms of the effect of treatment (e.g., STZ or another incubation) in addition to the effect of the applied drug concentration (i.e., x-axis), as detailed in Chapters 3 and 4). Significance observed with two-way ANOVA was presented on the side of the graph next to the last concentration (i.e., time point), whereas post hoc significance was shown on the top of the specific concentration or time point. By contrast, one-way ANOVA was conducted to examine the effect of a single independent variable on more than two groups—for instance, when iNOS expression was examined in the presence of MGO with and without L-arginine (Chapter 6) and the effect of insulin on STZ-diabetic ECs compared with naïve nondiabetic ECs (Chapter 5). A two-tailed Student's t-test was applied to examine the effect of a single independent variable on two groups—for example, when TRPV4 expression in ASMCs was compared (Chapter 6) and when the effect of AMTB was studied in terms of MGO-induced intracellular calcium elevation in CHO cells (Chapter 7). Paired or matched analysis was conducted when the same sample was subjected to two different conditions, such as with STZ-diabetic ECs treated with insulin (Chapter 6) and

when CHO and rTRPM8 cells were compared to CHO and rTRPM8 cells incubated with AMTB (Chapter 7).

2.10. Chemicals and drugs

Table 3 Chemical and drug suppliers, solvents used, and specifications

Chemical	**Supplier**	**Specification**	**Solvent**
Streptozotocin (STZ)	Sigma Chemical, St. Louis, MO, USA	≥98.0% high performance liquid chromatography (HPLC), M.wt= 265.22g/mol	pH 4.5, 20-mM citrate buffer
Noradrenaline (NA)	Sigma Chemical	Min. 99%, M.wt= 337g/mol	Distilled water (DW)
Carbachol (CC)	Sigma Chemical	Min. 98% (TLC), M.wt= 182.65g/mol	DW
Methylglyoxal (MGO)	Sigma Chemical	40% (w/v) in H_2O	DW
L-NG-Nitro-L-arginine methyl ester hydrochloride (L-NAME)	Sigma Chemical	≥98.0% (TLC), M.wt= 269.69g/mol	DW
RN-1747	Tocris Bioscience, Bristol, UK	10 mg M.wt= 395.87g/mol	Dimethyl sulfoxide (DMSO)
4α-Phorbol 12,13-didecanoate (4αPDD)	Sigma Chemical	1mg M.wt= 672.93g/mol	DMSO
HC067047	Tocris Bioscience	10 mg M.wt= 471.15g/mol	DMSO
RN-1734	Sigma Chemical	10mg M.wt= 353.31g/mol	DMSO
Icilin	Tocris Bioscience	10mg	DMSO

		M.wt= 311.3g/mol	
AMTB hydrochloride	Tocris Bioscience	10 mg M.wt= 430.99g/mol	DW
Lipopolysaccharides	Sigma Chemical	100 mg from *Escherichia coli* 0111:B4	DW
Collagenase	Sigma Chemical	50mg from *Clostridium histolyticum*, sterile-filtered for general use, type I-S, 0.2-1.0 FALGPA units/mg solid, ≥125 CDU/mg	Serum-free media 199 or Dulbecco's modified Eagle's medium (DMEM)
Endothelial cell growth supplement	Sigma Chemical	15mg from bovine pituitary	Complete DMEM media
Heparin sodium salt	Sigma Chemical	10mg from porcine intestinal mucosa (25 KU)	Complete DMEM media
Collagen	Sigma Chemical	10mg from rat tail Bornstein and Traub Type I, powder, BioReagent, suitable for cell culture	Acetic acid (100%)
Poly-L-lysine solution	Sigma Chemical	50 ml M.wt= 150000-300000g/mol, 0.01%, sterile-filtered, BioReagent, suitable for cell culture	
Luminol	Sigma Chemical, St. Louis, MO, U.S.A	5g M.wt= 177.16g/mol	DMSO

p-Coumaric acid	Sigma Chemical	5g M.wt= 164.16g/mol	DMSO
Carestream® Kodak® autoradiography GBX developer/ replenisher	Sigma Chemical	1 gallon	DW
Carestream® Kodak® autoradiography GBX fixer/ replenisher	Sigma Chemical	1 gallon	DW
Ionomycin	Sigma Chemical	Calcium salt (1 mg) from *Streptomyces conglobatus* M.wt= 47.07g/mol	DMSO
Iberiotoxin	Sigma Chemical	10 µg recombinant from *Mesobuthus tamulus* M.wt= 4,248.86g/mol	DMSO
L-arginine	Sigma Chemical	25 g M.wt= 174.20	DW
DMEM (1×) liquid (low glucose) Invitrogen Gibco	Fisher Scientific	500 ml [with L-Glutamine 1,000mg/L D-glucose sodium pyruvate 25mM HEPES] with L-glutamine, D-glucose, sodium pyruvate, HEPES Invitrogen Gibco	
New-born bovine calf serum	Fisher Scientific	100 ml	

		Thermo Scientific HyClone	
Horse serum	Fisher Scientific	100 ml [Origin: New Zealand] in plastic container, E-Z hold, Invitrogen Gibco	
Antibiotic–antimycotic solution	Fisher Scientific	100 ml 100×, 10000U/ml penicillin G, 10000 µg/ml streptomycin, 25µg/ml amphotericin B (Fungizone), Thermo Scientific HyClone	
Trypsin solution	Fisher Scientific	100 ml 2.5% (10×) without EDTA or phenol red Thermo Scientific HyClone	
Medium 199	Fisher Scientific	500 ml 1× liquid [with Earle's salts L-glutamine] Invitrogen Gibco	
Hyperfilm ECL	Fisher Scientific	18 × 24cm	
Hank's Balanced Salt Solution (HBSS)	Fisher Scientific	500ml 10× liquid [without phenol red sodium bicarbonate] without phenol red (ce) Invitrogen Gibco	
Membrane filter	Fisher Scientific	Immobilon-P transfer membranes 0.45 µm, pore size 265mm × 3.75m	
Protein assay reagent B	Fisher Scientific	25 ml BCA, Thermo Scientific Pierce	

Protein assay reagent A	Fisher Scientific	1 L BCA Thermo Scientific Pierce	
Fura-2, AM	Life Technologies	Cell permeant (20 × 50 µg)	DMSO
Pluronic® F-127	Life Technologies	0.2 µm filtered (10% solution in water, 30 ml) + A11	
Biotinylated Protein Ladder Detection Pack	New England Biolabs	650 µL	
Antibiotin	New England Biolabs	1 ml HRP-linked antibody	
Interferon-γ (IFN-γ)	Merck Chemicals	10µg (1000000 U) Rat, Recombinant, *E. coli*	Sterile distilled water (SDW)
Anti-SM22 alpha antibody	Abcam	Polyclonal rabbit anti-rat (100 µg)	SDW
Anti-TRPV4 antibody	Abcam	Polyclonal rabbit anti-rat (100 µl)	
Anti-iNOS antibody	Abcam	Polyclonal rabbit anti-rat (200 µl)	
Anti-rabbit antibody	Abcam	Goat IgG H&L (Biotin), 1 mg	SDW
Caveolin-1 antibody	Thermo–Fisher Scientific	Polyclonal rabbit anti-rat antibody (100 µl)	
eNOS antibody	Thermo–Fisher Scientific	Polyclonal rabbit anti-rat antibody (100 µl)	
TRPV4 antibody	Thermo–Fisher Scientific	Polyclonal rabbit anti-rat antibody (100 µl)	

Mounting medium	Vector Laboratories	With DAPI (10 ml), VECTASHIELD HardSet	
Fluorescein antibody	Vector Laboratories	Goat anti-rabbit IgG (1.5 mg)	
Rat oxidised low-density lipoprotein enzyme-linked immunosorbent assay (ELISA) kit	H2bioscience	96 assays	
OxiSelect Methylglyoxal (MGO) Competitive ELISA kit	Cambridge Bioscience	Rat selective 96 assays	
Acetylated low-density lipoprotein (Dil-Ac-LDL)	Bioquote Limited	200 µg	Serum-free DMEM
Sodium nitrite ($NaNO_2$)	Fisher Scientific	500 g (≥97%) M.wt = 69g/mol	DDW
Griess A		Sulphanilamide (1% v/v)	5% phosphoric acid
Griess B		Naphthyl ethylenediamine dihydrochloride (0.1% v/v)	DDW
Chloroform	Sigma Chemical	500 ml (≥99.5%) M.wt= 119.38g/mol	
Hydrochloric acid	Fisher Scientific	2.5 L M.wt= 36.46g/mol	
Ammonium persulfate	Fisher Scientific	25 g M.wt= 228.19	DDW
NNN'N'-tetramethylethylene diamine	VWR Chemicals, Auckland, New Zealand	25 ml M.wt= 116.21g/mol	DDW

(TEMED)			
Hygromycin B from *Streptomyces hygroscopicus*	Sigma Chemical	M.wt = 527.52	MEM AQmedia
Acrylamide	National Diagnostics, Yorkshire, UK	450 ml 30% acrylamide, 0.8% bis-acrylamide stock solution (37.5:1)	DDW
Sodium dodecyl disulphate (SDS)	Fisher Scientific	500 g (99% min) M.wt= 288.38g/mol	DDW
Glycine	Fisher Scientific	500 g (98%) M.wt= 75.07g/mol	DDW
Insulin	Sigma Chemical	100mg from bovine pancreas M.wt= 5733.49g/mol	Hydrochloric acid pH 2-3
Probenecid	Sigma Chemical	25g M.wt= 285.36g/mol	DDW
Acetic acid	Sigma Chemical	2.5 L (≥99%) M.wt= 60.05g/mol (A6283)	
HEPES	Sigma Chemical	BioPerformance Certified, ≥99.5% (titration), cell culture tested M.wt= 238.8g/mol	DW
Minimum essential medium eagle (MEM AQMedia)	Sigma Chemical	With Earle's salts, L-alanyl-glutamine, and sodium bicarbonate, liquid, sterile-filtered, suitable for cell culture	
Anti-phospho p38 MAPK	Cell Signalling	Polyclonal rabbit anti-rat antibody (200 µl)	
Anti-phospho Akt	Cell Signalling	Polyclonal rabbit anti-rat Antibody (100 µl)	

Chapter 3: The effect on muscarinic, TRPV4 and TRPM8 agonists on rat aortic rings

3.1. Introduction

Blood vessels are primarily composed of three layers: the outer layer (tunica adventitia), the medial layer (smooth muscle cells, or tunica media), and the inner layer (endothelium or tunica intima) (C. W. Chen et al., 2012). The endothelium is composed of endothelial cells (ECs) and sub-endothelial layer forming a relatively impermeable layer that separate the passive diffusion of the circulation's components to the supplied tissues (M. G. Davies & Hagen, 1993).

The endothelium regulates vascular tone by releasing numerous vasodilators, including NO, PG, and EDHF, in addition to vasoconstrictors such as ET-1 and Ang II (Tabit et al., 2010). NO is among the vasodilators released in response to shear stress and TRPV4 activation (Sena et al., 2013; Sukumaran et al., 2013). NO in ECs is generated by way of eNOS, which oxidises L-arginine into L-citrulline (M. I. Lin et al., 2003). eNOS or NOS-3 is a constitutively active enzyme in the ECs that can be further stimulated by receptor-dependent agonists that increase $[Ca^{2+}]i$ and compromise plasma membrane phospholipid symmetry (Cines et al., 1998; A. Dhar et al., 2010). NO diffuses to VSMCs where it activates the sGC that generates cGMP to yield vasodilation (van den Oever et al., 2010). cGMP inhibits the voltage-gated calcium channels (VGCC)-mediated Ca^{2+} entry into the VSMCs to inhibit the vasoconstriction. At the same time, cGMP activates potassium channels such as BKca, K_{ATP}, and Kv, which induces membrane hyperpolarisation and vasodilation (Dong et al., 1998; Murphy & Brayden, 1995b). cGMP also activates PKG, which in turn activates MLCP that dephosphorylates the MLC and causes further vasodilation (Cohen et al., 1999).

In addition to NO, COX-1 in ECs metabolises AA to produce prostacyclin, which is a potent vasodilator (Mitchell et al., 2008). AA is liberated from the ECs membrane through the action of PLA2 (Lambert et al., 2006). Prostacyclin mediates vasodilation by activating the BKca, K_{ATP} channels in VSMCs, which prompts membrane hyperpolarisation and, in turn, vasodilation (Clapp et al., 1998; Jackson et al., 1993). Moreover, prostacyclin induces the release of Ca^{2+} from ER stores to mediate endothelium Ca^{2+} entry, which is a crucial step in initiating endothelium-dependent vasodilation (Murata et al., 2007).

In addition to NO and prostacyclin, the 3rd endothelial vasodilatory pathway is the EDHF (G. Chen et al., 1988), which involves SKca, IKca, BKca and EET as essential elements in mediating vasodilation (Hecker et al., 1994; A. Huang et al., 2000; Murphy & Brayden,

1995a; Popp et al., 1996; Rosolowsky & Campbell, 1993; Widmann et al., 1998; Zygmunt & Högestätt, 1996).

In addition to the three mentioned pathways, Western blotting, RT-PCR and immunohistochemistry studies recognised at least 20 distinct TRP channels in the VSMCs and the endothelium (Earley et al., 2010; H. Y. Kwan et al., 2007; Watanabe et al., 2008). As cation channels, TRP channels exert vascular tone regulation in both systemic and pulmonary circulations (Watanabe et al., 2008). Highly expressed in ECs, TRPV4 induces NO and EDHF release and thereby controls the vascular tone (Köhler et al., 2006). Furthermore, TRPV4 is essential in muscarinic-mediated endothelium-dependent vasodilation via a novel mechanism that involves Ca^{2+} influx and by way of endothelium derived factor (11, 12 EET)-induced TRPV4 complex formation with RyR and BKca in VSMCs and thereby facilitate vasodilation (Earley et al., 2005). In addition to TRPV4, TRPM8 is expressed in both ECs and VSMCs in numerous vascular beds, including rat aorta, mesenteric arteries, femoral arteries, and tail artery (Earley, 2010; H. Y. Kwan et al., 2007). The co-expression of TRPM8 and TRPV4 channels in the aortic vasculature was concluded as novel Ca^{2+} entry pathways that might control the systemic circulation by way of EDHF (Garland et al., 1995; X. R. Yang et al., 2006).

Therefore, as mentioned in section 1.7, the main objectives this chapter were to investigate the relationships between muscarinic receptors, TRPV4 and TRPM8 channels through organ bath studies using aortic rings from Wistar rats. Moreover, the dependence of these three pathways on NO was investigated through incubating the rings with the NOS blocker, L-NAME. Further studies were conducted to investigate the involvement of BKca in the vasodilatory pathways induced by muscarinic agonist (carbachol), TRPV4 agonist (4-αPDD) and TRPM8 agonist (icilin). These investigations were conducted using the selective BKca blocker, iberiotoxin. Lastly, carbachol-, 4-αPDD-, and icilin-induced vasodilation was investigated after endothelium removal to investigate the endothelium-dependent vasodilation in muscarinic, TRPV4, and TRPM8 pathways.

3.2. Materials and methods

Organ bath studies were conducted to examine the muscarinic, TRPV4 and TRPM8-induced vasodilation through inhibiting TRPV4 and/or TRPM8, or inhibiting selected downstream cascade components such as NOS and BKca. Additionally, the endothelium was removed (denuded endothelium) to examine the endothelium-dependence of the muscarinic, TRPV4 and TRPM8 pathways. Fresh aortic rings were isolated and prepared as mentioned in section 2.3.1. To examine the vasodilation of an agonist, the tissue was initially contracted with NA (300nM) which was found as the EC_{80} (Figure 14). The extent of vasoconstriction and vasodilation was calculated as mentioned in general methodology section 2.3.2.

3.3. Results

3.3.1. NA EC_{80} determination

NA EC_{80} was estimated to spare the time for prospective experiments by curtailing NA concentration response curve (CRC) to avoid possible tissue damage or desensitisation through repeated maximum contraction as described in section 2.3.3.

When NA CRC experiments were analysed, the mean maximum contraction force (Emax) was 0.468 ± 0.041g obtained from 9 different rats (N= 9) from which 36 aortic rings were studied (n= 36) which were then normalised to the maximum response to yield an EC_{80} of FBC= 629.2 ± 86.7nM. However, when NA (629nM) was applied as a single dose, it yielded 100% vasoconstriction. NA (300nM) showed EC_{80} submaximal response Emax= 0.468 ± 0.04g, 100 ± 13.5% was achieved with NA final bath concentration (FBC) = 300µM (Figure 14).

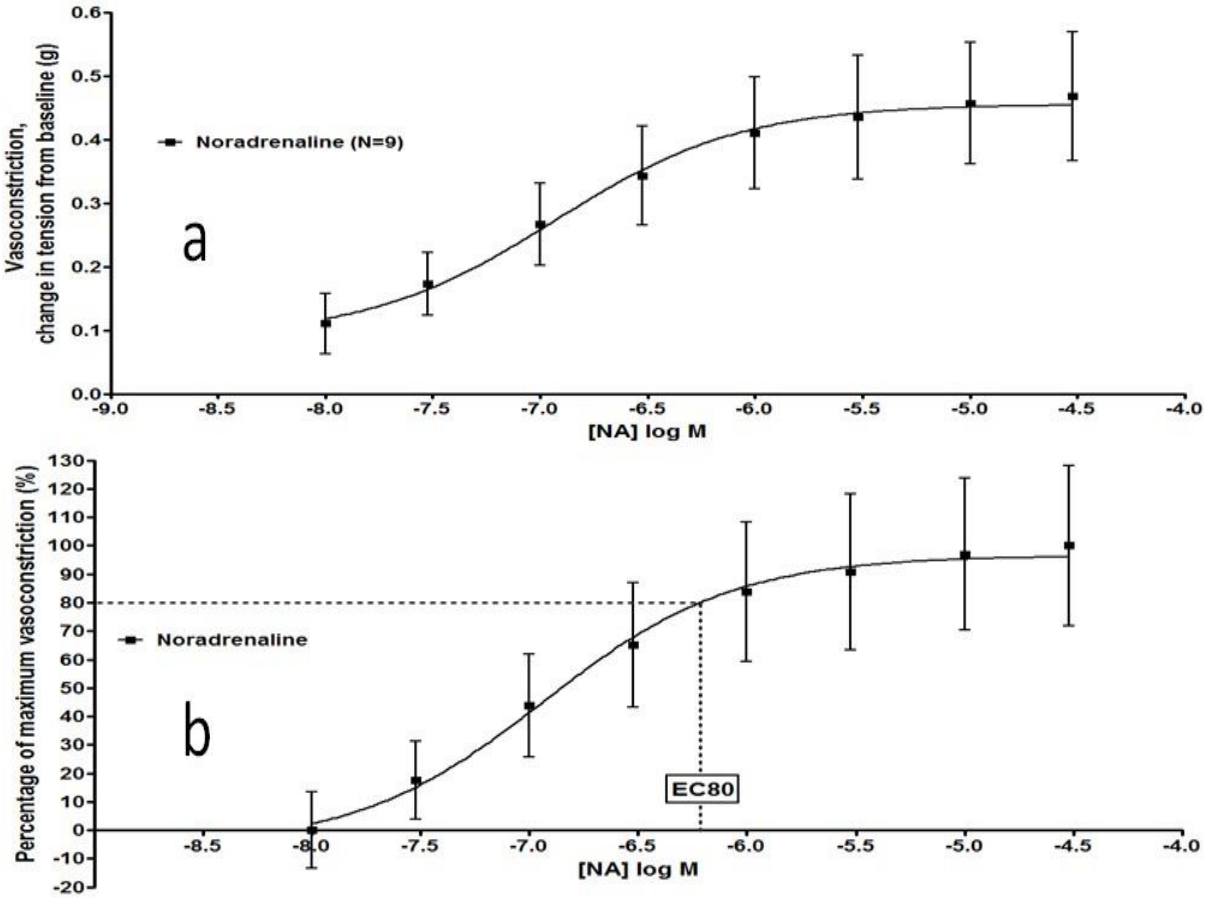

Figure 14. Noradrenaline (NA) concentration response curve in rat aortic rings. NA-induced vasoconstriction in gram scale (a). NA-induced vasoconstriction normalised to the maximum response % (b). Data is shown as mean ± SEM (N=9).

3.3.2. TRPV4 and TRPM8 antagonists' studies

As the vehicle for TRPV4 agonists (RN-1747 and 4-αPDD) and TRPM8 agonist (icilin) is DMSO, therefore, DMSO CRC was applied to investigate whether DMSO has an effect on vascular tone. DMSO stock solution 100% w/v which is equivalent to 12.8M was diluted by 1:1000 serial dilutions. DMSO did not show significant difference on vascular tone when compared to NA-induced contraction (N=3, $p \geq 0.05$, DMSO Emax= -3.6 ± 2.3% vs NA-induced contraction, Emax= 0.00 ± 2.4%) (Figure 15).

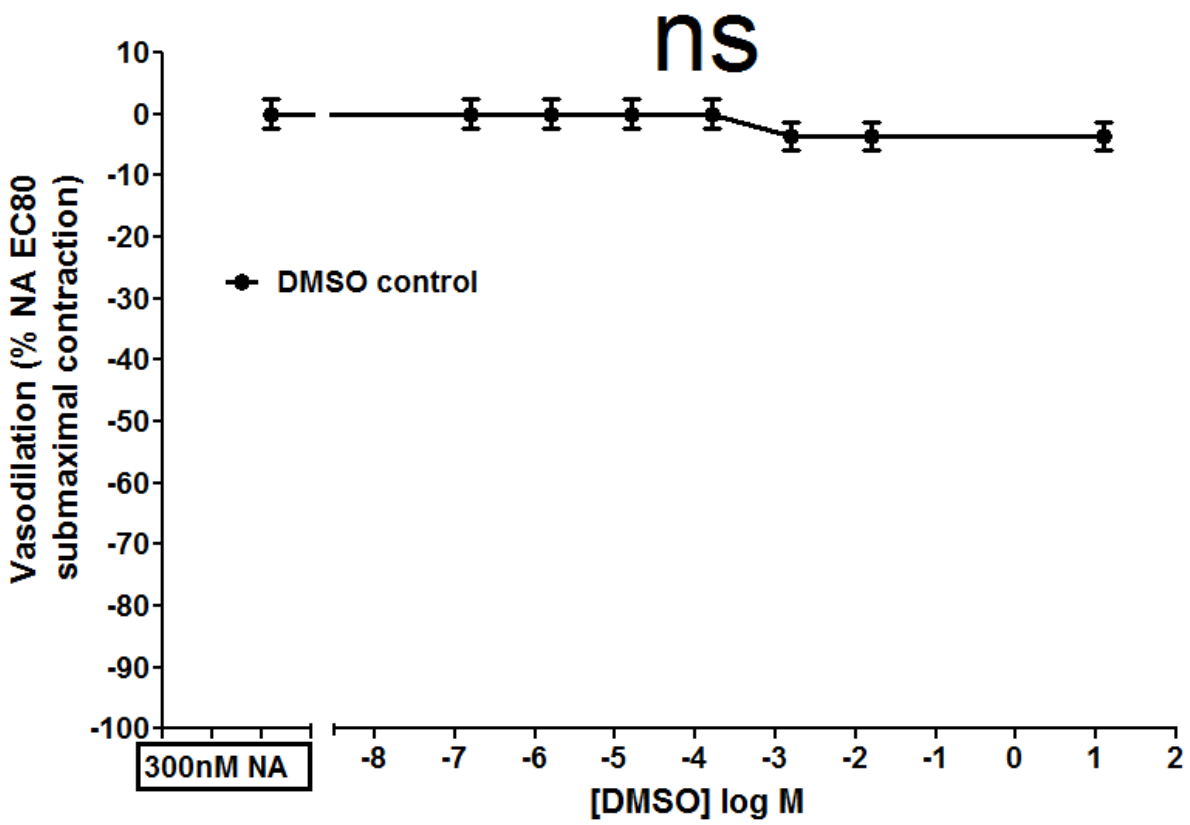

Figure 15. Dimethyl sulfoxide (DMSO) effect on NA-induced vasoconstriction in aortic rings. Non significance is represented as ns $p \geq 0.05$ analysed through one-way ANOVA vs NA-induced contraction (N= 3), Data is shown as mean ± SEM.

These studies were conducted to estimate the required concentration of the antagonist to block the targeted channel, whether TRPV4 (HC067047 and RN-1734) or TRPM8 (AMTB). As a previous study conducted by L. Zhang, Papadopoulos, and Hamel (2013) revealed that HC067047 is a competitive antagonist of TRPV4 and an unpublished findings from Professor Stuart Bevan's laboratory in Wolfson centre for age related diseases revealed that AMTB is a competitive TRPM8 antagonist (Unpublished data). Therefore, pA2 was estimated for each antagonist through constructing a Schild plot. pA2 is the negative logarithm of the molar concentration of an antagonist which reduces the effect of a dose of agonist to that of half the dose (Tallarida, Cowan, & Adler, 1979). pA2 measures the affinity of a competitive

antagonist to a certain receptor. The presence of an antagonist shifts the concentration response curve rightward as more agonist is required to exert a certain response (Tallarida & Murray, 1987).

- TRPV4 antagonist

Thoracic aortic rings were incubated with 3 different concentrations of TRPV4 antagonist (HC067047); 1µM, 1nM and 1pM for 60 minutes. Afterward, the aortic rings were contracted with NA (300nM) and relaxed with TRPV4 agonist, RN-1747 CRC. pA2 was obtained graphically as shown in Figure 16a&b and 17. The time period selected (60 minutes) was more than stated by Jin, Berrout, Chen, and O'Neil (2012) who stated that HC067047 (100nM) pre-incubation for 5 minutes was sufficient to block the effect of TRPV4 selective agonist, GSK1016790A in mouse cortical duct collect cells (M1 cells). In Figure 17b, the maximum control RN-1747-induced vasodilation was re-calculated as 100% to obtain an accurate pA2 using the Schild plot. The Schild plot represents the relationship between log (DR-1) and –log antagonist concentration (the ratio of the dose of agonist to produce a specific effect (e.g., half maximal effect) in the presence of the antagonist to the dose of agonist required in the absence of the antagonist is calculated). The obtained relationship was approximately linear revealing surmountable antagonism where pA2= 8.75 (Figure 17).

HC067047 showed significant effect on RN-1747-induced vasodilation at the highest applied concentration (1µM) [N=3, ns $p \geq 0.05$, HC067047 (1pM) EC_{50}= 28.9 ± 10.5nM Emax= -41.2 ± 9.5%, HC067047 (1nM) EC_{50}= 54.3 ± 39.5nM and Emax= -44.1 ± 4.4% and N=4 * $p < 0.05$ HC067047 (1µM) EC_{50}= 103.7 ± 42.0nM and Emax= -26.8 ± 4.2% vs RN-1747 without HC067047 EC_{50}= 46.7 ± 35.3nM and Emax= -52.6 ± 3.9%] (Figure 16a). The control response was calculated as 100% and each antagonist data were calculated according to the maximum concentration of the corresponding control data (Figure 16b). HC067047 showed significant effect on RN-1747-induced vasodilation at the highest applied concentration [N=3, ns $p \geq 0.05$, HC067047 (1pM) EC_{50}= 25.8 ± 10.8nM and Emax= -75.8 ± 17.8%, HC067047 (1nM) EC_{50}= 46.1 ± 32.9nM and Emax= -80.3 ± 7.7% and N=4, * $p < 0.05$, HC067047 (1µM) EC_{50}= 65.8 ± 24.6nM and Emax= -50.82 ± 7.0% vs RN-1747 without HC067047 EC_{50}= 37.7 ± 28.8nM and Emax= -100.0±0.00%] (Figure 16b).

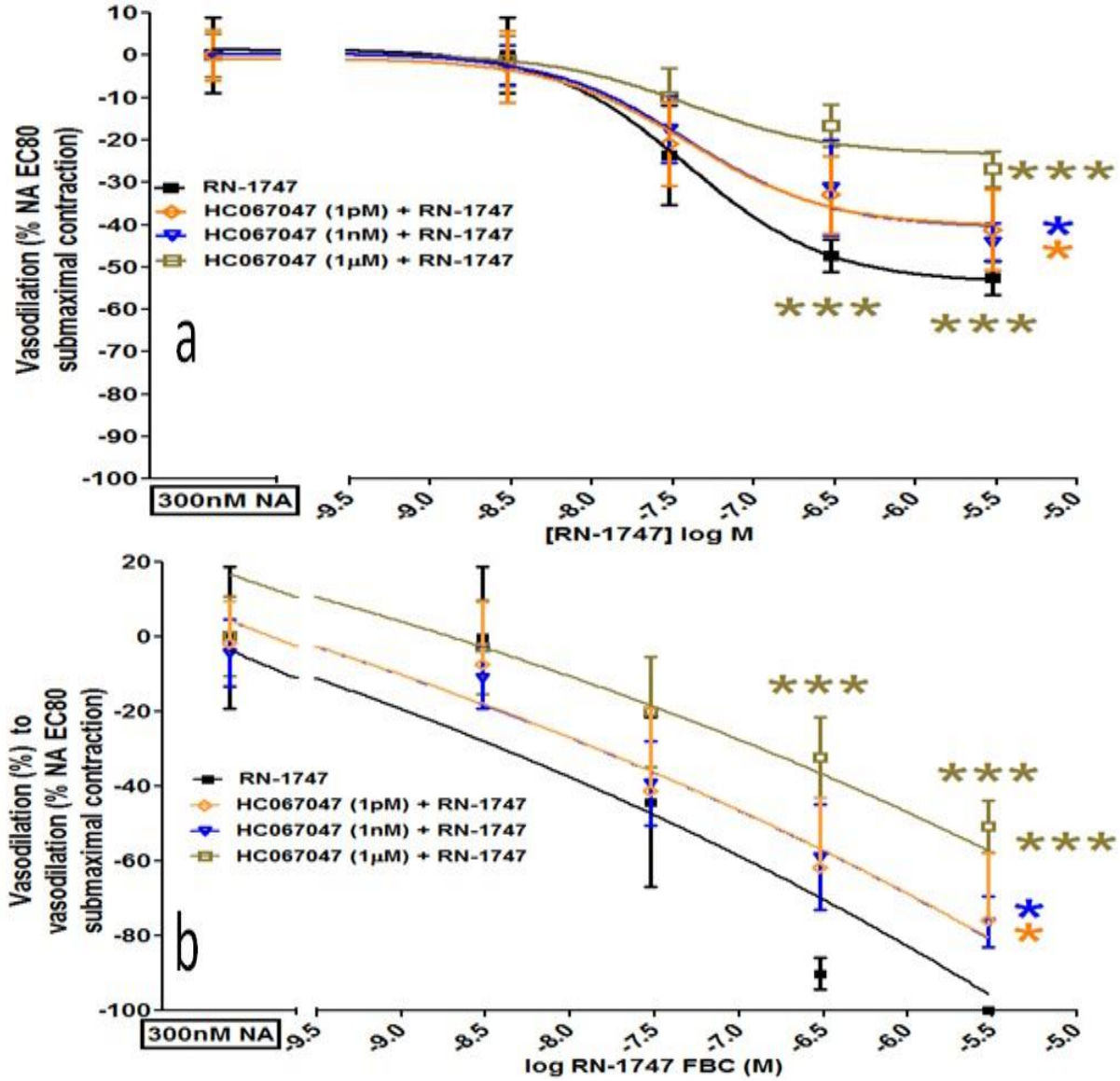

Figure 16. TRPV4 agonist (RN-1747) concentration response curve in the presence of three different concentrations of TRPV4 antagonist (HC067047). RN-1747-induced vasodilation normalised to noradrenaline EC80 submaximal contraction (a). RN-1747-induced vasodilation normalised to RN-1747 only-induced vasodilation (b). Analysed through two-way ANOVA with Bonferroni post-hoc test. Significance is represented as *** $p < 0.001$ compared with RN-1747 without HC067047. Data is shown as mean ± SEM (RN-1747, N= 4, HC067047 1pM+RN-1747, N= 3, HC067047 1nM+RN-1747, N= 3 and HC067047 1μM+RN-1747, N= 4).

Table 4 Schild plot parameters for TRPV4 antagonists (HC067047) applied against TRPV4 agonist (RN-1747)

Antagonist concentration (HC067047) M	**-log HC067047**	**Dose ratio (DR)**	**Log (DR-1)**	**EC_{50} (nM)**	**Emax %**
Control	-	-	-	37.7 ± 28.8	100.0 ± 0.0
1pM	12	1.14	-0.85	25.8 ± 10.8	75.8 ± 17.8
1nM	9	(1.64)[1]	-0.2	46.1 ± 32.9	80.3 ± 7.7
1μM	6	7.46	0.81	65.8 ± 24.6	50.82 ± 7.0

[1] Estimated from the original data set (not from the 100% recalculated data)

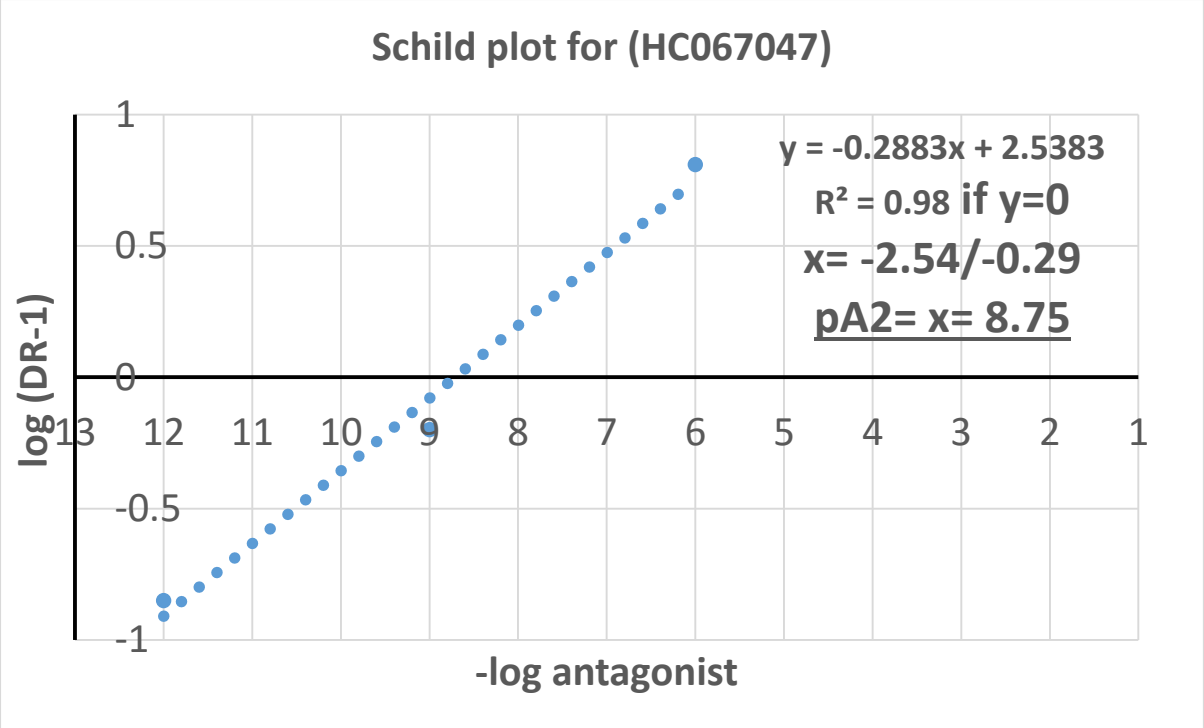

Figure 17. Schild plot for TRPV4 antagonist (HC067047) versus TRPV4 agonist (RN-1747). pA2 is the point of intersection at x-axis and is graphically estimated as 8.75.

- TRPM8 antagonist

Naïve aortic rings were incubated with 3 different concentrations of TRPM8 antagonist (AMTB); 1µM, 100nM and 1nM for 60 minutes. Afterward, the aortic rings were pre-contracted with NA (300nM) and relaxed with TRPM8 agonist, icilin CRC. pA2 was obtained graphically as shown in Figure 18a&b and 19. The incubation period (60 minutes) was more than what was applied by Lashinger et al. (2008) when they incubated hTRPM8 HEK293 cells with AMTB (1nM-100µM) for 10 minutes. In Figure 18b, the maximum control icilin-induced vasodilation was re-calculated as 100% to obtain an accurate pA2 using the Schild plot. The Schild plot represents the relationship between log (DR-1) and –log antagonist concentration. The obtained relationship was approximately linear revealing surmountable antagonism where pA2= 10.4.

AMTB showed significant effect on icilin-induced vasodilation at the highest applied concentration (1µM) [N=3, ns $P \geq 0.05$, AMTB (1pM) EC_{50}= 238.7 ± 92.2nM and Emax= -72.6 ± 12.2%, AMTB (1nM) EC_{50}= 3.8 ± 3.1µM and Emax= -71.2 ± 11.2% and *** $P<0.001$ AMTB (1µM) EC_{50}= 13.6 ± 3.4µM and Emax= -34.1 ± 10.5% vs icilin without AMTB EC_{50}= 223.4 ± 125.6nM and Emax= -83.8 ± 2.0%] (Figure 18a). The control response was calculated as 100% and each antagonist data were calculated according to the maximum concentration of the corresponding control data. AMTB showed significant effect on icilin-

induced vasodilation at the highest applied concentration (1μM) [N=3, ns $P \geq 0.05$, AMTB (1pM) EC_{50}= 246.1 ± 95.7nM and Emax= -86.5 ± 14.1%, AMTB (1nM) EC_{50}= 3.9 ± 2.2μM and Emax= -85.2 ± 14.0% and *** $P < 0.001$, AMTB (1μM) EC_{50}= 13.3 ± 3.5μM and Emax= -40.1 ± 11.6% vs icilin without AMTB EC_{50}= 228.6 ± 131.5nM and Emax= -100.0 ± 0.0%] (Figure 18b).

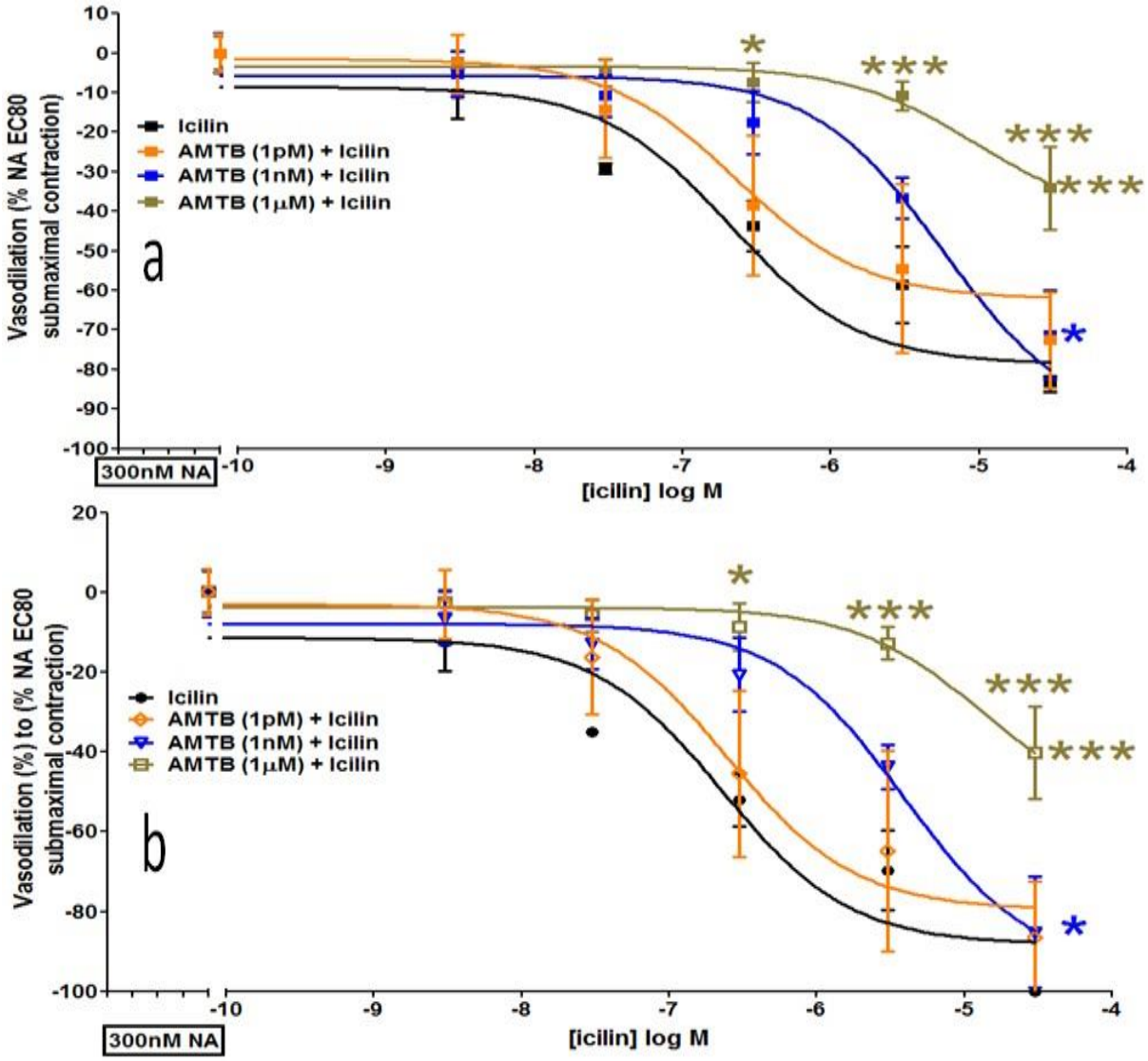

Figure 18. TRPM8 agonist (icilin) concentration response curve in the presence of three different concentrations of TRPM8 antagonist (AMTB). Icilin-induced vasodilation normalised to noradrenaline EC_{80} submaximal contraction (a). Icilin-induced vasodilation normalised to icilin only-induced vasodilation (b). Analysed through two-way ANOVA with Bonferroni post-hoc test. Significance is represented as * $p < 0.05$ and *** $p < 0.001$ vs icilin without AMTB. Data is shown as mean ± SEM (Icilin, N= 3, AMTB 1pM+icilin, N=3, AMTB 1nM+icilin, N=3 and AMTB 1μM+icilin, N=3).

Table 5 Schild plot parameters for TRPM8 antagonists (AMTB) applied against TRPM8 agonist (Icilin)

Antagonist concentration (AMTB) M	**-log AMTB**	**Dose ratio (DR)**	**Log (DR-1)**	**EC_{50} (µM)**	**Emax %**
Control	-	-	-	0.23 ± 0.13	100.0 ± 0.0
1pM	12	1.08	-1.08	0.25 ± 0.01	86.5 ± 14.1
1nM	9	22.5	1.33	3.9 ± 2.2	85.2 ± 14.0
1µM	6	41.7	1.61	13.3 ± 3.5	40.1 ± 11.6

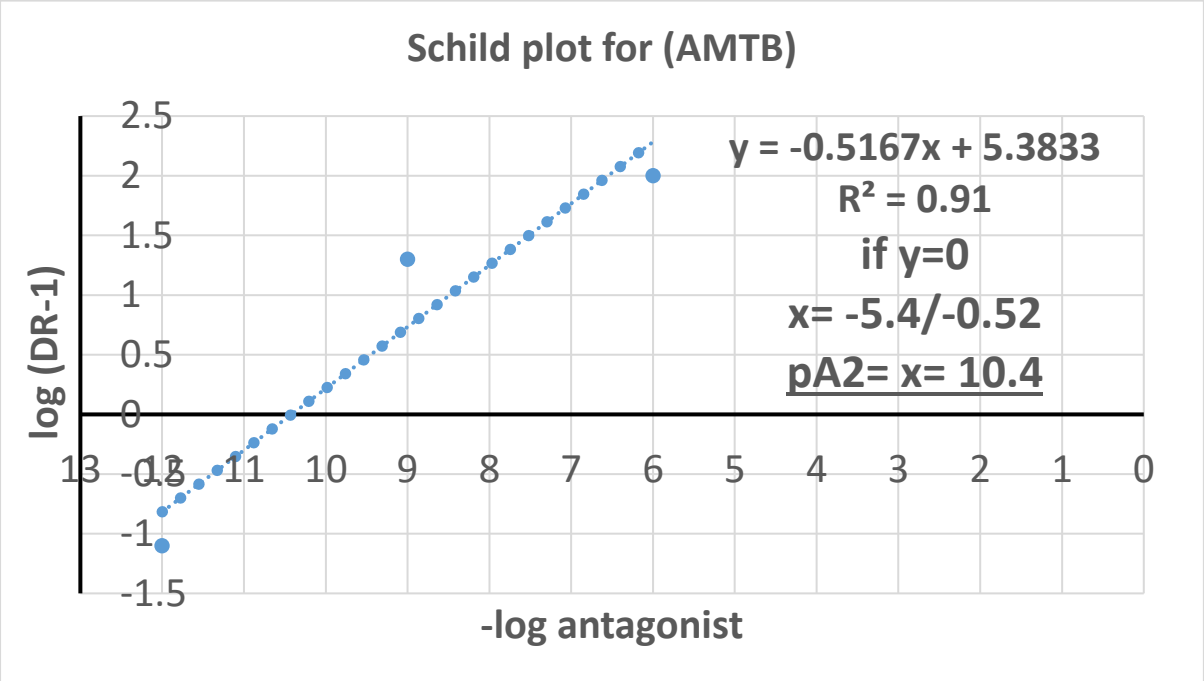

Figure 19. Schild plot for TRPM8 antagonist (AMTB) versus TRPM8 agonist (Icilin). pA2 is the point of intersection at x-axis and is graphically estimated as 10.4.

3.3.3. Carbachol-induced vasodilation in the presence of TRPV4 and TRPM8 antagonists

Carbachol-induced vasodilation was studied to examine the effect of blocking TRPV4 and/or TRPM8. These studies were conducted through utilising the TRPV4 antagonist (HC067047) and the TRPM8 antagonist (AMTB).

- TRPV4 antagonist did not significantly influence carbachol-induced vasodilation

Carbachol-induced vasodilation was examined before and after incubating the aortic ring with HC067047 (1µM). HC067047 was added for 1 hour before the aortic rings were constricted with NA (300nM) followed by carbachol CRC (30nM-300µM). TRPV4 antagonism did not show significant effect on carbachol CRC ($p \geq 0.05$). HC067047 did not show significant effect of carbachol-induced vasodilation (N=4, ns $p \geq 0.05$, EC_{50}= 2.0 ± 1.23µM and Emax= -64.0 ± 5.5% vs carbachol only EC_{50}= 1.02 ± 0.84µM and Emax= -76.1±3.0%) (Figure 20).

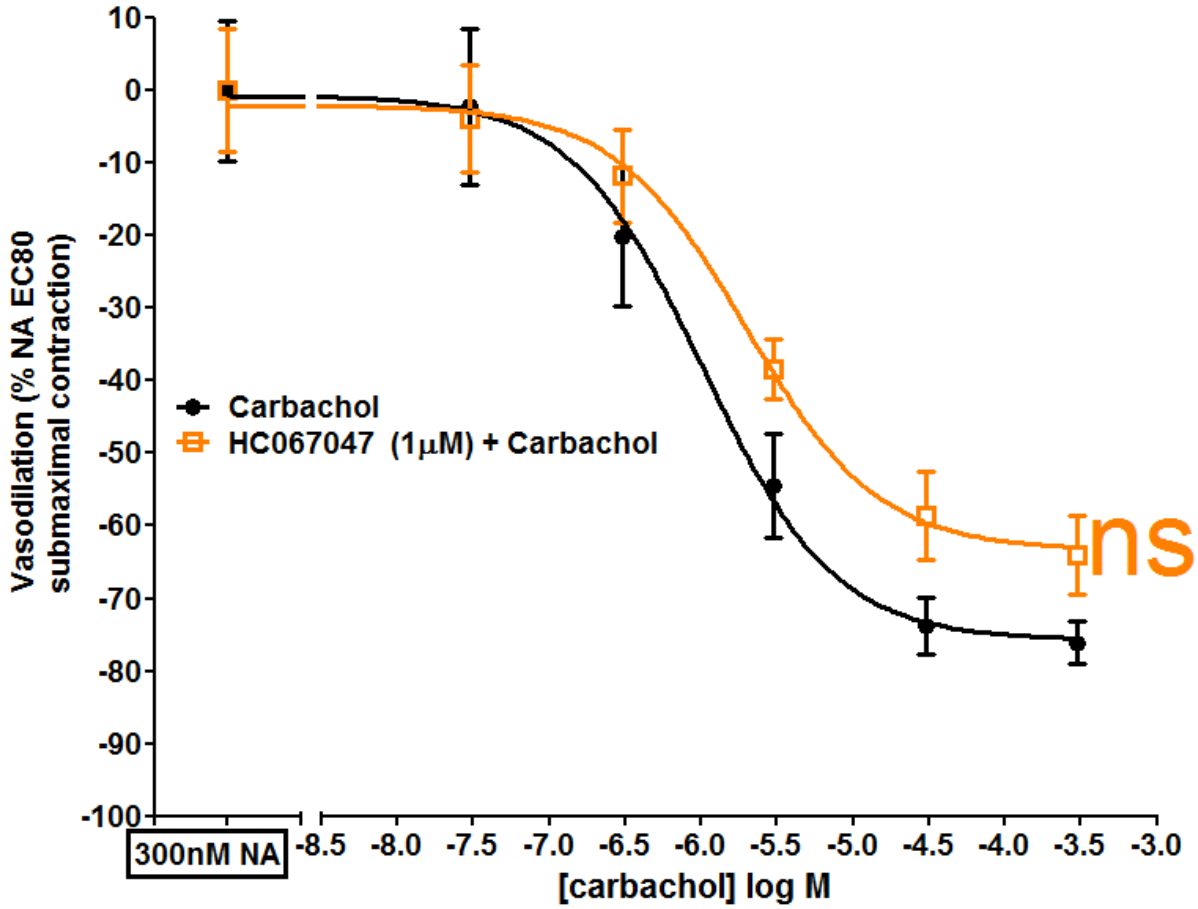

Figure 20. Carbachol cumulative concentration response curve in the presence and absence of TRPV4 antagonist (HC067047) (1µM). Analysed through two-way ANOVA with Bonferroni post-hoc test (ns $p \geq 0.05$) compared with carbachol in the absence of HC067047. Data is shown as mean ± SEM (Carbachol, N= 4, HC067047 1µM+carbachol, N=4).

- TRPM8 antagonist (AMTB) significantly compromised carbachol-induced vasodilation

Carbachol-induced vasodilation was examined in the presence and absence of AMTB (1μM). The antagonist was added for 1 hour before the aortic rings were contracted with NA (300nM) followed by carbachol cumulative concentration response curve (30nM-300μM). TRPM8 antagonism showed significant effect on carbachol CRC (*** $p < 0.001$) with significant reduction in carbachol-induced vasodilation (N=4, ns $p \geq 0.05$, EC_{50}= 2.7 ± 1.7μM vs carbachol only EC_{50}= 1.8 ± 1.05μM, and ** $p < 0.05$, Emax= 59.0 ± 10.4% vs carbachol only Emax= 80.8 ± 13.8%) (Figure 21).

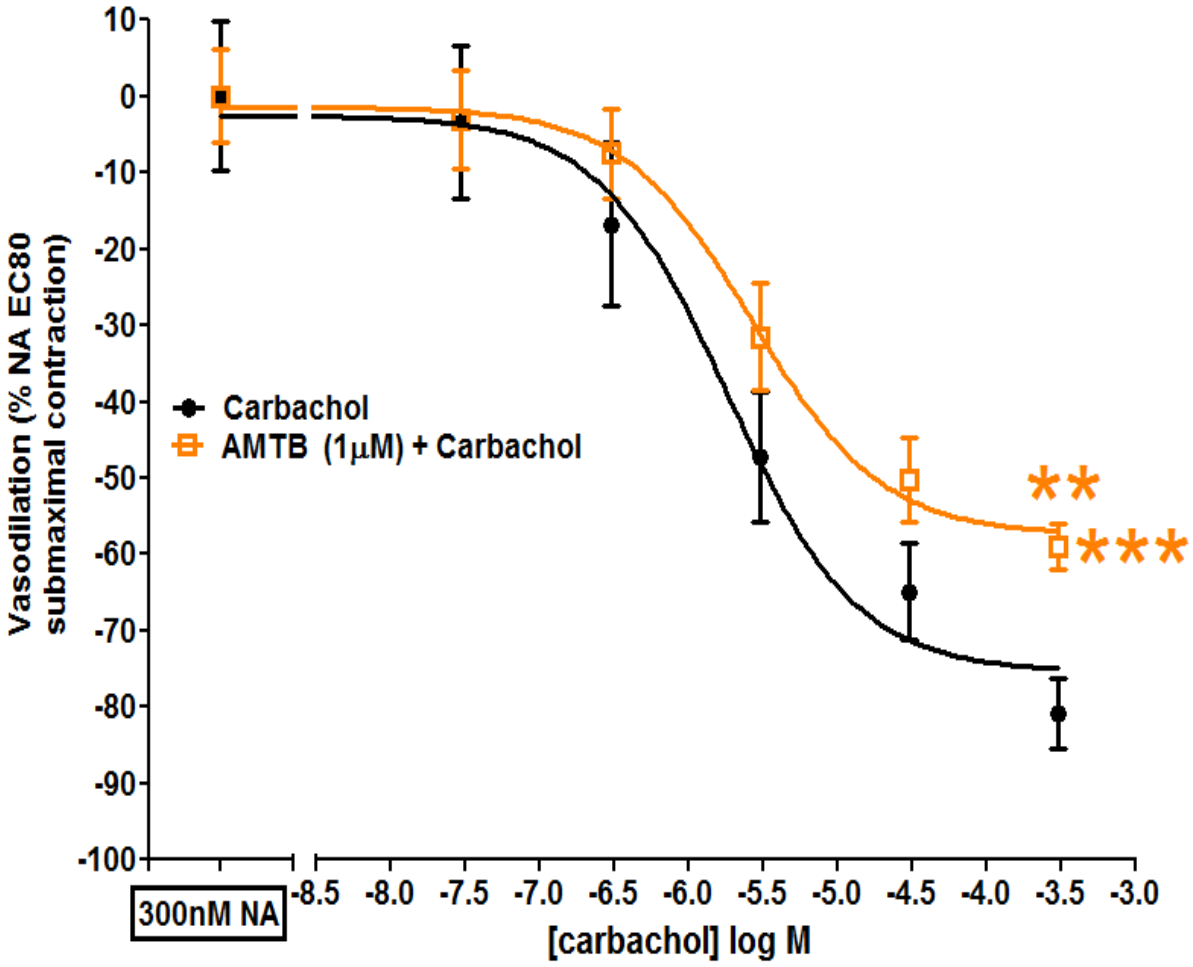

Figure 21. Carbachol cumulative concentration response curve in the presence and absence of TRPM8 antagonist (AMTB) (1μM). Analysed through two-way ANOVA with Bonferroni post-hoc test. Significance is shown as ** $p < 0.01$ and *** $p < 0.001$ compared with carbachol in the absence of AMTB. Data is shown as mean ± SEM (Carbachol, N= 4, AMTB 1μM+carbachol, N=4).

- TRPM8 antagonist (AMTB) and TRPV4 antagonist (HC067047) significantly compromised carbachol-induced vasodilation

Carbachol-induced vasodilation was examined in the presence and absence of both AMTB (1μM) and HC067047 (1μM). Both antagonists were added for 1 hour before the aortic rings were contracted with NA (300nM) followed by carbachol CRC curve (30nM-300μM) (Figure 22). The co-incubation of AMTB and HC067047 showed significant effect on carbachol CRC (*** $p < 0.001$) with significant reduction in carbachol-induced vasodilation (N=4, ns $p \geq 0.05$, EC_{50}= 3.1 ± 1.1μM vs carbachol only EC_{50}= 3.9 ± 2.2μM, and * $p < 0.05$, Emax= -44.3 ± 9.4% vs carbachol only Emax= -72.7 ± 6.9%) (Figure 22).

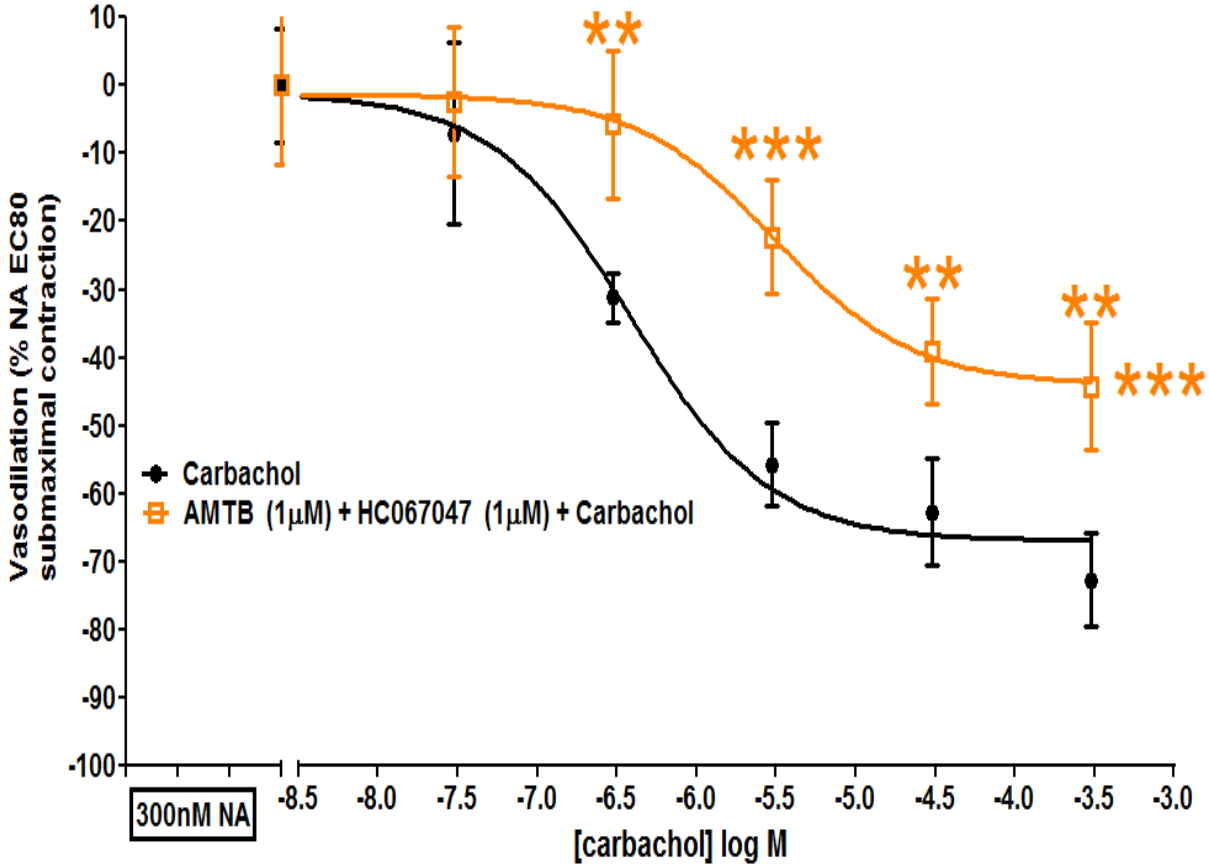

Figure 22. Carbachol cumulative concentration response curve in the presence and absence of both TRPM8 antagonist (AMTB) (1μM) and TRPV4 antagonist (HC067047) (1μM). Analysed through two-way ANOVA with Bonferroni post-hoc test. Significance is shown as ** $p < 0.01$ and *** $p < 0.001$ compared to carbachol in the absence of AMTB and HC067047. Data is shown as mean ± SEM (Carbachol, N= 4, AMTB 1μM+HC067047 1μM+carbachol, N= 4).

When comparing the effect of the application of both AMTB and HC067047 to the effect of each antagonist on the carbachol-induced vasodilation, there was significant change induced by the additional treatment (* $p < 0.05$). To investigate whether TRPM8 antagonism through AMTB added a significant effect to TRPV4 antagonism on carbachol-induced vasodilation, AMTB and HC067047 co-incubation (green) was compared with HC067047 incubated aortic rings (pink) through one-way ANOVA to investigate the treatment effect. Accordingly, TRPV4 antagonism showed non-significant effect on carbachol-induced vasodilation in the presence AMTB (green) when compared to the effect of HC067047 alone (pink) (N=4, ns $p \geq 0.05$ EC_{50}= 3.1 ± 1.0μM and Emax= 44.3 ± 9.4% vs EC_{50}= 2.0 ± 1.2μM and Emax 65.0 ± 5.5%) (Figure 23). Similarly, to investigate whether TRPV4 antagonism through HC067047 added a significant effect to TRPM8 antagonism on carbachol-induced vasodilation, AMTB and HC067047 co-incubation (green) was compared with AMTB incubated aortic rings (orange) through one-way ANOVA to investigate the treatment effect. Accordingly, HC067047 showed non-significant effect to AMTB (green) when compared to AMTB incubated artic rings (orange) (N=4, ns $p \geq 0.05$ EC_{50}= 3.1 ± 1.0μM and Emax= 44.3 ± 9.4% vs EC_{50}= 2.7 ± 1.7μM and Emax 65.0 ± 5.5%) (Figure 23).

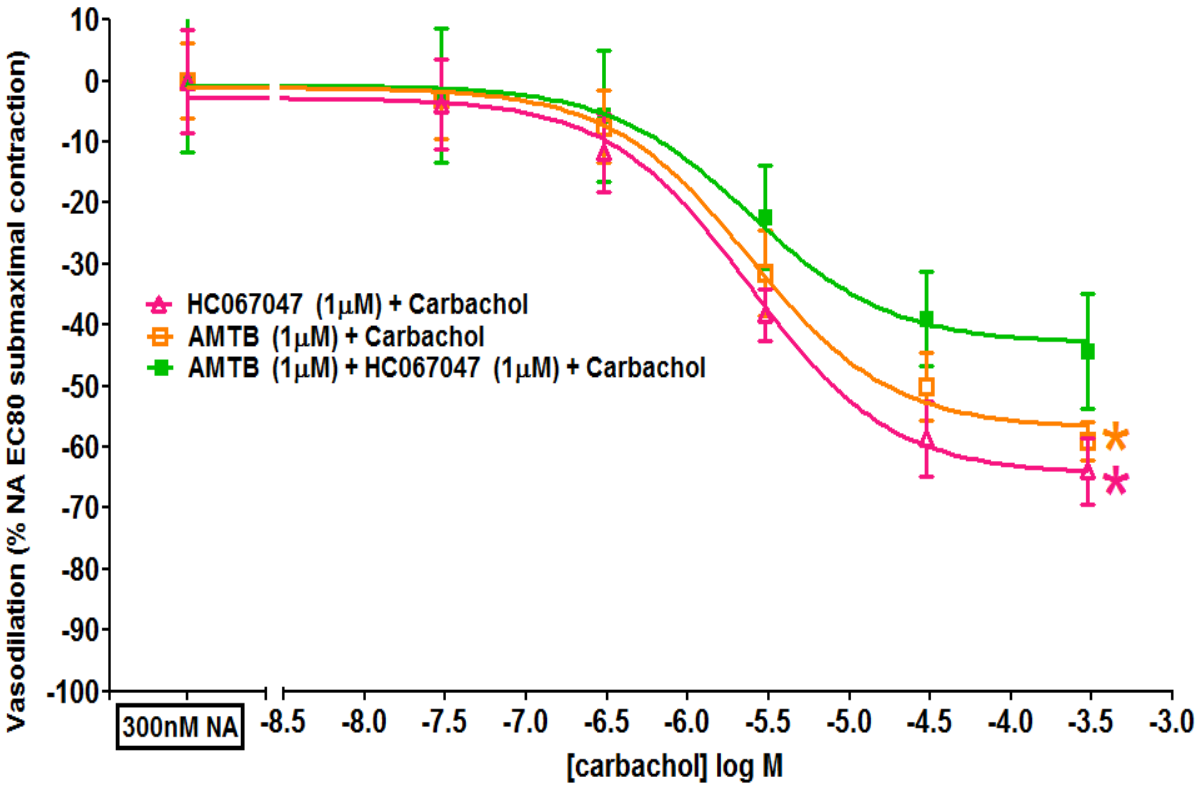

Figure 23. Carbachol-induced vasodilation in the presence of either TRPV4 antagonist (HC067047) or TRPM8 antagonist (AMTB) or both of the antagonists. Significance is shown as * $p < 0.05$ analysed through one-way ANOVA with Tukey post-hoc test.

3.3.4. TRPV4-induced vasodilation in the presence of TRPM8 antagonist

TRPV4-induced vasodilation was studied through examining the effect of blocking TRPM8. These studies were conducted through utilising TRPM8 antagonist (AMTB).

- TRPM8 antagonist (AMTB) did not show significant effect on TRPV4-induced vasodilation

TRPV4-induced vasodilation was examined in the presence and absence of AMTB (1μM). AMTB (1μM) was added for 1 hour before the aortic rings were contracted with NA (300nM) followed by 4-αPDD cumulative concentration response curve (3pM-3μM). AMTB (1μM) showed significant effect on 4-αPDD CRC (ns $p \geq 0.05$) without showing significant effect on 4-αPDD-induced vasodilation in Bonferroni post-hoc test (N=4, EC_{50}= 142 ± 89.6nM and Emax= -90.9 ± 2.8% vs 4-αPDD only EC_{50}= 156.3 ± 96.4nM and Emax= -74.3±8.2%) (Figure 24).

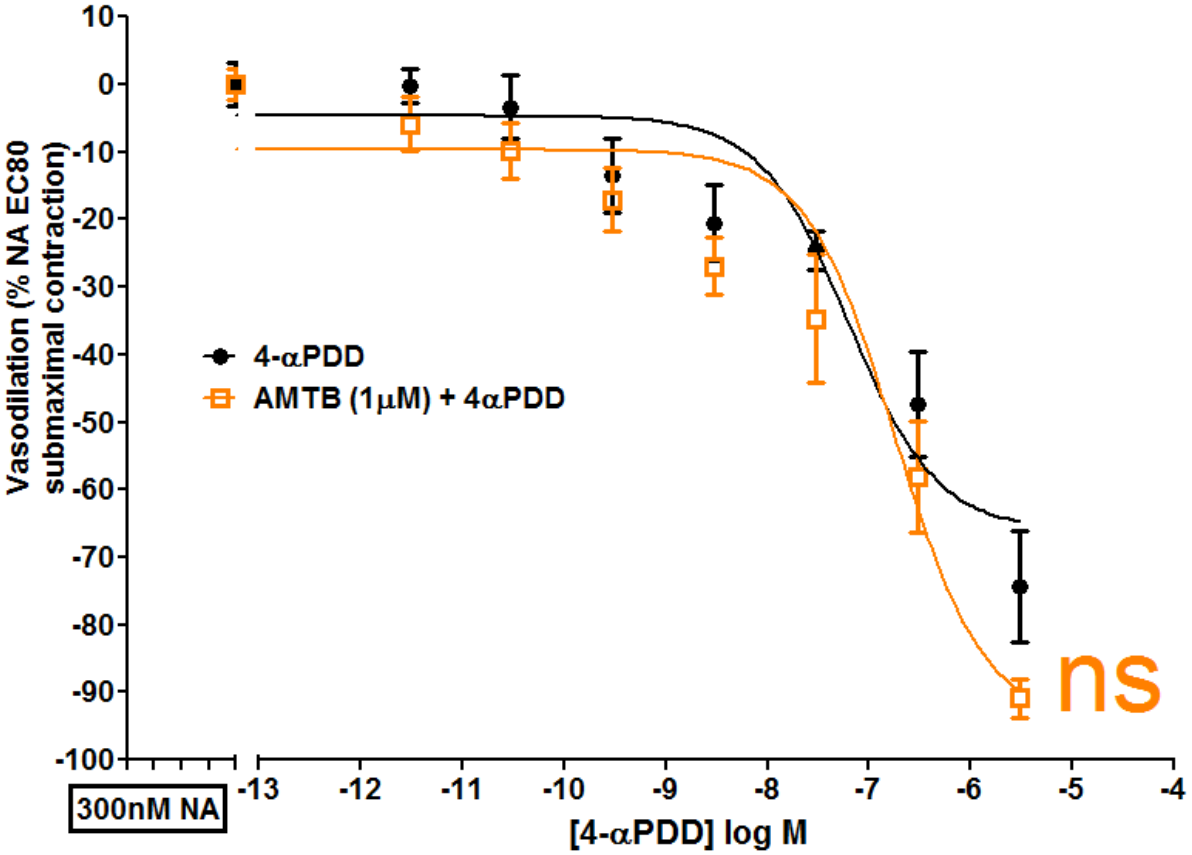

Figure 24. 4-αPDD cumulative concentration response curve in the presence and absence of TRPM8 antagonist (AMTB) (1μM). Analysed through two-way ANOVA (ns $p \geq 0.05$) with Bonferroni post-hoc test (ns $p \geq 0.05$) compared with 4-αPDD only. Data is shown as mean ± SEM (4α-PDD, N= 4, AMTB 1μM+4α-PDD, N= 4).

3.3.5. TRPM8-induced vasodilation in the presence of TRPV4 antagonist

TRPM8-induced vasodilation was studied through examining the effect of blocking TRPV4. These studies were conducted through utilising TRPV4 antagonist (HC067047).

- TRPV4 antagonist did not show significant effect on TRPM8-induced vasodilation

TRPM8-induced vasodilation was examined before and after incubating the aortic ring with HC067047 (1μM). HC067047 was added for 1 hour before the aortic rings were contracted with NA (300nM) followed by icilin cumulative concentration response curve (3nM-30μM). HC067047 (1μM) did not show significant effect on icilin CRC ($p \geq 0.05$). Icilin-induced vasodilation was not significantly affected through HC067047 incubation (N=3, Emax= -68.6 ± 13.1% vs icilin only Emax= -72.9 ± 8.4%) (Figure 25).

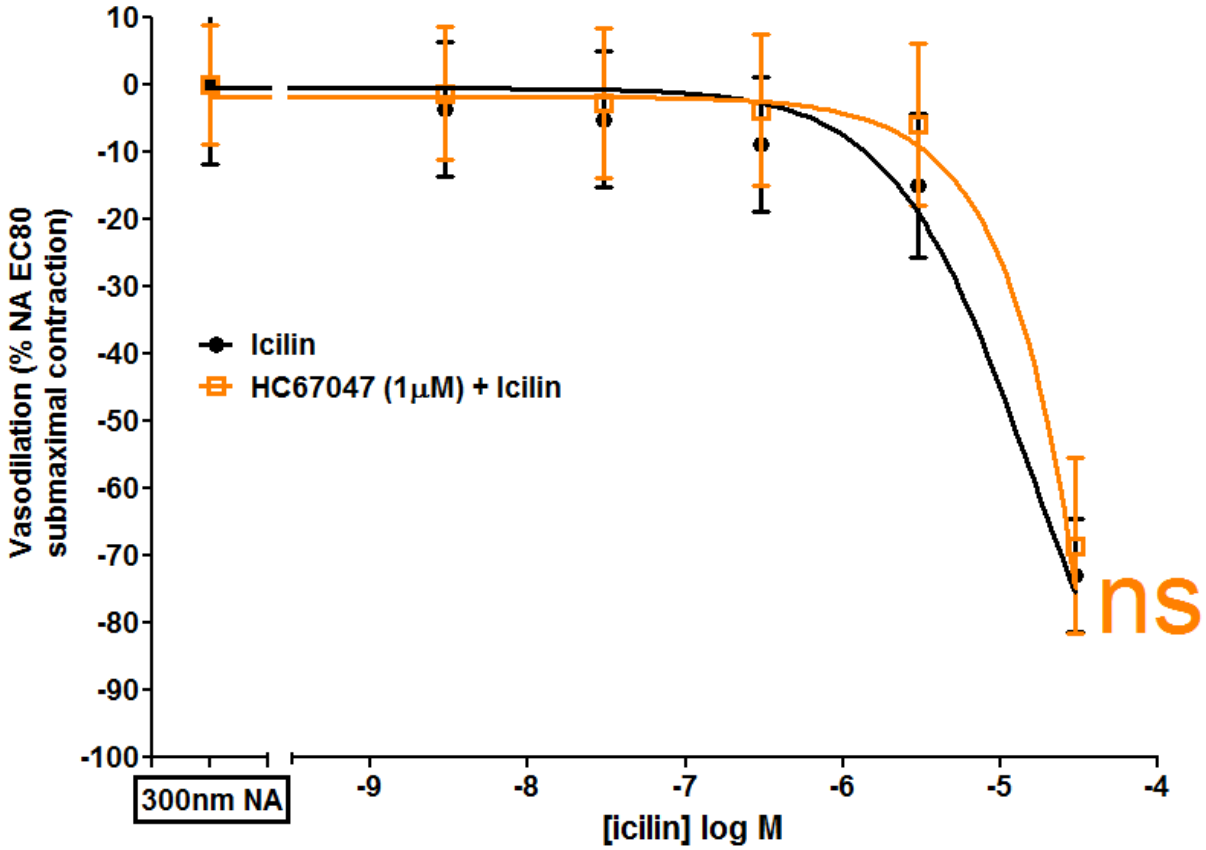

Figure 25. Icilin cumulative concentration response curve in the presence and absence of TRPV4 antagonist (HC067047) (1μM). Analysed through two-way ANOVA with Bonferroni post-hoc test (ns $p \geq 0.05$) compared with icilin in the absence of HC067047. Data is shown as mean ± SEM (Icilin, N= 3, HC067047 1μM+icilin, N= 3).

3.3.6. Nitric oxide synthase involvement in carbachol, TRPV4 and TRPM8-induced vasodilation

The role of NO and NOS in the muscarinic, TRPV4 and TRPM8-induced vasodilation was investigated through inhibiting NOS through incubating the freshly isolated aortic rings with L-NG-Nitro-L-arginine methyl ester (L-NAME) (100µM).

- L-NAME significantly reduced carbachol-induced vasodilation

Carbachol-induced vasodilation was examined in the presence and absence of NOS inhibitor, L-NAME (100µM). L-NAME was added for 30 minutes before the aortic rings were contracted with NA (300nM) followed by carbachol cumulative concentration response curve (30nM-300µM). L-NAME significantly influenced carbachol CRC (*** $p < 0.001$) with significant reduction in carbachol-induced vasodilation (N=4, *** $p < 0.001$, Emax= -11.3 ± 1.6% vs carbachol only Emax= -68.4 ± 2.3%). However, EC_{50} was not significantly influenced through L-NAME incubation (N=4, ns > 0.05, EC_{50}= 12.6 ± 1.6µM vs carbachol only EC_{50}= 2.2 ± 1.7µM) (Figure 26).

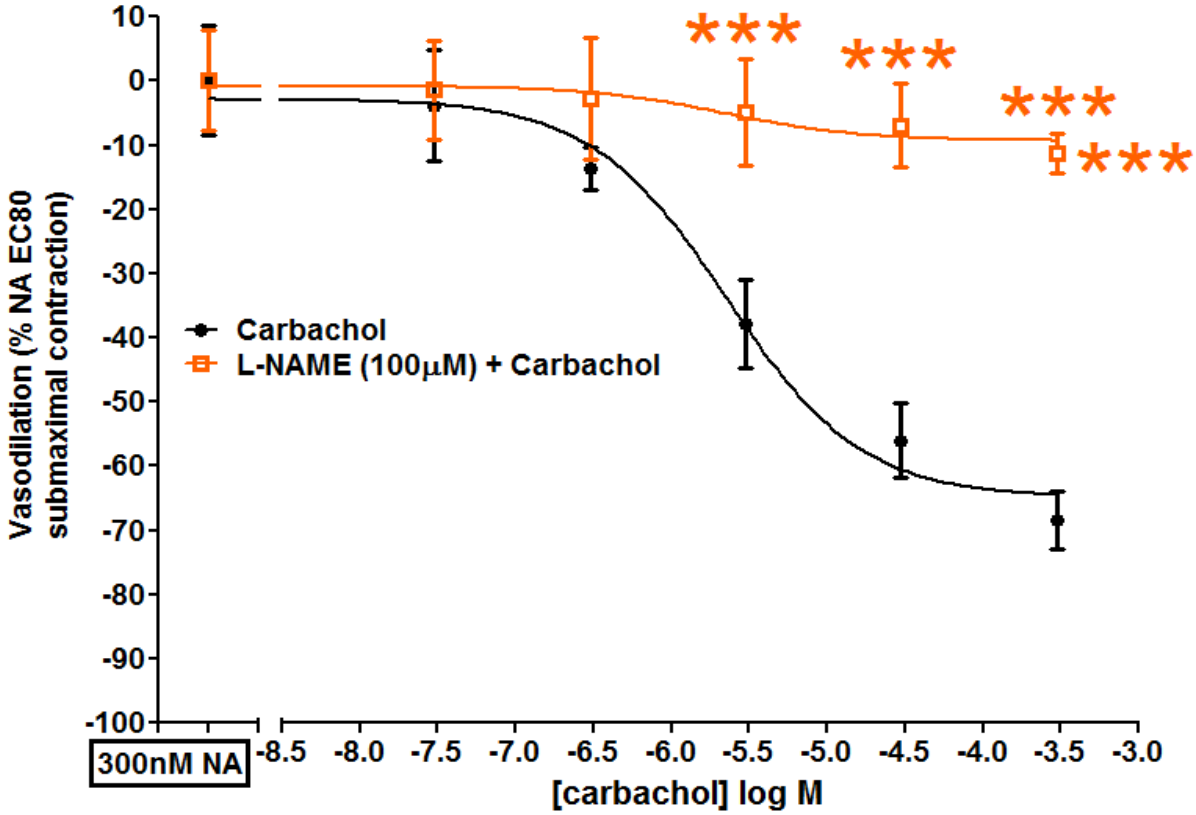

Figure 26. Carbachol cumulative concentration response curve in the presence and absence of the non-selective NOS inhibitor, L-NAME (100µM). Analysed through two-way ANOVA with Bonferroni post-hoc test. Significance is shown as *** $p < 0.001$ compared with carbachol in the absence of L-NAME. Data is shown as mean ± SEM (Carbachol, N= 4, L-NAME 100µM+carbachol, N= 4).

- L-NAME significantly influenced TRPV4-induced vasodilation

TRPV4-induced vasodilation was examined in the presence and absence of L-NAME (100µM). L-NAME was added for 30 minutes before the aortic rings were contracted with NA (300nm) followed by 4-αPDD cumulative concentration response curve (3pM-3µM). L-NAME significantly influenced 4-αPDD (*** $p < 0.001$) with significantly compromising 4-αPDD-induced vasodilation (N=4, *** $p < 0.001$, EC_{50}= 1.5 ± 1.0µM vs 4-αPDD only EC_{50}= 5.2 ± 3.4nM). Emax did not show significant difference (ns $p \geq 0.05$, Emax in the presence of L-NAME= -87.4 ± 2.2% vs 4-αPDD only Emax= -90.7 ± 4.7%) (Figure 27).

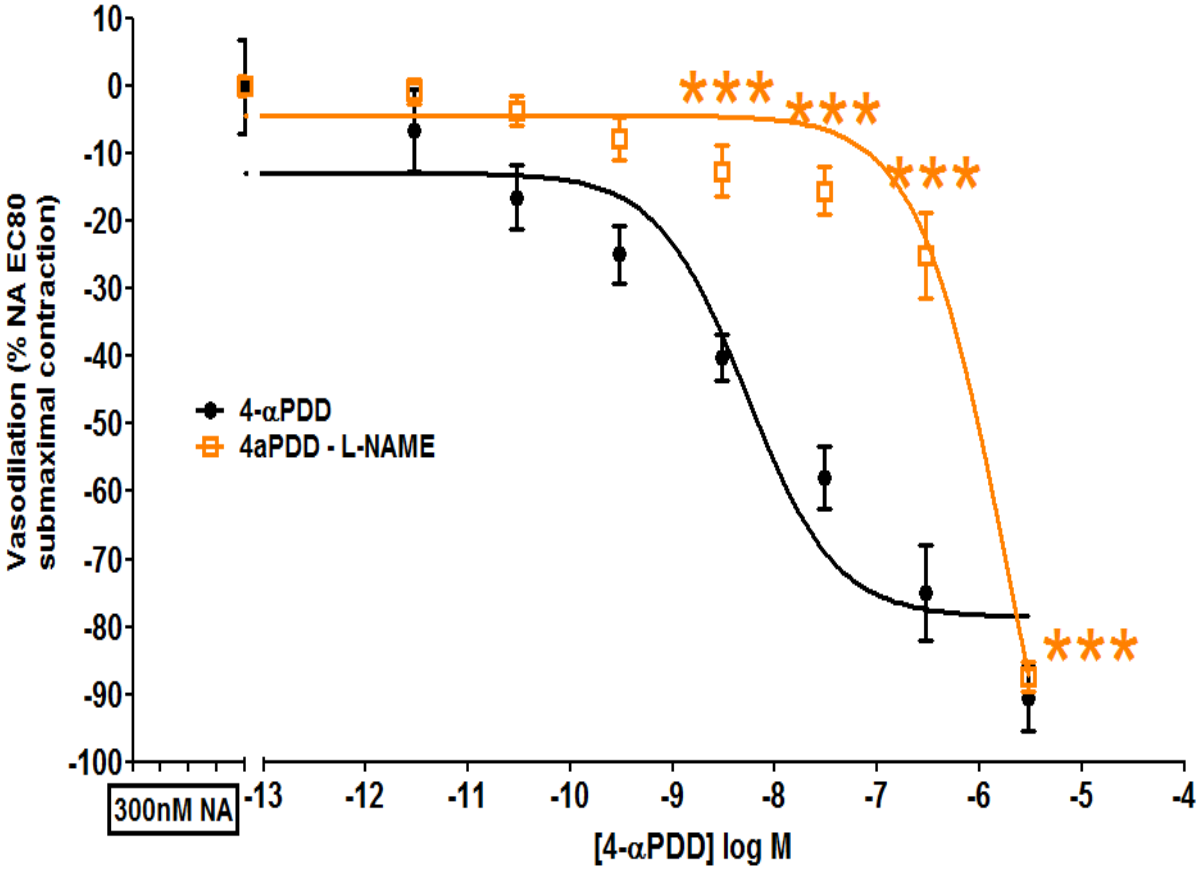

Figure 27. 4-αPDD cumulative concentration response curve in the presence and absence of NOS inhibitor (L-NAME) (100µM). Analysed through two-way ANOVA with Bonferroni post-hoc test. Significance is shown as *** $p < 0.001$ compared with 4-αPDD in the absence of L-NAME. Data is represented as mean ± SEM (4α-PDD, N= 4, L-NAME 100µM+4α-PDD, N= 4).

- L-NAME did not show significant effect on TRPM8-induced vasodilation

TRPM8-induced vasodilation was examined in the presence and absence of L-NAME (100µM). L-NAME was added for 30 minutes before the aortic rings were contracted with NA (300nM) followed by icilin cumulative concentration response curve (3nM-30µM). L-NAME did not show significant effect on icilin-induced vasodilation (N=6, ns $p \geq 0.05$, EC_{50}= 21.3 ± 9.7µM and Emax= -94.0 ± 2.4% vs icilin only EC_{50}= 7.5 ± 4.2µM and Emax= -79.4 ± 6.4%) (Figure 28).

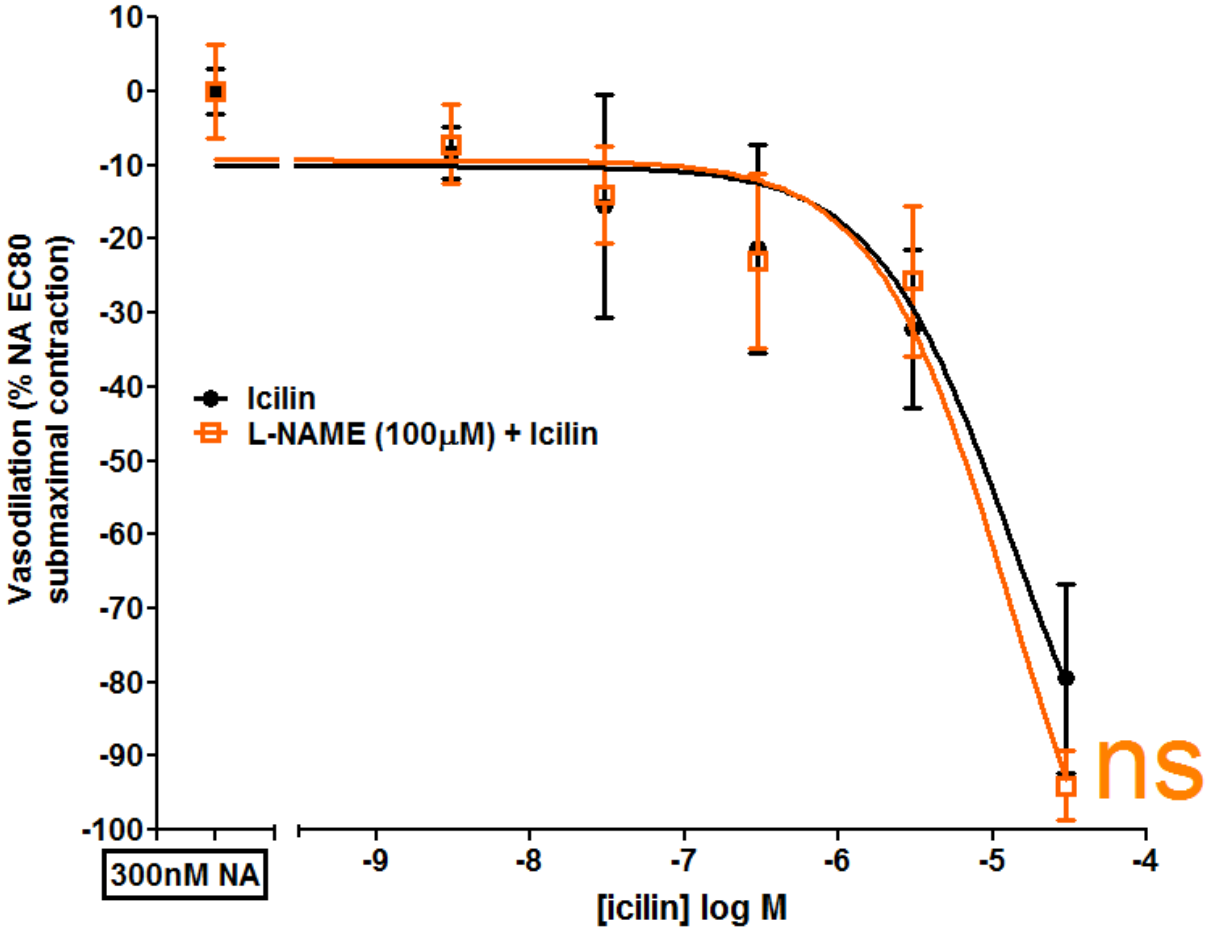

Figure 28. Icilin cumulative concentration response curve in the presence and absence of NOS inhibitor (L-NAME) (100µM). Analysed through two-way ANOVA with Bonferroni post-hoc test (ns $p \geq 0.05$) compared with icilin in the absence of L-NAME. Data is represented as mean ± SEM (Icilin, N= 4, L-NAME 100µM+icilin, N= 4).

3.3.7. The large conductance calcium-dependent potassium channels (BKca) involvement in carbachol, TRPV4 and TRPM8-induced vasodilation

The role of BKca in the carbachol, TRPV4 and TRPM8-induced vasodilation was investigated through inhibiting BKca by incubating the freshly isolated aortic rings with iberiotoxin (1-10nM).

- Iberiotoxin significantly compromised carbachol-induced vasodilation

Carbachol-induced vasodilation was examined in the presence and absence of BKca blocker, iberiotoxin (1nM). Iberiotoxin was added for 1 hour before the aortic rings were contracted with NA (300nM) followed by carbachol cumulative CRC (30nM-300µM). Iberiotoxin showed significant effect on carbachol CRC (*** $p < 0.001$) with significant reduction in carbachol-induced vasodilation (N=4, ns $p \geq 0.05$, EC_{50}= 1.5 ± 1.0µM vs carbachol only EC_{50}= 0.3 ± 0.19µM, and ** $p < 0.001$ Emax= -57.3 ± 3.5% vs carbachol only Emax= -87.9 ± 7.6%) (Figure 29).

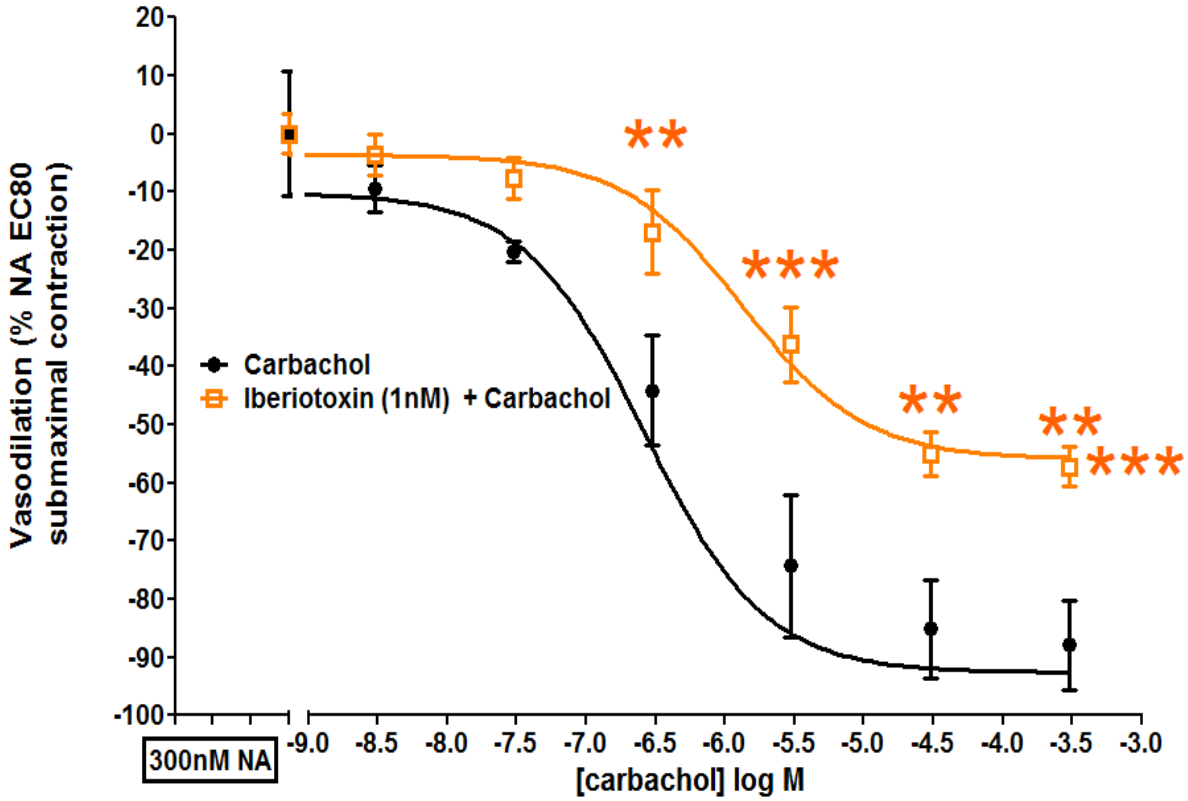

Figure 29. Carbachol cumulative concentration response curve in the presence and absence of BKca blocker (iberiotoxin) (1nM). Analysed through two-way ANOVA with Bonferroni post-hoc test. Significance is shown as ** $p < 0.01$ and *** $p < 0.001$ compared with carbachol-induced vasodilation in the absence of iberiotoxin. Data is represented as mean ± SEM (Carbachol, N= 4, iberiotoxin 1nM+carbachol, N= 4).

- Iberiotoxin significantly reduced TRPV4-induced vasodilation

TRPV4-induced vasodilation was examined in the presence and absence of iberiotoxin (1nM & 10nM). Iberiotoxin was added 1 hour before the aortic rings were contracted with NA (300nm) followed by 4-αPDD cumulative CRC (3pM-3μM). Iberiotoxin (10nM) significantly compromised 4-αPDD-induced vasodilation (*** $p < 0.001$) (N=4, * $p < 0.05$, EC_{50}= 403.7 ± 101.4nM vs 4-αPDD only EC_{50}= 25.1 ± 14.1nM). Maximum vasodilation showed significant difference (* $p < 0.05$, Emax= -46.2±12.0% vs 4-αPDD only Emax= -81.4±5.7%) (Figure 30a). However, iberiotoxin (1nM) did not show significant effect on TRPV4 function. Iberiotoxin (1nM) showed significant effect on 4-αPDD potency (N=2, * $p < 0.05$, EC_{50}= 3.0 ± 1.5nM vs 4-αPDD only EC_{50}= 38.4 ± 18.0nM). However, iberiotoxin (1nM) did not show significant effect on the maximum vasodilation (N=2, $p \geq 0.05$, Emax= -92.4 ± 5.0% vs 4-αPDD only Emax= -93.7 ± 2.2%) (Figure 30b).

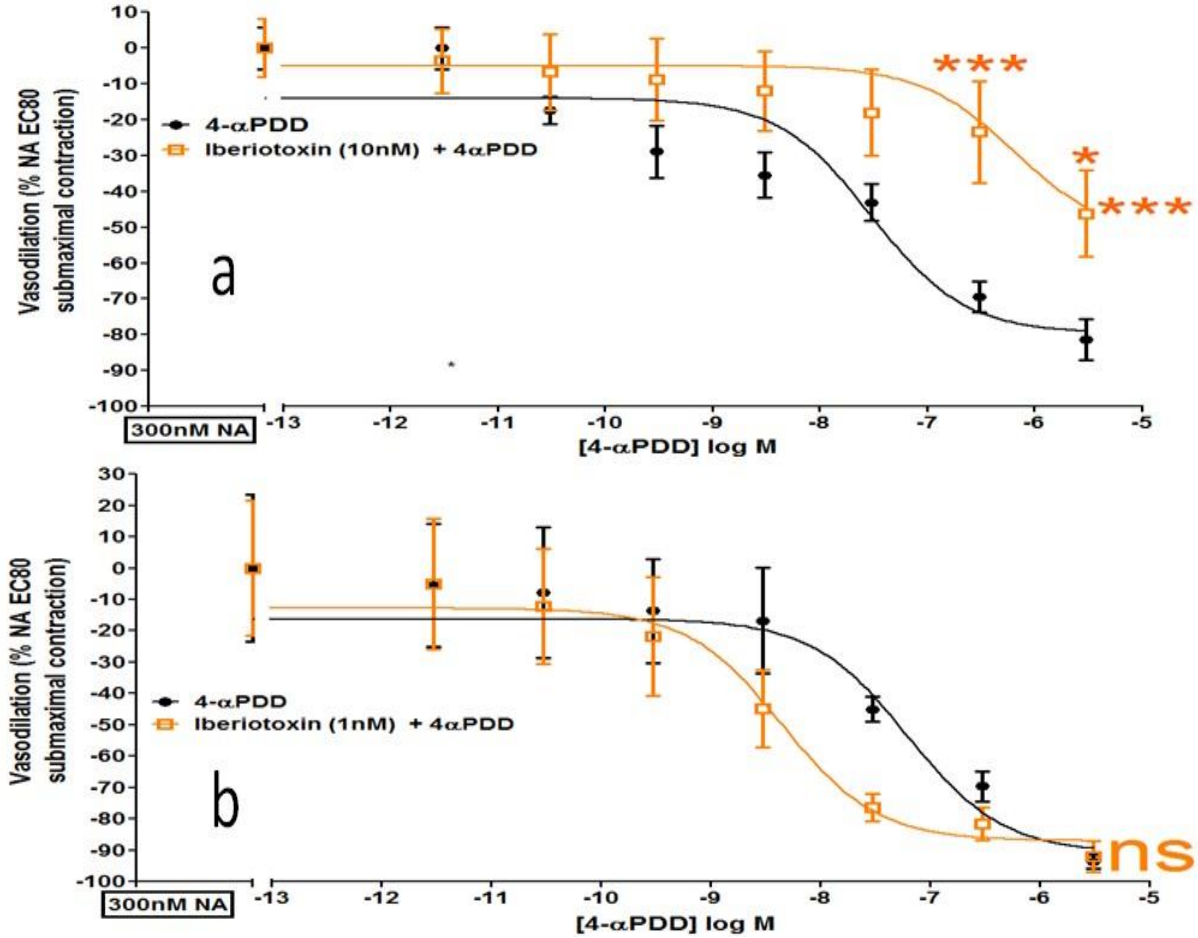

Figure 30. 4-αPDD cumulative concentration response curve in the presence of BKca blocker (Iberiotoxin) (1nM & 10nM). Analysed through two-way ANOVA with Bonferroni post-hoc test. Significance is represented as * $p < 0.05$ and *** $p < 0.01$ compared with 4-αPDD only. Data is represented as mean ± SEM (4-αPDD, N= 4, iberiotoxin 10nM+4-αPDD, N= 4 and iberiotoxin 1nM+4-αPDD, N= 2).

- Iberiotoxin showed significant effect on TRPM8-induced vasodilation

TRPM8-induced vasodilation was examined in the presence and absence of iberiotoxin (1nM). Iberiotoxin was added for 1 hour before the aortic rings were contracted with NA (300nM) followed by icilin cumulative CRC (3nM-30μM). Iberiotoxin showed significant effect on icilin-induced vasodilation (* $p < 0.05$) (N=3, ns $p \geq 0.05$, EC_{50}= 6.6 ± 1.9μM vs icilin only EC_{50}= 5.7 ± 2.5μM, and * $p < 0.05$ Emax= -40.1 ± 5.7% vs carbachol only Emax= -82.7 ± 6.9%) (Figure 31).

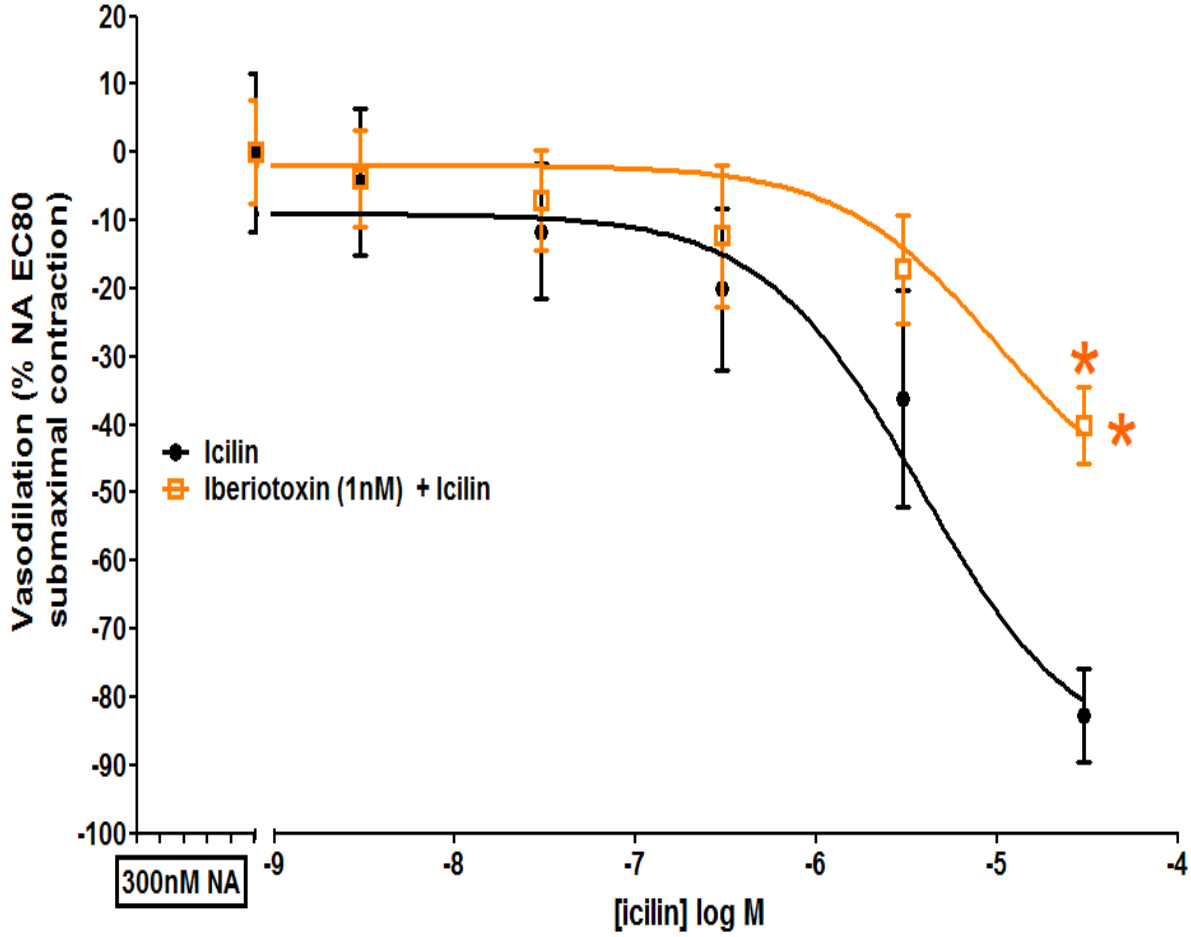

Figure 31. Icilin cumulative concentration response curve in the presence and absence of BKca blocker (Iberiotoxin) (1nM). Analysed through two-way ANOVA with Bonferroni post-hoc test. Significance is represented as * $p < 0.05$ versus icilin only CRC. Data is represented as mean ± SEM (Icilin, N= 3, iberiotoxin 1nM+icilin, N= 3).

3.3.8. Endothelium involvement in carbachol, TRPV4 and TRPM8-induced vasodilation

Since, NOS inhibition showed significant compromise of the muscarinic and TRPV4-induced vasodilation, but not TRPM8-induced vasodilation. Endothelium denuding was proposed as a strategy to investigate the role of endothelium components including eNOS and whether the targeted receptors or channels are expressed in the tunica media.

- Endothelium denuding showed significant suppression of carbachol-induced vasodilation

Aortic rings were rubbed with a cotton thread to mechanically remove the endothelium. Afterward, the aortic rings were contracted with NA (300nM) followed by carbachol cumulative CRC (30nM-300µM). Endothelium denuding showed significant reduction in carbachol-induced vasodilation (N=5, *** $p < 0.001$, Emax= -16.6 ± 4.8% vs intact endothelium carbachol induced-vasodilation Emax= -68.4 ± 2.3%) (Figure 32). However, the EC_{50} was not significantly influenced (N=5, $p \geq 0.05$, EC_{50}= 3.8 ± 0.6µM and vs intact endothelium carbachol induced-vasodilation EC_{50}= 1.8 ± 1.1µM) (Figure 52).

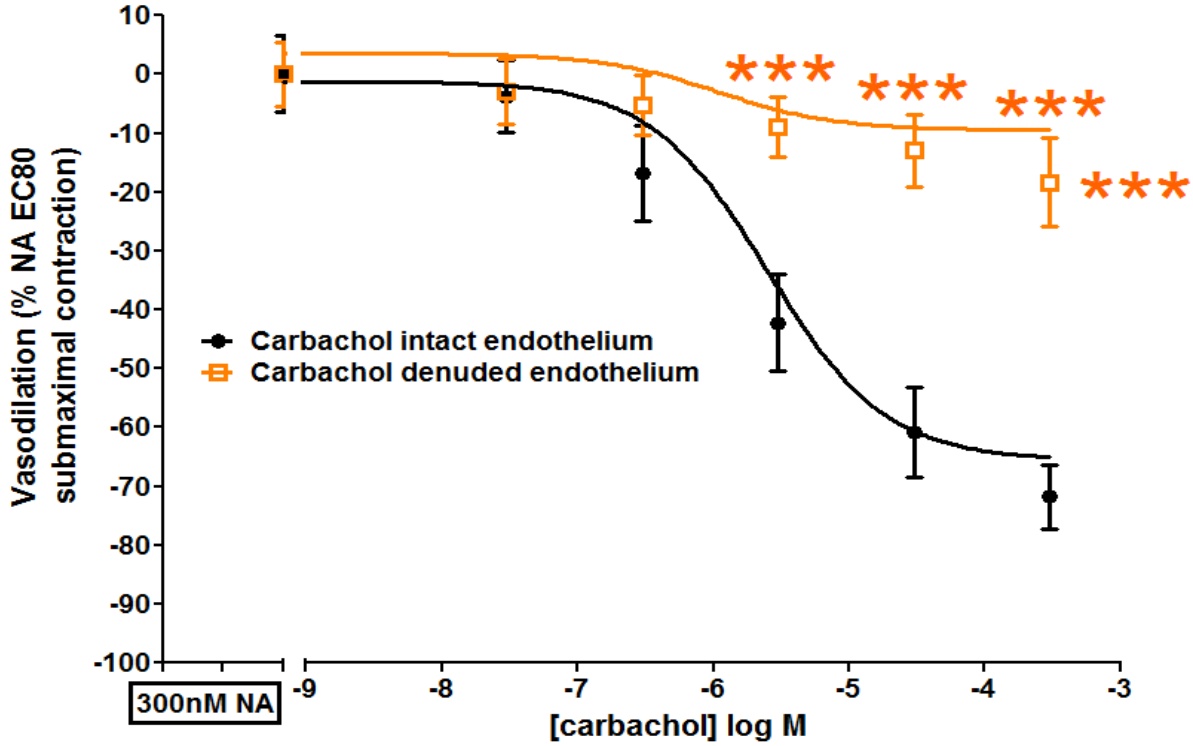

Figure 32. Carbachol cumulative concentration response curve when endothelium was denuded. Analysed through two-way ANOVA with Bonferroni post-hoc test. Significance is shown as *** $p<0.001$ versus carbachol-induced vasodilation in intact endothelium aortic rings. Data is represented as mean ± SEM (Carbachol, N= 5, denuded endothelium + carbachol, N= 5).

- Endothelium denuding showed significant suppression of TRPV4-induced vasodilation

After confirming the removal of the endothelium through the significant impairment of carbachol-induced vasodilation (Figure 32), the aortic rings were contracted with NA (300nM) followed by 4-αPDD cumulative CRC (3pM-3μM). Endothelium denuding showed significant reduction in 4-αPDD-induced vasodilation (*** $p < 0.001$). Endothelium denuding significantly compromised 4-αPDD-induced vasodilation (N=4, * $p < 0.05$ maximum vasodilation -58.7 ± 9.5% vs intact endothelium 4-αPDD-induced maximum vasodilation -89.3 ± 4.0%). However, endothelium denuding did not show significant influence on 4-αPDD potency (N=4, ns $p \geq 0.05$, EC_{50}= 7.5 ± 2.9nM vs intact endothelium with 4-αPDD-induced vasodilation EC_{50}= 5.4 ± 3.5nM) (Figure 33).

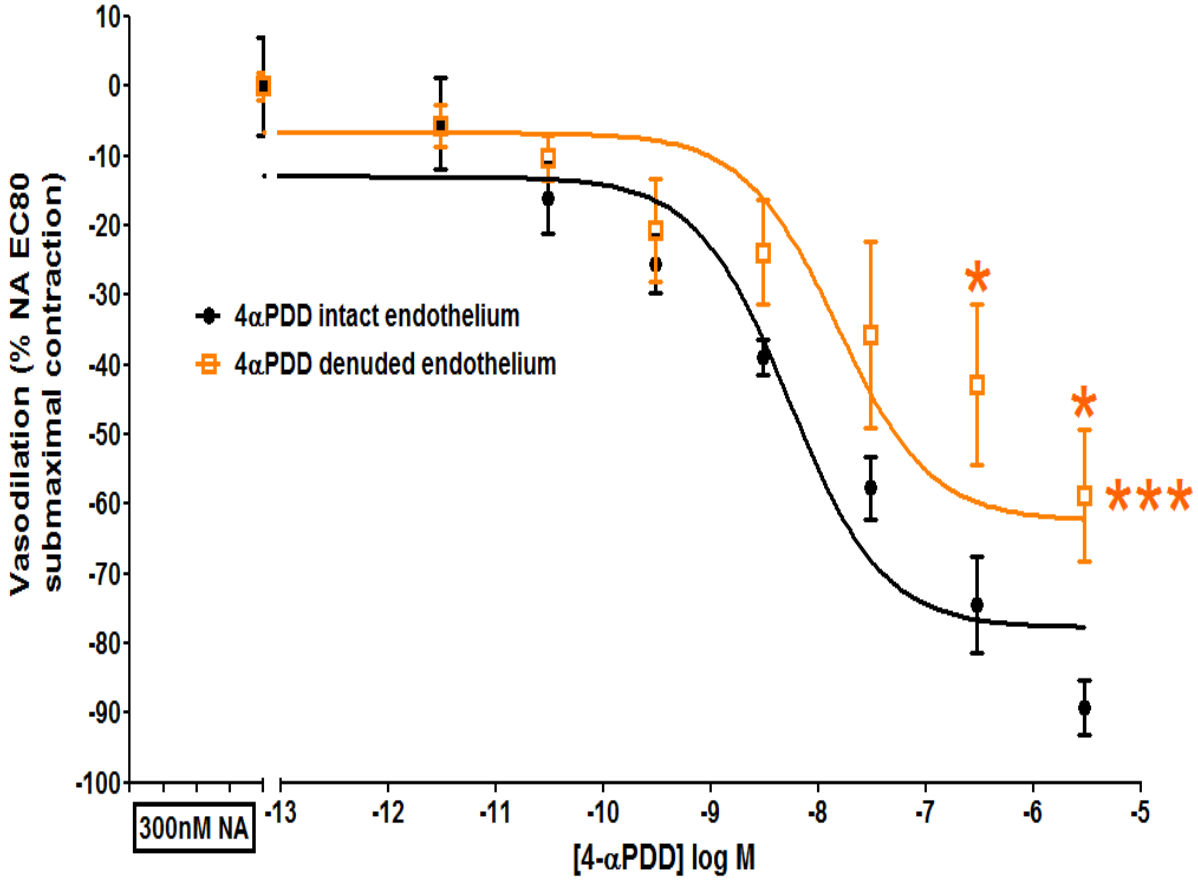

Figure 33. 4-αPDD cumulative concentration response curve when endothelium was denuded. Analysed through two-way ANOVA with Bonferroni post-hoc test. Significance is shown as * $p < 0.05$ and *** $p < 0.01$ versus 4-αPDD-induced vasodilation in intact endothelium aortic rings. Data is represented as mean ± SEM (4α-PDD, N= 4, L-denuded endothelium+4α-PDD, N= 4).

- Endothelium denuding did not show significant suppression of TRPM8-induced vasodilation

After confirming the removal of the endothelium through the significant impairment of carbachol-induced vasodilation (Figure 32), the aortic rings were contracted with NA (300nM) followed by icilin cumulative CRC (3nM-30μM). Endothelium denuding showed significant reduction in icilin-induced vasodilation (** $p < 0.01$). However, Bonferroni post-hoc test did not show significant difference among the applied concentrations (N=3, ns $p \geq 0.05$, EC_{50}= 5.3 ± 3.2μM and maximum vasodilation -67.4±9.67% vs intact endothelium icilin-induced vasodilation EC_{50}= 1.3 ± 0.7μM and maximum vasodilation -82.1 ± 1.3%) (Figure 34).

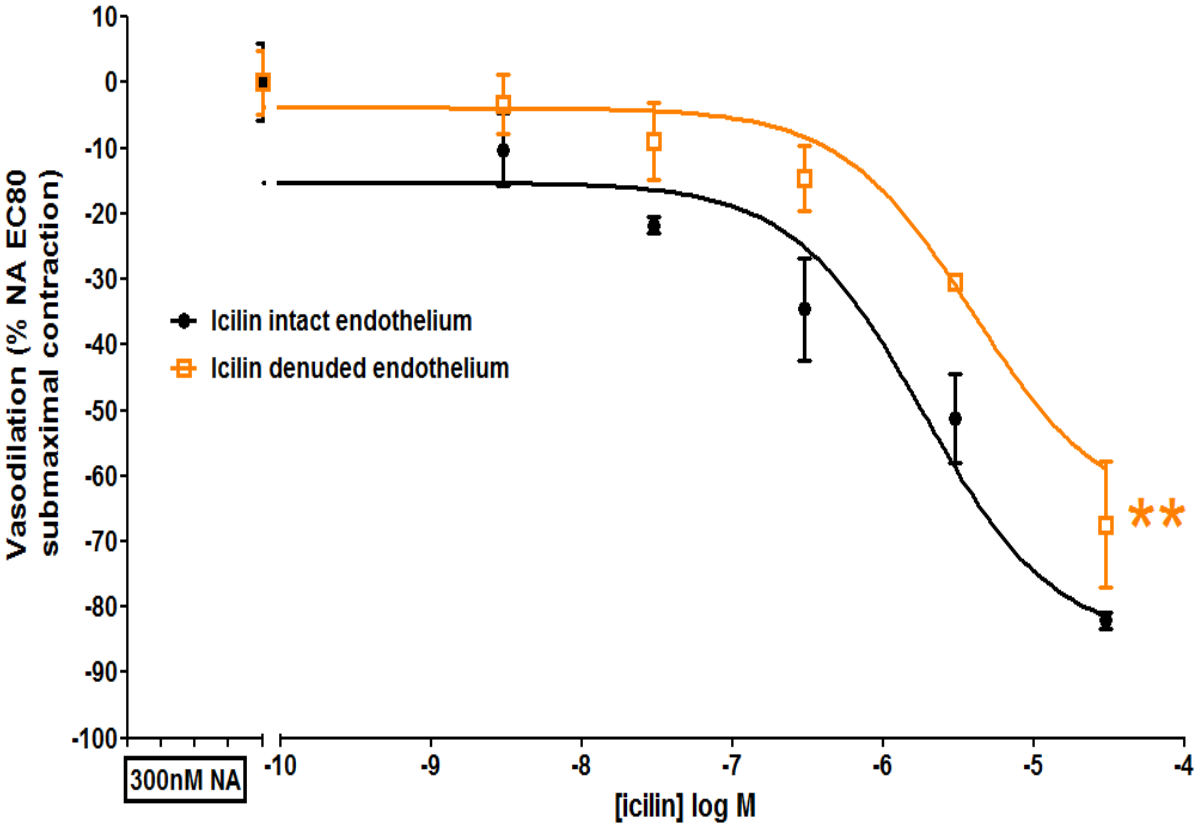

Figure 34. Icilin cumulative concentration response curve when endothelium was denuded. Analysed through two-way ANOVA with Bonferroni post-hoc test versus icilin-induced vasodilation in intact endothelium aortic rings. Data is represented as mean ± SEM (Icilin, N= 3, denuded endothelium+icilin, N= 3).

3.3.9. Experiments visual summary

The conducted experiments are summarised in the following figure where the arrow is stemmed from the blocked channel (TRPM8 ⟶cc-induced vasodilation, means the effect of blocking TRPM8 on carbachol-induced vasodilation).

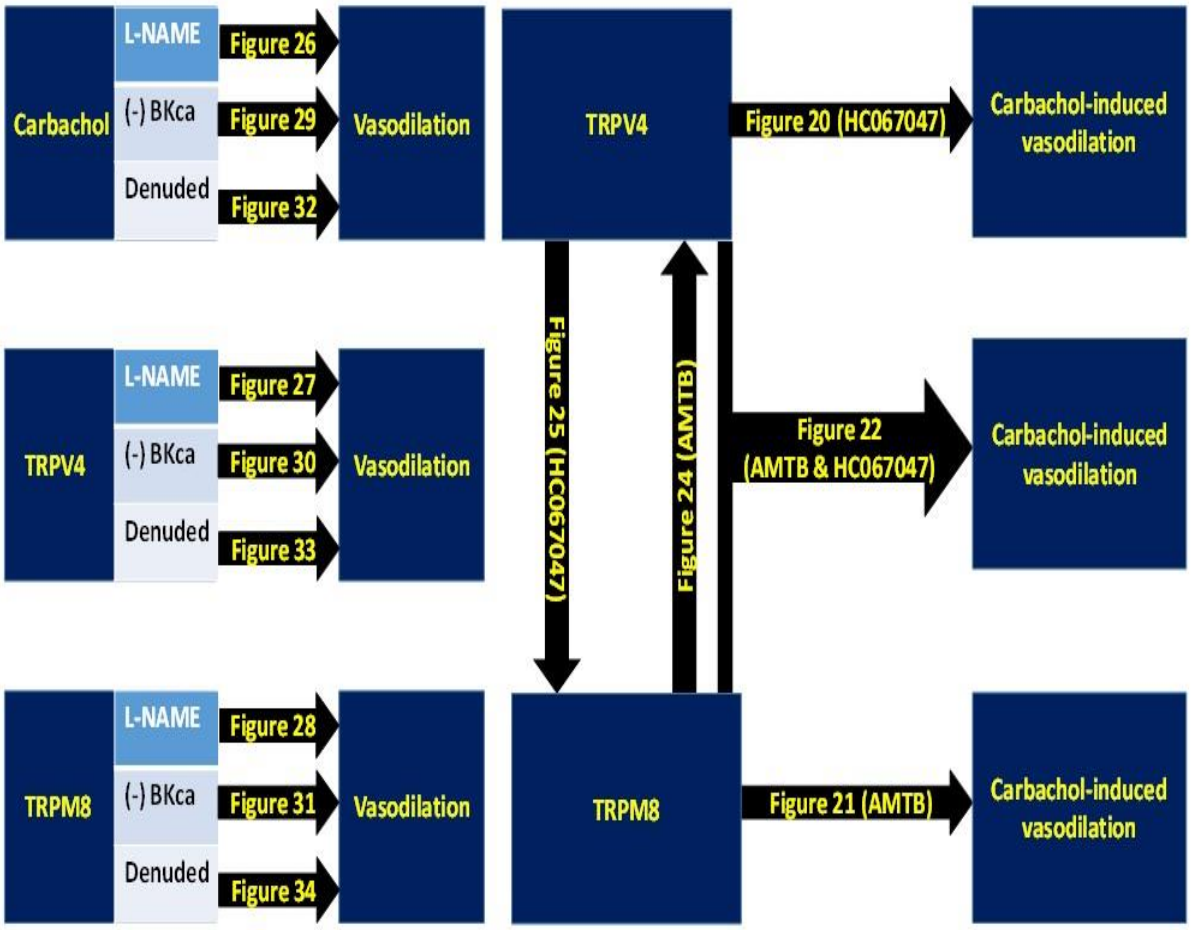

Figure 35. Chapter 3 experiments summary. The arrows are stemmed from the blocked channels/cellular components and labelled with the correspondent figure.

3.4. Discussion

In this chapter, firstly, consensus EC_{80} of NA (300nM) (Figure 14) was estimated which was similar to what was found previously (Verbeuren et al., 1986). Such experiment was conducted to spare the time for further experiments instead of constructing NA CRC for every tissue which might stress the tissue upon cumulative repeated contractions.

Antagonists' studies were conducted to estimate the pA2 and to prove that the applied concentrations are relevant to block the targeted channel. Therefore, when HC067047 (1μM) was applied for 1 hour incubation period, it showed significant suppression with EC_{50}= 103.7 ± 42.0nM and Emax= 26.8 ± 4.2% vs RN-1747 without HC067047 EC_{50}= 46.7 ± 35.3nM and Emax= 52.6 ± 3.9% (Figure 16). pA2 was calculated and estimated as 8.7 which was around the value estimated through previous research where pA2= 7.8 (L. Zhang et al., 2013). Previous studies showed that the efficacy of RN-1747 (EC_{50}= 4.1μM) is similar to 4-αPDD (EC_{50}= 4.4μM) against rat TRPV4 (Vincent & Duncton, 2011). However, RN-1747 activates human TRPV1 with 25% of the capsaicin's Emax and antagonises TRPM8 (Vincent & Duncton, 2011). Therefore, the residual RN-1747-induced vasodilation might be attributed to TRPV1 activation. By contrast, 4-αPDD is a small phorbol ester molecule that activates TRPV4 selectively (Vincent & Duncton, 2011).

TRPM8 antagonist, AMTB showed significant effect on icilin-induced vasodilation at the highest applied concentration (1μM). Therefore, when AMTB (1μM) was applied for 1 hour incubation period, it showed significant suppression with EC_{50}= 13.6 ± 3.4μM and Emax= 34.1 ± 10.5% vs icilin without AMTB EC_{50}= 223.4 ± 125.6nM and Emax= 83.8 ± 2.0% (Figure 18). Icilin is a TRPM8 agonist (EC_{50}= 7μM) that was shown to activate TRPA1 when applied to hTRPA1 expressing *Xenopus laevis* oocytes at 100μM (Sherkheli, Gisselmann, Vogt-Eisele, Doerner, & Hatt, 2008; Sherkheli et al., 2010). Accordingly, icilin vasodilation might include some paradoxical pathways to TRPM8, through TRPA1 activation in the presence of the selective TRPM8 antagonist, AMTB. AMTB's pA2 was estimated graphically= 10.4 (Figure 19). To the best of our knowledge and according to the AMTB manufacturers' email, there has not been any published data regarding AMTB's pA2 (Lefevre, 2016).

Carbachol studies were conducted to examine the endothelium function where muscarinic receptors (M3) mediate eNOS phosphorylation and hence causes NO-dependent vasodilation (A. Dhar et al., 2010). The cross studies were conducted to investigate the involvement of

TRPV4 and TRPM8 in the muscarinic-induced vasodilation. Accordingly, TRPV4 inhibition through HC067047 (1μM) did not significantly influence the carbachol-induced vasodilation as shown in Figure 20. However, previous data showed significant effect of HC067047 (1μM) on acetylcholine-induced vasodilation in mouse cerebral arteries (D. X. Zhang et al., 2009). This might be attributed to species or vascular bed differences, if not both. However, AMTB (1μM) significantly decreased carbachol induced vasodilation (Figure 21). Blocking TRPV4 and TRPM8 showed further inhibition of carbachol-induced vasodilation with EC_{50}= 3.1 ± 1.1μM and Emax= 44.3 ± 9.4% vs carbachol only EC_{50}= 3.9 ± 2.2μM and Emax= 72.7±6.9% (Figure 22). When compared together, there was not significant difference among blocking TRPV4 alone (EC_{50}= 2.0 ± 1.2μM and Emax= 65.0±5.5%), TRPM8 alone (EC_{50}= 2.7 ± 1.7μM and Emax 65.0 ± 5.5%) or both TRPV4 and TRPM8 (EC_{50}= 3.1 ± 1.0μM and Emax= 44.3 ± 9.4%), suggesting that TRPV4 or TRPM8, if not both, might be involved in muscarinic-induced vasodilation (Figure 23). These findings suggested that carbachol, TRPV4 and TRPM8 might play major roles in mediating vasodilation.

Furthermore, TRPV4 cross studies were conducted which showed that TRPM8 has a significant effect on TRPV4 CRC without showing significant effect on any of the applied 4-αPDD concentrations (Figure 24). Moreover, TRPM8-induced vasodilation was studied through treating the freshly isolated rat aortic rings with icilin. HC067047 did not show a significant effect on TRPM8-induced vasodilation (Figure 25). Therefore, these findings confirm the selectivity of each applied blocker at the applied concentrations.

Further investigation on the muscarinic, TRPV4 and TRPM8 pathways included L-NAME studies. L-NAME is a non-selective blocker of NOS that competes with L-arginine, the NOS substrate required to generate NO (Buxton et al., 1993). The aortic rings were cleaned from the connective tissue including the removal of the outer vascular layer, adventitia neurons that express neuronal nitric oxide synthase predominantly. Moreover, the VSMCs express iNOS that generates synthesise NO independent from CaM complex and phosphorylation (Arnal, Dinh-Xuan, Pueyo, Darblade, & Rami, 1999; Lüscher & Barton, 1997). However, eNOS is the predominant NOS isoform in the endothelium and it generates NO through a signalling cascade that requires CaM complex and enzyme phosphorylation to become active (Lüscher & Barton, 1997). Therefore, L-NAME treatment was hypothesised to inhibit eNOS as it is the constitutively expressed NOS isoform found in the endothelium (Cines et al., 1998).

Muscarinic endothelial vasodilation was NO-dependent, as eNOS inhibition with L-NAME showed significant suppression of carbachol-induced vasodilation (Figure 26). Moreover, TRPV4-induced vasodilation through 4-αPDD was also NO-dependent, however, other significant vasodilation pathways might be involved as the concentration response curve in the presence of L-NAME was surmountable with Emax of approximately 90% (Figure 27). By contrast, NO might not play a major role in TRPM8-induced vasodilation, as icilin treatment was not significantly affected by L-NAME incubation (Figure 28). These findings suggest that muscarinic and TRPV4 vasodilatory effects are NO-mediated, however TRPM8 exerts its vasodilation effect through different pathways. Therefore, although blocking TRPM8 with or without TRPV4 showed significant effect on muscarinic vasodilatory pathway (Figure 21 & 30), the intracellular pathway of TRPM8-induced vasodilation was not NO-dependent (Figure 28). This suggests TRPM8 as an extra signalling pathway to muscarinic-induced vasodilation. Moreover, muscarinic and TRPV4 vasodilatory pathways might share eNOS as a major vasodilatory intracellular component since both pathways were significantly inhibited by L-NAME (Figure 26 & 35).

These findings were in agreement with previous studies that revealed the dependence of endothelial muscarinic receptors on NO pathway for vasodilation (Buxton et al., 1993; Lopacinska & Strosznajder, 2005). Moreover, TRPV4 binds to a docking lipid raft, caveolae that is found in the ECs plasma membrane (Everaerts et al., 2010). Such lipid rich complexes might link TRPV4 to eNOS, so the TRPV4-facilitated Ca^{2+} influx will encourage NO release (Köhler et al., 2006).

TRPM8 showed NO-independent vasodilation, which is similar to a previous in vivo study on Sprague-Dawley rats demonstrated NO-independence of TRPM8-induced vasodilation in cutaneous arteries. However, this study indicated that TRPM8 is able to induce vasodilation as well as vasoconstriction, depending on the previous vasomotor tone as it related such effects to VSMCs only (C. D. Johnson et al., 2009).

To sum up the NO-dependent study, L-NAME abolished carbachol-induced vasodilation and partially inhibited TRPV4-induced vasodilation, revealing that NO is not the only vasodilation contributor in aorta (Figure 27). Whereas, TRPM8 might exert its vasodilatory function independent of NO (Figure 28).

EDHF provides a secondary vasodilation system to NO pathway (Garland et al., 1995; McCulloch, Bottrill, Randall, & Hiley, 1997). Furthermore, elevated $[Ca^{2+}]_i$ as consequence

of TRPV4 activation, activates Kca channels, SKca and IKca that yield endothelium hyperpolarisation which propagates through gap junctions into VSMCs and thereby causes vasodilation (Edwards, Félétou, & Weston, 2010).

Further studies were conducted to examine the involvement of BKca in muscarinic, TRPV4 and TRPM8-induced vasodilatory pathways. Incubating the aortic rings with iberiotoxin (1nM) showed significant suppression to carbachol-induced vasodilation (Figure 29). A previous study revealed that iberiotoxin (100nM) significantly reduces carbachol-induced vasodilation in rat isolated renal arteries (Jiang, Li, & Rand, 2000).

TRPV4-induced vasodilation required 10-fold higher concentration of iberiotoxin (10nM) to show significant inhibition of TRPV4-mediated vasodilation (Figure 30a), this is in agreement with numerous studies that have demonstrated significant suppression of TRPV4-induced vasodilation through iberiotoxin (100nM) in mice mesenteric arteries and renal collecting duct cells (Earley et al., 2009; Jin et al., 2012). These findings suggest what was concluded by Earley et al. (2005), that TRPV4 forms a signalling complex with BKca to generate VSM hyperpolarisation and vasodilation. Moreover, TRPV4 mediates Ca^{2+} influx through cooperative gating in the MEPs that activates Kca channels to yield VSM hyperpolarisation and hence causes vasodilation (Bagher & Garland, 2014).

Additionally, TRPM8-induced vasodilation was significantly compromised when BKca was blocked with iberiotoxin (1nM) (Figure 31). A small number of cardiovascular researches have been conducted on icilin-activated TRPM8 and iberiotoxin, while most of the studies on TRPM8 were conducted on macrophages cell lines. A study conducted on macrophage cell line raw 264.7 have found that iberiotoxin (200nM) does not have any effect on icilin-stimulated cation current (S. N. Wu, Wu, & Tsai, 2011). Another cardiovascular studies have concluded lysophosphatidylinositol as an extracellular mediator and an intracellular messenger affecting a number of ion channels including BKCa and TRPM8 (D. A. Andersson et al., 2007; Bondarenko et al., 2011a; Bondarenko et al., 2011b). Accordingly, BKca might form a signalling complex with TRPM8 through lysophosphatidylinositol, and therefore, inhibiting BKca with iberiotoxin (1nM, IC50= 500pM) might interfere with the signalling complex and hence block the TRPM8-induced hyperpolarisation and vasodilation.

In addition to NO, these findings suggest that BKca is another major component of the vasodilation cascade in aorta. Moreover, BKca is a common vasodilatory component between muscarinic, TRPV4 and TRPM8 pathways.

Further experiments were conducted to examine the endothelium dependence of these three main pathways, muscarinic, TRPV4 and TRPM8, as previous studies demonstrated that endothelium expresses at least 20 TRP channels (Earley et al., 2010; H. Y. Kwan et al., 2007; Watanabe et al., 2008).

As shown in Figure 32, muscarinic-induced vasodilation was significantly suppressed when endothelium was denuded. Such suppression was reproduced by NOS inhibition via L-NAME (Figure 30), revealing that L-NAME (100μM) incubation for 30 minutes could be a possible simple model to of endothelium removal for muscarinic studies. Moreover, the removal of endothelium showed significant reduction in TRPV4-induced vasodilation, with Emax= 58.7 ± 9.5% vs intact endothelium Emax= 89.3 ± 4.0% (Figure 33). A previous study showed TRPV4 channels were expressed in MEPs in cremaster and mesenteric arteries (Bagher et al., 2012). TRPV4 expression in MEPs was suggested to activate VSM's Kca, hence induce hyperpolarisation and vasodilation (Bagher & Garland, 2014). Therefore, TRPV4 might induce vasodilation in endothelium-dependent and endothelium-independent manners.

TRPM8-mediated vasodilation was significantly influenced by endothelium removal without showing significant effect at any specific concentration of icilin-induced vasodilation (N=3, ns $p \geq 0.05$, EC_{50}= 5.3 ± 3.2μM and maximum vasodilation 67.4±9.67% vs intact endothelium icilin-induced vasodilation EC_{50}= 1.3 ± 0.7μM and maximum vasodilation 82.1±1.3%) (Figure 34). These findings suggest that TRPV4 and TRPM8 are not exclusively expressed in the endothelium, but also in the VSMCs. The expression of TRP channels in vasculature was studied through molecular assays such as Western blotting, RT-PCR and immunohistochemistry which recognised approximately 21 TRP channels in VSMCs (TRPC1-7, TRPM1-8, TRPV1-TRPV4, and TRPP1 and TRPP2) (H. Y. Kwan et al., 2007; Watanabe et al., 2008). The co-expression of TRPM8 and TRPV4 channels in the aortic vasculature was concluded as novel Ca^{2+} entry pathways that might control the systemic circulation (X. R. Yang et al., 2006).

To sum up, inhibiting NOS showed significant inhibition of muscarinic and TRPV4 vasodilatory pathways but not TRPM8, while blocking BKca with iberiotoxin showed significant reduction in all muscarinic, TRPV4 and TRPM8-induced vasodilation. Muscarinic receptors are known to stimulate PLC, an enzyme hydrolyses the membranous PIP2 into IP3 and DAG from which IP3 is capable to activate TRPV4 and bind to ER's IP3-R to induce

Ca^{2+} release from ER (Everaerts et al., 2010; Lawler et al., 2001; Murata et al., 2007). Such cellular Ca^{2+} storage depletion will trigger the extracellular Ca^{2+} influx through Ca^{2+} channels including CaM-activated TRPV4 channels (Haworth, Goknur, Hunter, Hegge, & Berkoff, 1987; Lopacinska & Strosznajder, 2005; Ma, Cheng, Wong, et al., 2011). However, TRPM8 is activated through TRP-domain bound PIP2, therefore when endothelial muscarinic and TRPV4 pathways are activated, TRPM8 might be inhibited as its cytoplasmic activator, PIP2 level is reduced through upon PLC activation (B. Liu & Qin, 2005; Rohács et al., 2005).

In conclusion, endothelial muscarinic, TRPV4 and TRPM8 pathways might be integrated in BKca-mediated vasodilation. However, inhibiting TRPM8 or TRPV4, if not both, is shown to interfere with muscarinic-induced vasodilation. NO is an essential part in muscarinic and TRPV4-vasodilatory pathways but not TRPM8-induced vasodilation. Muscarinic-induced vasodilation showed complete endothelium dependence, while the TRPV4-induced vasodilation is partially endothelium-dependent. Therefore, the endothelial muscarinic and TRPV4 pathways might be linked mainly through eNOS and BKca. Additionally, endothelial TRPM8 acts mainly as a hyperpolarisation inducer as it showed BKca and slightly endothelium dependent but NO-independent. This conclusion will be the base of the hypothesis to study the diabetic endothelial function in STZ diabetic-rats model. In the next chapter, endothelial function through carbachol, TRPV4 and TRPM8-induced vasodilation will be investigated with through main focus on TRPV4.

Chapter 4: The effect of STZ-induced diabetes on muscarinic, TRPV4 and TRPM8 responses on rat aortic and mesenteric arteries

4.1. Introduction

In the previous chapter, muscarinic, TRPV4 and TRPM8 pathways showed to play essential roles in mediating aortic rings vasodilation. Such vasodilation was through NO pathway in addition to BKca. Endothelial dysfunction is a common diabetes complication that renders the diabetic patients vulnerable to limbs fungal infections, nephropathy, and retinopathy (F. M. Ashcroft & Rorsman, 2012; A. Dhar et al., 2010).

Endothelial dysfunction is a common diabetes complication in which endothelium-dependent vasodilation becomes impaired (Kolluru et al., 2012). The principal determinant of endothelial dysfunction is decreased NO bioavailability, with increased ET-1 biosynthesis as a close second (Bakker et al., 2009). The primary factors govern the bioavailability of endothelial NO: the generation of NO from eNOS and the elimination of active NO (van den Oever et al., 2010). Numerous studies have revealed different pathways of accelerated NO elimination. Under physiological circumstances, NO is produced from the dimeric eNOS that utilises L-arginine and molecular oxygen parallel to NADPH, FMN, FAD and BH4 as co-substrates (M. I. Lin et al., 2003). BH4 downregulation contributes to eNOS uncoupling (Alp et al., 2003). Superoxide anions quench NO to produce $ONOO^-$ that compromise NO bioavailability and oxidise BH4 to BH2, as well as suppress GCH expression and thereby reduce BH4 expression (Alp et al., 2003; Milstien & Katusic, 1999). Elevated BH2 reduces NO production in addition to aggravating eNOS uncoupling due to BH4 reduction (Alp et al., 2003; Milstien & Katusic, 1999). Arginase upregulation or hyperactivity, if not both, compromises L-arginine availability to induce eNOS uncoupling that culminates with ROS production and suppressed NO generation (Kashyap et al., 2008; Kim et al., 2009). Endothelial dysfunction might also be attributed to the impairment of the eNOS signalling cascade, such as PI3K/Akt/eNOS culminates with reduced NO production (Kolluru et al., 2012; Liang et al., 2009; Tabit et al., 2010).

Another NO pathway component is the TRPV4 channel, which is highly expressed in the endothelium. H. Y. Kwan et al. (2007) hypothesised that a dysfunction in TRPV4 might contribute to endothelial dysfunction. Moreover, Köhler et al. (2006) provided the first evidence of TRPV4 dysfunction involvement in endothelial dysfunction. A recent study demonstrated TRPV4 downregulation in STZ-rats' mesenteric endothelium (Ma et al., 2013). Moreover, TRPV4 downregulation was concluded to be involved in diabetic endothelial

dysfunction and retinopathy (Monaghan et al., 2015). These studies provide a very robust foundation that correlates TRPV4 alteration with endothelium dysfunction in diabetes.

MGO inhibits eNOS phosphorylation and induces endothelial dysfunction (I. Dhar, Dhar, Wu, & Desai, 2012), and MGO generation is increased in diabetes as a consequence of accelerated glycolysis, lipolysis and proteins metabolism (Shamsaldeen et al., 2016).

In response to these studies and findings, and as mentioned in section 1.7, the main objectives of this chapter were to investigate possible serum markers alteration in STZ-induced diabetes such as MGO and ox-LDL through ELISA. Moreover, since Hogikyan, Galecki, Halter, and Supiano (1999) showed that NA infusion induces exaggerated vasoconstriction in T2DM patients, therefore, NA-induced vasoconstriction was studied in both STZ-diabetic and non-diabetic aortic rings. Moreover, investigating STZ-induced diabetes endothelial dysfunction through muscarinic and TRPV4 agonists in both aortic and mesenteric arteries. Finally, another TRP channel, TRPM8 will be investigated in parallel with muscarinic, TRPV4 and sodium nitroprusside (SNP)-induced vasodilation.

4.2. Materials and methods

4.2.1. ELISA studies

- MGO determination in naïve and STZ-diabetic rats' serum samples

Serum samples were analysed through sandwich ELISA according to the manufacturer's instructions. Briefly, a sterile 96-well plate was coated with MGO conjugate (100µl of 50ng/ml) which was prepared by the supplier through reacting BSA with MGO, followed by extensive dialysis and column purification. Samples (50µl) were incubated at 25°C for 10 minutes prior to the addition of primary monoclonal mouse anti-MGO antibody (50µl). Afterward, the samples were incubated at room temperature on an orbital shaker for 1 hour. All samples were washed with washing buffer before the addition of secondary horseradish peroxidase labelled goat anti-mouse antibody (100µl) for 1 hour on orbital shaker. The loaded wells were washed three times and then incubated with TMB substrate solution (100µl) for 5 minutes. The reaction was stopped using sulphuric acid stop solution (100µl) and absorbance measured at 450nm. MGO standard curve was used to estimate the samples MGO concentrations (Figure 36). Eight different standard solutions of MGO conjugated bovine serum albumin (MGO-BSA) were prepared (0, 0.2, 0.39, 0.78, 1.56, 3.13, 6.26. 12.5 and 25µg/ml) were read at 450nm wavelength. X-axis represents the concentration in logarithmic scale (0.2, 0.39, 0.78, 1.56, 3.13, 6.25, 12.5 and 25). R2 value showed approximately 97% strong correlation between absorbance and increased ox-LDL. The curve was used to estimate the sample (log) concentration (x-axis).

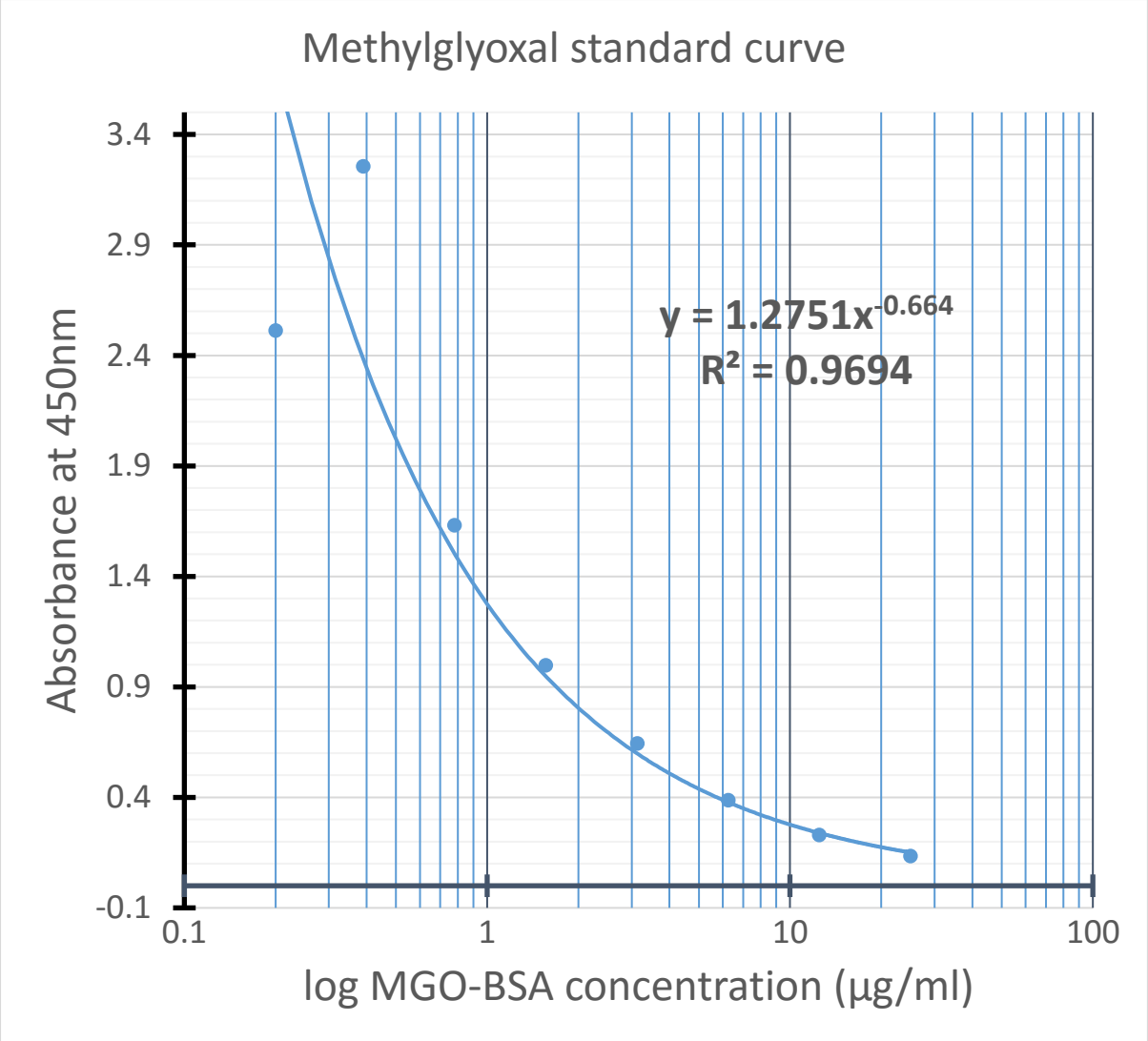

Figure 36. Methylglyoxal standard curve. The blue dotted line showed trend line robust fit.

- Oxidised LDL (ox-LDL) determination in serum

All samples were analysed through sandwich ELISA according to the manufacturer's instructions. Briefly, a sterile coated 96-well plate was loaded with serum samples (100µl). Thereafter, the plate was covered and incubated in 37°C for 2 hours. Afterward, the samples were aspirated and the wells were added with primary biotin-conjugated monoclonal mouse antibody specific to Ox-LDL (100µl) (detection reagent A) and the plate was incubated in 37°C for 1 hour. Detection reagent A was aspirated and wells were washed for 3 times with washing buffer (350µl) (provided by the supplier). The wells were then loaded with secondary polyclonal avidin-conjugated horseradish peroxidase labelled rabbit anti-mouse antibody (100µl) (detection reagent B), and incubated at 37°C for 30 minutes. Detection reagent B was aspirated and wells were washed for 5 times with washing buffer (350µl). The wells were then added with TMB substrate solution (100µl) and incubated at 37°C for 25

minutes. The reaction was stopped using sulphuric acid stop solution (100µl) and the absorbance was measured at 450nm. Ox-LDL standard curve was used to estimate the samples ox-LDL concentrations (Figure 37). Eight different standard solutions of oxidised-LDL (0, 31.25, 62.5, 125, 250, 500, 1000 and 2000pg/ml) were read at 450nm wavelength. R2 value showed approximately 98% correlation between absorbance and increased ox-LDL. The curve was used to estimate the sample concentration (x-axis).

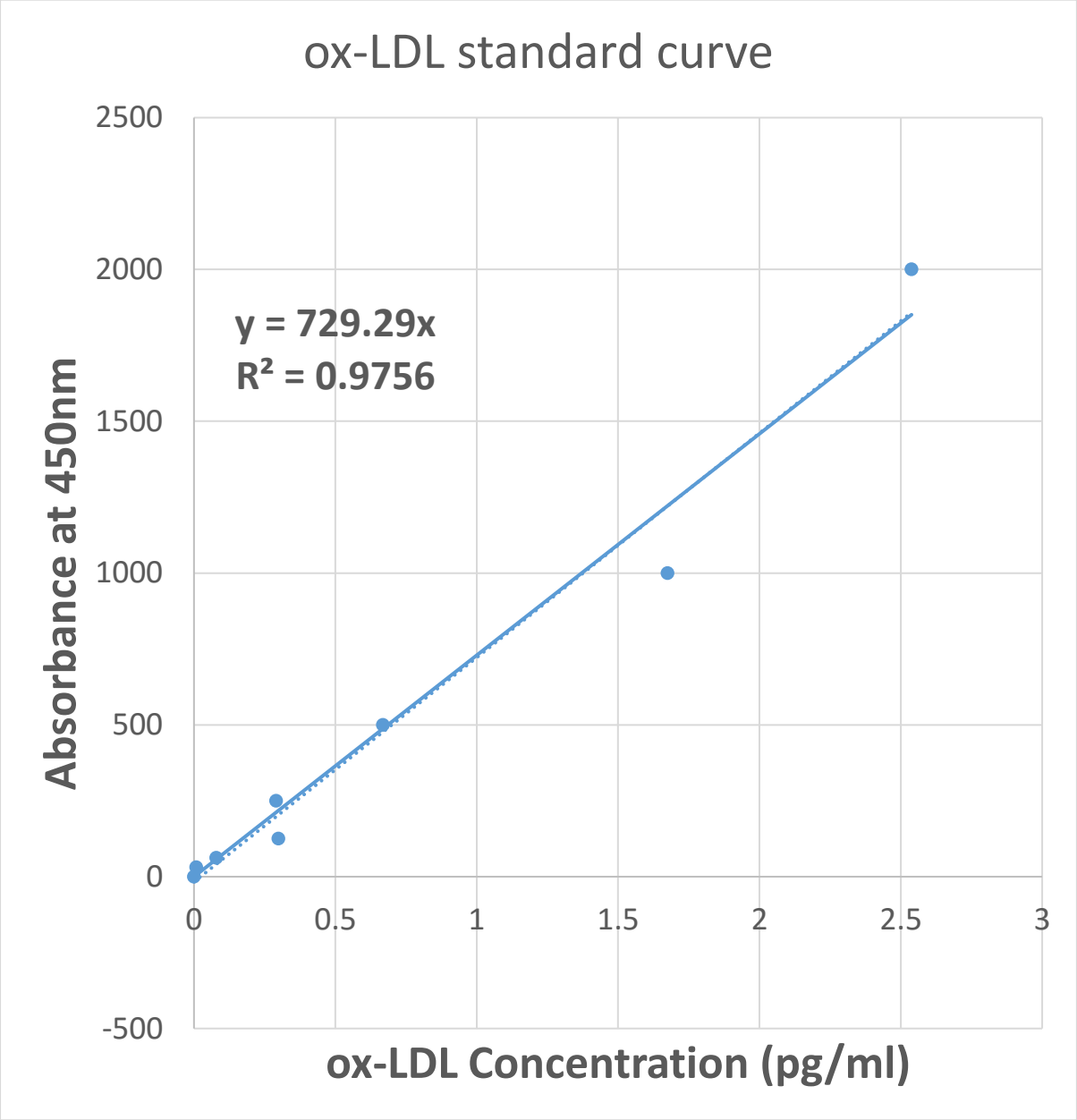

Figure 37. Oxidised LDL (ox-LDL) standard curve. The blue dotted line showed trend line robust fit.

4.2.2. Total serum proteins measurement

The same serum samples were used for serum protein determination through BCA assay to investigate whether diabetes is associated with hypoproteinaemia. BCA standard curve was constructed and used for serum samples total proteins determination. Seven different standard solutions of bovine serum albumin (BSA) in deionised distilled water (0, 20, 40, 60, 100, 200, 300 and 400µg/100µl) were read at 620nm wavelength. R-square showed approximately 100% correlation between absorbance and concentration. The linear equation was applied to estimate the sample concentration (x) (Figure 38).

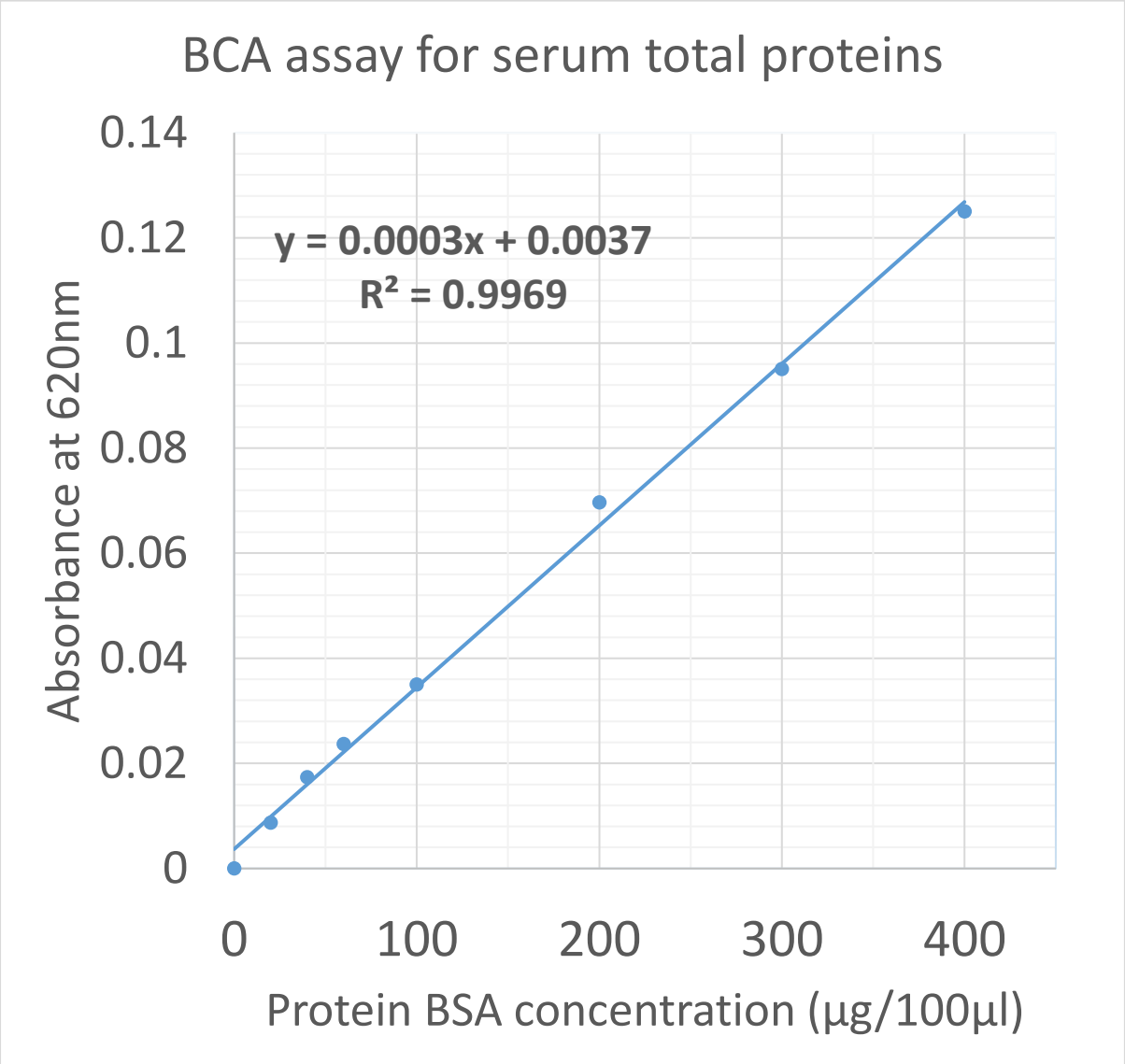

Figure 38. Bicinchoninic acid (BCA) assay standard curve for serum samples analysis. The blue dotted line showed trend line robust fit. Bovine serum albumin= BSA

4.2.3. Naïve, control and STZ rats comparison

- Vascular studies

Vascular functions were evaluated in diabetic, control and naïve rats. Aortic rings from control rats' injected with citrate buffer (control), or STZ diabetic rats were studied for 1-5 weeks post injection and compared with naïve rats. Aortic rings (2-3mm) were isolated and left to equilibrate for approximately 60-90 minutes in Bennett isolated tissue vessel organ bath of 95% O_2 / 5% CO_2 Krebs solution pH 7.4 at 37°C ± 1°C as described in section 2.3.1. All aortic rings were initially contracted with NA CRC to determine the NA EC_{80}. The NA EC_{80} was applied to pre-contract the aortic rings before being treated with either carbachol (CC) CRC (30nM- 300µM), TRPV4 agonists (RN1747 or 4-αPDD) CRC (3nM–30µM and 3pM-3µM, respectively), TRPM8 agonist (icilin) CRC (3nM-3mM), or the direct vasodilator, SNP CRC (1nM-1mM).

The vasodilation experiments started with pre-contracting the aortic rings and the mesenteric arteries (section 2.3.2.) with NA EC_{80} until the reading trace reached the plateau. Afterward, the vasodilator was added starting from the minimum concentration, and waiting for any response's plateau before adding the higher concentration, until reaching the maximum CRC concentration. The extent of vasodilation was measured through iWORKS (version 1.817). Each value of the CRC was estimated in regard to the baseline value, the value of the trace before adding the NA EC_{80}, which is approximately 1g (Figure 39). The extent of vasoconstriction and vasodilation was measured as described in 2.3.2.

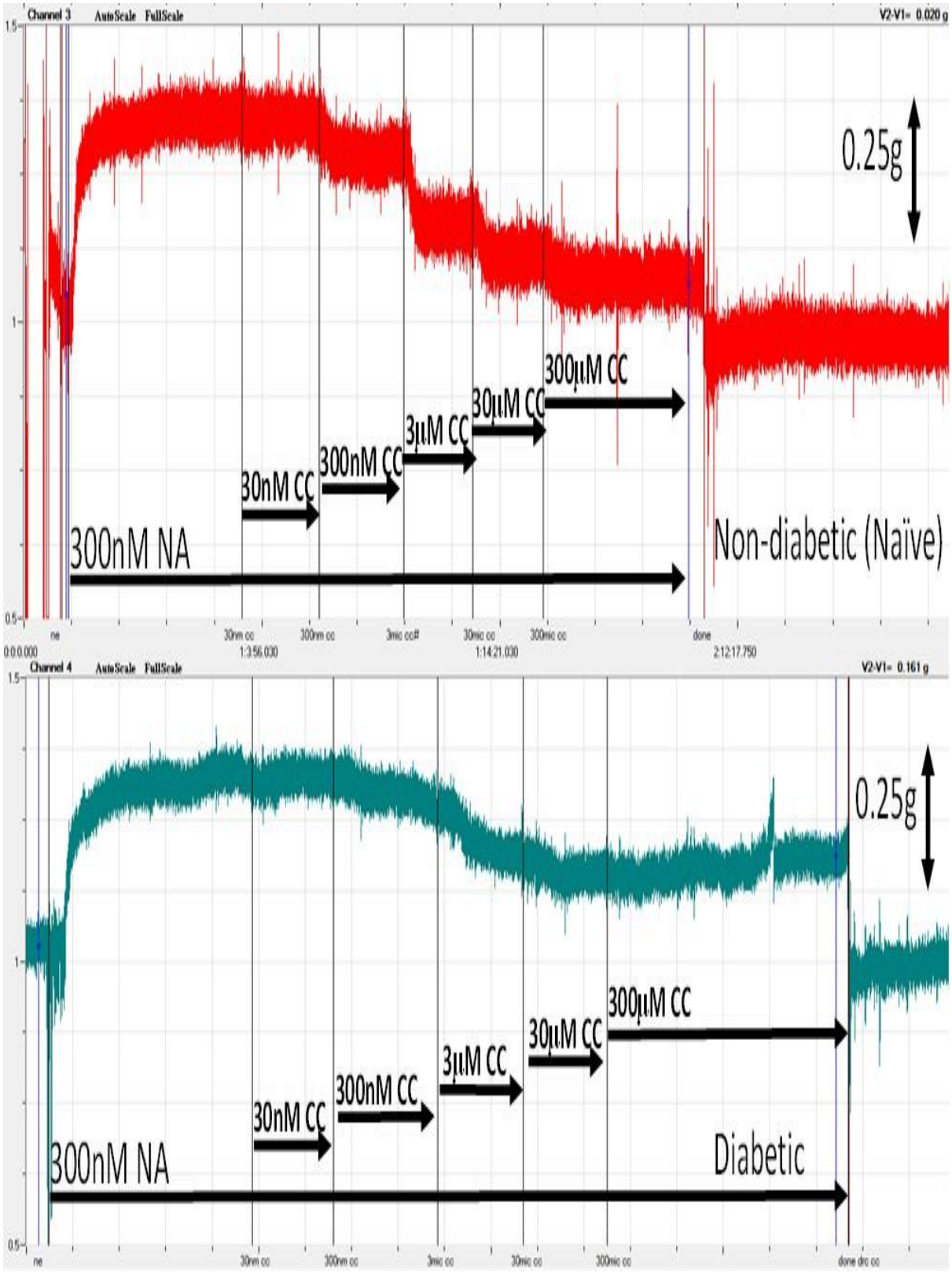

Figure 39. Carbachol-induced vasodilation representative traces. Non-diabetic aortic rings showed vasodilation (upper trace: red). STZ-diabetic aortic rings showed impaired vasodilation (lower trace: turquoise). After noradrenaline EC_{80}-induced vasoconstriction, aortic ring was treated with a series of carbachol concentrations to induce vasodilation. Once a plateau was reached, another higher concentration of carbachol (RN-174, 4-αPDD or icilin) was added until reaching the maximum vasodilation.

4.3. Results

4.3.1. STZ model characteristics

- Blood glucose was significantly elevated in STZ-diabetic rats:

Approximately 95% of the STZ-injected rats developed diabetes as indicated by elevated blood glucose > 16mmol/L. Blood glucose was significantly elevated in STZ-injected rats when measured at the day of sacrifice (N=28, *** $p < 0.001$, 31 ± 1.1mmo/L vs pre-injection 6.6 ± 0.13mmol/L). STZ-injected rats showed significant blood glucose increment from the 1st week to the 5th week post injections [1st week: N=9, 31.7 ± 2mmol/L vs 6.5 ± 0.3mmol/L, 2nd week: N=5, 28.0 ± 1.3mmol/L vs 6.3 ± 0.17mmol/L, 3rd week: N=6, 33.1 ± 2.7mmol/L vs 6.5 ± 0.25, 4th week: N=4, 30.3 ± 3.1mmol/L vs 6.6 ± 0.3 & 5th week: N=4, 36.4 ± 2.6mmol/L vs 7.2 ± 0.2mmol/L].

The mean blood glucose for naïve (non-injected) and control (injected with citrate buffer) rats did not show significant difference ($p \geq 0.05$ naïve N=14: day of sacrifice 6.8 ± 1.4mmol/L vs pre-injection 6.8 ± 0.14mmol/L, control N=4: day of sacrifice 7.7 ± 0.34mmol/L vs pre-injection 6.15 ± 1.9mmol/L) (Figure 40).

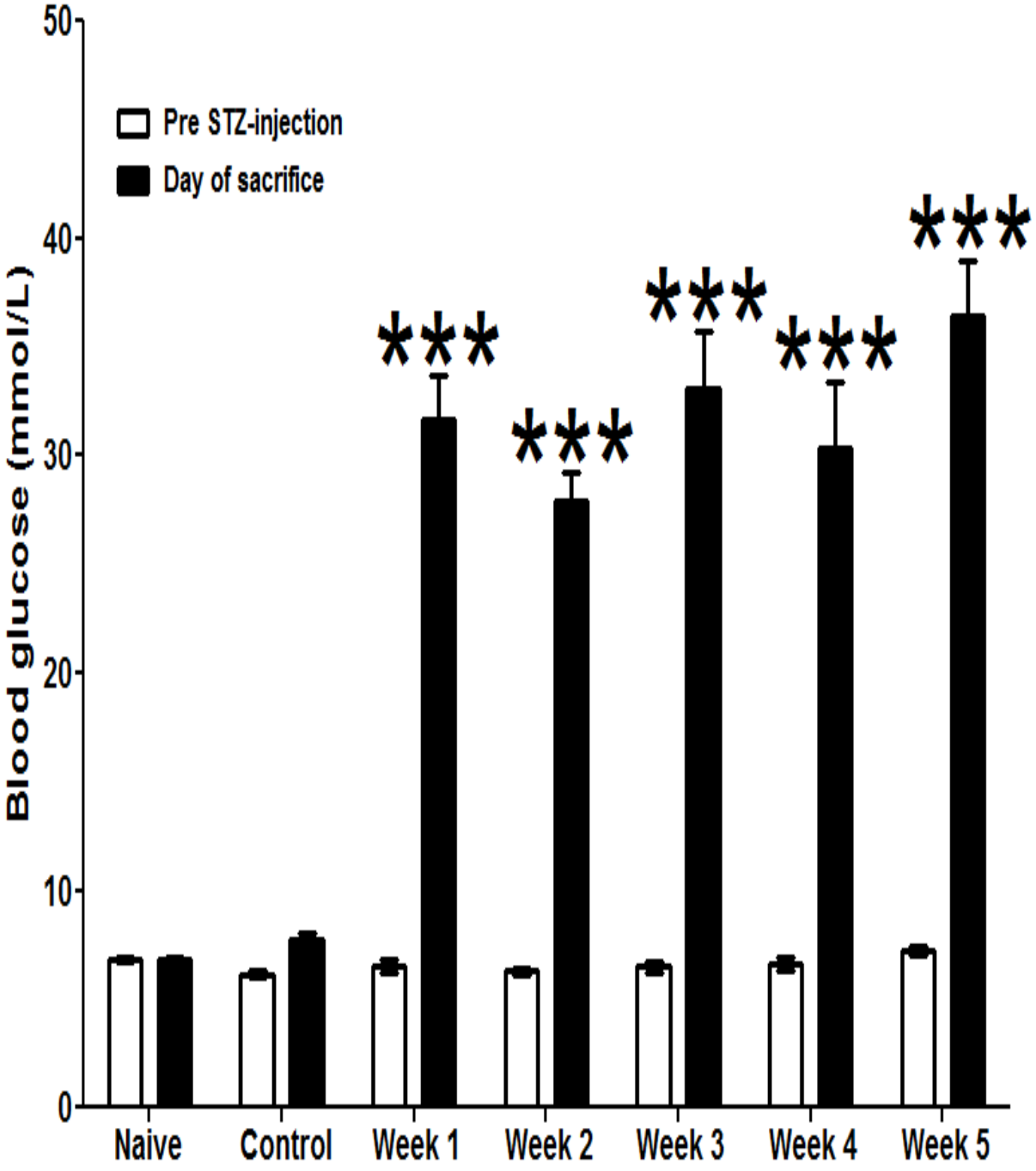

Figure 40. Naïve and STZ-diabetic rats blood glucose concentrations. Blood glucose was significantly increased in STZ rats among the 5 weeks course of study. Compared with respective pre-injection blood glucose levels versus respective pre-injection analysed through two-way ANOVA post hoc Bonferroni test. Significance is represented as *** $p < 0.001$. Data presented as mean blood glucose ± SEM (Naïve, N=14, control, N=4, STZ-diabetic week 1, N= 9, STZ- diabetic week 2, N= 5, STZ- diabetic week 3, N= 6, STZ- diabetic week 4, N= 4 and STZ- diabetic week 5, N= 4).

Moreover, body weight did not increase during the study as seen with naive rats. Naïve rats across the 5 weeks showed significant weight gain (N=14, *** $p < 0.001$, day of sacrifice 445 ± 20.7g vs when starting the study 336.8 ± 8.6g) while control rats across the 5 weeks did not show significant body weight increment (N=4, $p \geq 0.05$, 420 ± 6.4g vs pre-injection 450 ± 12.1g,). STZ-injected rats did not show significant weight gain. The 1st week showed insignificant weight loss while from the 2nd week – 5th week body weight was not significantly increased (1st week: N=9, $p \geq 0.05$, 355.6 ± 10.0g vs 381.2 ± 11.0g, 2nd week: N=5, $p \geq 0.05$, 405.0 ± 6.8g vs 387.2 ± 20.0g, 3rd week: N=6, $p \geq 0.05$, 372.7 ± 9.9g vs 357.2 ± 13.7g, 4th week: N=4, $p \geq 0.05$, 369.7 ± 10.8g vs 359.3 ± 13.3g, & 5th week: N=4, $p \geq 0.05$, 385.8 ± 21.1g vs 339.5 ± 4.1g) (Figure 41).

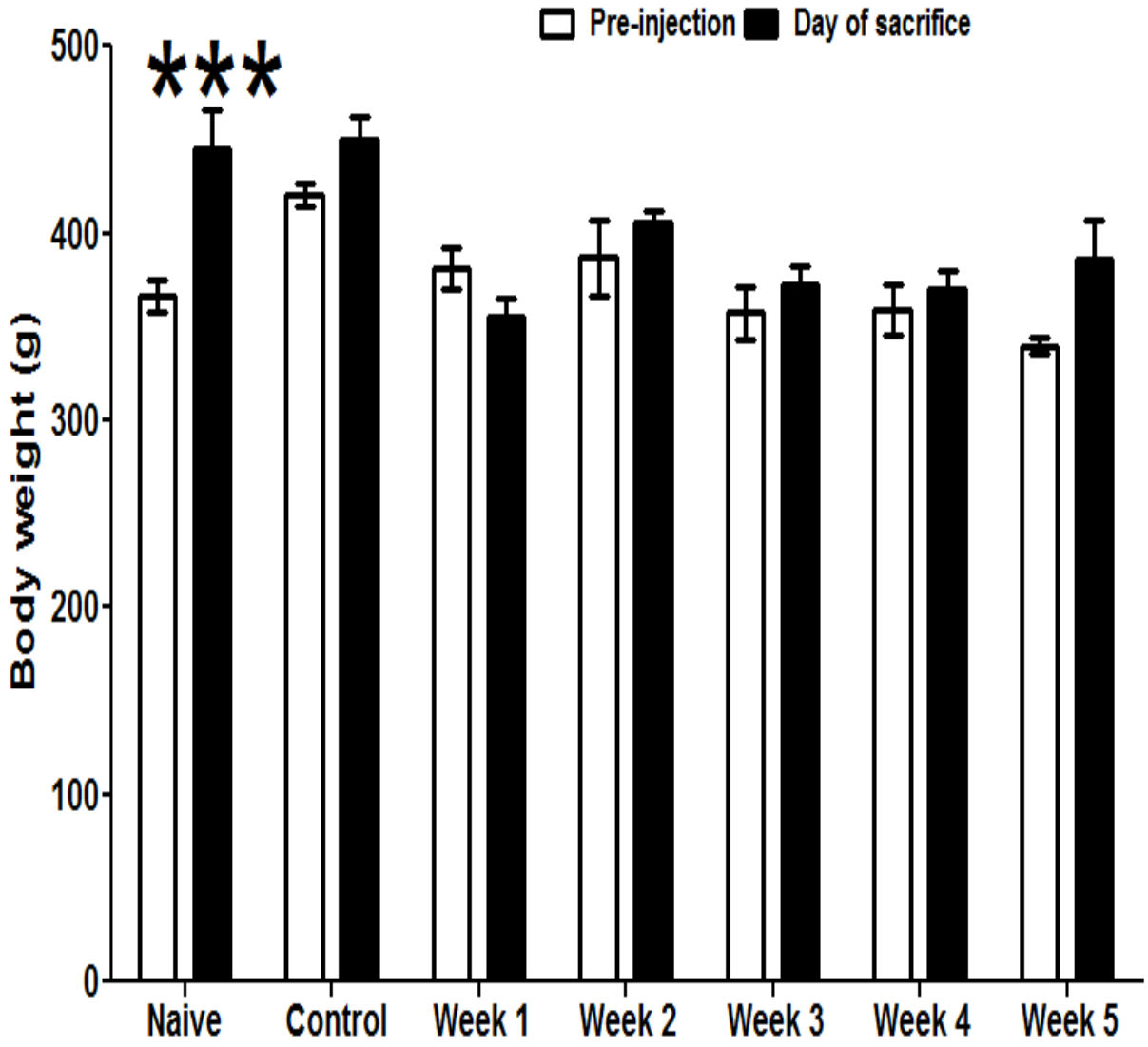

Figure 41. Naïve and STZ-diabetic rats body weights. Body weight was not significantly changed in STZ rats compared to naive and control on the day of sacrifice. Analysed through two-way ANOVA with Bonferroni post hoc test $p < 0.001$ *** versus respective pre-injection. Data presented as mean body weight ± SEM (Naïve, N=14, control, N=4, STZ- diabetic week 1, N= 9, STZ- diabetic week 2, N= 5, STZ- diabetic week 3, N= 6, STZ- diabetic week 4, N= 4 and STZ- diabetic week 5, N= 4).

Additionally, diabetic rat's aorta showed reduced adipose tissue as a consequence of diabetic-lipolysis which was associated with cloudy plasma from the 1st week of diabetes-induction (Figure 42).

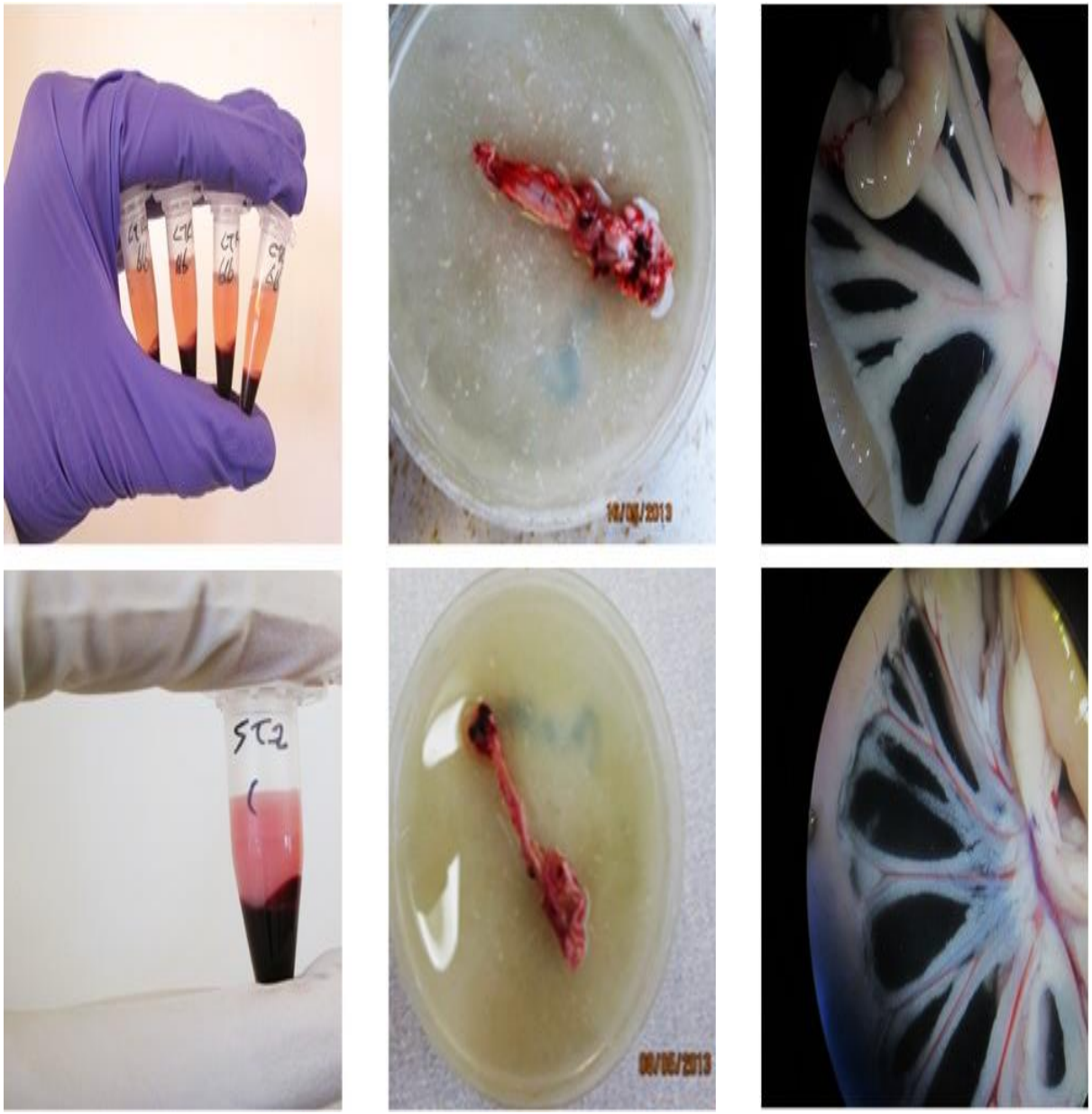

Figure 42. Diabetic lipolysis was shown evidently in diabetic rats in different compartments. Normal rats samples (upper row) of clear plasma, thick connective tissue surrounding the aorta and mesentery, whereas turbid and cloudy serum which was accompanied with thinned connective tissue surrounding the aorta and mesentery revealing lipolysis (lower three pictures).

- MGO and ox-LDL were significantly elevated in STZ-diabetic rats' serum:

Serum samples from naïve, control and STZ-diabetic rats were isolated as described in section 2.3.4 for ELISA studies. MGO and ox-LDL were both investigated in serum samples. MGO is a glycolytic metabolite that was attributed to endothelial dysfunction and diabetic complications such as neuropathy and nephropathy (M. Davies et al., 2006; A. Dhar et al., 2010). According to these studies, serum MGO was measured through ELISA. As shown in Figure 43, MGO was significantly increased in STZ-diabetic rats' serum (STZ week 1, N=4, * $p < 0.05$, 124.0 ± 16.5μM, STZ week 2, N=5, * $p < 0.05$, 121.4 ± 11.2μM, STZ week 3, N=4, *** $p < 0.001$, 201.2 ± 44.4μM, STZ week 4, N= 4, $p \geq 0.05$, 97.0 ± 26.4μM and STZ week 5, N= 4, * $p < 0.05$,142.2±3.5μM vs naïve, N=5, 27.5 ± 9.2μM) (Figure 43a). Pooled STZ weeks showed significant MGO increase (STZ, N=21, *** $p < 0.001$, 136.4 ± 12.2μM vs naïve, N=5, 27.5 ± 9.2μM) (Figure 43b).

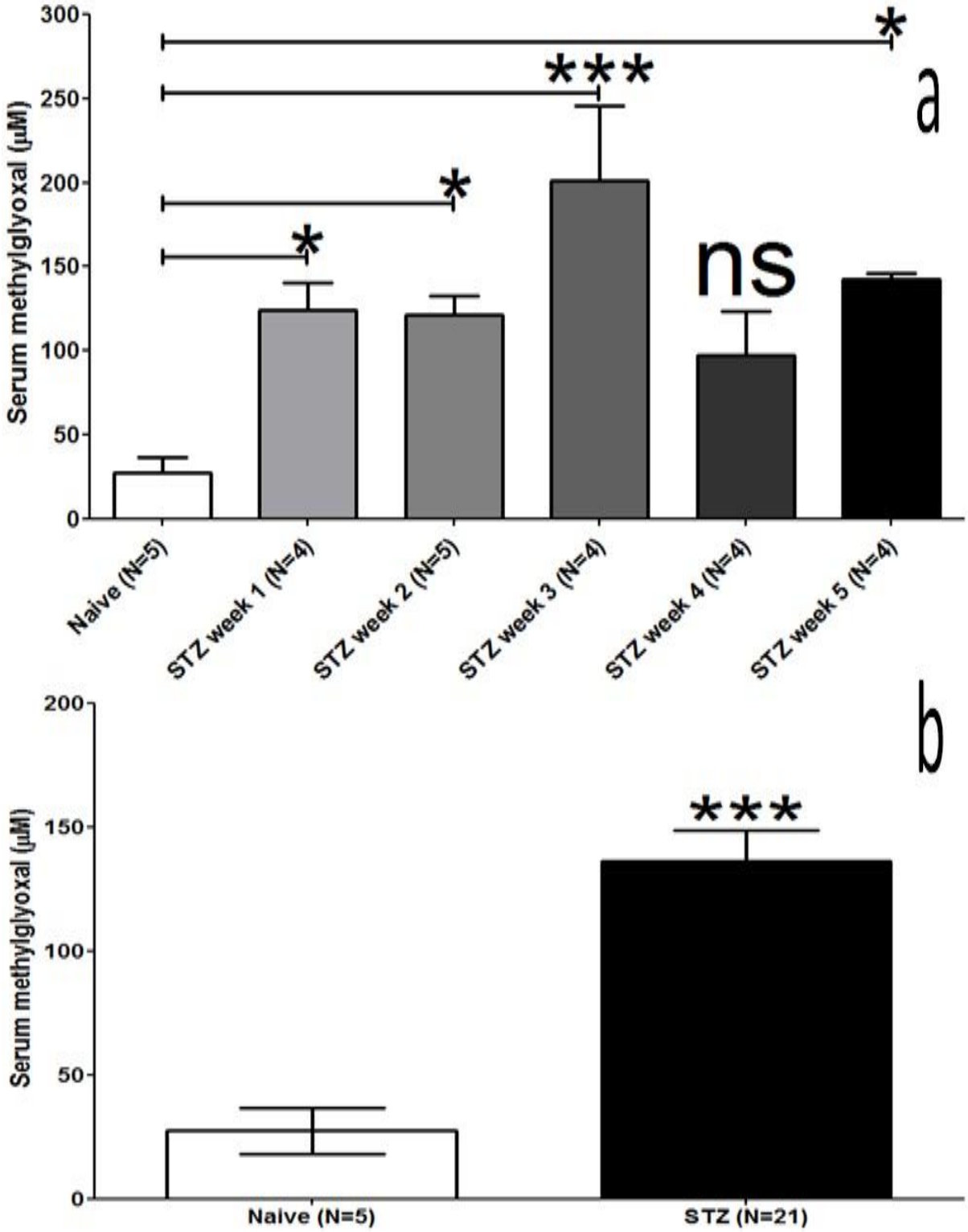

Figure 43. Serum methylglyoxal concentration. STZ-diabetic rats' serum showed significant increase in methylglyoxal across the studied timeframe (week 1- week 5) analysed through one-way ANOVA, post-hoc Tukey test (a). Pooled STZ weeks analysed through unpaired Student's t-test (b). Significance is represented as * $p < 0.05$ and *** $p < 0.001$ compared with naïve serum MGO. Data shown as mean serum methylglyoxal concentration ± SEM (Naïve, N=5, STZ- diabetic week 1, N= 4, STZ- diabetic week 2, N= 5, STZ- diabetic week 3, N= 4, STZ- diabetic week 4, N= 4 and STZ- diabetic week 5, N= 4).

Previous studies correlated elevated serum ox-LDL with diabetic complications, neuropathy, nephropathy and vascular dysfunction (Tsuzura et al., 2004). Serum samples were isolated from naïve, STZ-diabetic rat at week 2 and randomised pooled samples from STZ-diabetic rats' serum week 1-5 without week 2. Serum ox-LDL was estimated which showed significant increase in STZ-diabetic rats' serum. STZ-diabetic rats' serum showed significant increase in ox-LDL (STZ weeks 1-5, N= 8, * $p < 0.05$, 1407 ± 178.1pg/ml, STZ week 2, N= 4, * $p < 0.05$, 1486 ± 78.1pg/ml vs naïve serum, N=5, 732.6 ± 160.6pg/ml) (Figure 44).

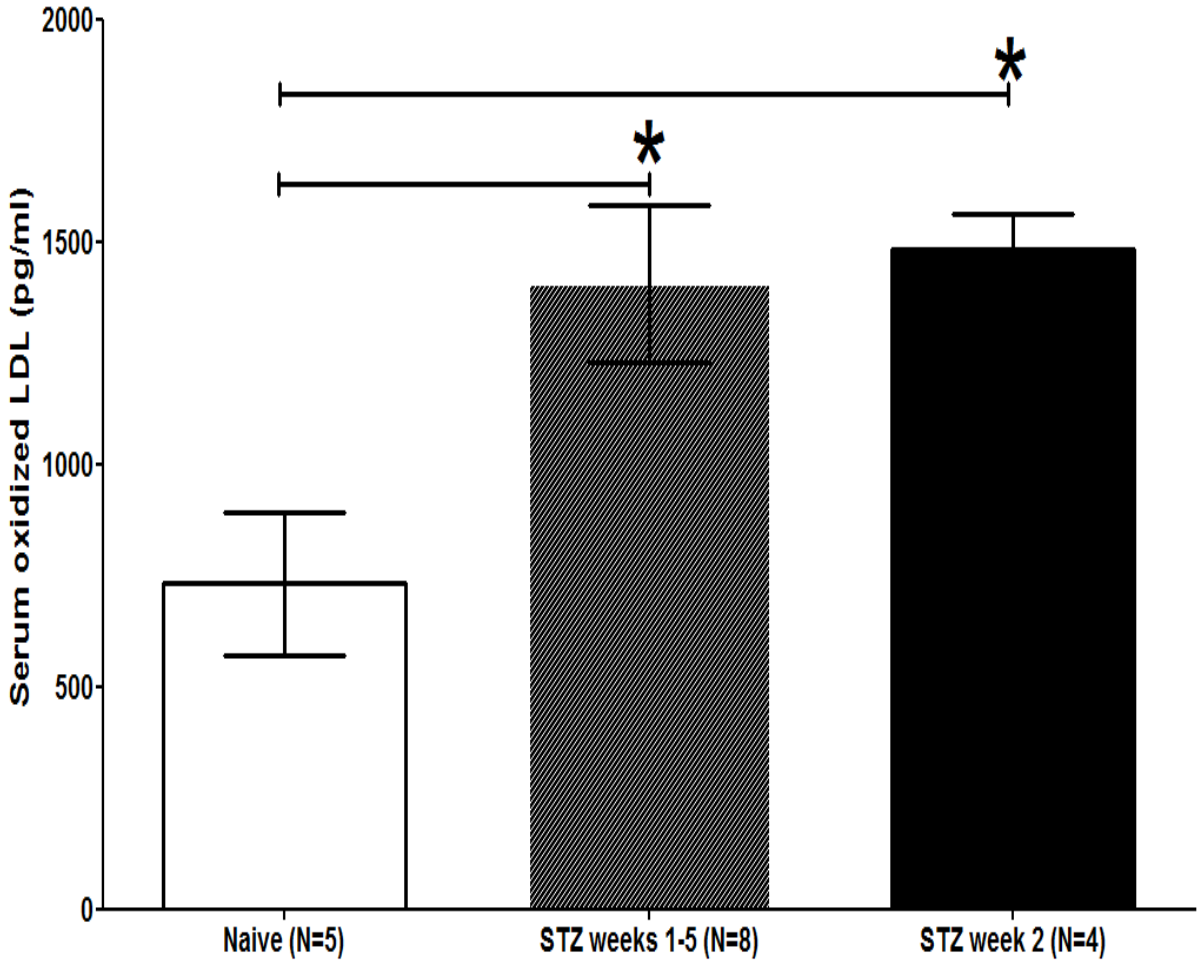

Figure 44. Serum ox-LDL concentration. Analysed through one-way ANOVA, post-hoc Tukey test. Significance is represented as * $p < 0.05$ against naïve serum ox-LDL. Data shown as mean serum ox-LDL concentration ± SEM (Naïve, N=5, STZ- diabetic week 1-5, N= 8 and STZ- diabetic week 2, N= 4).

- STZ-diabetic rats' serum showed significant hypoproteinaemia

The same serum samples were used for serum protein determination through BCA assay to investigate whether diabetes is associated with hypoproteinaemia. Significant reduction in total serum proteins was shown in STZ-diabetic rats' serum (*** $p < 0.001$). STZ-diabetic week 1 did not show significant difference (N=4, $p \geq 0.05$, serum proteins= 8.8 ± 1.03g/dl), STZ-diabetic week 2 showed significant difference (N=5, * $p < 0.05$, serum proteins= 8.7 ±

0.6g/dl), STZ-diabetic week 3 showed significant difference (N=4, ** $p < 0.01$, serum proteins= 7.7 ± 0.9g/dl), STZ-diabetic week 4 showed significant difference (N=4, *** $p < 0.001$, serum proteins= 5.7±0.3g/dl), STZ-diabetic week 5 showed significant difference (N=2, ** $p < 0.01$, serum proteins= 6.4±0.8g/dl) when compared with naïve serum proteins (N=5, serum proteins= 12.0 ± 0.8g/dl) (Figure 45a). Pooled STZ-diabetic samples showed significant difference (N=19, *** $p < 0.001$, serum proteins= 7.6 ± 0.4g/dl vs naïve, N=5, serum proteins= 12.0 ± 0.8g/dl) (Figure 45b).

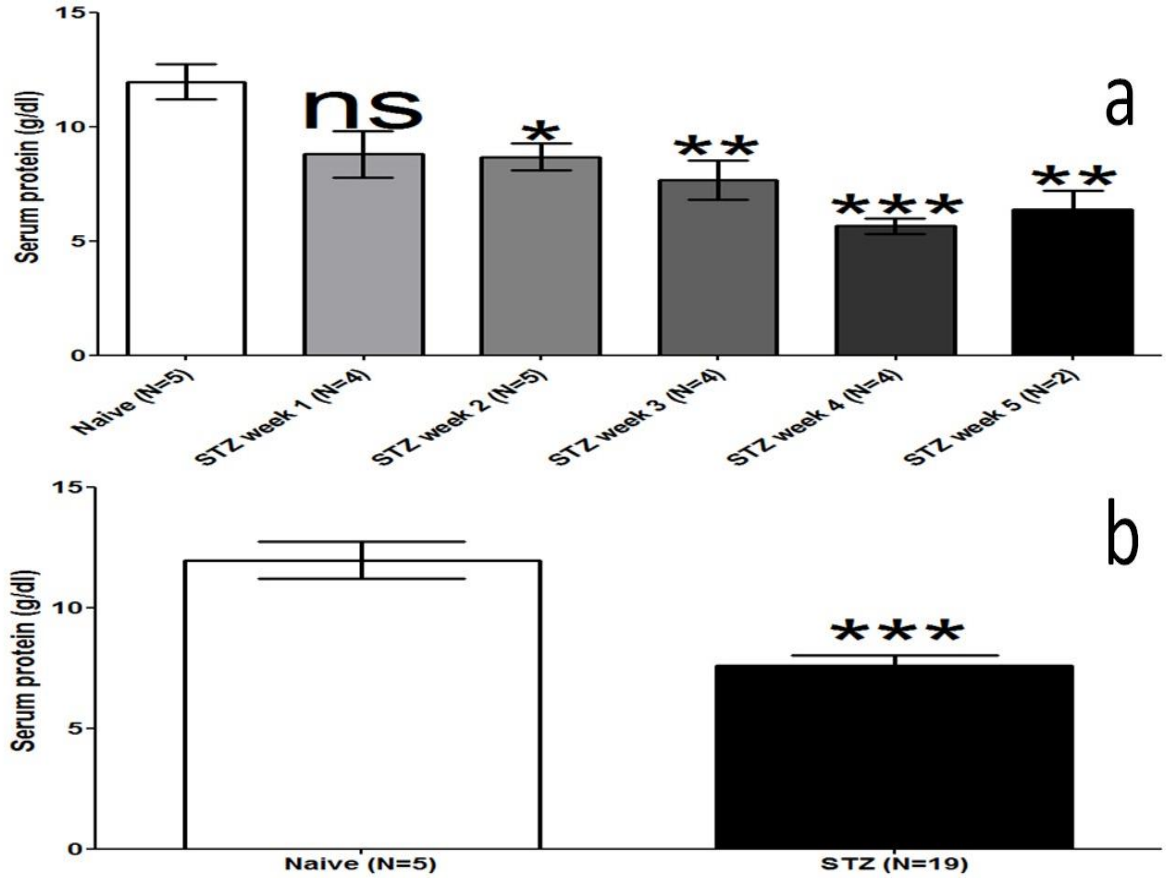

Figure 45. Total serum proteins. Diabetic total serum protein in STZ-diabetic rats from week 1-week 5 analysed through one-way ANOVA post hoc Tukey test (a). Pooled STZ-diabetic samples analysed through unpaired Student's t-test. Significant is represented as * $p < 0.05$, ** $p < 0.01$ and *** $p < 0.001$ when compared with naïve serum samples. Data shown as mean serum proteins concentration ± SEM (Naïve, N=5, STZ- diabetic week 1, N= 4, STZ- diabetic week 2, N= 5, STZ- diabetic week 3, N= 4, STZ- diabetic week 4, N= 4 and STZ-diabetic week 5, N= 2).

4.4. Vascular characteristics of naïve, control and STZ-diabetic rats

A 5 weeks experiment was conducted to investigate vascular alterations throughout the STZ-induced diabetes induction timeframe. STZ-induced diabetes rats were compared to control (injected with citrate buffer only) and non-injected naïve rats.

4.4.1. STZ-diabetic rats' aortic rings showed similar noradrenaline EC_{80} to naïve aortic rings with significantly higher response

As shown in Figure 14 in chapter 3, the NA EC_{80} was be 300nM in naïve aortic rings. Therefore, STZ-diabetic aortic rings were studied to investigate any significant difference in EC_{80}. STZ-diabetic aortic rings vasoconstriction showed significant difference (** $p < 0.01$) when compared to naïve aortic rings (N=2, Emax= 0.55 ± 0.07g vs naïve, N=9, Emax= 0.41 ± 0.03%). However, STZ-diabetic aortic rings did not show significant difference in EC_{80} ($p \geq 0.05$) when normalised to maximum contraction and compared to naïve aortic rings (N=2, EC_{50}= 121.2 ± 87.8nM, EC_{80}= 794 ± 575.2nM and Emax= 100.0 ± 15.4% vs naïve, N=9, EC_{50}= 112.0 ± 69.1, EC_{80}= 630 ± 388.5nM and Emax= 100.0 ± 8.8%) (Figure 46). Therefore, the NA EC_{80} determined in chapter 3 was also applicable for STZ-diabetic aortic rings, 300nM noradrenaline.

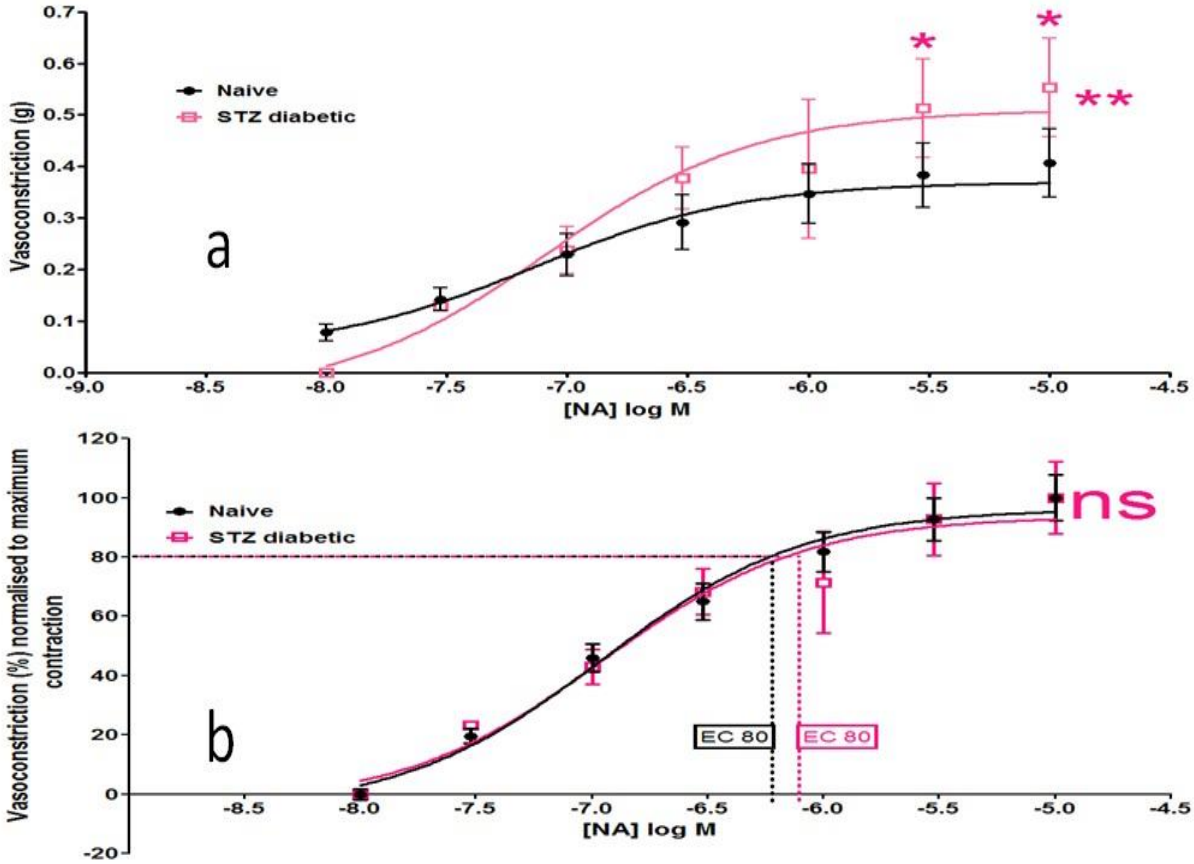

Figure 46. Noradrenaline (NA) concentration response curve in STZ and naïve aortic rings. STZ aortic rings showed significant difference in vasoconstriction force (g) (a). STZ aortic rings did not show significant difference in EC_{80} (ns $p \geq 0.05$) (b) Data analysed through two-way ANOVA post hoc Bonferroni test. Significance is represented as * $p < 0.05$ and ** $p < 0.01$. Data shown as mean contraction % ± SEM (Naïve, N=9 and STZ-induced diabetes, N= 2).

When NA (300nM) was applied to the freshly isolated aortic rings, STZ-diabetic aortic rings showed significantly higher contraction force compared to naïve aortic rings showed significantly higher contraction (N=21, *** $p < 0.001$, vasoconstriction= 0.402 ± 0.02g vs naïve, N=12, vasoconstriction= 0.29 ± 0.02g) (Figure 47).

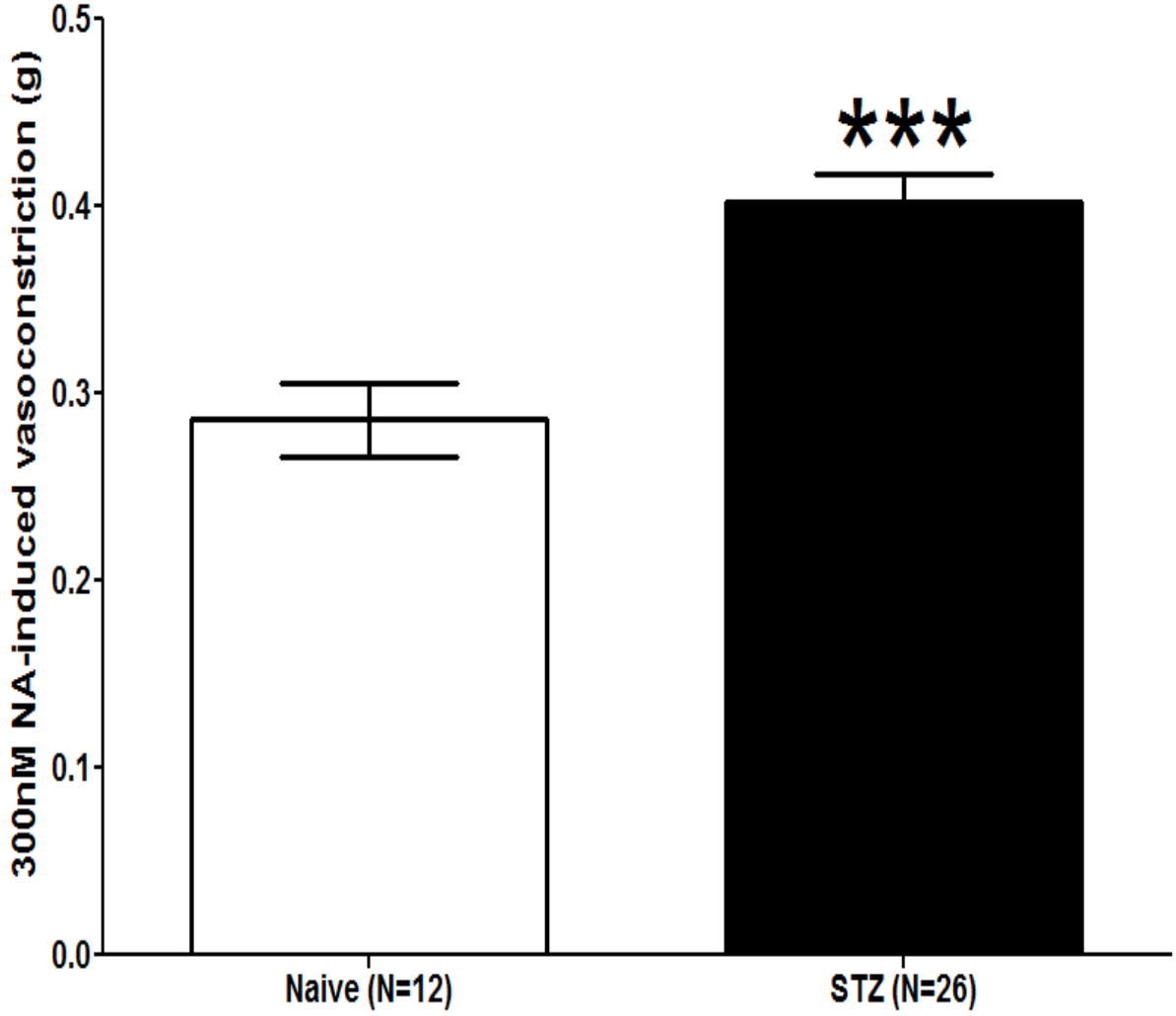

Figure 47. Aortic rings contraction to noradrenaline (NA) EC_{80} (300nM). Significance is represented as *** $p < 0.001$ when compared against naïve aortic rings. Analysed through unpaired two-tailed Student's t-test. Data shown as tension force (g) ± SEM (Naïve, N=12, STZ-diabetic rats, N=26).

Moreover, mesenteric arteries resemble the peripheral vasculature where peripheral arterial resistance is found and contributes to hypertension and diabetic vascular complications. For this reason the effects of STZ treatment were also examined in this resistance artery. Vasoconstriction in mesenteric STZ rat's mesenteric arteries showed significant difference (* $p < 0.05$) when compared to naïve mesenteric arteries, however, there was not any significant difference at any applied noradrenaline concentration when analysing the data through Bonferroni post-hoc test (N=6, $p \geq 0.05$, Emax= 17.6 ± 2.5g vs naïve, N=4, Emax= 22.4 ±

1.8g). When normalised to maximum vasoconstriction, STZ-diabetic mesenteric arteries did not show significant different when compared to naïve mesenteric arteries (N=6, $p \geq 0.05$, EC_{50}= 3.5 ± 2.5µM, N=6, EC_{80}= 6.31 ± 4.5µM and Emax= 100.0 ± 14.4% vs naïve, N=4, EC_{50}= 2.1 ± 1.4µM, N=6, EC_{80}= 6.3 ± 4.3µM and Emax= 100.0 ± 8.1%) (Figure 48) and therefore, the EC_{80} was also applicable for STZ-diabetic aortic rings, 10µM noradrenaline.

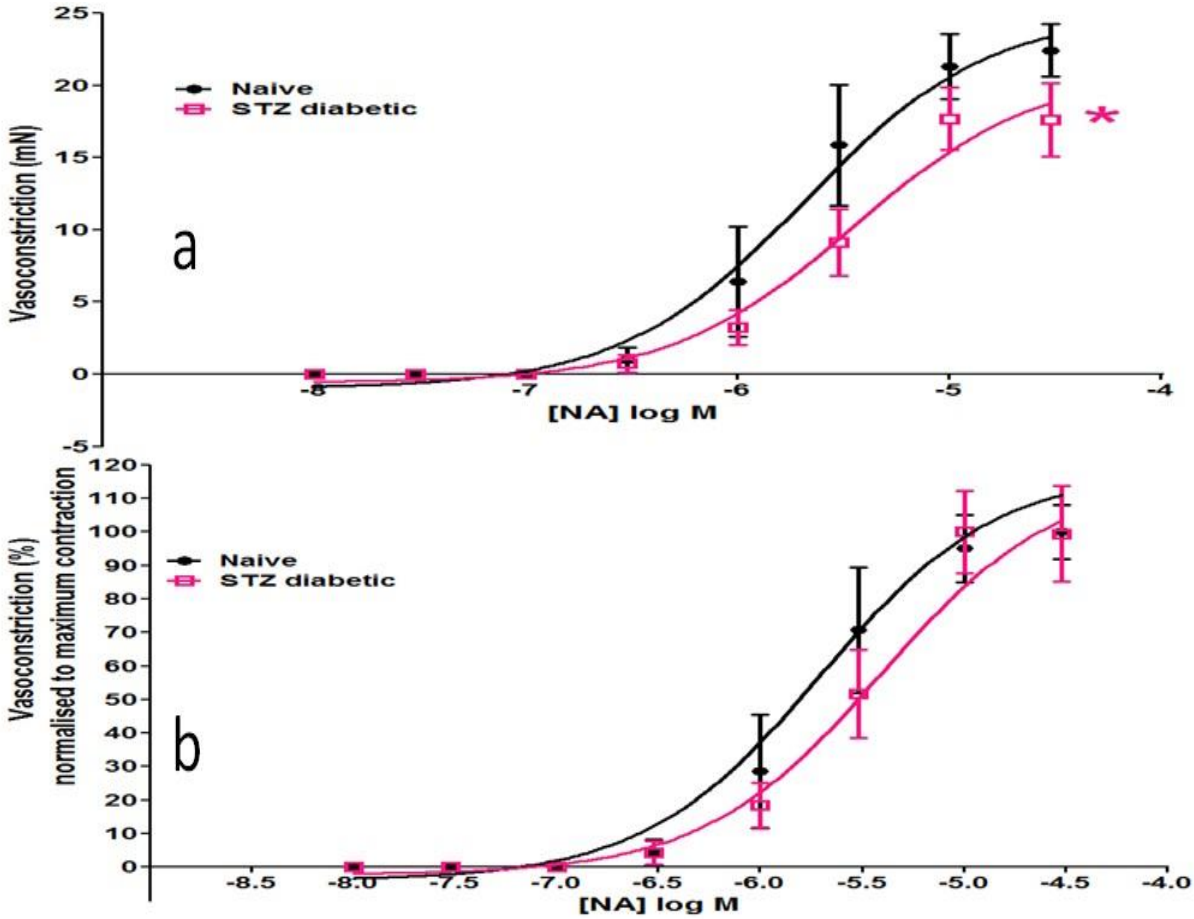

Figure 48. Noradrenaline (NA) concentration response curve in STZ and naïve mesenteric arteries. STZ mesenteric arteries did not show significant difference in vasoconstriction force (g) (a). STZ-diabetic rats' mesenteric arteries did not show significant difference in vasoconstriction force in EC_{80} when analysed through two-way ANOVA post hoc Bonferroni test (b). Data shown as mean contraction ± SEM (Naïve, N=4 and STZ-diabetic rats, N=6).

4.4.2. Carbachol-induced vasodilation was significantly compromised in STZ-diabetic aortic and mesenteric arteries

Since carbachol-induced vasodilation was endothelium-dependent (Figure 32), accordingly, pre-contracted rats' aortic rings were treated with carbachol CRC, to investigate the viability of endothelium in STZ-diabetic models. STZ rats showed significant (*** $p < 0.001$) alteration in vascular response in contrast to naïve rats as shown in Figure 49 with the maximum alteration was shown in the 2nd week as maximum vasodilation reduced by approximately 75%.

As shown in Figure 49, control and STZ-diabetic EC_{50} values did not show significant difference throughout the course study when compared to naïve EC_{50} ($p \geq 0.05$). The main significant difference was in the maximum vasodilation (Emax %). Early significant vascular dysfunction was shown in the 1st week (red) (N= 4, *** $p < 0.05$, EC_{50}= 0.95 ± 0.7µM & Emax= -55.3% ± 3.4%). The 2nd STZ-induced diabetes week (pink) showed the most retarded vascular dysfunction (N= 6, *** $p < 0.001$, EC_{50}= 0.6 ± 0.2µM & Emax= -29.6 ± 9.3%). The 3rd week (green) showed significant endothelial dysfunction (N= 5, *** $p < 0.001$, EC_{50}= 1.3 ± 0.5µM & Emax= -58.6 ± 12.4%). However, endothelial dysfunction was significant in week 4 (blue) (N= 7, *** $p < 0.001$, EC_{50}= 0.6 ± 0.15µM & Emax= -35.1 ± 11.0%) and 5th week (grey) (N= 5, *** $p < 0.001$, EC_{50}= 1.02 ± 0.4µM & Emax= -52.3 ± 18.4%) when compared to carbachol-induced vasodilation in naïve aortic rings (N= 7, EC_{50}=0.6 ± 0.3µM & Emax= 89.4 ± 4.4%). Control rats showed significant difference when compared to carbachol-induced vasodilation through two way ANOVA (* $p < 0.05$) without showing any significant difference through Bonferroni post-hoc test in naïve aortic rings (N= 5, ns $p \geq 0.05$, EC_{50}= 0.6 ± 0.4µM & Emax= -77.2 ± 2.5% vs EC_{50}=0.6 ± 0.3µM & Emax= -89.4 ± 4.4%) (Figure 49).

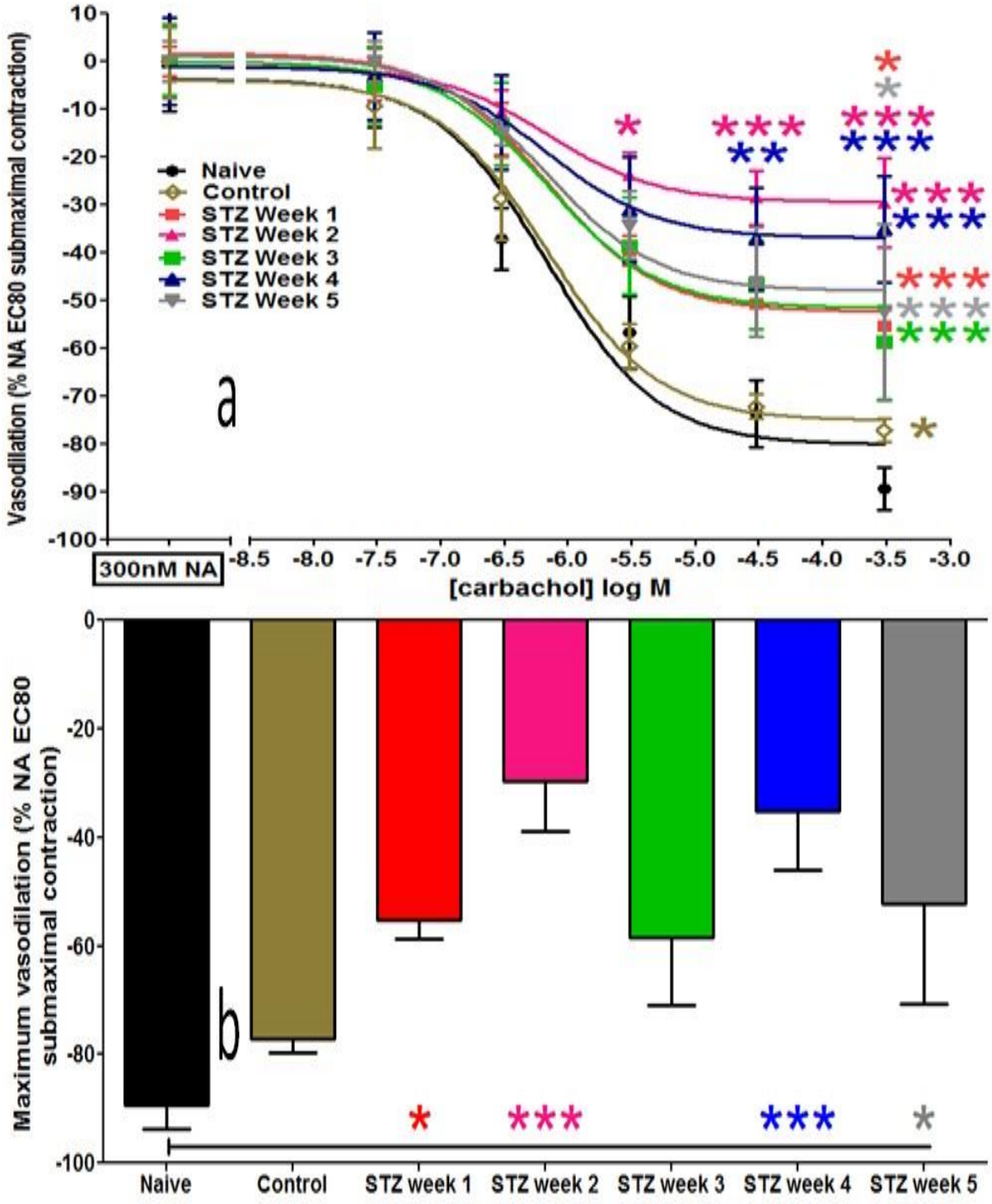

Figure 49. Concentration response curves of carbachol normalised to NA EC_{80} contraction in STZ-diabetic rats aorta (1st week – 5th week) compared to naïve (a). Maximum response induced by carbachol when normalised to NA-induced contraction (b). Analysed through two-way ANOVA post hoc Bonferroni test. All compared against naïve rats' aorta. Data presented as mean ± SEM (Naïve, N= 7, control, N= 5, STZ-induced diabetes week 1, N=4, STZ-induced diabetes week 2, N=6, STZ-induced diabetes week 3, N=5, STZ-induced diabetes week 4, N=7 and STZ-induced diabetes week 5, N=4). Significance is represented as * $p < 0.05$, ** $p < 0.01$ and *** $p < 0.001$.

Carbachol-induced vasodilation experiments were also performed on secondary mesenteric arteries in order to assess the level of dysfunction in these small resistance arteries. There was a significant reduction in carbachol-induced vasodilation due to the induction of diabetes when week 2 STZ-diabetic mesenteric arteries were compared to naïve mesenteric arteries (*** $p < 0.001$). However, Bonferroni's post-hoc test did not show significant difference at any concentration (Figure 50). STZ treatment showed to significantly affect the overall response compared to naïve (N=5, ns $p \geq 0.05$, EC_{50}= 157.7 ± 80.9nM and Emax= -63.5 ± 9.9% vs naïve N=4 EC_{50}= 90.9nM ± 62.8 and Emax= -91.2 ± 4.6).

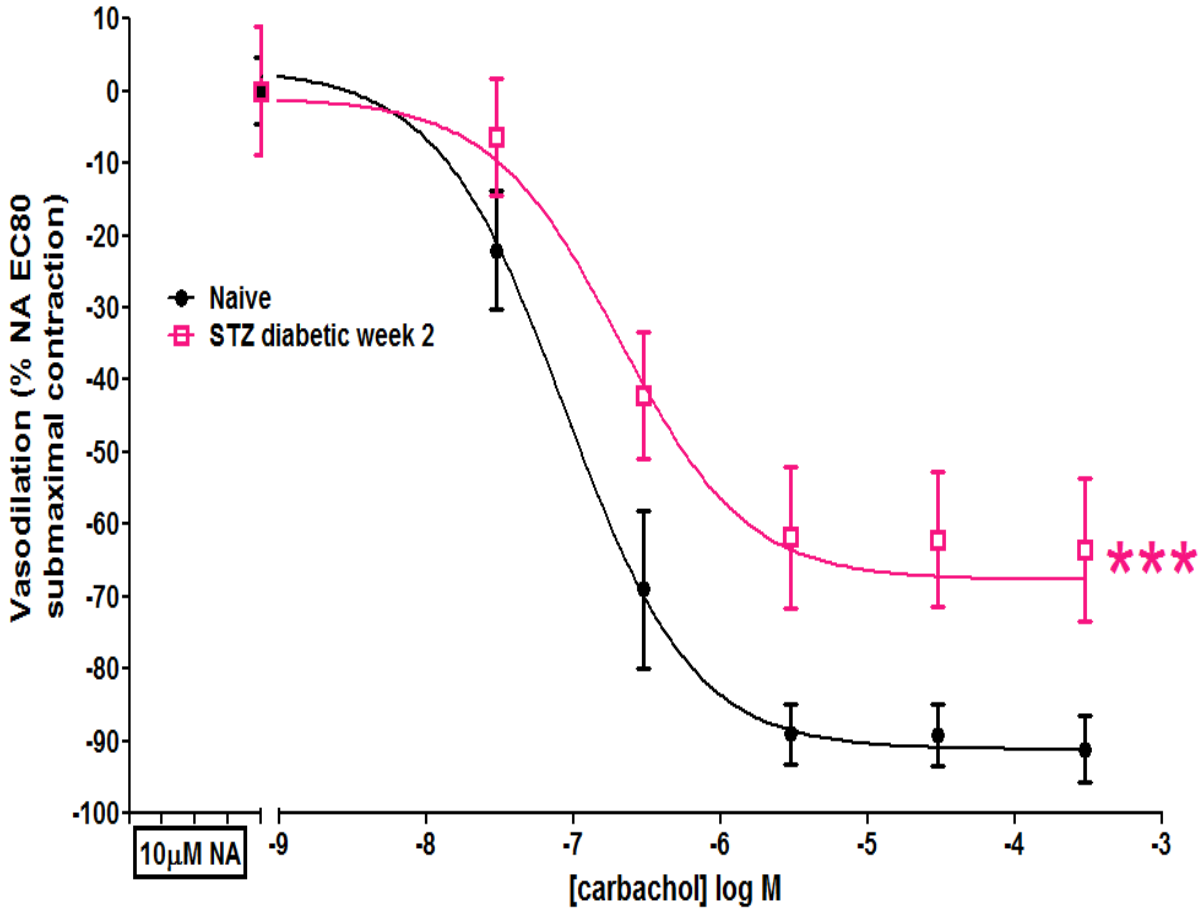

Figure 50. Mesenteric artery response to carbachol concentration response curve of normalised to NA EC_{80} contraction in STZ rats' mesenteric artery. Analysed through two-way ANOVA with Bonferroni's post-hoc analysis did not show significance among the applied carbachol concentrations. Data presented as mean ± SEM (Naïve, N= 4 and STZ-diabetic week 2, N=5).

4.4.3. MGO significantly impaired the carbachol-induced vasodilation in naïve aortic rings

A previous study conducted by A. Dhar et al. (2010) showed that MGO induces vascular dysfunction. As shown in Figure 43, MGO was significantly elevated in diabetic serum. Moreover, figure 49 showed significant impairment of carbachol-induced vasodilation in diabetic aortic rings. Therefore, MGO might contribute to diabetic endothelial dysfunction. To test this hypothesis, naïve aortic rings were exposed to MGO (100µM) ex vivo. This cannot be done over a period of two weeks as in the in vivo experiment, however normal function of aortic rings was retained over 12 hours ex vivo. Accordingly, aortic rings were kept for 12 hours as time control (control 12 hours), figure 51 shows the vasodilation to carbachol of control aorta rings after 12 hours compared to 1 hour after sacrifice (time control). Carbachol-induced full vasodilation was maintained across the 12 hours and the aortic rings became more sensitive to carbachol. The time factor showed significant influence on aortic rings response to carbachol (*** $p < 0.001$). Aortic rings control 12 hours showed increased sensitivity to carbachol with significant EC_{50} reduction when compared to aortic rings time 0 (N= 4, *** $p < 0.001$, EC_{50}= 23.05 ± 13.3nM & Emax= -96.3±2.3% vs time control time, N= 6, EC_{50}= 664.8 ± 449.5nM & Emax= -88.1 ± 3.6%) (Figure 51).

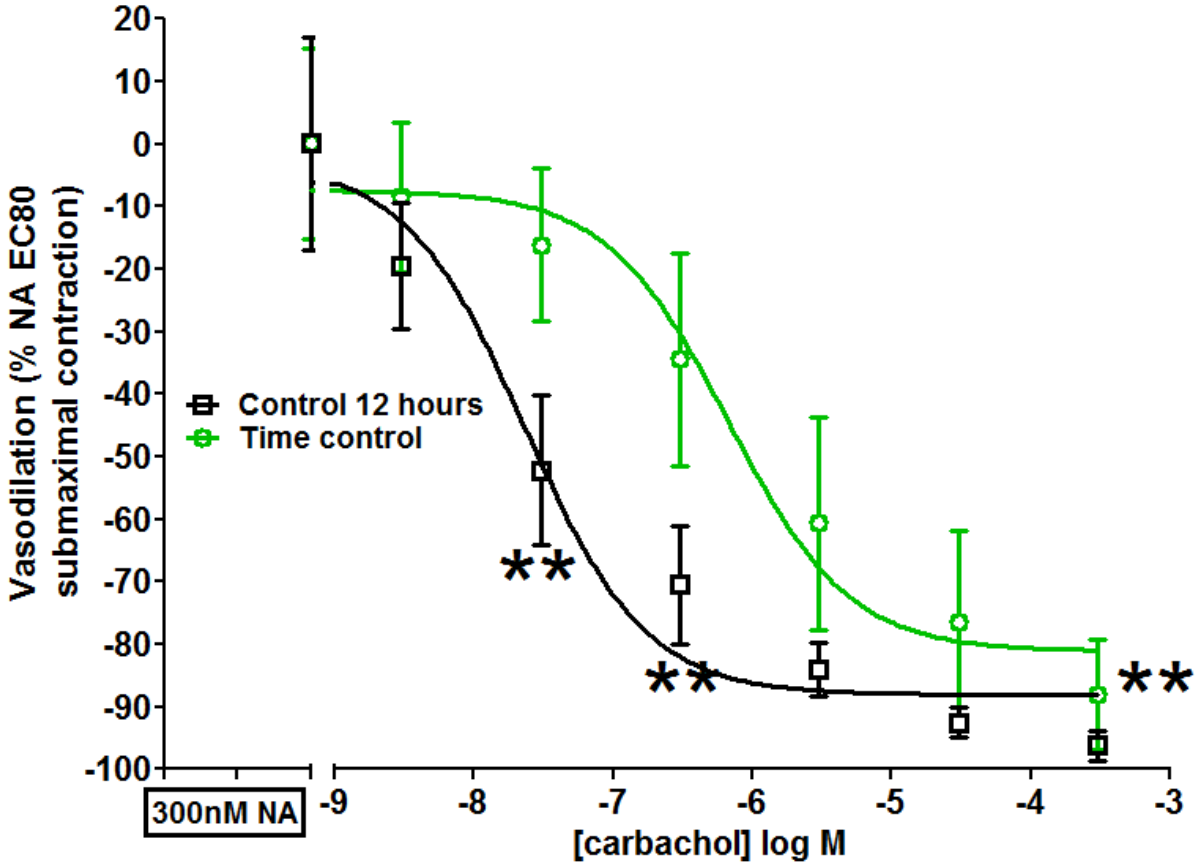

Figure 51. Carbachol concentration response curves normalised to NA EC_{80} contraction in fresh rat aortic rings (time control time) (green) compared to 12 hour time control aortic rings in the organ bath (control 12 hours) (black). Analysed through two-way ANOVA post hoc Bonferroni test. Significance is represented as ** $p < 0.01$ when compared with time control. Data is presented as mean ± SEM (Control 12 hours, N=4 and time control, N=6).

Afterwards, MGO effect on endothelial function was investigated through incubating the aortic rings with MGO (100µM) for 12 hours. Moreover, L-arginine (100µM) was added to MGO (100µM) based on a previous study which concluded that L-arginine acts as MGO scavenger (I. Dhar et al., 2012). MGO (100µM) incubated aortic rings showed significant reduction in carbachol-induced vasodilation. Aortic rings incubated with MGO (100µM) for 12 hours showed significant endothelial dysfunction when compared with time 12 hours control aortic rings (N= 4, *** $p < 0.001$, EC_{50}= 233.4 ± 125.3nM and Emax= -49.1 ± 5.0% vs control 12 hours: N= 4, EC_{50}= 23.05 ± 13.3nM and Emax= -96.3 ± 2.3%). L-arginine showed significant influence on MGO-induced impaired vasodilation [N= 4, $$$ $p < 0.001$, EC_{50}= 33.6 ± 15.0nM & Emax= -84.6 ± 3.3% vs MGO (100µM), N= 4, EC_{50}= 233.4 ± 125.3nM and Emax= -49.1 ± 5.0%). However, aortic rings incubated with MGO (100µM) and L-arginine (100µM) did not show significant difference when compared to control 12 hours (Figure 52).

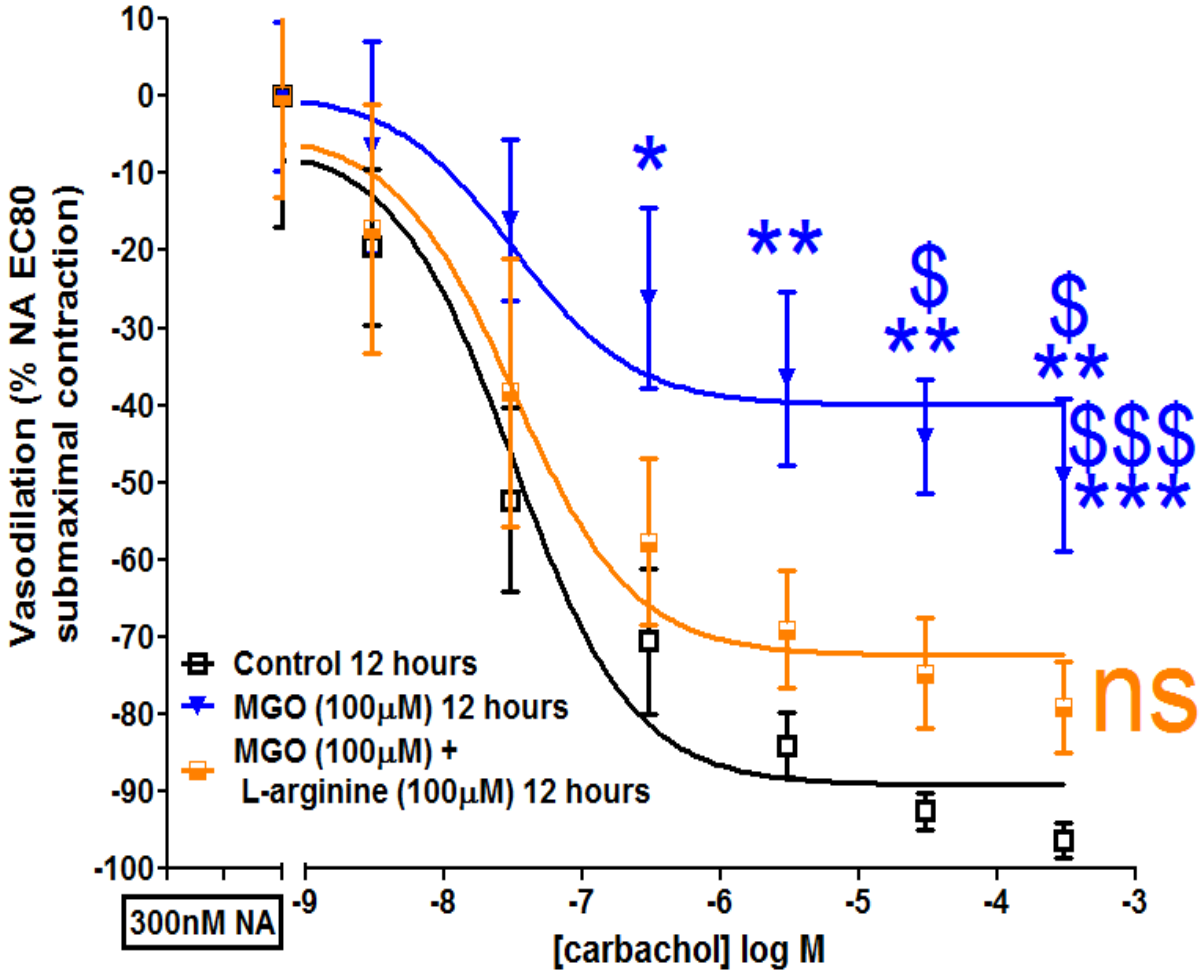

Figure 52. Carbachol concentration response curves normalised to NA EC_{80} contraction in fresh rat aortic rings (control 12 hours) compared to aortic rings incubated with MGO for 12 hours in the organ bath. Analysed through two-way ANOVA post hoc Bonferroni test. Significance is represented as * $p < 0.05$ and ** $p < 0.01$ and *** $p < 0.001$ when compared to control 12 hours and $ $p < 0.05$ and $$$ $p < 0.05$ when compared to MGO (100µM) + L-arginine (100µM), and ns $p \geq 0.01$ when MGO (100µM) and L-arginine (100µM) compared to control 12 hours. Data is presented as mean ± SEM (Control 12 hours, N=4, MGO (100µm), N=4 and MGO (100µm) + L-arginine (100µM) (N=4).

4.4.4. TRPV4-induced vasodilation was significantly impaired in STZ-diabetic aortic and mesenteric arteries

As the endothelial response to carbachol was compromised in STZ-diabetic aortic rings (Figure 49), together with the previous findings that revealed the TRPV4 involvement in endothelium-dependent vasodilation (Figure 33). Experiments were performed to investigate if TRPV4 mediated vasodilation were altered in STZ-diabetic aortic rings. Pre-contracted aortic rings were treated with the TRPV4 agonist RN-1747, to examine the TRPV4-induced vasodilation. STZ vascular responses were significantly altered (*** $p < 0.001$) with the most compromised vascular function in the 2nd week post STZ-injection as TRPV4-induced vasodilation was reduced by approximately 60%, while control rats aorta did not show any significant difference to naïve (Figure 53). Control and STZ-diabetic EC_{50} values did not show significant difference throughout the course study when compared to naïve EC_{50} ($p \geq 0.05$). Diabetes contributed to a significant alteration to the RN-1747 CRC (*** $p < 0.001$). TRPV4-induced vasodilation was reduced among the STZ weeks except the 3rd week (N= 5, ns $p \geq 0.05$, EC_{50}= 122.4 ± 48.7nM & Emax= -68.0 ± 11.2%) which showed similar pattern to naïve (N=7, EC_{50}= 63.3 ± 33.2nM & Emax= -62.4 ± 8.7%) and control aortic rings (N=5, EC_{50}= 36.5 ± 14.5nM & Emax= -56.2 ± 8.6%). RN-1747-induced vasodilation was significantly impaired in the 1st week STZ-diabetic aortic rings (N=4, *** $p < 0.001$, EC_{50}= 35.0 ± 10.1nM & Emax= -19.0 ± 3.0%), 2nd week (N= 6, *** $p < 0.001$, EC_{50}= 431.7 ± 86.1nM & Emax= -21.4 ± 7.7%), the 4th week diabetes showed significant vascular dysfunction (N= 6, *** $p < 0.05$, EC_{50}= 47.6 ± 11.4nM & Emax= -33.0 ± 6.8%) and the 5th week (N= 4, ** $p < 0.01$, EC_{50}= 63.1 ± 5.4nM & Emax= -19.4 ± 9.3%) (Figure 53).

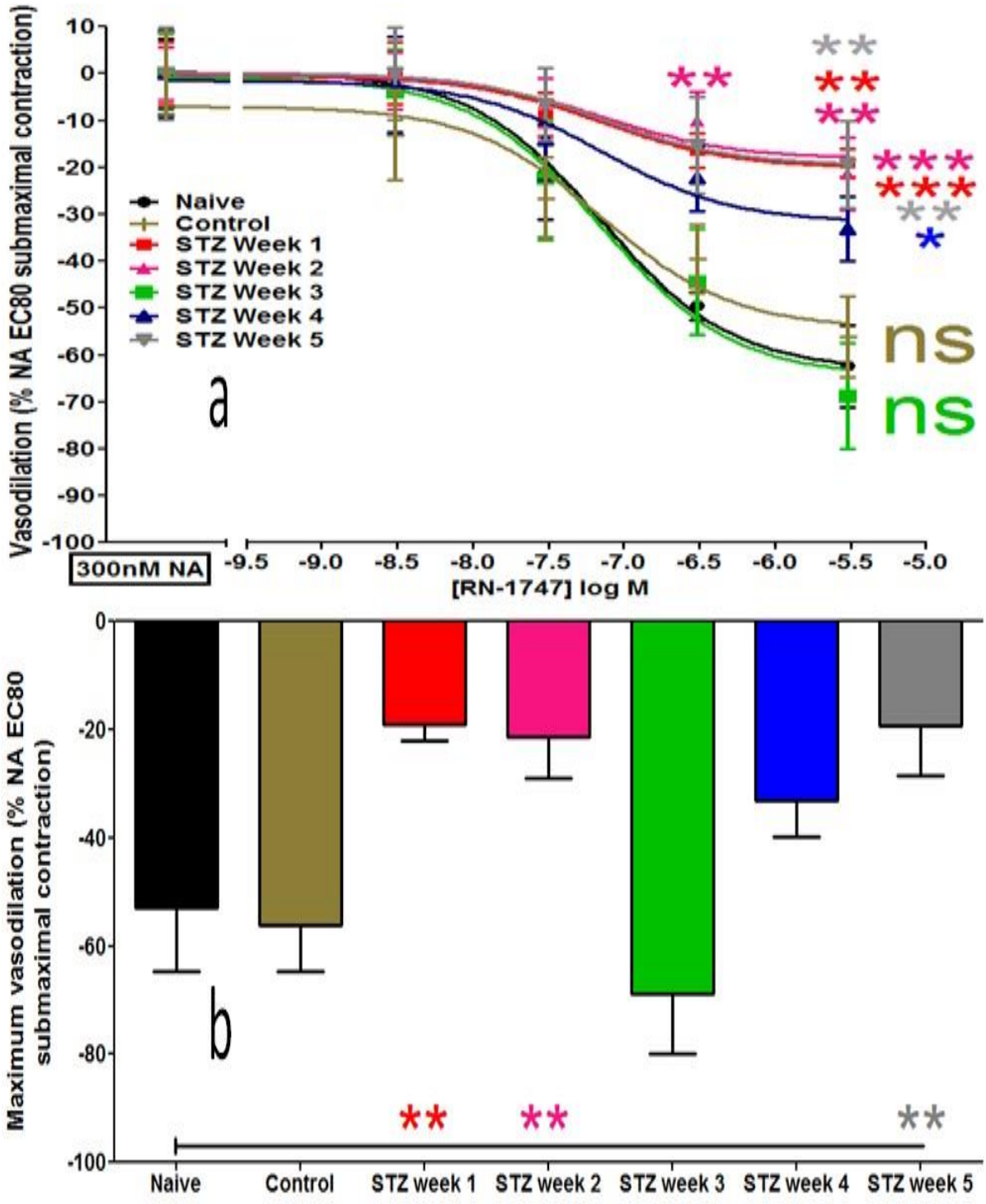

Figure 53. TRPV4-induced vasodilation normalised to maximum NA-induced contraction in naïve and STZ-diabetic aortic rings (a). Maximum response induced by RN-1747 when normalised to NA-induced contraction (b). Analysed through two-way ANOVA post hoc Bonferroni test. Significance is represented as ns $p \geq 0.05$, p * < 0.05, ** < 0.01 and *** $p < 0.001$ versus naïve aortic rings. Data presented as mean ± SEM (Naïve, N= 5, control, N= 5, STZ-induced diabetes week 1, N=4, STZ-induced diabetes week 2, N=6, STZ-induced diabetes week 3, N=6, STZ-induced diabetes week 4, N=6 and STZ-induced diabetes week 5, N=4).

Another TRPV4 agonist, 4-αPDD was examined to confirm the observation with RN-1747. As shown in Figure 54, diabetes contributed to a significant alteration to the 4-αPDD CRC (*** $p < 0.001$). Diabetic aortic rings showed significant impairment in 4-αPDD –induced vasodilation (N=4, EC_{50}= 526.2 ± 317.1nM and Emax= 56.0 ± 5.5% vs naïve EC_{50}= 92.9 ± 54.7nM and Emax= 81.1 ± 2.1%) (Figure 54). However, STZ-diabetic EC_{50} values did not show significant difference when compared to naïve EC_{50} ($p \geq 0.05$).

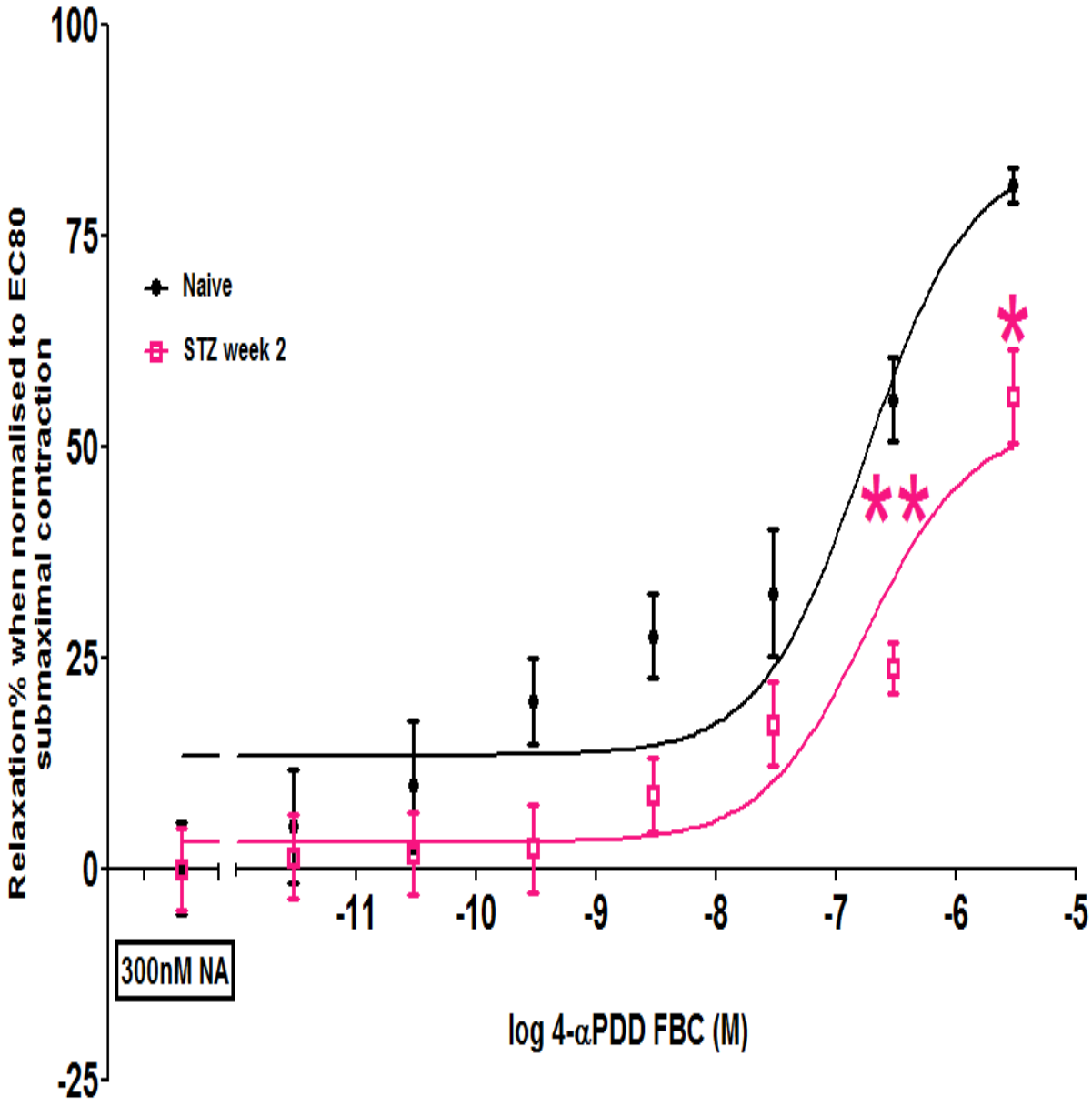

Figure 54. 4-αPDD reduced vasodilation in STZ-diabetic aortic rings. Analysed through two-way ANOVA with Bonferroni post-hoc test. Significance is represented as * $p < 0.05$ and ** $p < 0.01$ when compared with naïve aortic rings. Data shown as percentage ± SEM (Naïve, N= 5 n= 11 and STZ-diabetic week 2, N=4 n= 8).

Mesenteric arteries' response toward RN-1747 was recorded to compare STZ-diabetic with naïve rats' mesenteric arteries. As shown in Figure 55, STZ-diabetic EC_{50} values did not show significant difference when compared to naïve EC_{50} ($p \geq 0.05$), however, diabetes contributed to a significant alteration to the RN-1747 CRC (* $p < 0.05$). STZ-diabetic rats' mesenteric arteries showed significant compromise in RN-1747-induced vasodilation in week 2 STZ-diabetic mesenteric arteries compared to naïve mesenteric arteries. Diabetic mesenteric arteries showed significant vascular dysfunction N=5, EC_{50}= 0.3 ± 0.11μM and Emax= -41.5 ± 5.7% vs naïve EC_{50}= 2.3 ± 1.02μM and Emax= -79.1 ± 6.1% (Figure 55).

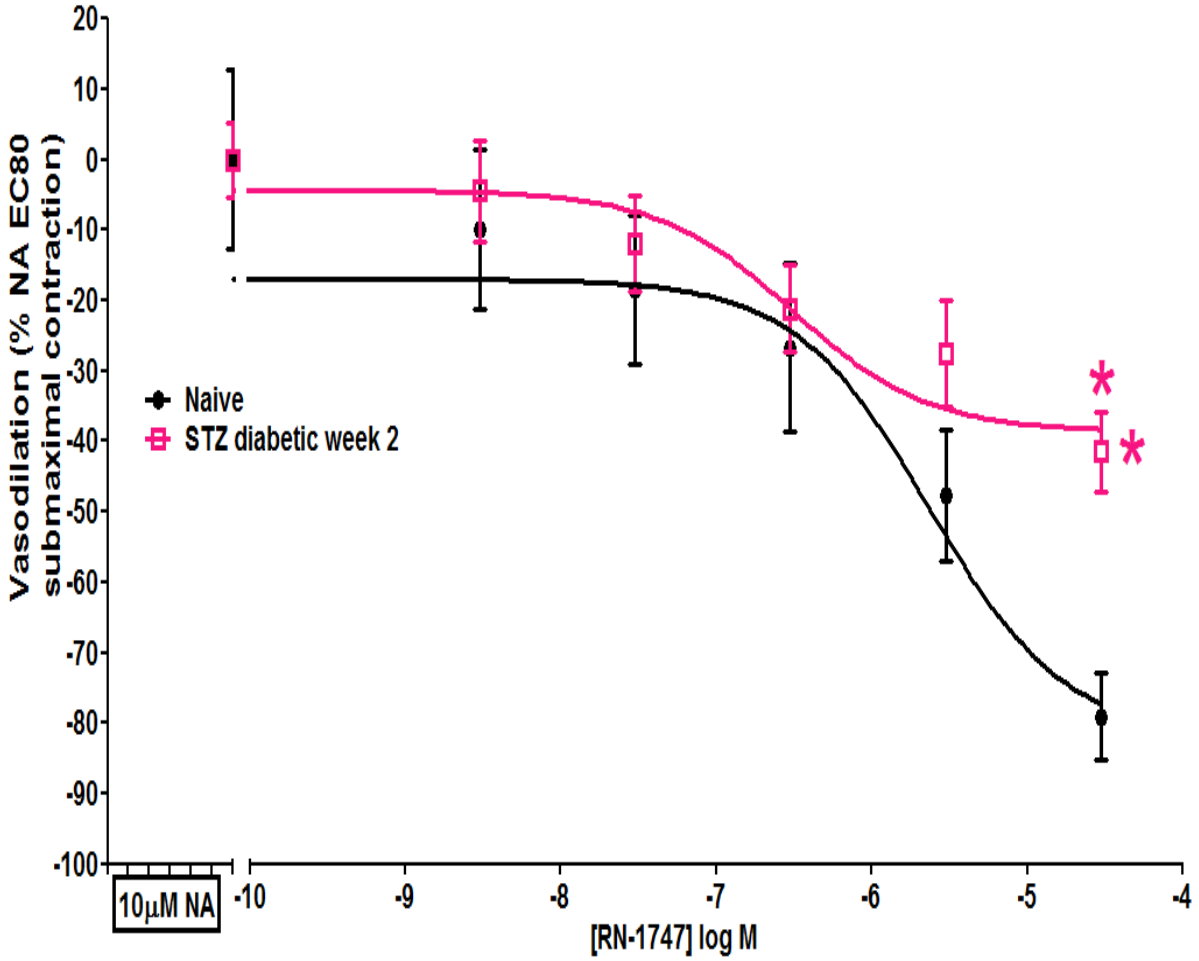

Figure 55. TRPV4-induced vasodilation in naïve and STZ-diabetic mesenteric arteries. RN-1747-induced vasodilation was significantly reduced in STZ-diabetic mesenteric arteries. Analysed through two-way ANOVA post hoc Bonferroni test. Significance is represented as * $p < 0.05$ when compared with naïve mesenteric arteries. Data shown as percentage ± SEM (Naïve, N= 4 and STZ-diabetic week 2, N=5).

4.4.5. TRPM8-induced vasodilation was not significantly influenced in STZ-diabetic aortic arteries

Previous findings in chapter 3 showed that TRPM8-induced vasodilation was not significantly compromised when endothelium was removed (Figure 34). Additionally, significant alteration in carbachol and TRPV4-mediated vasodilation was shown in endothelium denuded aortic ring (Figure 32 & 41). Moreover, both carbachol and TRPV4-induced vasodilation was impaired in STZ-diabetic aortic rings (Figure 49-58 & 61-63). Therefore, pre-contracted aortic rings were relaxed with TRPM8 agonist, icilin CRC to investigate whether TRPM8 is impaired in the STZ-diabetic endothelium. As shown in Figure 56, TRPM8 was not affected in STZ-diabetic aortic rings ($p \geq 0.05$). Icilin-induced vasodilation showed overlapping concentration response curve with naïve aortic rings (N=5, $p \geq 0.05$, EC_{50}= 0.82 ± 0.53μM and Emax= -76.3 ± 5.3% vs naive EC_{50}= 2.7 ± 1.7μM and Emax= -78.3 ± 2.2%) (Figure 56).

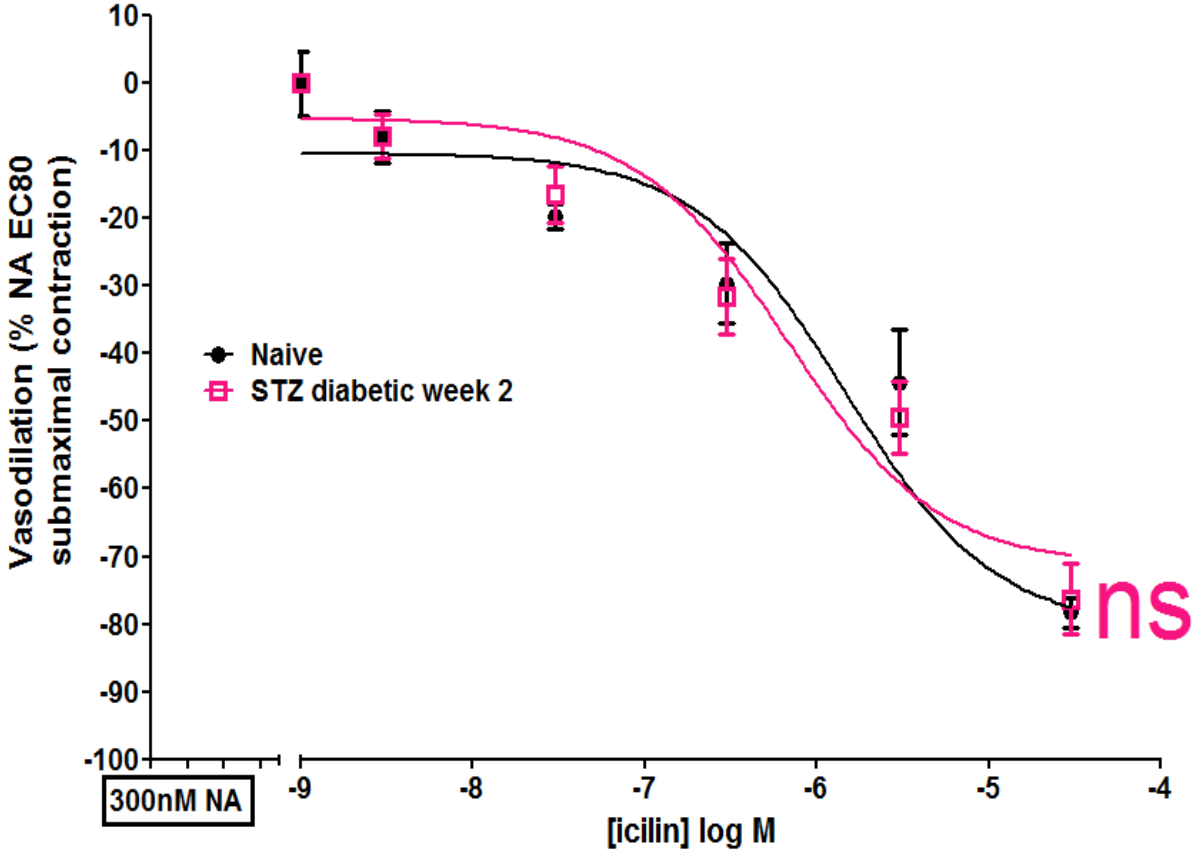

Figure 56. TRPM8 mediated vasodilation in naïve and STZ-diabetic aortic rings. Analysed through two-way ANOVA post hoc Bonferroni test compared with naïve aortic rings. Data shown as percentage ± SEM (Naïve, N= 4 and STZ-diabetic week 2, N=5).

4.4.6. SNP-induced vasodilation did not show significant difference between STZ-diabetic and naïve aortic rings

To investigate whether the diabetic vascular dysfunction is mainly attributed to endothelium or both endothelium and VSM, SNP, a direct vasodilator was applied to pre-contracted aortic rings. This vasodilator acts independently from the endothelium and hence activates the VSM's sGC (Boese, Busse, Miilsch, & Kerth, 1996). As illustrated in Figure 57, diabetic aortas showed a similar SNP-induced vasodilation pattern as naive aorta. SNP-induced vasodilation showed overlapping concentration response curve with naïve aortic rings (N=4, ns $p \geq 0.05$, EC_{50}= 5.2 ± 3.6nM Emax= 113.4 ± 7.2% vs naive N=6, EC_{50}= 1.9 ± 1.2nM and Emax= 103.2 ± 2.8%) (Figure 57).

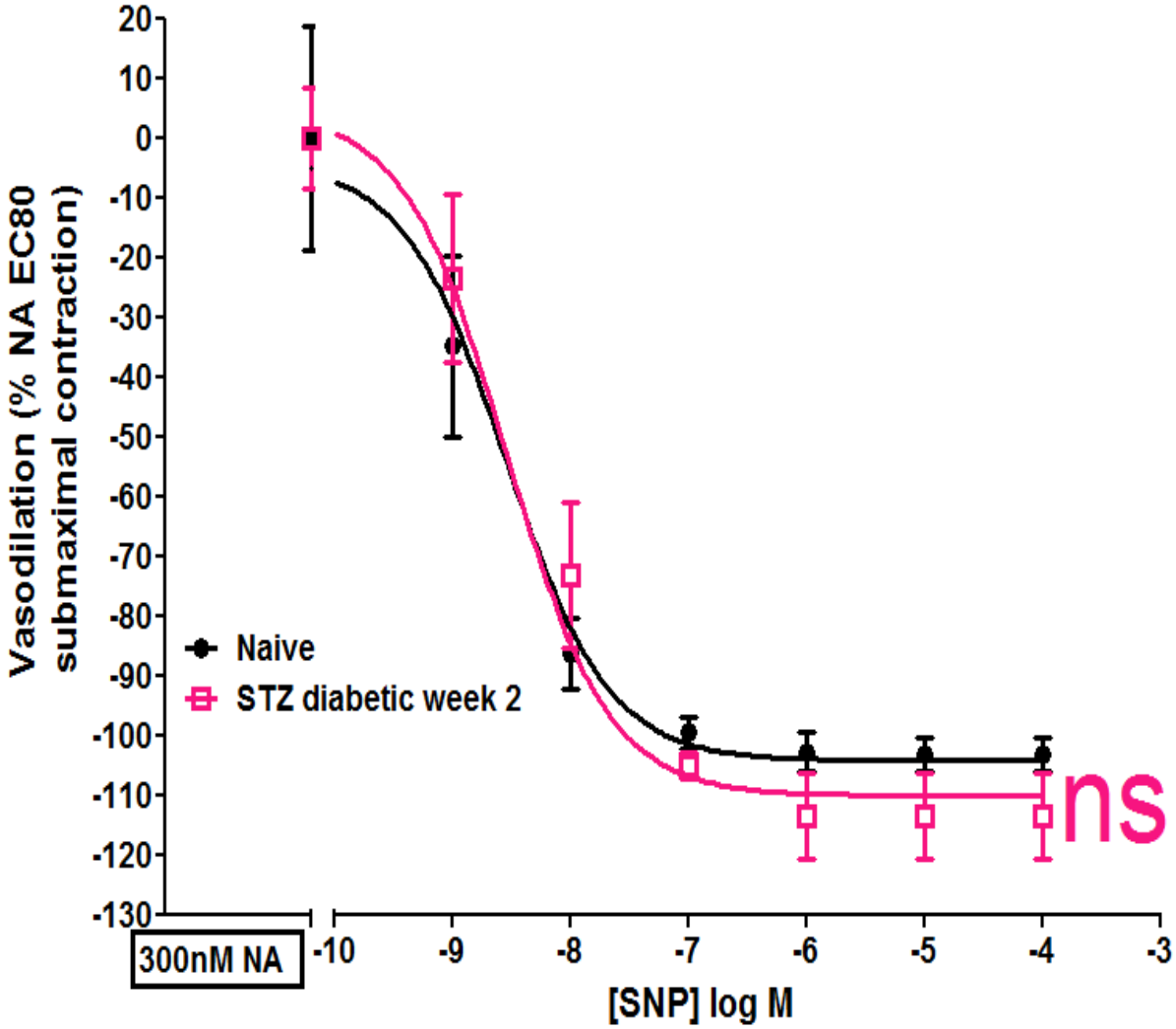

Figure 57. SNP-induced vasodilation in naïve and STZ-diabetic aortic rings. Analysed through two-way ANOVA post hoc Bonferroni test compared with naïve aortic rings. Data shown as percentage ± SEM (Naïve, N= 6 and STZ-diabetic week 2, N=4).

4.5. Discussion

In this chapter, STZ-induced diabetes model was used in these experiments and characterised through a number of parameters. Blood glucose concentration was the main diabetes marker as rats were considered diabetics when their blood glucose readings exceeded 16mmol/L. STZ induced hyperglycaemia with fourfold blood glucose increase in 95% of the STZ-injected rats (Figure 40). These findings were similar to what was reported in a previous study (Bagri, Ali, Aeri, Bhowmik, & Sultana, 2009).

ELISA studies were conducted to correlate hyperglycaemia and diabetes vascular dysfunction with selected circulating markers, MGO and ox-LDL. MGO showed significant increase in STZ-diabetic rats' serum samples (Figure 43). The fourfold increase in serum MGO (Figure 43b) was accompanied with fourfold increase in blood glucose concentration (Figure 40). Therefore, chronic hyperglycaemia, where blood glucose concentration exceeds 7mmol/L might contribute as the major endogenous MGO source (Kalapos, 2013). The glycolytic-derived MGO is mainly attributed to triose phosphates, glyceraldehyde 3-phosphate and glycerone phosphate pathway through non-enzymatic or enzymatic reactions, if not both (Philips & Thornalley, 1993). Additionally, since lipolysis and proteins metabolism are accelerated in diabetes, MGO generation is increased through lipid peroxidation and SSAO, respectively (Boomsma et al., 1999; Mahendran et al., 2013; Mitch et al., 1999; Shamsaldeen et al., 2016). MGO is involved in common diabetes complications such as endothelial dysfunction, insulin resistance, and neuropathic pain (A. Dhar et al., 2010; A. Dhar, Dhar, Jiang, Desai, & Wu, 2011; Eberhardt et al., 2012).

Serum ox-LDL showed significant increase in STZ-diabetic rats' serum (Figure 44). Ox-LDL molecule is recognised by CD36 endothelial scavenger receptor that facilitates the uptake and the endocytosis of ox-LDL (Y. Zeng, Tao, Chung, Heuser, & Lublin, 2003). Additionally, ox-LDL is a cholesterol acceptor that competes with caveolae to deplete the caveolae from cholesterol and hence causes caveolae disruption (Blair, Shaul, Yuhanna, Conrad, & Smart, 1999). Caveolae disruption inhibits eNOS attachment to CAV-1 which contributes to endothelial dysfunction (Blair et al., 1999). Moreover, previous studies revealed the correlation between elevated serum ox-LDL and diabetic complications, neuropathy, nephropathy and vascular dysfunction (Tsuzura et al., 2004). Daily consumption of tomato juice (500ml/day for 4 weeks) improves the serum antioxidant, lycopene concentration by 3–fold. Such improvement is associated with decrease in LDL susceptibility to oxidation and decreased CRP aiming for reducing the risk of diabetes associated myocardial infarction

(Upritchard, Sutherland, & Mann, 2000). Moreover, HMG-CoA reductase inhibitors, statins (simvastatin and lovastatin) protects eNOS activity from ox-LDL-induced downregulation (Laufs, Fata, Plutzky, & Liao, 1998). High density lipoprotein (HDL) binds mainly on scavenger receptor class B isoform I (SR-BI) where it delivers the circulating cholesterol to the caveolae and hence maintains the caveolae integrity and enhances eNOS activity (Malerød, Juvet, & Berg, 2002; Thomas & Smart, 2008; Yuhanna et al., 2001).

STZ-induced hyperglycaemia was associated with significant hypoproteinaemia (Figure 45). Serum total protein measurement showed significant time-dependent reduction in STZ-diabetic rats (Figure 45a). Such hypoproteinaemia reveals the progression of diabetes as the 1st week STZ-diabetic rats' serum did not show significant serum hypoproteinaemia, while significant hypoproteinaemia was observed afterwards, (2nd week – 5th week). A previous study showed proteinuria as a common diabetes complication that is associated with plasma hypoproteinaemia (Bhonsle et al., 2012). Hypoproteinemia is mainly attributed to nephropathy and such finding was reported in previous study which was associated with significant eightfold increase in urine protein (Niwa et al., 1997). However, Niwa et al. (1997) did not show significant hypoproteinaemia although the STZ-induced diabetes was 3 months duration revealing the robust diabetes model demonstrated in this study.

Thereafter, NA-induced vasoconstriction was investigated. Both naïve and STZ-diabetic aortic rings showed similar EC_{80} of NA, 300nM (Figure 46), which went in agreement with Verbeuren et al. (1986) findings. However, STZ-diabetic rats' aortic rings treated with NA (300nM) showed significant higher vasoconstriction compared to naïve aortic rings (Figure 47). Such finding can be attributed to impaired endothelium hyperpolarisation which causes higher arterial response to exogenous vasoconstrictor than the naïve aortic rings (Fukao, Hattori, Kanno, Sakuma, & Kitabatake, 1997). Moreover, TRP channels-mediated striking influx of Ca^{2+} that might lead to vasoconstriction through agonist-induced membrane depolarisation-activated TRP channels as for instance in α1-adrenergic receptor-stimulated TRPC6 that is commonly found in rat's aorta and cerebral arteries (Inoue et al., 2009). Additionally, previous studies revealed that ox-LDL induces the expression of endothelin-1, a potent vasoconstrictor which might exacerbate the vascular complications in diabetes (Galley & Webster, 2004). Therefore, in addition to being implicated in endothelial dysfunction, elevated serum ox-LDL (Figure 44) might be related to the significant increase in STZ-vasoconstriction shown in Figure 47. Naïve and STZ-diabetic rats' mesenteric arteries

showed similar NA EC_{80} at 10μM, which matched the concentration applied by Lewis, Surprenant, and Evans (1998) on the second order rats' mesenteric arteries (Figure 48).

Afterward, STZ rats were studied as diabetic models to examine the vascular function over a 5 week period. Aortic rings were examined through applying vasodilators; carbachol or TRPV4 agonist (RN1747 or 4-αPDD) after being pre-contracted with NA (300nM). STZ-diabetic rats showed significant vascular dysfunction which was started from the first couple of days post-injection and continued for the whole 5 weeks experiment timeframe. The most significant vascular dysfunction was shown in the 2nd week in STZ-induced diabetes model as shown in Figures 49 and 50. Therefore, the 2nd week (8th - 14th day) post-STZ injection was applied as a representative time-point for diabetic vascular dysfunction. Muscarinic-induced vasodilation was significantly impaired in aortic rings and mesenteric arteries (Figures 49 & 50). These findings match with a previous study's conclusion that vascular function of STZ-diabetic rats is attributed to impaired muscarinic-induced endothelium-dependent vasodilation (Fukao et al., 1997).

Carbachol-induced vasodilation was endothelium dependent (Figure 32). Therefore, STZ-impaired muscarinic-induced vasodilation might be regarded as endothelial dysfunction. As a consequence of diabetes, endothelial dysfunction is a common complication where endothelium-dependent vasodilation is impaired that contributed to peripheral artery disease, foot ischemia, ulceration and even amputation (A. Dhar et al., 2010; Ruiter et al., 2012).

To examine whether elevated MGO is implicated in inducing diabetic endothelial dysfunction, naïve aortic rings were incubated with MGO (100μM) for 12 hours. Carbachol-induced vasodilation was significantly impaired (Figure 52). To ensure that the effect was not due to tissue failure, control rings were experimented in parallel which did not show endothelial alteration (Figure 51). Such finding is supported by previous study which found that MGO inhibits the phosphorylation of serine-1177 of eNOS and hence reduces endothelial NO release (A. Dhar et al., 2010). This finding is supported by STZ-diabetic endothelial dysfunction (Figure 49 & 58) which was correlated with the significant increase in serum MGO (Figure 43). Therefore, MGO might play a major role in diabetic endothelial dysfunction (Brownlee, 2001). L-arginine (100μM) restored the endothelial function in the presence of MGO (100μM) (Figure 52). Such finding is attributed to the ability of L-arginine to scavenge MGO (I. Dhar et al., 2012). However, further studies such as high performance liquid chromatography (HPLC) are required to prove the ability of L-arginine to scavenge

MGO. Moreover, incubating aortic rings with L-arginine (100μM) only, as L-arginine control should be investigated in parallel to the conditions applied in Figure 52, since L-arginine could potentiate eNOS activity to enhance NO generation (Böger, 2004)

The deterioration in endothelium-dependent vasodilation characterised by impaired muscarinic-induced vasodilation (Figure 49 & 58) was in parallel with impaired TRPV4-induced vasodilation in both aortic and mesenteric arteries (Figures 53 - 55). Therefore, muscarinic and TRPV4 impaired vasodilation reveals possible mechanistic collaboration of the muscarinic receptors and TRPV4 channels. Additionally, TRPV4 blocking was shown to significantly influence muscarinic-induced vasodilation (Figures 22 & 23). Muscarinic and TRPV4 cascades might be integrated through GPCR-activated PLC that hydrolyses the membranous PIP2 into DAG and IP3, IP3 binds to its corresponding smooth ER's IP3-R to facilitate Ca^{2+} release from cellular stores (Clapham, 2003; Ying, Aaron, & Sanders, 2014). Moreover, TRPV4 is activated through the muscarinic downstream cascade element, DAG-activated PKC binding (Rohacs & Nilius, 2007). Additionally, TRPV4 mice KO study have revealed its essential role in muscarinic-mediated endothelium-dependent vasodilation through novel mechanism that involves Ca^{2+} influx through endothelium derived factor, 11, 12 EET-activated TRPV4 which enhances Ca^{2+} entry that activates and opens the BKCa to yield membrane hyperpolarisation and vasodilation (Earley et al., 2005; M. Freichel et al., 2005).

Among the channels of interest was TRPM8, which was elicited specifically for two main reasons: firstly, not like TRPV4 that mediates both BKca and NO-dependent vasodilation (Figure 27 & 39), TRPM8 showed to mediate vasodilation through BKca-dependent (Figure 31) and NO-independent pathways (Figure 28). The second reason was for the commonly available and applicable agonist as it is activated by menthol or icilin (D. A. Andersson et al., 2007). Pre-contracted diabetic aortic rings were relaxed through icilin CRC without any significant difference from non-diabetic aortic rings (Figure 56). This supports the previous findings (Figure 28 & 39) that TRPM8 is suggested to mediate vasodilation through different pathways to TRPV4 which was significantly compromised in diabetes.

SNP study was conducted to investigate the viability of sGC (Boese et al., 1996). As illustrated in Figure 57, STZ-diabetic aortic rings showed similar SNP-induced vasodilation pattern as naive aortic rings revealing that sGC activity might not be significantly compromised in diabetic aortic rings.

To sum up, STZ-diabetic rats showed significant endothelial dysfunction through impaired carbachol-induced vasodilation. Such endothelial dysfunction was accompanied with compromised TRPV4-induced vasodilation. By contrast, TRPM8 vascular function was not significantly compromised in STZ-induced diabetes which might suggest that TRPM8 is acting through different pathways than TRPV4. ELISA studies showed significant increase in diabetic serum ox-LDL and MGO. Ox-LDL might explain the diabetic endothelial dysfunction and the exaggerated vasoconstriction. Elevated MGO serum concentration in STZ-diabetic rats' serum might also explain the diabetic endothelial dysfunction as incubating naïve non-diabetic aortic rings with MGO (100μM) for 12 hours compromised endothelial function. To examine the mechanism of the compromised TRPV4-induced vasodilation and the involvement of MGO in endothelial TRPV4 dysfunction, the next chapter will include further MGO investigations.

Chapter 5: The effect of diabetes on TRPV4 function and expression in rat primary aortic ECs

5.1. Introduction

In the last chapter, muscarinic and TRPV4-induced vasodilation were significantly compromised in STZ-diabetic aortic and mesenteric arteries. However, TRPM8-induced vasodilation was not significantly influenced in STZ-diabetic aortic rings.

Endothelial dysfunction is a common diabetes complication in which endothelium-dependent vasodilation becomes impaired (Kolluru et al., 2012). TRPV4 is highly expressed in the ECs and a major vascular tone controller (Köhler et al., 2006). H. Y. Kwan et al. (2007) hypothesised that a dysfunction in TRPV4 might contribute to endothelial dysfunction. Moreover, Köhler et al. (2006) provided the first evidence of TRPV4 dysfunction involvement in endothelial dysfunction when the flow-induced vasodilation was abolished by TRPV4 blockers, ruthenium red, and the PLA2 inhibitor, arachidonyl trifluoromethyl ketone in rat carotid arteries. A recent study demonstrated TRPV4 downregulation in STZ-rats' mesenteric endothelium (Ma et al., 2013). Moreover, TRPV4 downregulation is involved in diabetic endothelial dysfunction and retinopathy (Monaghan et al., 2015). These studies provide a very robust foundation that correlates TRPV4 alteration with diabetes endothelium dysfunction. TRPV4 is coupled and functionally regulated by CAV-1 (Saliez et al., 2008). Additionally, CAV-1 is coupled with eNOS and both were downregulated in STZ-diabetic rats' kidneys and bovine aortic ECs, and such downregulation was reversed through insulin treatment (Komers et al., 2006; H. Wang et al., 2009).

As described in section 1.7., the main objectives of this chapter were to investigate whether TRPV4-induced $[Ca^{2+}]i$ elevation is influenced in diabetic ECs through fura-2 Ca^{2+} imaging studies. Moreover, to investigate the contribution of diabetes on TRPV4 expression in ECs through LSCM studies, and whether other cellular proteins are influenced such as eNOS and CAV-1. Ex vivo insulin treatment of the ECs was conducted to examine the importance of insulin to maintain the endothelial function. Further investigations were conducted on the effect of MGO (100μM) on TRPV4 function through fura-2 Ca^{2+} imaging studies and LSCM. Moreover, TRPM8 fura-2 Ca^{2+} imaging studies were conducted to test the hypothesis that the vascular TRPM8 function is not influenced by diabetes.

5.2. Materials and methods

5.2.1. Primary endothelial cells studies

Primary aortic ECs were isolated and grown in t-25 collagen I-coated culture flasks as described in section 2.4. The primary aortic ECs showed morphological characteristics which became clearer under the LSCM when the ECs were tagged with Dil-Ac-LDL. After becoming fully confluent, the ECs were plated on poly-l-lysine coated glass coverslips. STZ-diabetic ECs were treated with insulin (1 and 10µg/ml equivalent to 270mIU/ml and 2.7mIU/ml) for 5 days. The expression level of TRPV4, CAV-1 and eNOS was studied through LSCM as described in section 2.7.1. Each ECs' coverslip was initially tagged with Dil-Ac-LDL that is a selective marker for ECs in the vasculature. The Dil-Ac-LDL is taken-up by the ECs that hydrolyse the acetyl bond to release the fluorescence LDL which is trapped intracellularly, endowing red fluorescence to the ECs. The Dil-Ac-LDL-tagged coverslips were then washed-out to remove any extracellular Dil-Ac-LDL. Afterward, the coverslips were incubated with the primary antibody to tag the protein of interest: TRPV4, CAV-1 or eNOS. Thereafter, the coverslips were washed-out of any unbound antibodies before being incubated with the secondary green fluorescence antibody that binds to the primary antibody. Thereafter, the unbound secondary antibodies were washed-out and the coverslips were added with mounting media containing the nucleus staining DAPI, which stains the nucleus in blue. The LSCM pictures were analysed through ImageJ. The nucleated, Dil-Ac-LDL tagged ECs were considered as ROI. Therefore, the expression of the protein of interest was measured only in the ROI. STZ-diabetic ECs were treated with insulin for 5 days to examine the effect of insulin treatment on TRPV4, CAV-1 and eNOS expression and distribution.

In another experiment, the naïve control aortic ECs were treated with MGO (100µM) to examine the effect of MGO on TRPV4 expression and distribution.

Fura-2 Ca^{2+} imaging studies were conducted to compare the STZ-diabetic and naïve primary aortic ECs response to 4-αPDD (1mM) and icilin (1mM) as described in section 2.6. Additionally, the effect of insulin on TRPV4 function was investigated in STZ-diabetic aortic ECs cells through fura-2 Ca^{2+} imaging. The naïve control aortic ECs were treated with MGO (100µM) to examine the effect of MGO on TRPV4 function. Additionally, L-arginine (100µM) was added to MGO (100µM) to examine the protective effect of L-arginine against MGO on TRPV4 function.

5.3. Results

5.3.1. TRPV4 was significantly downregulated in STZ-diabetic ECs and restored through insulin treatment

As previously shown in Figures 53-55, TRPV4-induced vasodilation was significantly impaired in diabetic aortic and mesenteric arteries. Moreover, TRPV4-induced vasodilation was significantly endothelium dependent (Figure 33). Therefore, naïve and STZ-diabetic ECs were visualised under the LSCM (figure 58). Additionally, STZ-diabetic ECs were treated with insulin (1 and 10μg/ml equivalent to 270mIU/ml and 2.7mIU/ml) for 5 days before being studied through LSCM. As shown in Figure 58, TRPV4 showed distribution around the nucleus and at the edge of plasma membrane in naïve aortic ECs (a2). STZ-diabetic ECs showed disrupted TRPV4 distribution with less green fluorescence emission (b2). Insulin treatment 270mIU/ml/day (c2) and 2.7IU/ml/day (d2) for 5 days restored TRPV4 distribution in STZ-ECs. Images were combined to matching endothelial marker (red), nucleus marker (blue) and TRPV4 florescence antibody (green) (a3, b3, c3 & d3).

Label	AC-Dil-LDL	TRPV4 antibody	AC-Dil-LDL + TRPV4 antibody
Naïve (or control)	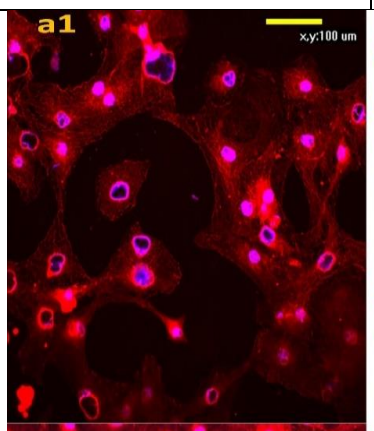	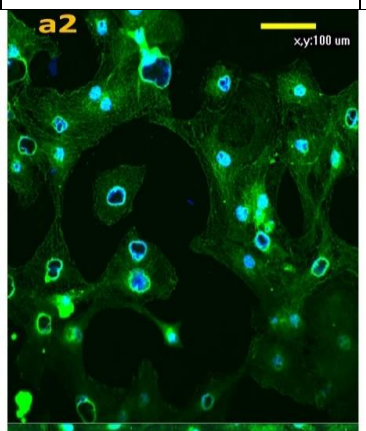	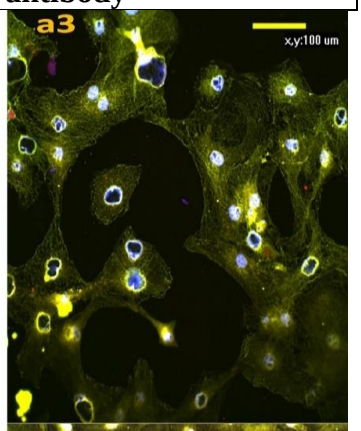
STZ-diabetic ECs	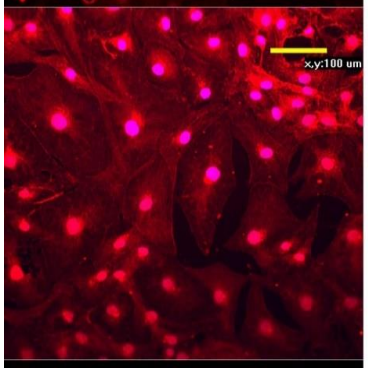	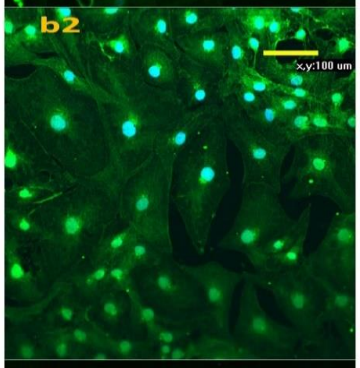	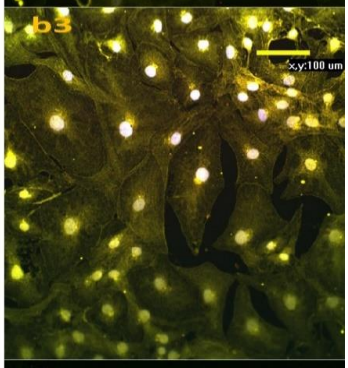
STZ-diabetic ECs treated with insulin 270mIU/ml	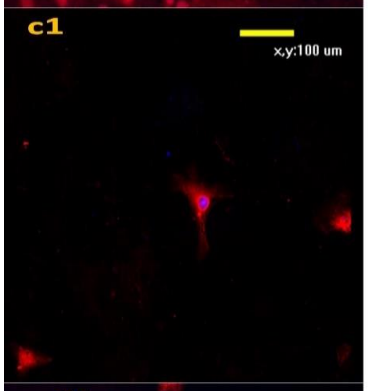	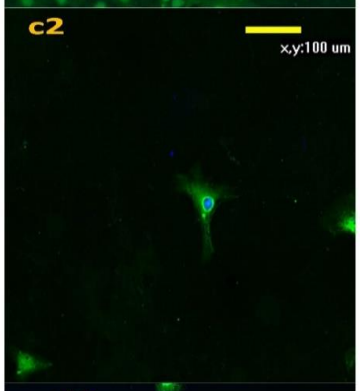	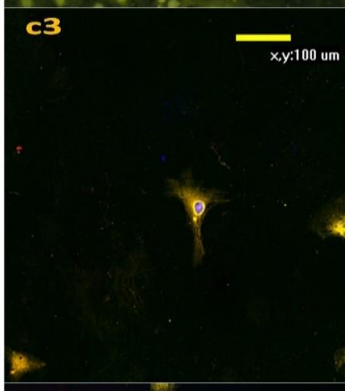
STZ-diabetic ECs treated with insulin 2.7IU/ml	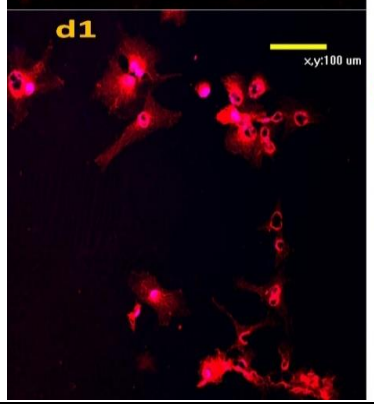	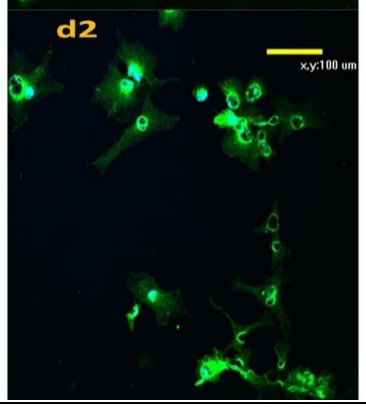	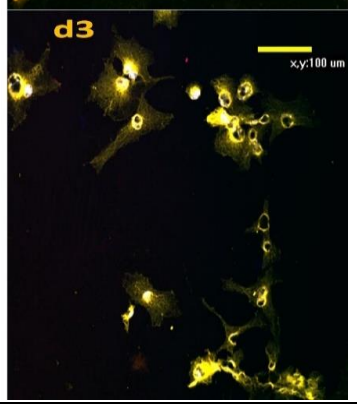

Figure 58. TRPV4 expression in primary aortic endothelial cells under laser scanning confocal microscope. Endothelial cells were probed with DAPI to label the nucleus in blue and marked with acetylated LDL (Dil-Ac-LDL) giving the cells the red colour (left: a1, b1, c1 & d1). Anti TRPV4 primary antibody probed with secondary green fluorescence antibody (middle: a2, b2, c2 & d2). Images were combined to match the selective ECs marker (red) with anti TRPV4 (green) and the nucleus marker (blue) (right: a3, b3 & c3 & d3) (200×) 488nm laser.

The confocal microscopy images were quantitatively analysed through ImageJ software (version 1.46r) and statistically analysed through GraphPad prism (version 5.00). Total TRPV4 expression showed significant difference when insulin treated STZ-ECs were compared to untreated STZ-diabetic ECs (* $p < 0.05$). As shown in Figure 59a, primary aortic ECs isolated from 3 different STZ-diabetic rats were treated with insulin (270mIU/ml & 2.7IU/ml). The three groups were compared through matched one way ANOVA analysis showing significant increase in TRPV4 expression when diabetic ECs were treated ex vivo with insulin (Insulin 270mIU/ml, N= 3, * $p < 0.05$, average TRPV4 expression= 101.6 ± 6.5% and insulin 2.7IU/ml, N= 3, average TRPV4 expression= 100.0 ± 10.9% vs STZ-diabetic ECs N= 3, average TRPV4 expression= 68.4 ± 12.03%) (Figure 59a).

When the whole data were pooled together and compared with naïve ECs, TRPV4 expression showed a significant increase through ex vivo insulin treatment (Figure 59b). Pooled data showed a significant reduction in STZ-diabetic ECs' TRPV4 expression compared to naïve ECs' TRPV4 (Naïve, N= 5, average TRPV4 expression= 100.0 ± 7.3% vs STZ-diabetic ECs N= 8, average TRPV4 expression= 58.9 ± 5.8%). Insulin treatment showed to significantly restore STZ-diabetic TRPV4 expression (270mIU/ml N= 3, * $p < 0.05$, average TRPV4 expression= 96.2 ± 6.2% and 2.7IU/ml N= 3, average TRPV4 expression= 94.7 ± 10.4% vs STZ N= 8, 58.9 ± 5.8%) (Figure 59b).

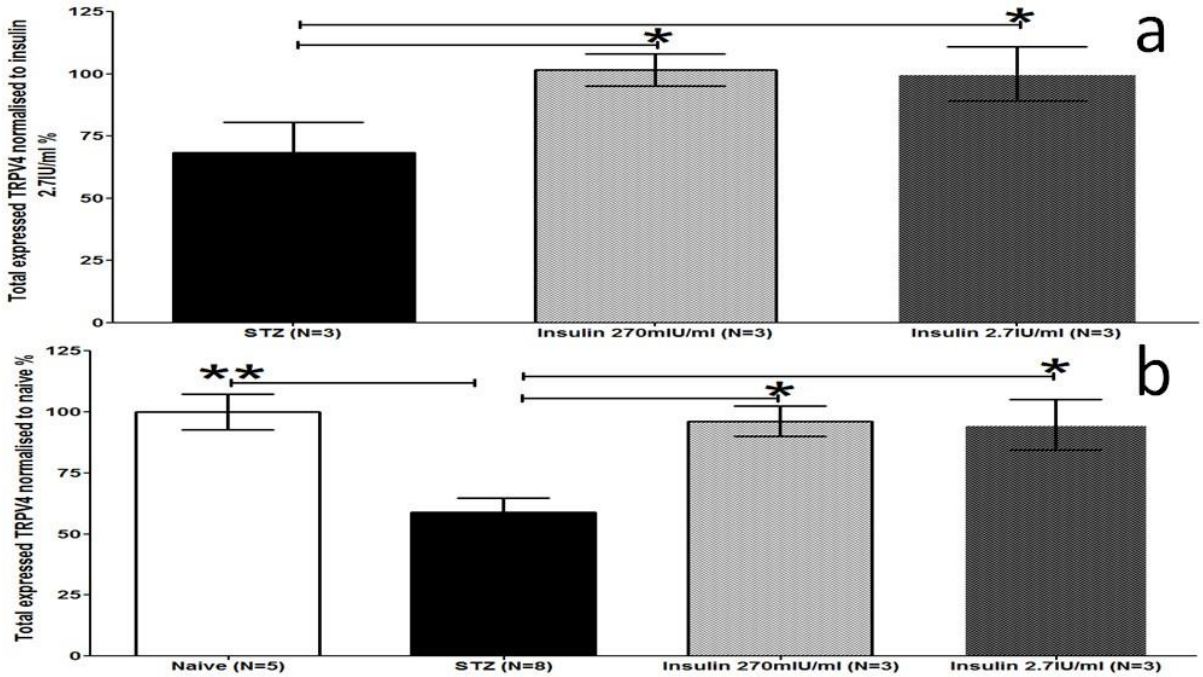

Figure 59. Total TRPV4 expression in primary aortic endothelial cells. Matched data analysed through repeated measure one-way ANOVA with Tukey post-hoc test (a). Pooled data analysed through one-way ANOVA with Tukey post-hoc test (b). Significance is represented as * $p < 0.05$ and ** $p < 0.01$ compared with TRPV4 expression in STZ endothelial cells. Data shown as average percentage ± SEM.

5.3.2. Caveolin-1 (CAV-1) was significantly downregulated in STZ-diabetic ECs and restored through insulin treatment

Caveolae are 50 to 100nm diameter lipid raft invaginations in the ECs membrane (X. Yao & Garland, 2005). Caveolae form approximately 95% of the ECs surface invaginations functioning as signalling platform that integrate the signalling molecules to facilitate their interactions (X. Yao & Garland, 2005). Among the signalling molecules docked in the caveolae is TRPV4 (Garland, Hiley, & Dora, 2010). CAV-1 is a major protein component of the endothelial caveolae. Previous studies showed CAV-1 is co-localised with TRPV4 (Saliez et al., 2008). Therefore, further studies were conducted on ECs to investigate whether CAV-1 is affected by diabetes and restored through insulin treatment.

As shown in Figure 60, CAV-1 showed distinct distribution around the nucleus and at the edge of plasma membrane in naïve aortic ECs (a2). STZ-diabetic ECs showed disrupted CAV-1 distribution with less green fluorescence emission (b2). Insulin treatment 270mIU/ml/day (c2) and 2.7IU/ml/day (d2) for 5 days restored CAV-1 distribution in STZ-diabetic ECs. Images were combined to matching endothelial marker (red), nucleus marker (blue) and CAV-1 florescence antibody (green) (a3, b3, c3 & d3).

Label	AC-Dil-LDL	CAV-1 antibody	AC-Dil-LDL + CAV-1 antibody
Naïve (or control)	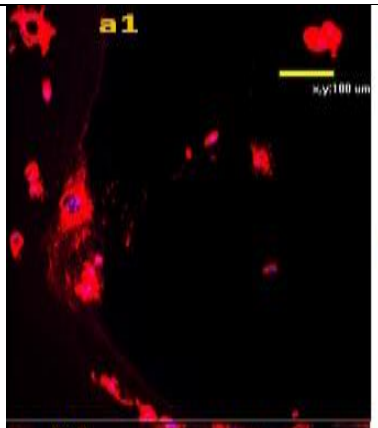	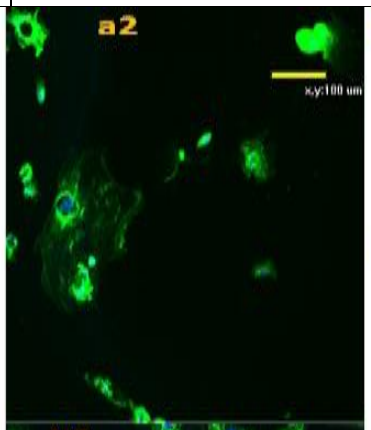	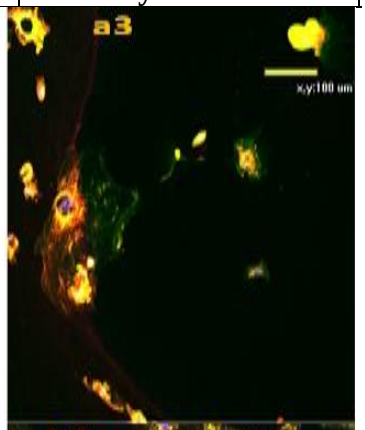
STZ-diabetic ECs	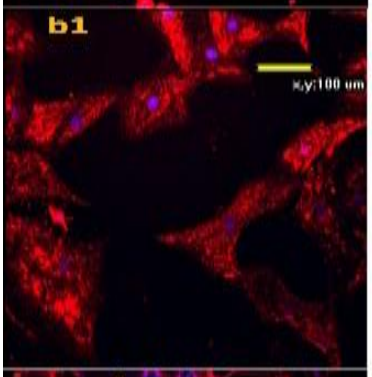	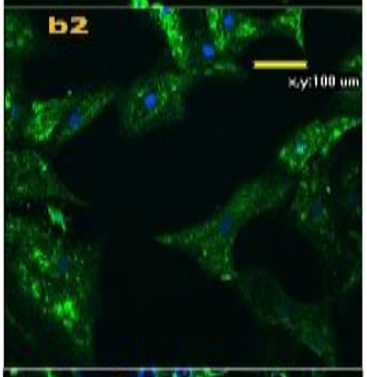	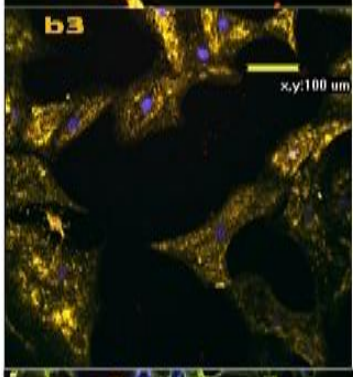
STZ-diabetic ECs treated with insulin 270mIU/ml	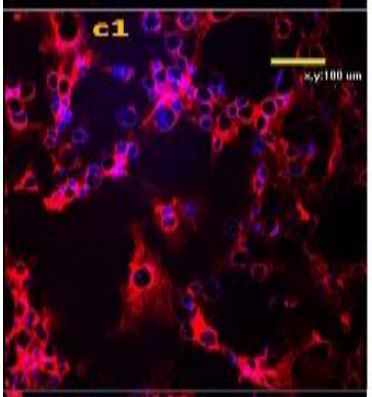	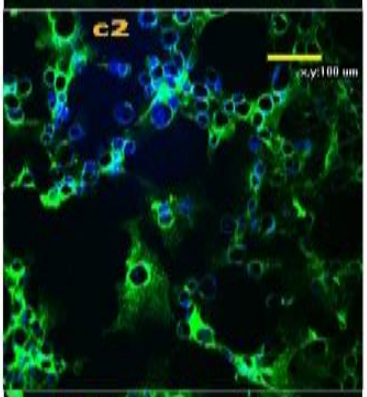	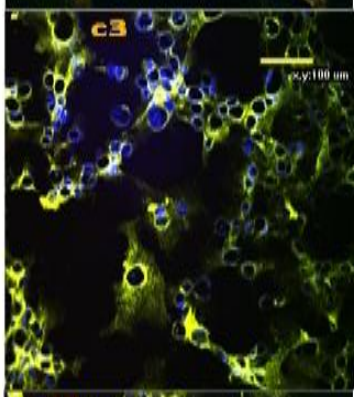
STZ-diabetic ECs treated with insulin 2.7IU/ml	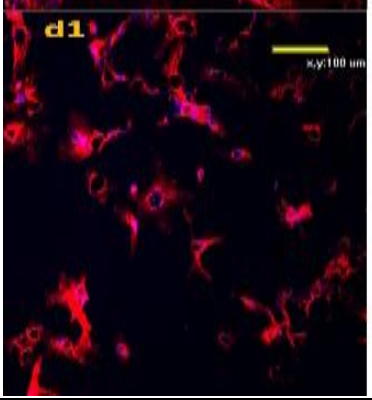	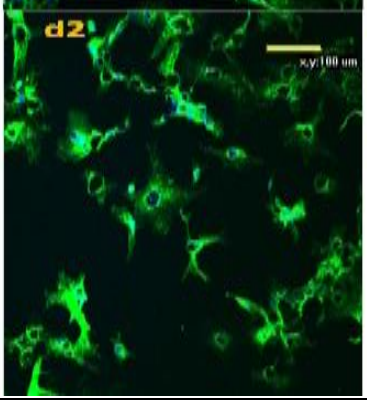	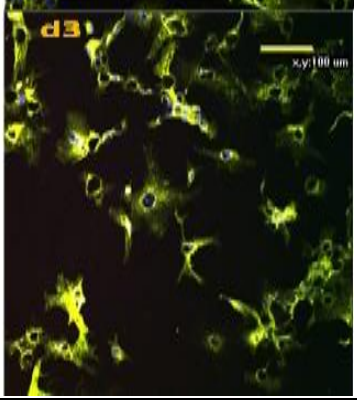

Figure 60. Caveolin-1 (CAV-1) expression in primary aortic endothelial cells under laser scanning confocal microscope. Endothelial cells were probed with DAPI to label the nucleus in blue and marked with acetylated LDL (Dil-Ac-LDL) giving the cells the red colour (left: a1, b1, c1 & d1). Anti caveolin-1 primary antibody probed with secondary green fluorescence antibody (middle: a2, b2, c2 & d2). Images were combined to match the selective ECs marker (red) with anti CAV-1 (green) and the nucleus marker (blue) (right: a3, b3 & c3 & d3) (200×) 488nm laser.

The confocal microscopy images were quantitatively analysed through ImageJ software (version 1.46r) and statistically analysed through Graph Pad prism (version 5.00). As shown in Figure 61a, primary aortic ECs isolated from 3 different STZ-diabetic rats were treated with insulin (270mIU/ml & 2.7IU/ml). The three groups were compared through matched one way ANOVA analysis showing significant increase in CAV-1 expression when STZ-diabetic ECs were treated ex vivo with insulin (Insulin 270mIU/ml, N= 3, * $p < 0.05$, average CAV-1 expression= 100.0 ± 3.0% and insulin 2.7IU/ml, N= 3, * $p < 0.05$, average CAV-1 expression= 100.0 ± 7.7% vs STZ-diabetic ECs, N= 3, average CAV-1 expression= 70.0 ± 5.5%) (Figure 61a).

When the whole data were pooled together and compared with naïve ECs, CAV-1 expression showed a significant increase following ex vivo insulin treatment (Figure 59b). Pooled data showed significant reduction in STZ-diabetic ECs' CAV-1 expression compared to naïve ECs' CAV-1 (Naïve, N= 5, average CAV-1 expression= 100.0 ± 3.0% vs STZ-diabetic ECs, N=4, average CAV-1 expression= 73.8 ± 4.3%). Insulin treatment significantly increased STZ-diabetic ECs' CAV-1 expression at higher concentration (270mIU/ml N= 3, ns $p \geq 0.05$, average CAV-1 expression= 99.3 ± 1.6% and 2.7IU/ml N= 3, * $p < 0.05$, average CAV-1 expression= 103.2 ± 8.0% vs STZ N= 4, 73.8 ± 4.3%).

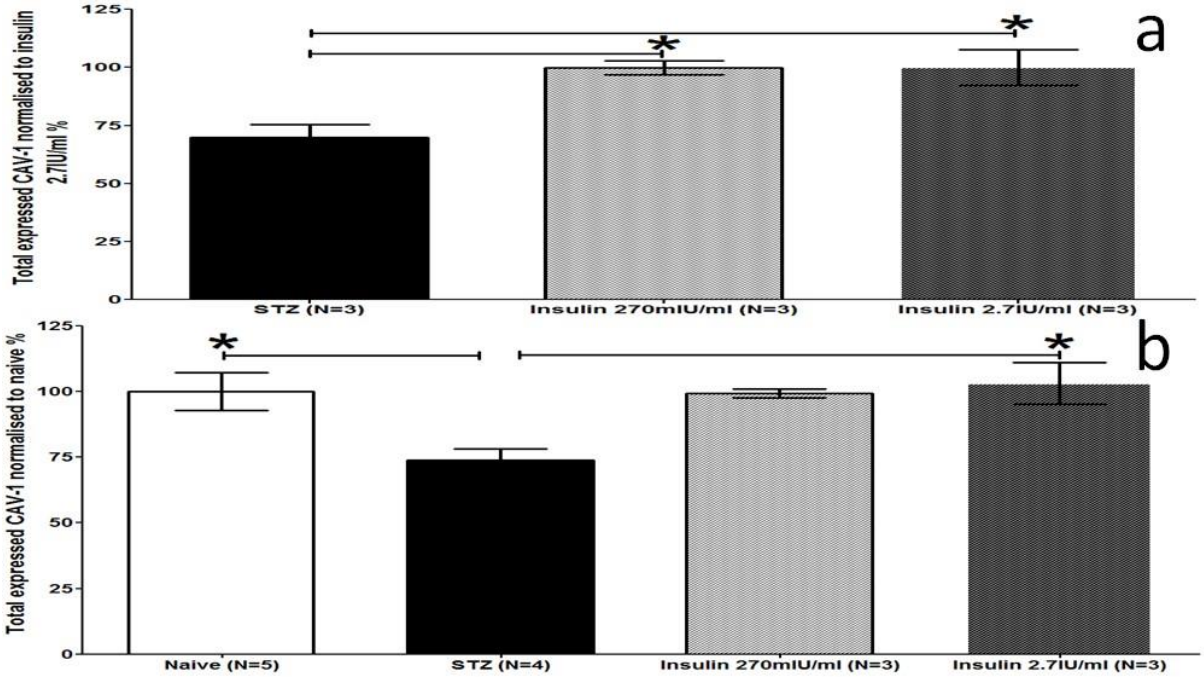

Figure 61. Total caveolin-1 (CAV-1) expression in primary aortic endothelial cells. Matched data analysed through repeated measure one-way ANOVA with Tukey post-hoc test (a). Pooled data analysed through one-way ANOVA with Tukey post-hoc test (b). Significance is represented as * $p < 0.05$ compared with CAV-1 expression in STZ endothelial cells. Data shown as average percentage ± SEM.

5.3.3. eNOS was significantly downregulated in STZ-diabetic ECs and restored through insulin treatment

Previous studies showed that eNOS and CAV-1 are co-localised in rat kidneys and cultured bovine aortic ECs (Komers et al., 2006; H. Wang et al., 2009). Additionally, being co-localised with CAV-1 and affected by shear stress, eNOS was hypothesised to be co-localised with TRPV4 and CAV-1 and affected in diabetic rat aortic ECs. Therefore, immunocytochemistry studies were conducted to examine whether eNOS will show similar patterns as TRPV4 and CAV-1. eNOS was significantly downregulated in diabetic aortic ECs which was restored through insulin treatment (Figure 62 and 72). As illustrated in Figure 62, eNOS showed distinct distribution around the nucleus and at the edge of plasma membrane in naïve aortic ECs (a2). STZ-diabetic ECs showed disrupted eNOS distribution with less green fluorescence emission (b2). Insulin treatment 270mIU/ml/day (c2) and 2.7IU/ml/day (d2) for 5 days restored eNOS distribution in STZ-diabetic ECs. Images were combined to matching endothelial marker (red), nucleus marker (blue) and eNOS florescence antibody (green) (a3, b3, c3 & d3).

Label	AC-Dil-LDL	eNOS antibody	AC-Dil-LDL + eNOS antibody
Naïve (or control)	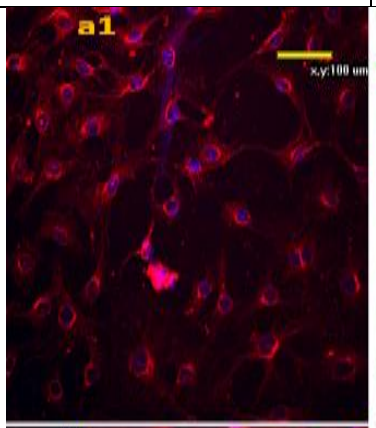	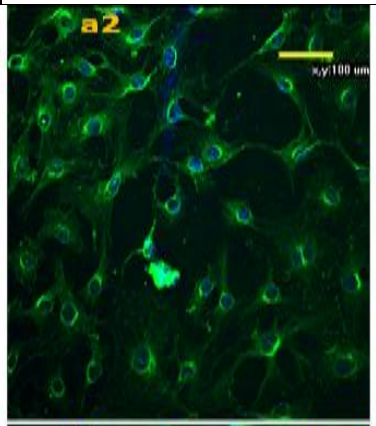	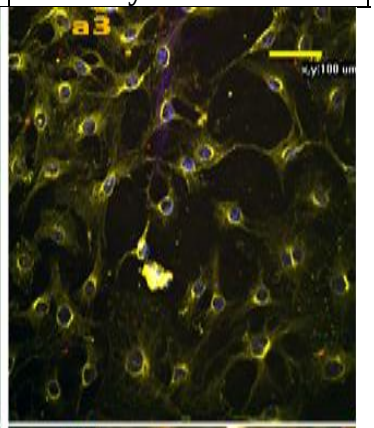
STZ-diabetic ECs	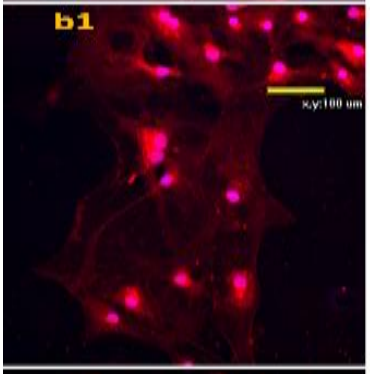	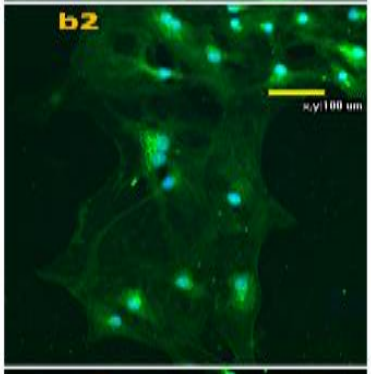	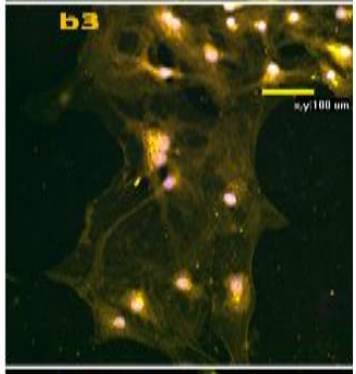
STZ-diabetic ECs treated with insulin 270mIU/ml	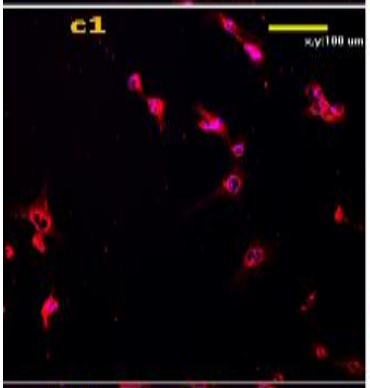	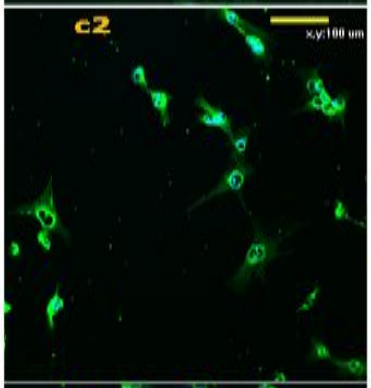	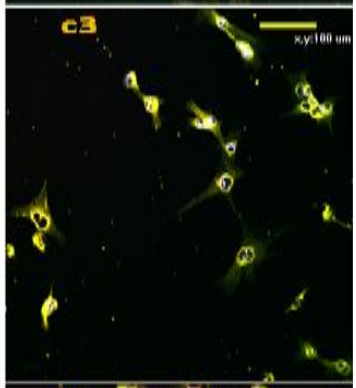
STZ-diabetic ECs treated with insulin 2.7IU/ml	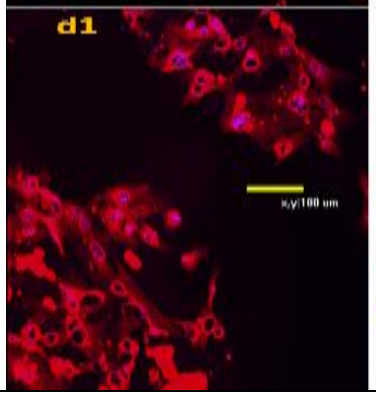	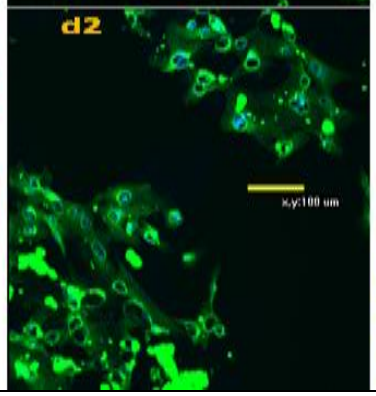	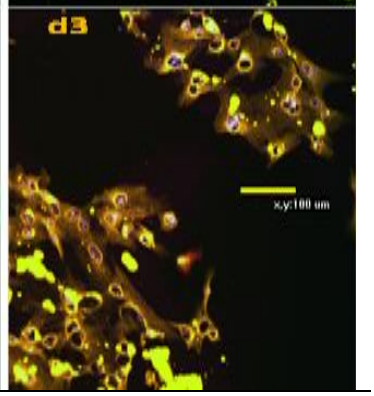

Figure 62. Endothelial nitric oxide synthase (eNOS) expression in primary aortic endothelial cells under laser scanning confocal microscope. Endothelial cells were probed with DAPI to label the nucleus in blue and marked with acetylated LDL (Dil-Ac-LDL) giving the cells the red colour (left: a1, b1, c1 & d1). Anti eNOS primary antibody probed with green secondary fluorescence antibody (middle: a2, b2 & c2 & d2). Images were combined to match the selective ECs marker (red) with anti eNOS (green) and the nucleus marker (blue) (right: a3, b3 & c3 & d3) (200×) 488nm laser.

The confocal microscopy images were quantitatively analysed through ImageJ software (version 1.46r) and statistically analysed through Graph Pad prism (version 5.00). As shown in Figure 63a, primary aortic ECs isolated from 3 different STZ-diabetic ECs were treated with insulin (270mIU/ml & 2.7IU/ml). The three groups were compared through matched one way ANOVA analysis showing significant improvement in eNOS expression when STZ-diabetic ECs were treated ex vivo with insulin (Figure 63a). Matched data showed significantly enhanced eNOS expression in STZ-ECs treated with insulin (Insulin 270mIU/ml, N= 3, * $p < 0.05$, average eNOS expression= 98.5 ± 4.8% and insulin 2.7IU/ml, N= 3, average eNOS expression= 100.0 ± 5.5% vs STZ-diabetic ECs, N=3, average eNOS expression= 59.6±5.13%) (Figure 63a).

Pooled data showed significant reduction in STZ-diabetic ECs' eNOS expression compared to naïve ECs' eNOS (Naïve, N= 5 average eNOS expression= 100.0 ± 4.3% vs STZ N=6, 62.1 ± 5.8%). Insulin treatment showed to significantly restore STZ-diabetic ECs' eNOS reduction (270mIU/ml N=3, average eNOS expression= 120.7 ± 5.8% and 2.7IU/ml N= 3, *** $p < 0.001$, average eNOS expression= 122.6 ± 6.7% vs STZ N= 6, 62.1 ± 5.8%) (Figure 63b).

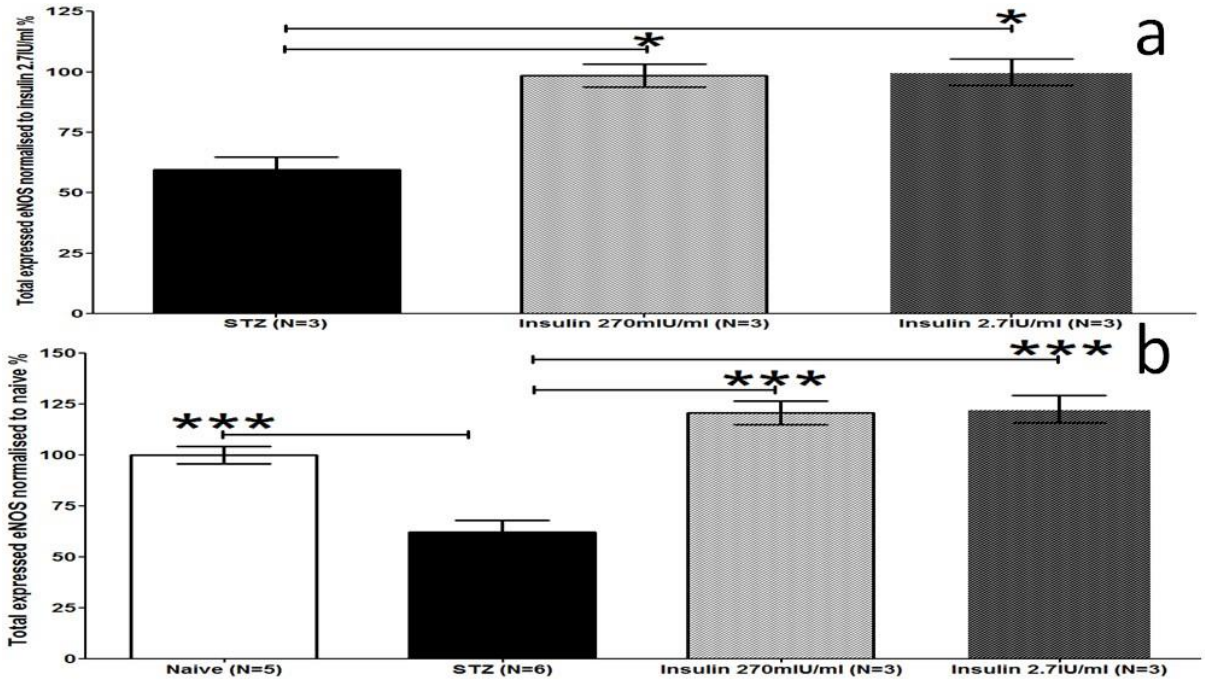

Figure 63. Total eNOS expression in primary aortic endothelial cells. Matched data analysed through repeated measure one-way ANOVA with Tukey post-hoc test (a). Pooled data analysed through one-way ANOVA with Tukey post-hoc test (b). Significance is represented as * $p < 0.05$ and *** $p < 0.01$ compared with eNOS expression in STZ endothelial cells. Data shown as average percentage ± SEM.

These findings suggest that TRPV4, CAV-1, and eNOS are all downregulated in STZ-diabetic rat aortic ECs and restored through insulin treatment. Therefore, further fura-2 Ca^{2+} imaging functional study was conducted to investigate whether TRPV4 downregulation influences the changes in $[Ca^{2+}]i$ following TRPV4 stimulation.

5.4. TRPV4-induced intracellular calcium concentration was significantly reduced in STZ-diabetic ECs and restored through insulin treatment

As shown in Figure 64, baseline fura-2 ratio was not significantly different across naïve ECs, STZ-diabetic ECs (untreated) and STZ-diabetic ECs treated with insulin (270mIU/ml/day for 5 days).

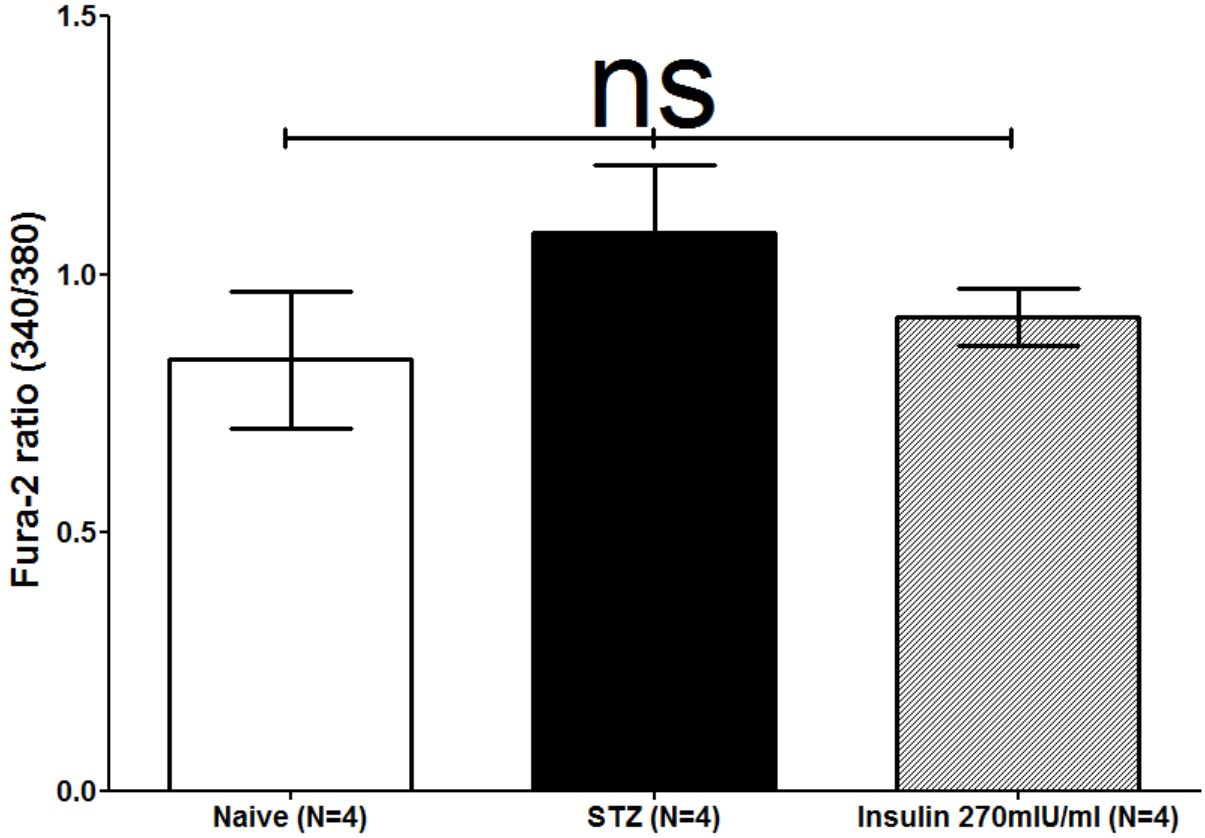

Figure 64. Baseline fura-2 ratio before 4-αPDD treatment. All studied groups were compared through Tukey's one-way ANOVA, and no significant difference was shown. Non-significance is represented as ns $p \geq 0.05$ when the groups were compared with each other. Data shown as average fura-2 ratio ± SEM.

However, TRPV4-induced $[Ca^{2+}]i$ showed a significant decrease in STZ-diabetic ECs compared to naïve ECs (* $p < 0.05$). In STZ-diabetic ECs treated with insulin 270mIU/ml/day for 5 days, the amplitude of the intracellular Ca^{2+} in response to TRPV4 activation was significantly restored. Naïve ECs (N=4, 1.0 ± 0.2 fura-2 ratio change) and STZ-diabetic ECs treated with insulin 270mIU/ml/day for 5 days (N=4, 1.1 ± 0.1 fura-2 ratio change) showed significant difference (* $p < 0.05$) compared to STZ-diabetic ECs (N=4, 0.5 ± 0.13 fura-2 ratio change) (Figure 65).

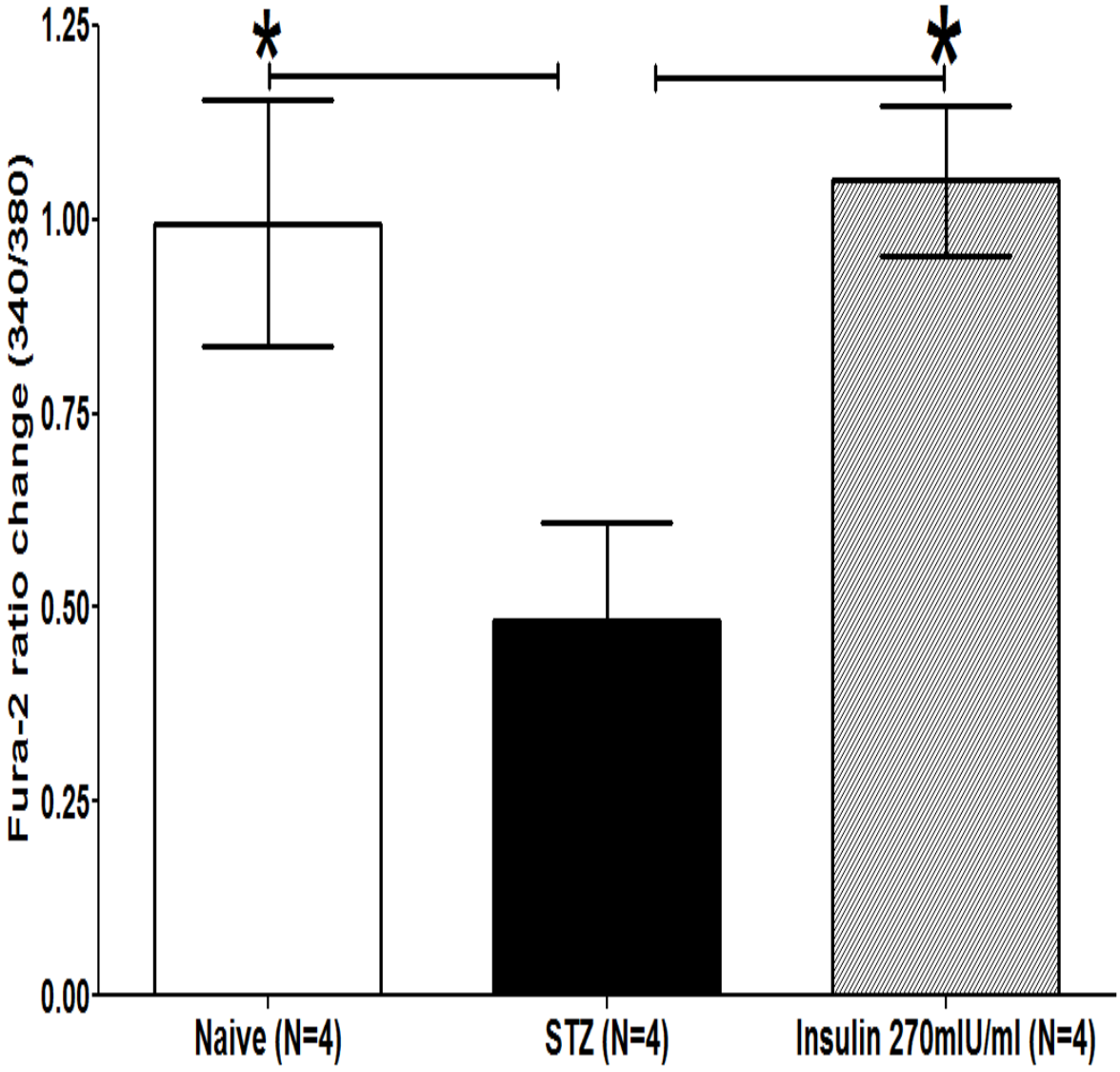

Figure 65 TRPV4 induced peak fura-2 ratio change through 4-αpdd (1mM) treatment. Analysed through one-way ANOVA with Tukey post-hoc test. Significance is represented as * $p < 0.05$ when compared to STZ ECs fura-2 ratio changes. Data shown as average fura-2 ratio ± SEM.

In addition to showing a reduced amplitude, the time course of the $[Ca^{2+}]i$ rise in the ECs isolated from STZ-diabetic rats was significantly delayed compared to naïve ECs. Naïve aortic ECs showed a significant difference in the required time to reach the fura-2 peak compared to STZ-diabetic ECs (Naïve, N= 4, * $p < 0.05$, peak time= 81.3 ± 13.5 seconds vs STZ-diabetic ECs, N= 4, peak time= 202 ± 23.5 seconds). STZ-diabetic ECs treated with insulin 270mIU/ml/day for 5 days did not show a significant difference when compared to untreated STZ-diabetic ECs (STZ-diabetic ECs treated with insulin 270mIU/ml/day, N= 4, $p \geq 0.05$, peak time= 154.5 ± 40.2 seconds vs STZ-diabetic ECs, N= 4, peak time= 202 ± 23.5 seconds) as shown in Figure 66.

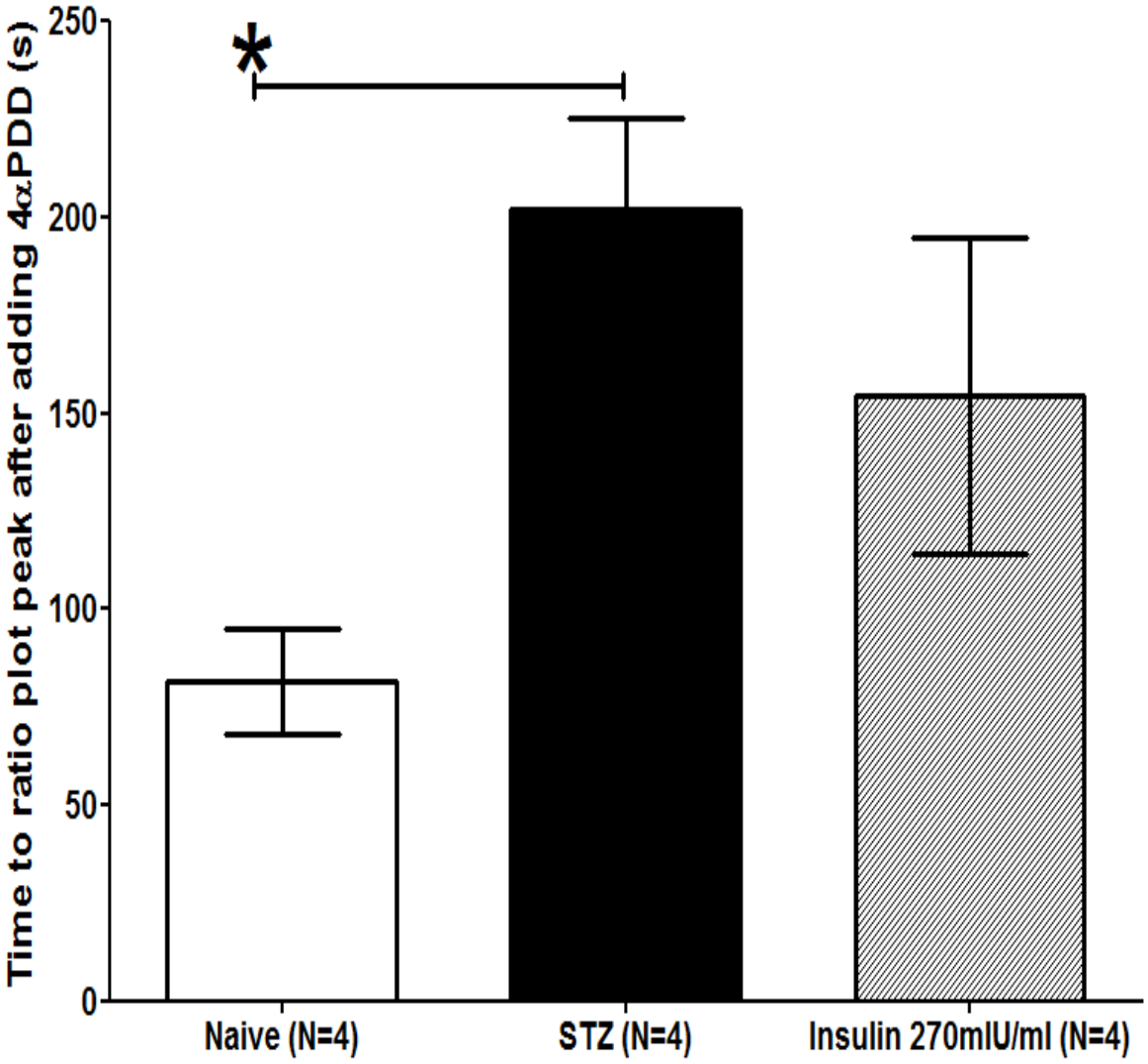

Figure 66 Time to reach peak 4-αPDD induced fura-2 ratio change. Analysed through one-way ANOVA with Tukey post-hoc test. Significance is represented as * $p < 0.05$ when compared to STZ ECs peak time. Data shown as mean ± SEM.

5.4.1. MGO significantly compromised the TRPV4-induced intracellular calcium concentration in naïve ECs, which was restored through L-arginine treatment

MGO was significantly elevated in diabetic serum (Figure 43), and MGO (100μM) inhibited endothelial-mediated vasodilation in whole naïve aortic rings (Figure 52). Additionally, TRPV4-mediated $[Ca^{2+}]i$ was significantly reduced in STZ-diabetic ECs (Figure 65). Accordingly, fura-2 Ca^{2+} imaging studies were conducted to examine whether TRPV4 function is compromised through MGO treatment, and if L-arginine co-treatment can restore MGO-induced TRPV4 dysfunction. After plating the ECs on poly-L-lysine coated glass coverslips, they were treated with MGO (100μM) or MGO (100μM) and L-arginine (100μM) once daily until becoming confluent. As shown in Figure 67, MGO (100μM) showed significant reduction in TRPV4-induced $[Ca^{2+}]i$ elevation, whereas L-arginine (100μM) showed significant reversal of MGO-induced TRPV4 dysfunction (* $p < 0.05$). Naïve ECs treated with MGO 100μM/day for 5 days (N=4, 0.54 ± 0.08 fura-2 ratio) showed significant difference in fura-2 ratio change (* $p < 0.05$) compared to untreated naïve ECs (N=4, 0.995 ± 0.16 fura-2 ratio) and naïve ECs treated with MGO 100μM and L-arginine100μM/day for 5 days (N=4, 0.89 ± 0.08 fura-2 ratio) (Figure 67a). Such MGO-reduced fura-2 ratio change was significantly similar to what was shown in STZ-diabetic ECs (N=4, 0.5 ± 0.13 fura-2 ratio) (Figure 67b).

Moreover, naïve ECs treated with MGO 100μM/day for 5 days (N=4, 1.1 ± 0.2 fura-2 ratio) did not show significant difference ($p \geq 0.05$) in the fura-2 ratio baseline when compared to naïve ECs (N=4, 0.84 ± 0.13 fura-2 ratio) and naïve ECs treated with MGO 100μM and L-arginine100μM/day for 5 days (N= 4, 0.84 ± 0.3 fura-2 ratio) (Figure 68a). Similarly, naïve ECs cells treated with MGO 100μM/day for 5 days (N= 4, 1.1 ± 0.2 fura-2 ratio) did not show a significant difference ($p \geq 0.05$) in the fura-2 ratio baseline when compared to STZ ECs (N= 4, 1.1 ± 0.1 fura-2 ratio) (Figure 68b).

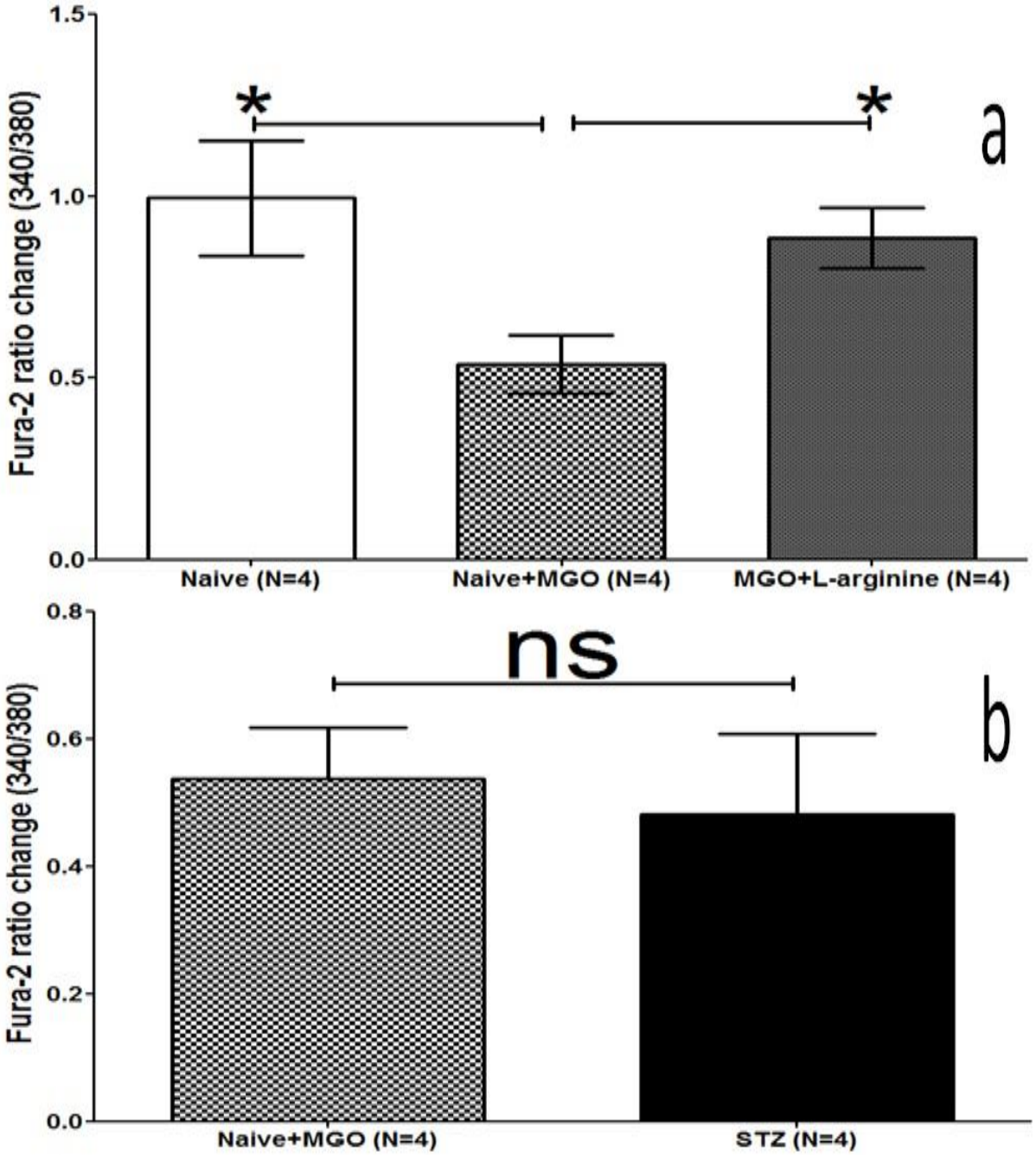

Figure 67 TRPV4 induced intracellular Ca^{2+} elevation in the presence of MGO. MGO reduced the 4-αPDD-induced fura-2 ratio change (a). Analysed through repeated measure one-way ANOVA with Tukey post-hoc test. Significance is represented as * $p < 0.05$ compared to untreated naïve endothelial cells. Naïve endothelial cells treated with MGO compared to STZ ECs (b). Analysed through unpaired two-tailed Student's t-test Non-significance is represented as ns $p \geq 0.05$. Data shown as average fura-2 ratio ± SEM.

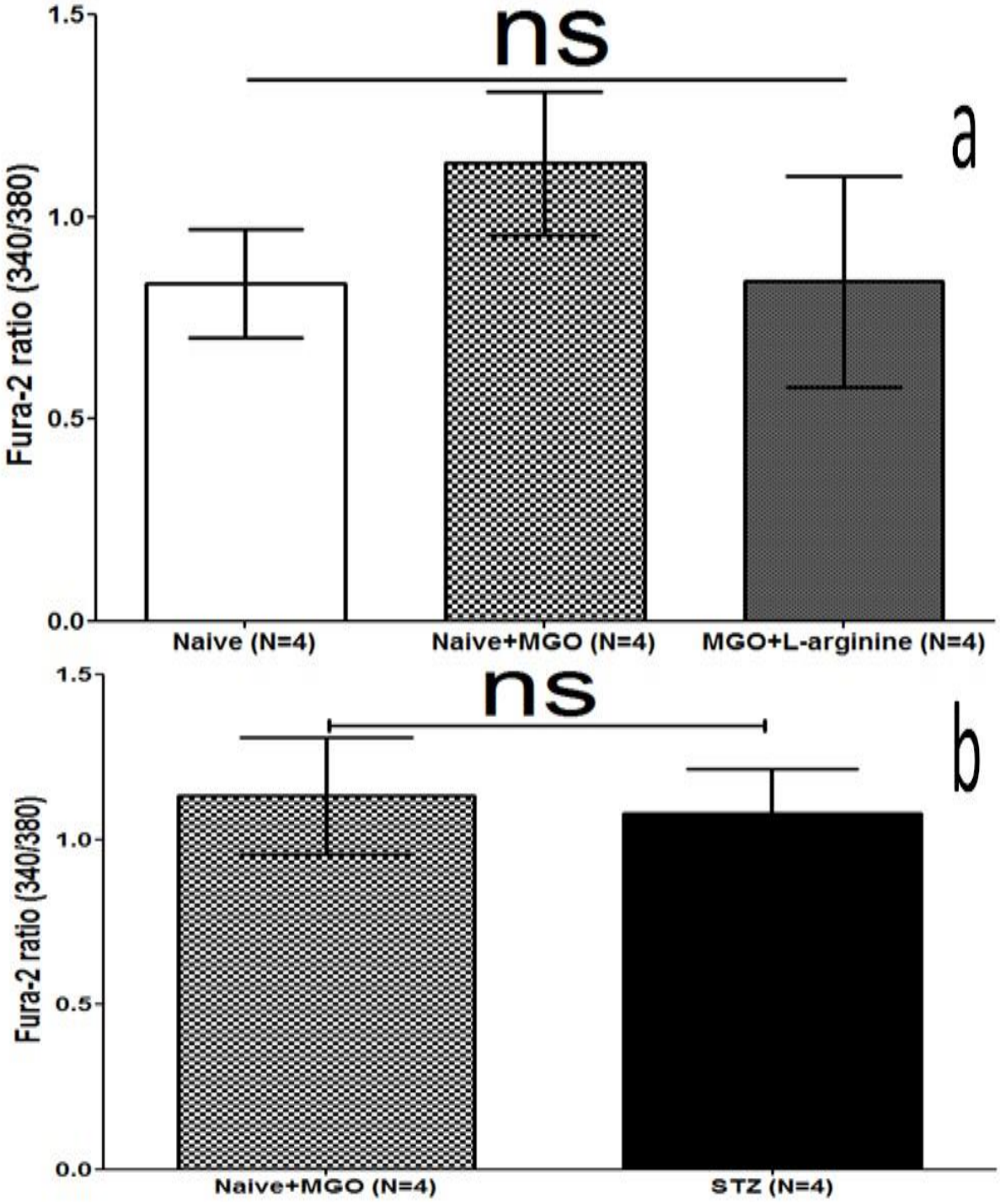

Figure 68 Baseline fura-2 ratio before 4-αPDD treatment. Naïve ECs compared with naïve ECs treated with MGO 100μM/day for 5 days and naïve endothelial cells treated with MGO 100μM and L-arginine100μM/day for 5 days. Analysed through repeated measure one-way ANOVA with Tukey post-hoc test. Non-significance is represented as ns $p \geq 0.05$ when the groups were compared with each other. (a). Naïve ECs treated with MGO 100μM/day for 5 days compared with STZ ECs analysed through un-paired two-tailed Student's t-test (b). Non-significance is represented as ns $p \geq 0.05$. Data shown as average fura-2 ratio ± SEM.

5.4.2. MGO significantly compromised the TRPV4 expression in naïve ECs

As shown in Figures 58 and 59, TRPV4 was downregulated in STZ-diabetic primary aortic ECs. Additionally, since MGO was significantly elevated in STZ-diabetic rats' serum (Figure 43), therefore, control naïve primary aortic ECs were treated with MGO (100μM/day) for 5 days and visualised under LSCM as described in section 2.7.1. As shown in Figure 69, TRPV4 expression was disrupted in control naïve ECs treated with MGO, showing similar distribution as STZ-diabetic aortic ECs.

Label	AC-Dil-LDL	eNOS antibody	AC-Dil-LDL + eNOS antibody
Naïve (or control) ECs	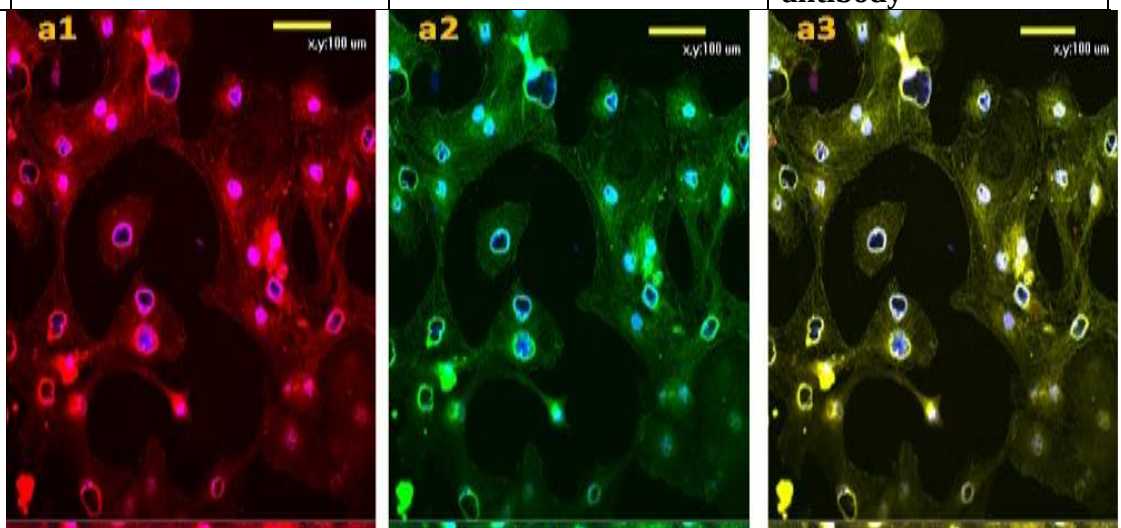		
STZ-diabetic ECs	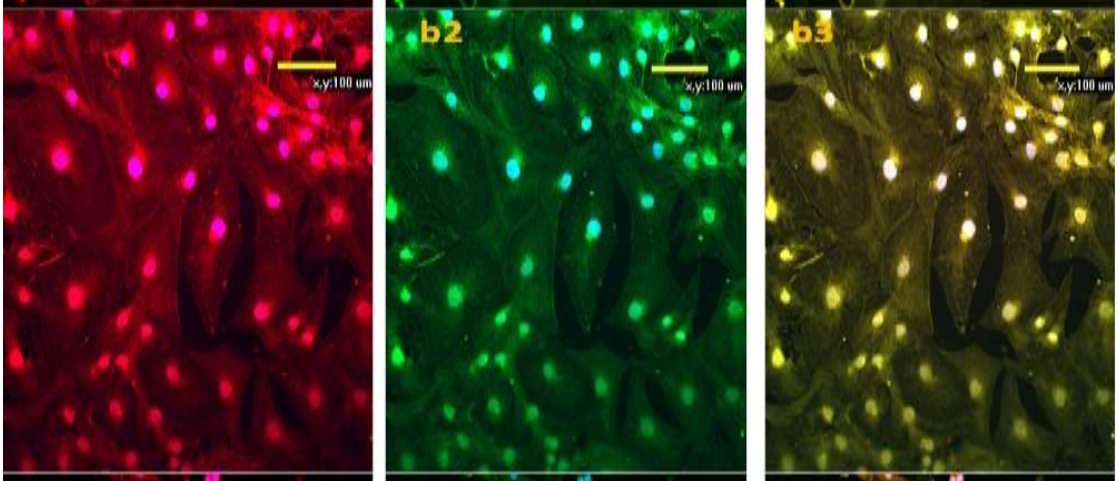		
Naïve (or control) ECs treated with MGO (100µM)	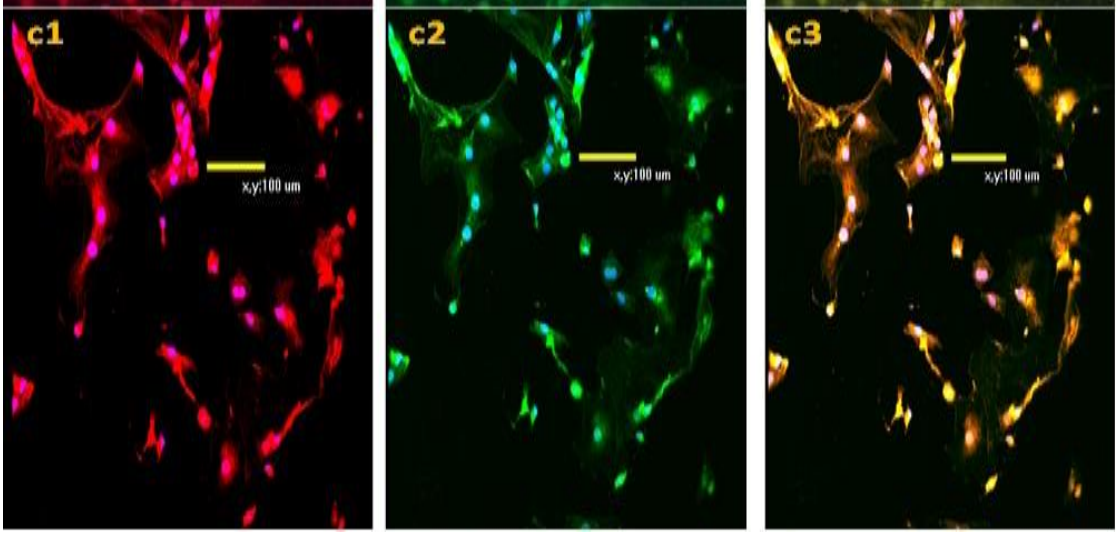		

Figure 69. MGO effect on TRPV4 expression in primary aortic endothelial cells under laser scanning confocal microscope. Endothelial cells were probed with DAPI to label the nucleus in blue and marked with acetylate LDL (Dil-Ac-LDL) giving the cells the red colour (left: a1, b1 & c1). Anti TRPV4 primary antibody probed with secondary fluorescence antibody. TRPV4 showed unique distribution around the nucleus and at the edge of plasma membrane in naïve aortic endothelial cells (a2). STZ-diabetic endothelial cells showed disrupted TRPV4 distribution with less fluorescence light emission (b2). Naïve endothelial cells treated with MGO (100µm/day) showed disrupted TRPV4 distribution with less fluorescence light emission. Images were combined to matching endothelial marker (red), nucleus marker (blue) and TRPV4 florescence antibody (green) (right: a3, b3 & c3) (200×) 488nm laser.

The LSCM images were quantitatively analysed through ImageJ software (version 1.46r) and statistically analysed through Graph Pad prism (version 5.00). As shown in Figure 70a, paired data showed significant TRPV4 downregulation in MGO-treated naïve ECs (N=4, ** $p < 0.01$, average total TRPV4 expression= 54.1 ± 6.6% vs naïve, N= 4, 100.0 ± 9.4%) Moreover, when the findings were pooled with STZ-diabetic ECs, control naïve ECs treated with MGO (100µM) for 5 days showed similar fura-2 ratio (ns $p \geq 0.05$). Naïve ECs treated with MGO (100µm/day for 5 days) showed similar TRPV4 expression to STZ-diabetic ECs, and showed significant difference in TRPV4 expression compared to naïve ECs (Naïve treated with MGO, N=4, ** $p < 0.01$, average TRPV4 expression= 53.6 ± 6.6% and STZ-diabetic ECs, N=8, average TRPV4 expression= 58.9±5.8% vs naïve, N=5 average TRPV4 expression= 100.0 ± 7.3%) (Figure 70b).

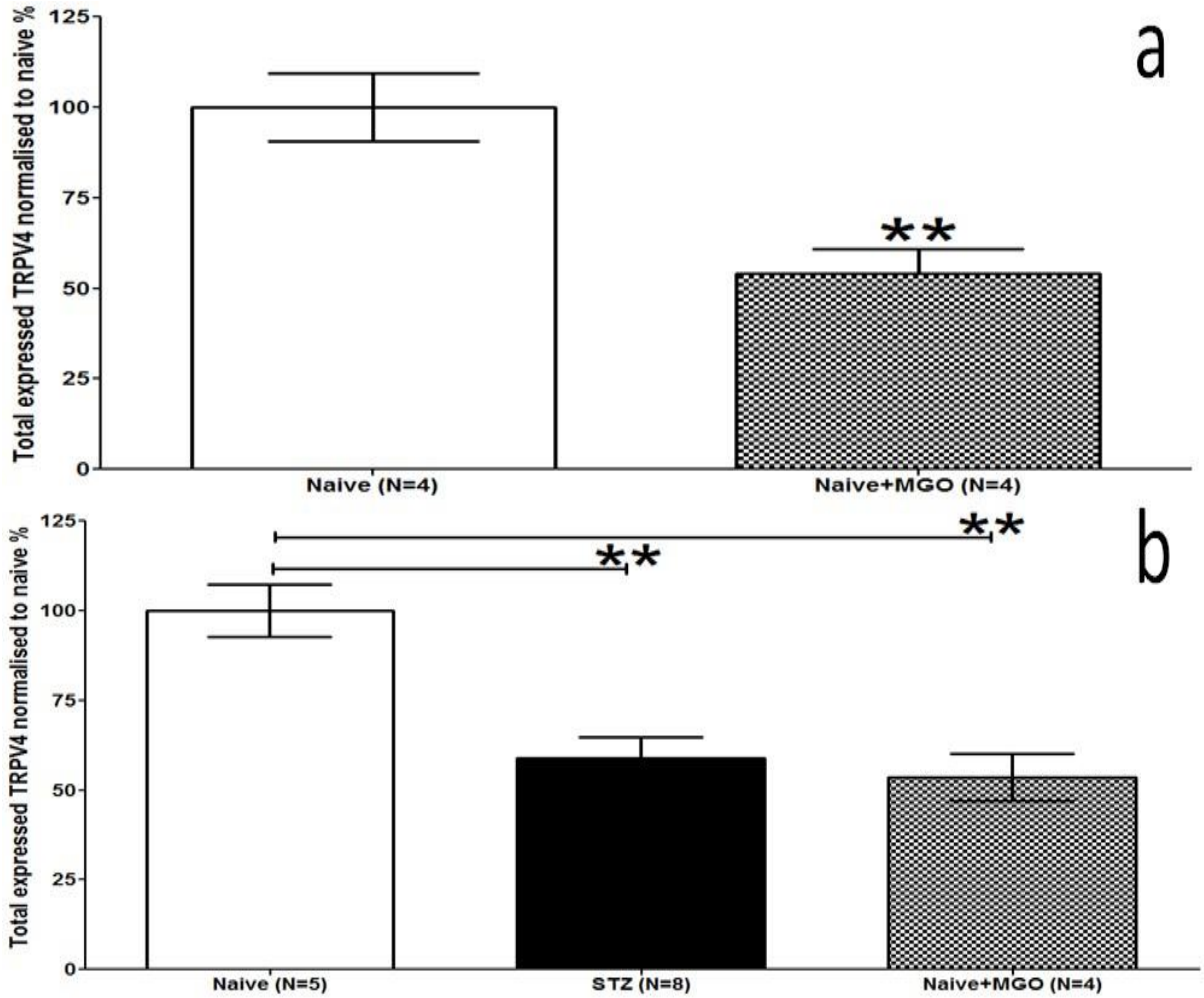

Figure 70 MGO treatment of primary aortic ECs cultures reduces total TRPV4 expression. Paired data analysed through paired two-tailed Student's t-test. Significance is represented as ** $p < 0.01$ (a). Naïve ECs treated with MGO (100µm/day for 5 days) showed significant difference in TRPV4 expression compared to untreated naïve ECs when analysed through one-way ANOVA with Tukey post-hoc test (b). Significance is represented as ** $p < 0.01$ when compared with untreated naïve endothelial cells. Data shown as average percentage ± SEM.

5.4.3. TRPM8-induced intracellular calcium elevation was not significantly affected in STZ-diabetic ECs

Previous findings showed that TRPM8-induced vasodilation was not significantly changed in STZ-diabetic aortic rings (Figure 56). Accordingly, fura-2 Ca^{2+} imaging functional study was conducted to investigate the TRPM8-increased $[Ca^{2+}]i$ in both naïve and STZ-diabetic ECs. Baseline readings were recorded for a minute before adding icilin (1mM) in HBS buffer. As shown in Figure 72, baseline ratios were not significantly different (STZ N=3, $p \geq 0.05$, 1.3 ± 0.2 fura-2 ratio vs naïve, N=3, 0.9 ± 0.1 fura-2 ratio).

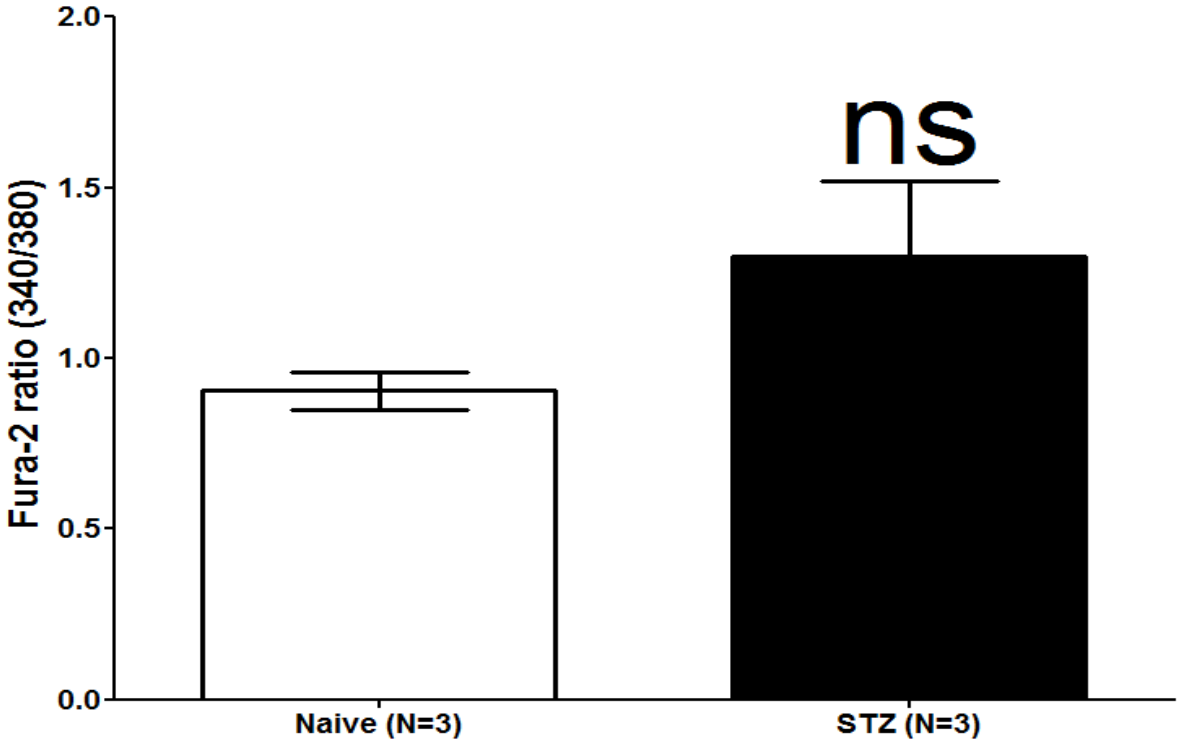

Figure 71 Baseline fura-2 ratio before icilin treatment. Analysed through unpaired two-tailed Student's t-test. Non-significance is represented as ns $p \geq 0.05$. Data shown as average fura-2 ratio ± SEM.

Fura-2 ratio change was recorded for further 9 minutes were recorded for measuring $[Ca^{2+}]i$ through icilin treatment. Icilin-induced $[Ca^{2+}]i$ did not show significant difference between STZ-diabetic aortic ECs and naïve ECs (N=3, $p \geq 0.05$, 1.2 ± 0.4 fura-2 ratio vs naïve, N=3, 1.80 ± 0.4 fura-2 ratio) (Figure 72).

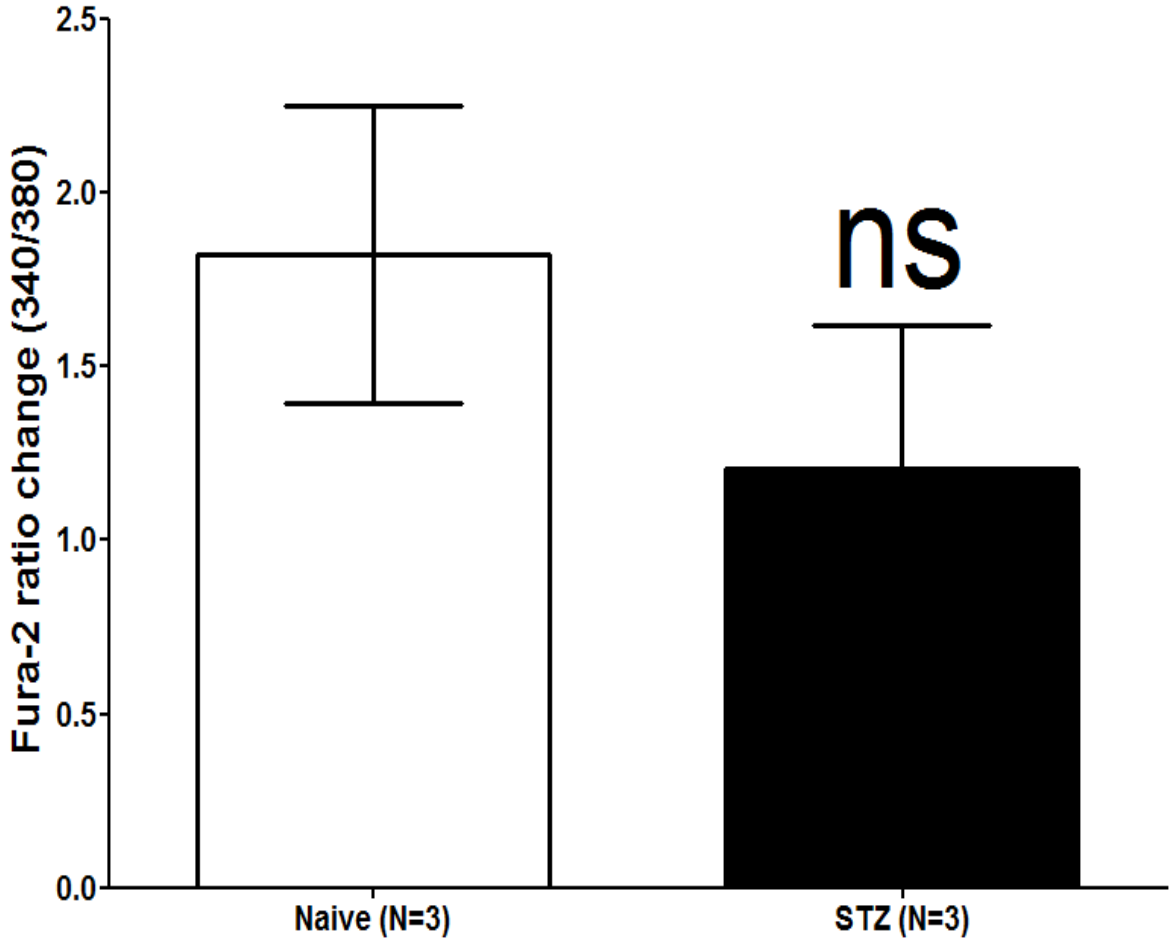

Figure 72 TRPM8 induced peak fura-2 ratio change through icilin (1mM) treatment. Analysed through unpaired two-tailed Student's t-test. Non-significance is represented as ns $p \geq 0.05$. Data shown as average fura-2 ratio ± SEM.

Additionally, the time required for fura-2 ratio to reach the peak did not show a significant difference. As shown in Figure 73, STZ-diabetic ECs did not show a significant difference in the required time to reach fura-2 peak compared to naïve ECs (N=3, $p \geq 0.05$, peak time= 190 ± 5.8 seconds vs Naïve, N=3, peak time= 152 ± 65.4 seconds).

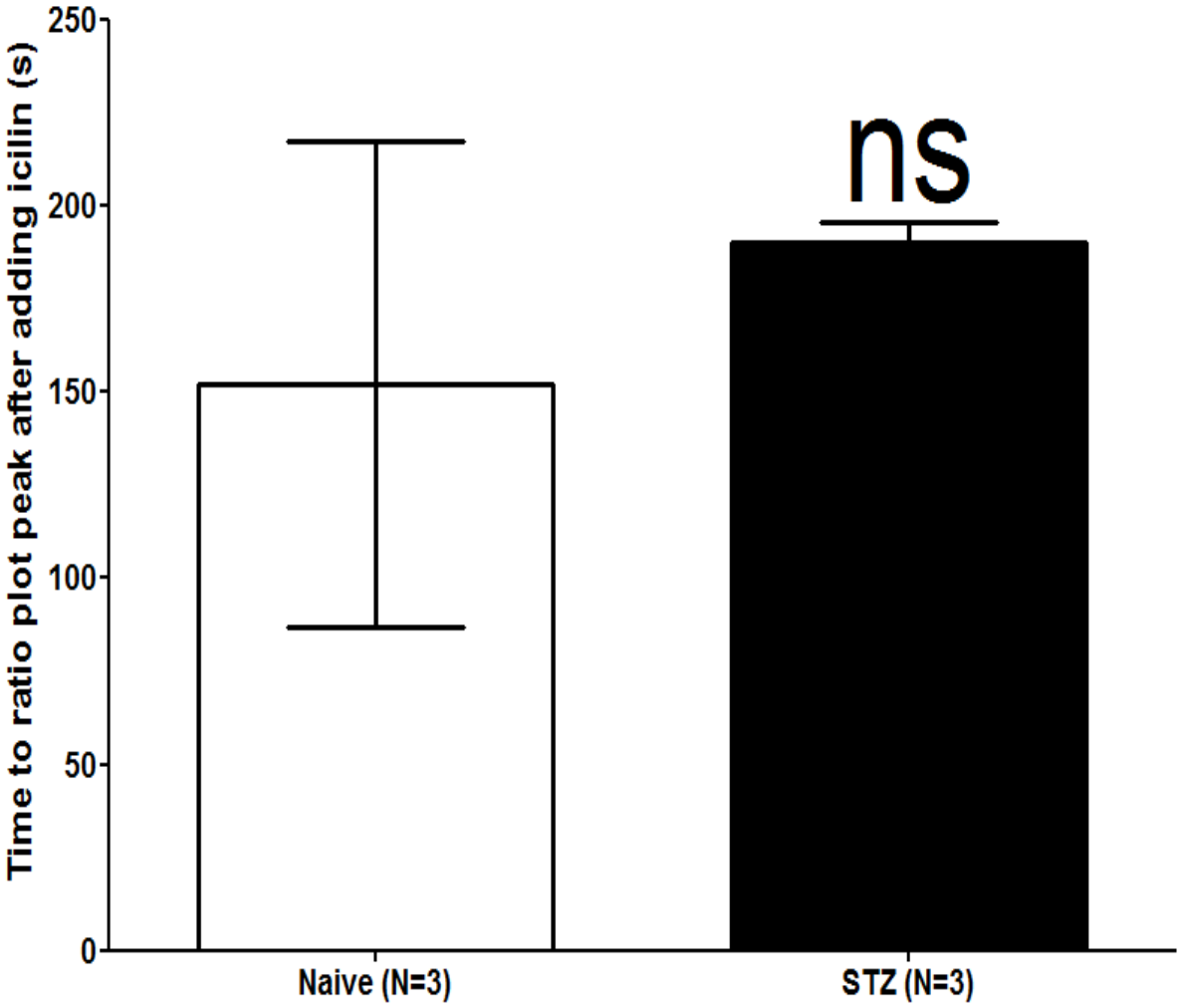

Figure 73 Peak time for icilin induced fura-2 ratio. Analysed through unpaired Student's t-test. Non-significance is represented as ns $p \geq 0.05$. Data shown as mean peak time ± SEM.

5.5. Discussion

As an extension to the compromised TRPV4-induced vasodilation in STZ-diabetic rats' aortic and mesenteric arteries shown in Figures 53-55, immunocytochemistry studies were conducted on primary aortic ECs in this chapter, to examine the molecular mechanism of TRPV4 dysfunction. The ECs were tagged with the selective marker (Dil-Ac-LDL), however, other antibodies are also applicable such as anti CD34 (Fina et al., 1990). Since other antibodies were used to target the expression of TRPV4, CAV-1 and eNOS, therefore, Dil-Ac-LDL labelling was applied to prevent any possible cross reaction between these antibodies with the selective ECs antibody marker. As shown in Figure 58 and 68, TRPV4 expression in primary aortic ECs was significantly reduced by approximately 50% in STZ-diabetic ECs. Moreover, TRPV4 channels distribution around the nucleus and the plasma membrane edges was disrupted in STZ-diabetic ECs (Figure 58). These findings may explain the TRPV4 endothelial dysfunction in diabetes that might be attributed to TRPV4 downregulation. Primary ECs TRPV4 downregulation match the findings of recent study by Monaghan et al. (2015) that showed TRPV4 downregulation in diabetic retinal microvascular ECs.

Furthermore, CAV-1 was investigated in parallel with TRPV4 in the primary ECs. Caveolae form highly organised microdomains in the ECs plasma membrane through providing docking sites for numerous signalling molecules such as TRPV4, GPCR and IKca (Frank, Woodman, Park, & Lisanti, 2003; Garland et al., 2010). CAV-1 is a principal protein and marker found in the endothelial caveolae (Frank et al., 2003). Previous studies showed that CAV-1 is an essential component in modulating TRPV4-induced vasodilation through modulating TRPV4 membrane localisation (Saliez et al., 2008). Moreover, a recent study showed that TRPV4 is co-localised with CAV-1 and SKca in human ECs (Fritz et al., 2015). Therefore, CAV-1 investigation was conducted for two main purposes: to confirm the TRPV4-CAV-1 co-localisation in naïve ECs, and accordingly, whether CAV-1 expression is affected through diabetes.

As shown in Figure 60 and 61, CAV-1 was significantly compromised by approximately 30% in STZ-diabetic aortic ECs. This finding match the previous study on diabetic kidneys that revealed CAV-1 significant reduction when compared to non-diabetic kidneys (Komers et al., 2006). CAV-1 is an essential ECs component in mediating TRPV4-induced EDHF and hence causes vasodilation (Saliez et al., 2008). This was supported through *CAV-1* gene deletion in mice mesenteric arteries which resulted in abolished EDHF-induced vasodilation (Saliez et

al., 2008). Additionally, diabetic kidneys showed significant reduction in CAV-1 when compared to non-diabetic kidneys (Komers et al., 2006).

A previous study concluded that CAV-1 reduction is accompanied with eNOS downregulation (Komers et al., 2006). CAV-1 is co-localised with eNOS in bovine aortic endothelial cells (H. Wang et al., 2009). Accordingly, further investigations were conducted on eNOS in parallel with TRPV4 and CAV-1 using the same ECs batch, which showed similar distribution of eNOS, TRPV4, and CAV-1 in naïve primary aortic ECs (Figures 58a3, 60a3 and 62a3) revealing the possible co-localisation of these three essential elements in endothelial cells plasma membrane. Moreover, eNOS showed significant downregulation in STZ-diabetic ECs (Figure 62 & 72). This is supported by H. Wang et al. (2009)'s findings that eNOS and CAV-1 are co-localised in bovine aortic ECs, and Saliez et al. (2008)'s conclusion of CAV-1 and TRPV4 co-localisation. Diabetic-induced eNOS and CAV-1 downregulation might be attributed to inhibited phosphatidylinositol 3-kinase/Akt (PI3K/Akt) pathway since PI3K inhibitor, wortmannin was shown to inhibit the eNOS and CAV-1 translocation to the plasma membrane (H. Wang et al., 2009). However, further studies such as co-immunoprecipitation are required to confirm the co-localisation of TRPV4, CAV-1 and eNOS in endothelial cells.

Further studies were applied to investigate the beneficial effect of insulin on endothelial TRPV4, CAV-1 and eNOS. The applied insulin concentrations were similar to what was applied by previous studies (Cuevas, Yang, Upadhyay, Armando, & Jose, 2014; Vaidya, Goyal, & Cheema, 2012). As shown in Figure 58c&d and 59, primary STZ-diabetic ECs treated with insulin for 5 days showed significant improvement in TRPV4 expression, distribution and function. Such TRPV4 restored expression and distribution was in parallel with CAV-1 (Figure 60c&d) and eNOS restored expression and distribution (Figure 62c&d). As explained by H. Wang et al. (2009), insulin induces the PI3K/Akt pathway to stimulate eNOS and CAV-1 translocation toward the plasma membrane. Insulin induces eNOS palmitoylation. eNOS and CAV-1 palmitoylation is governed through Golgi's palmitoyl acyl transferase, an enzyme that catalyses eNOS and CAV-1 acetylation and further translocation toward the plasma membrane (Hernando et al., 2006). Additionally, eNOS palmitoylation increases the CAV-1 coupling by 10-fold, a process that is required to optimise eNOS activity (Shaul et al., 1996).

The molecular mechanism of TRPV4 downregulation in diabetes is not fully understood. TRPV4 N-linked mannose glycosylation in the ER is followed by complex TRPV4 protein glycosylation in Golgi apparatus, both are vital post-translational modification steps for the channel maturation, membrane translocation and function (Lei et al., 2013). Deleting 857-838 residues of the TRPV4 c-terminus renders the channels immature and trapped in the ER that culminates in TRPV4 downregulation (Lei et al., 2013). Therefore, as shown in Figures 58b2&c2, TRPV4 was downregulated and seems to be trapped in a region that is overlapped with the nucleus which might be the endoplasmic reticulum. Additionally, TRPV4 downregulation might be exacerbated through CAV-1 disruption and downregulation as numerous studies showed that TRPV4 co-localisation with CAV-1 is essential for TRPV4 function to induce EDHF and vasodilation (Saliez et al., 2008; Serban, Nilius, & Vanhoutte, 2010). These researches have suggested the importance of CAV-1 and TRPV4 co-localisation to maintain the TRPV4 Ca^{2+} required for EDHF and NO generation (Saliez et al., 2008; Serban et al., 2010). Moreover, the TRPV4-CAV-1-eNOS co-localisation might provide a cooperative functional complex (Köhler et al., 2006; Saliez et al., 2008; H. Wang et al., 2009). ECs constitutively secrete NO which is generated from eNOS that oxidises L-arginine to L-citrulline (Cines et al., 1998). eNOS can be stimulated through shear stress (Lüscher & Barton, 1997). Moreover, increased blood shear stress activates the membrane bound PLA-2 which generates arachidonic acid (AA) from membrane cholesterol followed by series reactions that yield epoxyeicosatrienoic acid (EET) generation which is a direct TRPV4 activator (Inoue et al., 2009). These findings reveal the pivotal role of TRPV4 in regulating vascular tone and function through sustained endothelium Ca^{2+} entry that induces NO and PG activation and release (Watanabe et al., 2008). Additionally, TRPV4 was shown to regulate blood pressure (BP) in endothelium-dependent manner through enhancing calcium-influx and thereby generating NO and EDHF (Inoue et al., 2009; Serban et al., 2010).

TRPV4-elevated $[Ca^{2+}]i$ was significantly compromised when naïve ECs were treated with MGO (100µM/day for 5 days) (Figure 67). Such reduction in TRPV4-mediated $[Ca^{2+}]i$ elevation was similar to the $[Ca^{2+}]i$ reduction shown in STZ-diabetic ECs and significantly less than naïve control ECs (Figure 67). Moreover, LSCM pictures showed similar TRPV4 distribution and downregulation in STZ-diabetic ECs and naïve ECs treated with MGO (100µM/day for 5 days) compared to naïve control ECs' TRPV4 (Figures 69 & 70). Additionally, since MGO was significantly elevated in STZ-diabetic rats' serum (Figure 43).

Therefore, MGO-induced TRPV4 downregulation and dysfunction in naïve ECs might explain the STZ-diabetic TRPV4 downregulation in ECs.

As previously stated, TRPV4 N-linked mannose glycosylation in the ER and protein glycosylation in Golgi apparatus are vital post-translational modification steps for the channel maturation, membrane translocation and function (Lei et al., 2013). Immature channels are trapped in the ER that culminates in TRPV4 downregulation (Lei et al., 2013). Therefore, as shown in Figure 69, TRPV4 was downregulated and seems to be trapped in a region that is overlapped with the nucleus which might be the ER. In eukaryotic cells, the ER provides 3 main cellular functions: firstly, proteins folding before being transferred to the Golgi apparatus, secondly, ER provide a cellular Ca^{2+} storage, and lastly, it is a site for the synthesis of phospholipids, sterols and unsaturated fatty acids (FA) (Schröder, 2008). A perturbation in any of these functions contributes to ER stress and hence affects the overall ER performance (Schröder, 2008). Misfolded proteins accumulation in the ER lumen is a distinct hallmark of perturbation of any of the mentioned ER physiological functions (Schröder, 2008). Unlike the cytosolic reducing environment, the ER lumen is an oxidising environment with a high ratio of the reduced to oxidised glutathione (GSH:GSSG) (1-3:1), whereas the GSSG:GSH is approximately 50:1 in the cytoplasm (Malhotra & Kaufman, 2007). Being the primary Ca^{2+} storing organelle in the cell, enables the ER to use the Ca^{2+} stored in the ER lumen for both protein-folding reactions and protein chaperone functions (Malhotra & Kaufman, 2007). Moreover, N-linked glycosylation is a post-translational modification process performed in the ER (Malhotra & Kaufman, 2007). N-linked glycosylation is coupled with protein folding and chaperone interactions to ensure that only the properly folded proteins are released from the ER compartment (Malhotra & Kaufman, 2007). ER Ca^{2+} depletion induces protein misfolding (Lodish, Kong, & Wikstrom, 1992) and inhibits the ER-Golgi trafficking (Lodish & Kong, 1990). Ca^{2+} depletion from ER stores induces the accumulation of unfolded proteins through inhibiting endoplasmic reticulum-associated degradation (ERAD) due to decreased endoplasmic reticulum-a(1,2)mannosidase activity (Schröder, 2008). MGO induces ER Ca^{2+} release that contributes to the initial and the sustained $[Ca^{2+}]i$ elevation (Jan, Chen, Wang, & Kuo, 2005). Therefore, chronic MGO elevation, as shown in STZ-induced diabetes (Figure 43) might lead to ER Ca^{2+} stores perturbation that culminates in protein misfolding and ER stress and hence causes significant decrease in TRPV4 expression through MGO-treatment (Figures 69 & 70).

Misfolded proteins form hydrophobic patches that inhibit other proteins, especially the proteins that act through interacting with other proteins such as transcription factors (Schröder, 2008). To counteract the misfolded proteins complications, the ER monitors the protein misfolding through UPR's numerous transmembrane proteins such as protein kinase receptor (PKR)-like eukaryotic initiation factor 2 kinase (PERK) (Schröder, 2008). Activated PERK phosphorylates the eukaryotic initiation factor2α (eIF2α), a transcription factor which is inhibited by phosphorylation and accordingly, inhibiting new protein translation and hence reduces the ER stress (Marciniak & Ron, 2006). Phosphorylated eIF2α activates a downstream orchestrated cascade including the transcription factor ATF4 that induces the expression of other transcription factors such as GADD34 which relieves translational attenuation and ERO1α which promotes oxidative protein folding (Marciniak & Ron, 2006). Antioxidants buffer the increased ROS produced by ERO1α to maintain the redox status of ER (Marciniak & Ron, 2006). Since MGO induces ER Ca^{2+} release that contributes to the initial and the sustained intracellular Ca^{2+} elevation (Jan et al., 2005). Additionally, chronic MGO elevation might lead to ER Ca^{2+} stores perturbation that culminates in ER stress (Jan et al., 2005). Accordingly, when primary aortic ECs were incubated with MGO (100μM), TRPV4-induecd rise in $[Ca^{2+}]i$ was significantly reduced (Figure 67) which was in parallel with the significant TRPV4 downregulation (Figure 69 & 79). By contrast, when L-arginine (100μM) was added to the primary aortic ECs in the presence of MGO (100μM), TRPV4-induecd rise in $[Ca^{2+}]i$ was significantly restore (Figure 67). This might be attributed to 2 main factors: L-arginine ability to scavenge MGO (I. Dhar et al., 2012), in addition to the ability of L-arginine to facilitate the maintenance of ER redox status (Marciniak & Ron, 2006) and hence relieves ER stress induced by MGO-induced OS which was shown in Figure 69 and 79, and therefore, TRPV4 function might be restored when ECs were incubated with L-arginine in the presence of MGO (Figure 67). To the best of our knowledge, this is the first study that investigates the MGO-compromised TRPV4 function in ECs.

Since pre-contracted diabetic aortic rings were relaxed through icilin CRC without any significant difference from non-diabetic aortic rings (Figure 56). Moreover, fura-2 Ca^{2+} imaging studies did not show significant difference in TRPM8-mediated Ca^{2+} influx in primary ECs isolated from either naïve control or STZ-rats' ECs (Figure 72). This supports the previous findings (Figure 28 & 39) that TRPM8 might mediate vasodilation through different pathways to TRPV4 which was significantly compromised in diabetes.

To sum up, TRPV4 was significantly downregulated in STZ-diabetic ECs. Such downregulation was accompanied with TRPV4 dysfunction characterised by compromised TRPV4-induced vasodilation and reduced TRPV4-mediated $[Ca^{2+}]i$ elevation. STZ-diabetic ECs treated with insulin ex vivo showed restored TRPV4 function and expression. Additionally, CAV-1 and eNOS were both downregulated in parallel with TRPV4. STZ-diabetic ECs treated with insulin ex vivo showed restored CAV-1 and eNOS expression, revealing that TRPV4-CAV-1-eNOS might form an endothelial functional complex. Since the main objective was to examine the effect on insulin treatment on STZ-diabetic primary aortic ECs, therefore insulin was only applied to the STZ-diabetic primary aortic ECs. However, a control of naïve primary aortic ECs treated with insulin would show whether insulin would provide beneficial effect to naïve primary aortic ECs.

MGO was elevated in STZ-diabetic rats' serum to approximately 100µM. Incubating non-diabetic ECs with MGO (100µM/day for 5 days) compromised TRPV4 expression and function similar to what was shown in STZ-diabetic ECs. L-arginine showed vascular protection properties as a possible MGO scavenger through restoring ECs' TRPV4 function. Chronic MGO elevation as shown in STZ-induced diabetes might contribute to ER stress and hence causes protein misfolding. Not like TRPV4, TRPM8 function was not significantly affected in STZ-diabetic ECs. However, another group of naïve primary aortic ECs treated with L-arginine only would provide an idea of whether L-arginine treatment could induce TRPV4 expression.

In conclusions, insulin is might be involved in regulating vascular function and endothelial protein expression such as TRPV4, CAV-1 and eNOS. MGO might be a pivotal therapeutic target to manage diabetes complications. L-arginine was shown to act as a scavenger for MGO and hence it might play a major therapeutic strategy for MGO-related diabetic complications such as endothelial dysfunction (Bierhaus et al., 2012; A. Dhar et al., 2010).

Therefore, the next chapter will cover further vascular studies conducted on primary aortic smooth muscle cells (ASMCs) as a component of tunica media and the effect of MGO on ASMCs.

Chapter 6: The effect of diabetes on nitric oxide production and TRPV4 expression in primary rat ASMCs

6.1. Introduction

According to the last two chapters, both TRPV4-induced vasodilation and $[Ca^{2+}]i$ elevation in primary aortic ECs were significantly compromised in STZ-induced diabetes. Such significant TRPV4 dysfunction was accompanied with significant eNOS downregulation. Moreover, TRPV4-induced vasodilation was endothelium-dependent and independent, as the endothelium removal did not completely abolish the TRPV4-induced vasodilation. TRPV4 expression in MEPs was suggested to induce VSM hyperpolarisation through Kca activation and hence inducing vasodilation (Bagher & Garland, 2014). Moreover, the VSM's calcium-independent NOS isoform, iNOS releases NO that was shown to reduce the NA-induced vasoconstriction by activating Kca channels (Hall et al., 1996). Moreover, other studies showed that iNOS expression through LPS infusion reduces the NA-induced vasoconstriction through cGMP pathway (Gray et al., 1991; C.-C. Wu, Szabo, Chen, Thiemermann, & Vane, 1994). The blood vessels' hyporeactivity to NA was L-arginine-dependent, thus when extracellular L-arginine increases, the vascular reactivity to NA decreases (Schott, Gray, & Stoclet, 1993). Accordingly, the aim of this chapter is to investigate the influence of diabetes on iNOS and TRPV4 expression in primary ASMCs. iNOS was induced through incubating ASMCs with LPS and interferon gamma (IFN-γ) to induce inflammation and NO release (Arnal et al., 1999; Uemura et al., 2002).

The main objectives of these experiments were to investigate whether iNOS-generated NO from primary ASMCs was influenced by STZ-induced diabetes, through SDS-PAGE Western blotting and the Griess assay to measure iNOS expression and function, respectively. Moreover, further investigations were conducted on the effect of MGO (100μM) on iNOS expression and NO release, and to investigate if L-arginine was able to counteract the MGO effect. Moreover, TRPV4 expression was studied through SDS-PAGE Western blotting.

6.2. Materials and methods

6.2.1. Primary aortic smooth muscle cells studies

As described in section 2.5, primary aortic smooth muscle cells (ASMCs) were isolated to investigate iNOS and TRPV4 expression. iNOS was stimulated to release NO through incubating a 100% confluent naïve (or STZ-diabetic) primary ASMCs with IFN-γ (100IU/ml) and LPS (100µg/ml) for 24 hours. To study the effect of MGO on iNOS expression and NO release, naïve ASMCs were treated with MGO representing the pathological and physiological concentration (100 and 10µM, respectively) as well as without MGO (positive control) in addition to untreated cells (negative control), and ASMCs treated with IFN-γ (100IU/ml) and LPS (100µg/ml) with MGO (100µM) and L-arginine (100µM) for 24 hours. After being treated, the ASMCs cultures were incubated at 37°C CO_2 5% for 24 hours. Total nitrite (NO_2) was estimated through the Griess assay. The Griess assay was conducted for measuring NO indirectly through total NO_2 released from ASMCs. A total NO_2 standard curve was used to estimate the samples total NO_2 (Figure 74). The reaction based on oxidising NO into NO_2 from 100µl sample from the well which was then added with 100µl Griess mixed reagents A and B (1:1 Griess reagents ratio), Sulfanilamide and N-1-naphthylethylenediamine, respectively. The reaction generates a pink azo dye and its intensity is proportional to the NO_2 concentration. The total NO_2 was estimated through an automated spectrophotometer at 540nm (Coneski & Schoenfisch, 2012). Afterward, the ASMCs cultures were lysed for BCA to estimate the required volume of the cell lysate to load 20µg total proteins for western blotting as described in section 2.8.

Total TRPV4 expression in ASMCs was studied through growing the ASMCs primarily from the aortic rings in a six well plate. After 3-5 days, the wells become confluent and the cells were lysed and the cells lysate samples were studied through SDS-PAGE Western blotting for TRPV4 expression level as described in section 2.8.1.

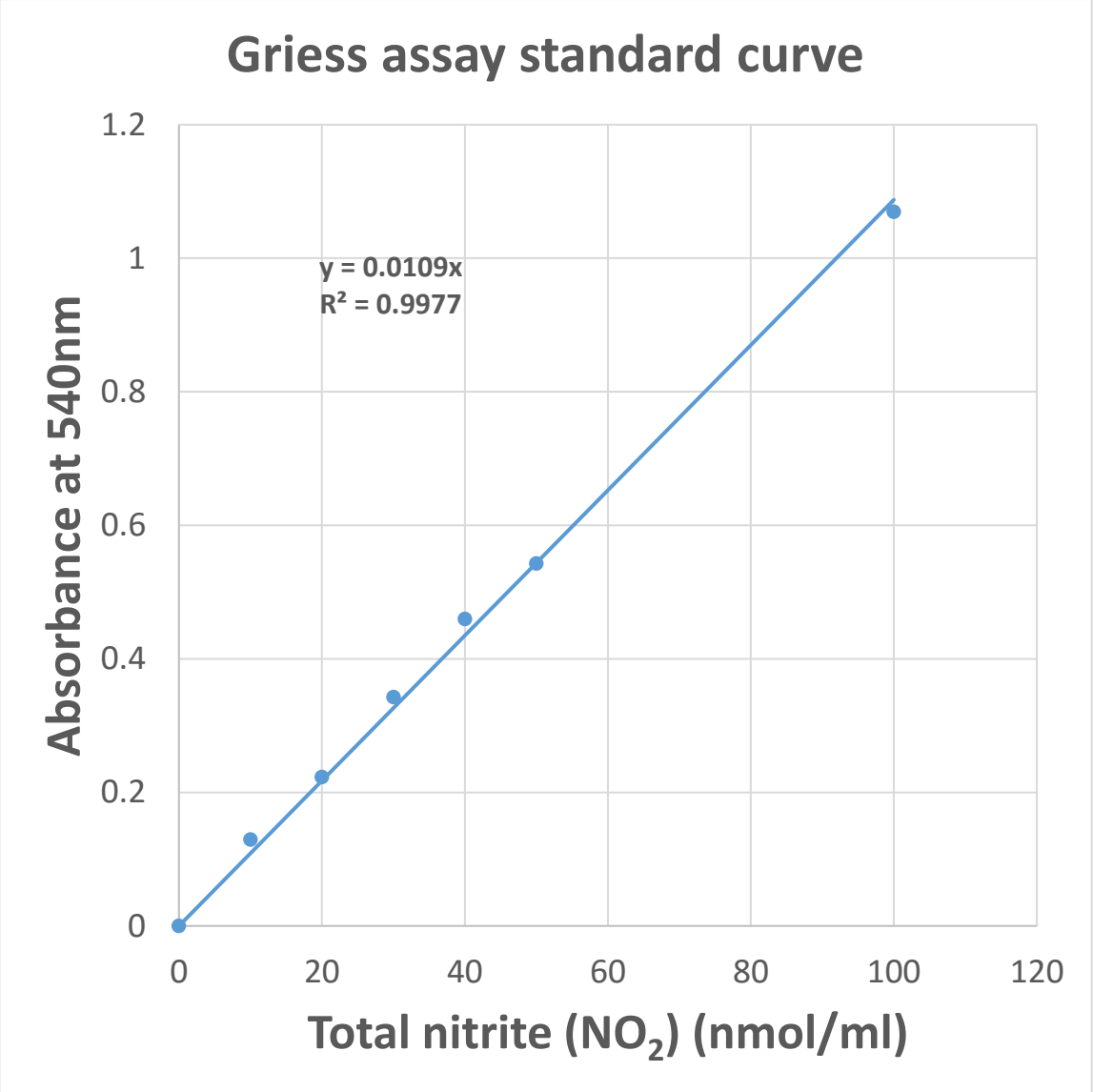

Figure 74. Griess assay standard curve. Seven different standard solutions of sodium nitrite in complete culture media (0, 10, 20, 30, 40, 50 and 100nmol/ml) were read at 540nm wavelength. The linear equation was applied to estimate the sample concentration (x). The blue dotted line showed trend line robust fit.

6.3. Results

6.3.1. Total NO_2 release was significantly elevated after incubating ASMCs with IFN-γ and LPS for 24 hours

A time course study was conducted to estimate the suitable required time for iNOS induction. Incubation time points were 1, 3, 6 and 24 hours. iNOS induction was evaluated through total NO_2 measurement. As shown in Figure 75, incubating ASMCs with IFN-γ (100IU/ml) and LPS (100µg/ml) for 24 hours was the most suitable time point to induce iNOS. Incubating ASMCs with IFN-γ (100IU/ml) and LPS (100µg/ml) for 24 hours was shown to significantly induce NO release which was measured through total NO_2 (N=3, total NO_2= 3.0 ± 1.0nmol/ml) when compared to negative control and the other groups of shorter time points (1-6 hours) or ASMCs treated with LPS only. LPS only groups were treated with LPS (100µg/ml) in cell culture complete media. The negative control was incubated with cell culture complete media only for 24 hours.

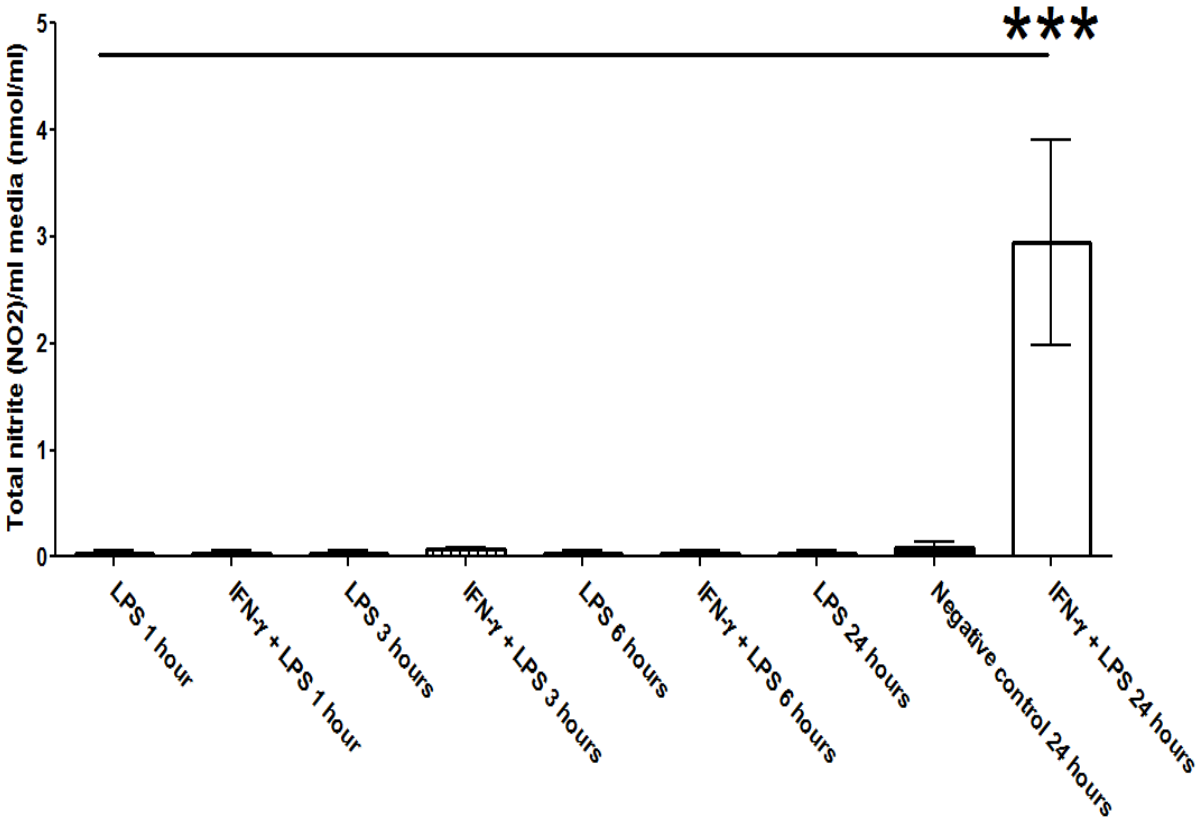

Figure 75. Time course study of total nitrite (NO_2) production from ASMCs. Analysed through one-way ANOVA with Tukey post-hoc test. ASMCs treated with IFN-γ (100IU/ml) and LPS (100µg/ml) compared with LPS only groups were treated with LPS (100µg/ml) and untreated ASMCs (negative control). Significance is represented as *** $P < 0.001$ compared with IFN-γ (100IU/ml) and LPS (100µg/ml) (positive control). Data shown as average total nitrite ± SEM (Every group, N= 3).

According to the previous time course finding (Figure 75), NO release and iNOS expression from primary ASMCs isolated from naïve STZ-diabetic rats were compared. iNOS was detected through SDS-PAGE western blotting (Figure 76 & 86a). STZ-diabetic ASMCs were incubated with IFN-γ and LPS (positive STZ) for 24 hours and showed a significant reduction in iNOS expression when compared to naïve ASMCs' (Figure 77b). The Griess assay showed significant suppression of total NO_2 release when STZ-diabetic ASMC were incubated with IFN-γ and LPS for 24 hours compared to naïve ASMCs (Figure 77c).

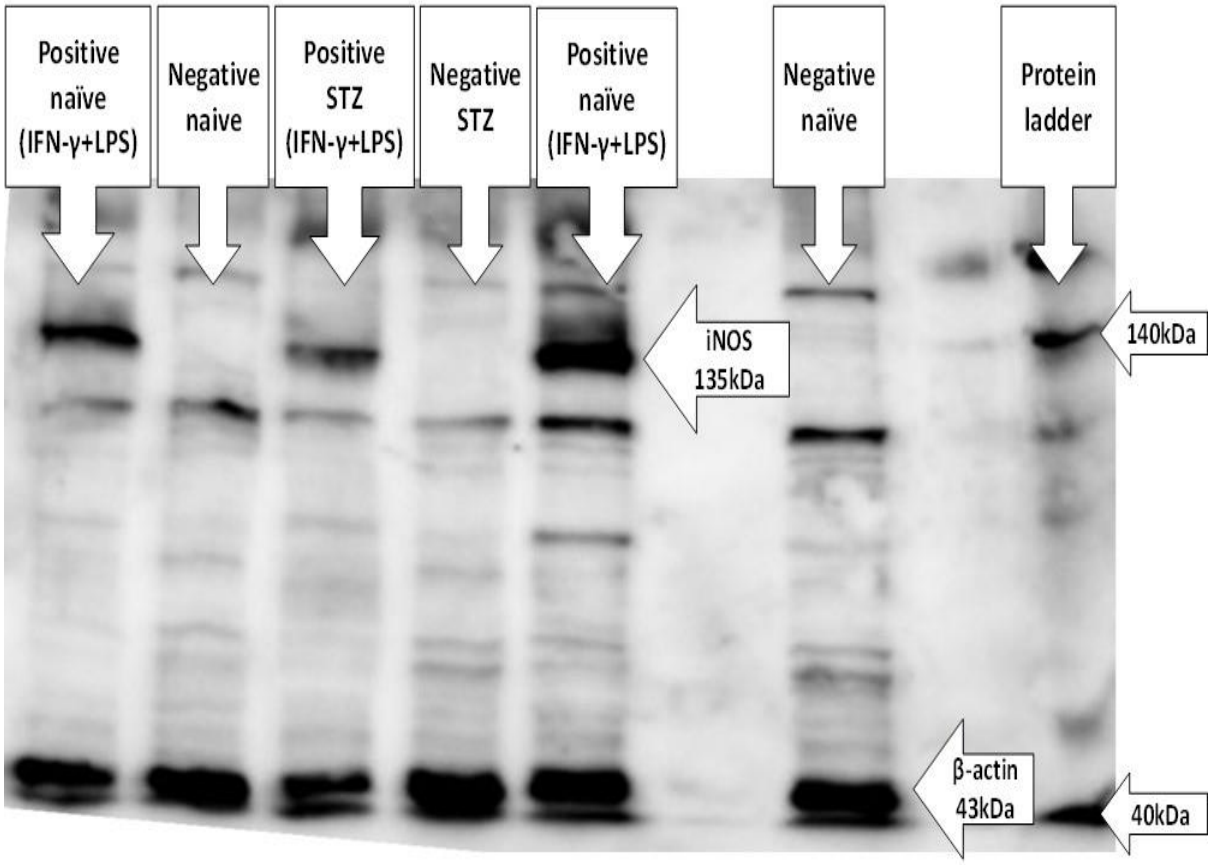

Figure 76. SDS-PAGE Western blotting for iNOS expression in STZ-diabetic and naïve ASMCs. iNOS was detected in positive control (IFN-γ and LPS) lanes but not in negative control (untreated). Positive control (IFN-γ and LPS) lanes were loaded with cell lysate that corresponds to 20µg. iNOS band was matched to approximately 135kDa through using the 140kDa band shown in protein ladder. β-actin protein was detected at approximately 43kDa just above the 40kDa band shown in protein ladder.

When the Western blot gels were analysed through densitometric analysis as describe in section 2.7, iNOS expression in STZ-diabetic rats' ASMCs was significantly suppressed (N= 5, * $p < 0.05$, average iNOS expression= 56.1 ± 13.4% vs naïve ASMCs' average iNOS expression= 100 ± 4.4%) (Figure 77b). Additionally, total NO_2 released from STZ-diabetic rats' ASMCs was significantly reduced (N= 6, * $p < 0.05$, total NO_2= 37.02 ± 13.8% vs naïve ASMCs' total NO_2= 100 ± 18.0%) (Figure 77c).

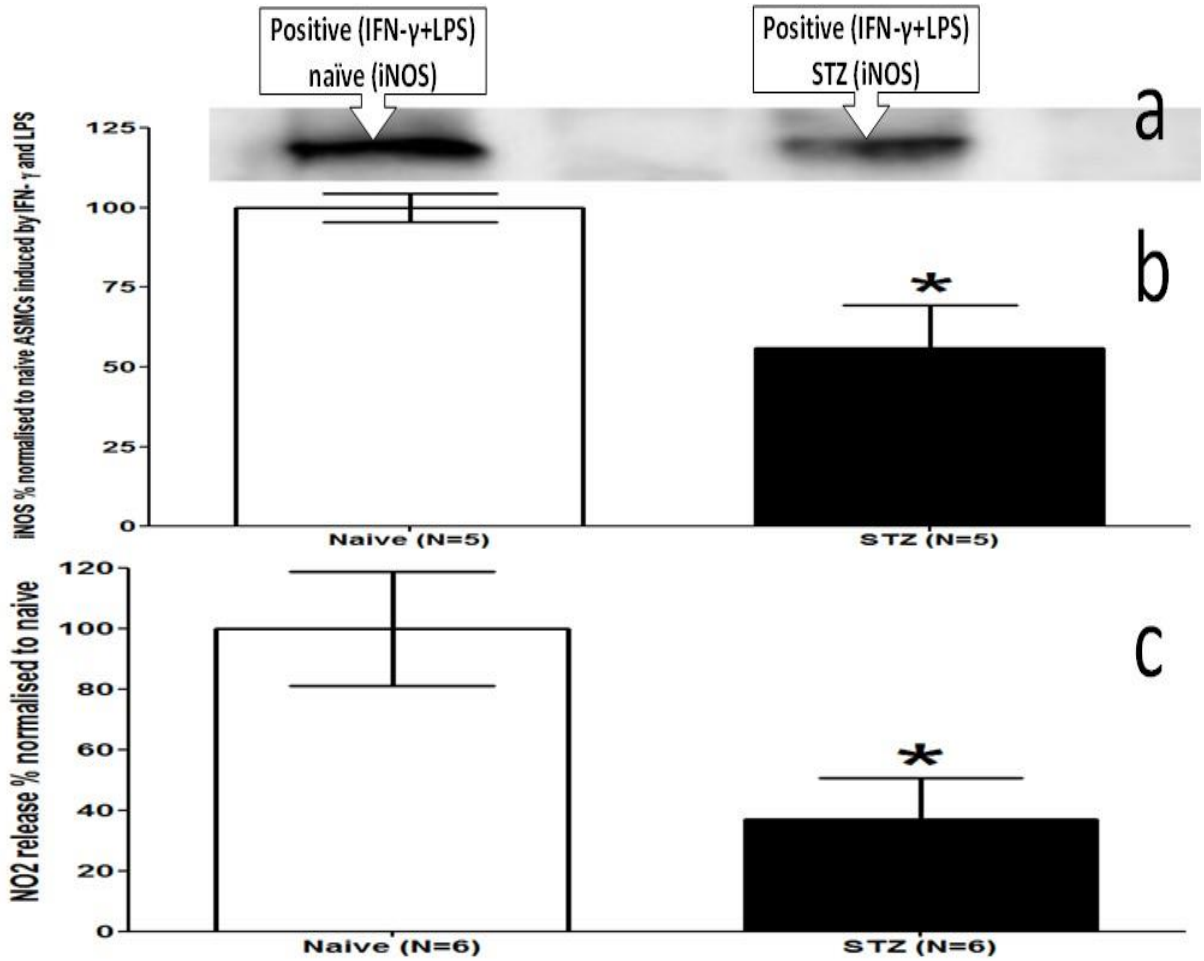

Figure 77. iNOS expression and total nitrite (NO_2) released from STZ-diabetic and naïve ASMCs. Western blotting of rats' aortic smooth muscle cells' (ASMCs) inducible nitric oxide synthase (iNOS) (a). iNOS expression in STZ-diabetic and naïve ASMCs (b). Total NO_2 released from STZ-diabetic rats' and naïve ASMCs (c). Data is presented as mean ± SEM. Significance is represented as * $p < 0.05$ versus naive analyses by unpaired two-tailed Student's t-test.

6.3.2. MGO studies on ASMCs

- MGO significantly increased the NA-induced vasoconstriction

A previous report showed that the VSM's calcium-independent NOS isoform, iNOS releases NO that was shown to reduce the NA-induced vasoconstriction through activating Kca channels (Hall et al., 1996). Moreover, other studies showed that iNOS expression through LPS infusion reduces the NA-induced vasoconstriction through cGMP pathway (Gray et al., 1991; C.-C. Wu et al., 1994). The blood vessels' hyporeactivity was enhanced through L-arginine incubation (Schott et al., 1993).

Since, MGO was elevated in STZ serum (Figure 43), and a previous study revealed that MGO inhibits the calcium-dependent NOS form, eNOS phosphorylation and activation (A. Dhar et al., 2010). Moreover, as iNOS and eNOS are NOS isoforms which are expressed predominantly in VSMCs and ECs, respectively. Therefore, it was hypothesised that freshly isolated STZ-rat aortic rings may show higher vasoconstriction than naïve aortic rings when treated with NA EC_{80} (300nM), due to the effect of MGO to reduce NO production from iNOS (Hall et al., 1996; C.-C. Wu et al., 1994).

Aortic rings were treated with NA (300nM) and showed time-dependent increased vasoconstriction. NA-induced vasoconstriction was significantly elevated in the 3^{rd} week STZ-diabetic rats (N= 5, * $p < 0.05$, vasoconstriction= 0.32 ± 0.03g), the 4^{th} week STZ-diabetic rats (N= 7, ***P<0.001, vasoconstriction= 0.36 ± 0.04g) and the 5^{th} week STZ-diabetic rats (N= 4, **P<0.01, vasoconstriction= 0.44 ± 0.01g) compared with control naïve rats (N= 12, vasoconstriction= 0.29 ± 0.02g). However, NA-induced vasoconstriction did not show significant difference (ns $p \geq 0.05$) in the first 2 weeks after STZ-induced diabetes induction (1^{st} week STZ-rats, N= 4, ns $p \geq 0.05$, , vasoconstriction= 0.31 ± 0.01g, 2^{nd} week STZ rats ns $p \geq 0.05$, N= 6, , vasoconstriction= 0.316 ± 0.02g vs control naive aortic rings, N= 12, , vasoconstriction= 0.29 ± 0.02g) (Figure 79a).

To investigate the iNOS contribution from smooth muscle cells in counteracting vasoconstriction, aortic rings were denuded from endothelium and incubated for 30 minutes with L-NAME (100μM) before being treated with NA (300nM). To ensure that the endothelium removal was effective in the denuded tissue we tested this by measuring the carbachol induced vasodilation of NA induced tension in control and denuded tissue (Figure 91). As expected the carbachol induced vasodilation was almost completely abolished in the denuded rings consistent with endothelium removal. Endothelium denuding showed

significant reduction in carbachol-induced vasodilation (N=5, *** $p < 0.001$, Emax= -16.6±4.8% vs intact endothelium carbachol induced-vasodilation Emax= -68.4±2.3%) (Figure 91). However, the EC50 was not significantly influenced (N=5, $p \geq 0.05$, EC50= 3.8 ± 0.6µM and vs intact endothelium carbachol induced-vasodilation EC50= 1.8 ± 1.1µM) (Figure 78).

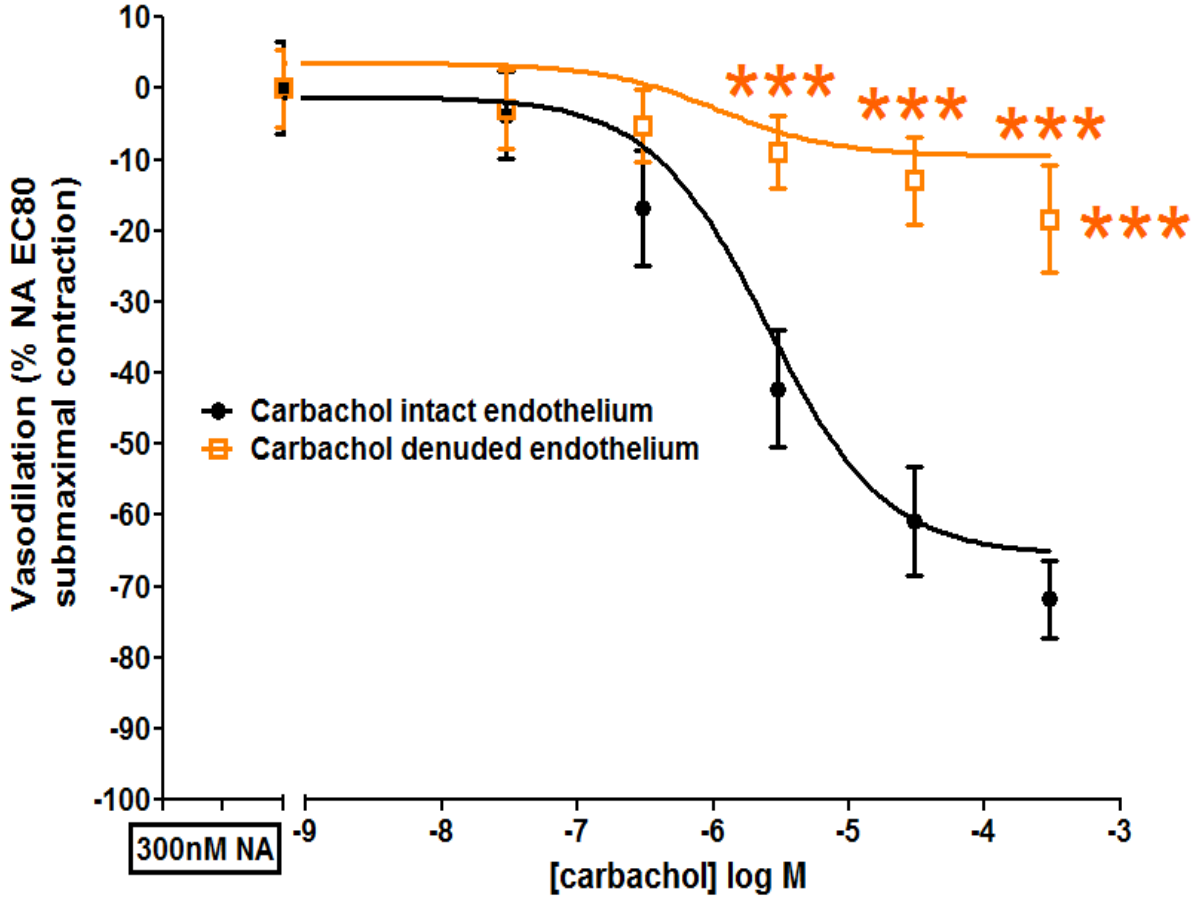

Figure 78. Carbachol cumulative concentration response curve when endothelium was denuded. Analysed through two-way ANOVA with Bonferroni post-hoc test. Significance is shown as *** $p < 0.001$ versus carbachol-induced vasodilation in intact endothelium aortic rings (N= 5).

Endothelial denuded rats' aortic rings incubated with L-NAME (100μM) were compared to untreated endothelial denuded aortic rings and intact aortic rings contraction. Denuded naïve aortic rings incubated with L-NAME showed significantly higher vasoconstriction compared to untreated denuded control aortic rings (** $p < 0.01$). Endothelium denuded control aortic rings did not show a significant difference when compared to intact aortic rings vasoconstriction (ns $P \geq 0.05$) (denuded control rings incubated with L-NAME, N= 4, ** $p < 0.01$, vasoconstriction= 0.47 ± 0.05g vs denuded aortic rings N= 7, vasoconstriction= 0.30 ± 0.02g and *** $p < 0.001$ vs intact aortic rings, N= 12, vasoconstriction= 0.29 ± 0.02g) (Figure 79b).

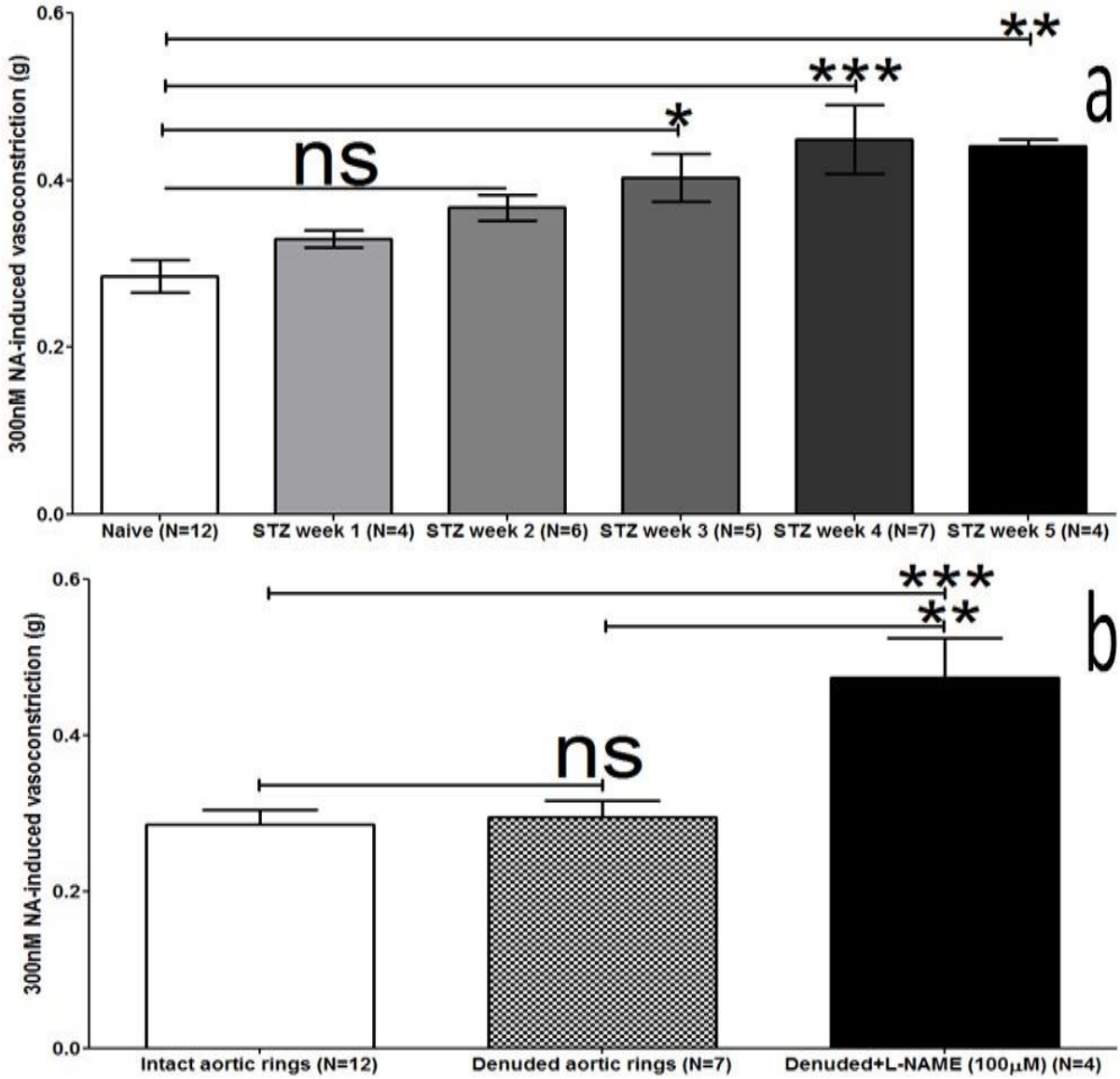

Figure 79. Fresh rats' aortic rings contractility with NA EC_{80} (300nM). STZ-diabetic aortic rings constricted through NA (300nM) compared with naïve aortic rings constriction (a). Denuded control aortic rings incubated with L-NAME compared to untreated denuded aortic rings and intact aortic rings (b). Analysed through one-way ANOVA and Tukey post-hoc test. Significance is represented as * $p < 0.05$, ** $p < 0.01$ and *** $p < 0.001$. Data is presented as mean ± SEM.

- MGO significantly suppressed iNOS expression and total NO_2 release in ASMCs

STZ-rat primary ASMCs showed significant reduction in NO_2 release and iNOS expression following IFN-γ and LPS induction (Figure 77). Additionally, MGO was significantly increased in STZ-diabetic rats' serum (Figure 43). Therefore, the effect of MGO on NO_2 release and iNOS expression in naïve rat primary ASMCs was investigated. When ASMCs were incubated with IFN-γ, LPS and MGO (100µM) for 24 hours it showed significant iNOS suppression (***$p < 0.001$) but not with MGO (10µM) (ns $p \geq 0.05$) compared to ASMCs incubated with IFN-γ and LPS only. Incubating ASMCs with LPS and IFN-γ for 24 hours in addition to MGO 100µM for 2 hours causes non-significant reduction to iNOS expression (ns $p \geq 0.05$). When ASMCs were incubated with IFN-γ, LPS and MGO (100µM) for 24 hours showed significant iNOS suppression (N= 9, *** $p < 0.001$, average iNOS expression= 35.3 ± 3.7% vs positive control, N= 9, average iNOS expression= 100 ± 7.6%) but not with MGO (10µM) (N= 6, ns $p \geq 0.05$, 113.4±6.3%). Incubating ASMCs with IFN-γ and LPS for 24 hours with MGO (100µM) added for 2 hours causes non-significant reduction to iNOS expression (N= 5, ns $p \geq 0.05$, average iNOS expression= 73.4±14.5% vs positive control, N= 5, average iNOS expression= 100 ± 7.6%). When ASMCs were incubated with media only it showed significant iNOS suppression (N= 9, *** $p < 0.001$, average iNOS expression= 16.3 ± 3.0% vs positive control, N= 9, average iNOS expression= 100 ± 7.6%) (Figure 81b). We next performed Griess assay to see if the changes in iNOS expression resulted in changes in total NO_2 release. The Griess assay showed significant suppression of NO_2 release when ASMC were incubated with IFN-γ and LPS with MGO 100µM for 24 hours (*** $p < 0.001$) but not with MGO (10µM) (ns $p \geq 0.05$). Incubating ASMC with LPS and IFN-γ for 24 hours with MGO (100µM) added for 2 hours did not cause significant reduction to NO2 release (ns $p \geq 0.05$). The Griess assay showed significant suppression of total NO_2 release when ASMC were incubated with IFN-γ and LPS with MGO (100µM) for 24 hours (N= 9 *** $p < 0.001$, total NO_2= 2.8 ± 15.1% vs positive control, N=9, total NO_2= 100 ± 17.8%) but not with MGO 10µM (N= 6, ns $p \geq 0.05$, total NO_2= 84.2 ± 16.2% vs positive control, N=9, total NO_2= 100 ± 17.8%). Incubating ASMC with LPS and IFN-γ for 24 hours with MGO 100µM added for 2 hours causes non-significant reduction to total NO_2 release (N=5, ns $p \geq 0.05$, total NO_2= 62.3 ± 24.4% vs positive control, N=9, total NO_2= 100 ± 17.8%) (Figure 81c).

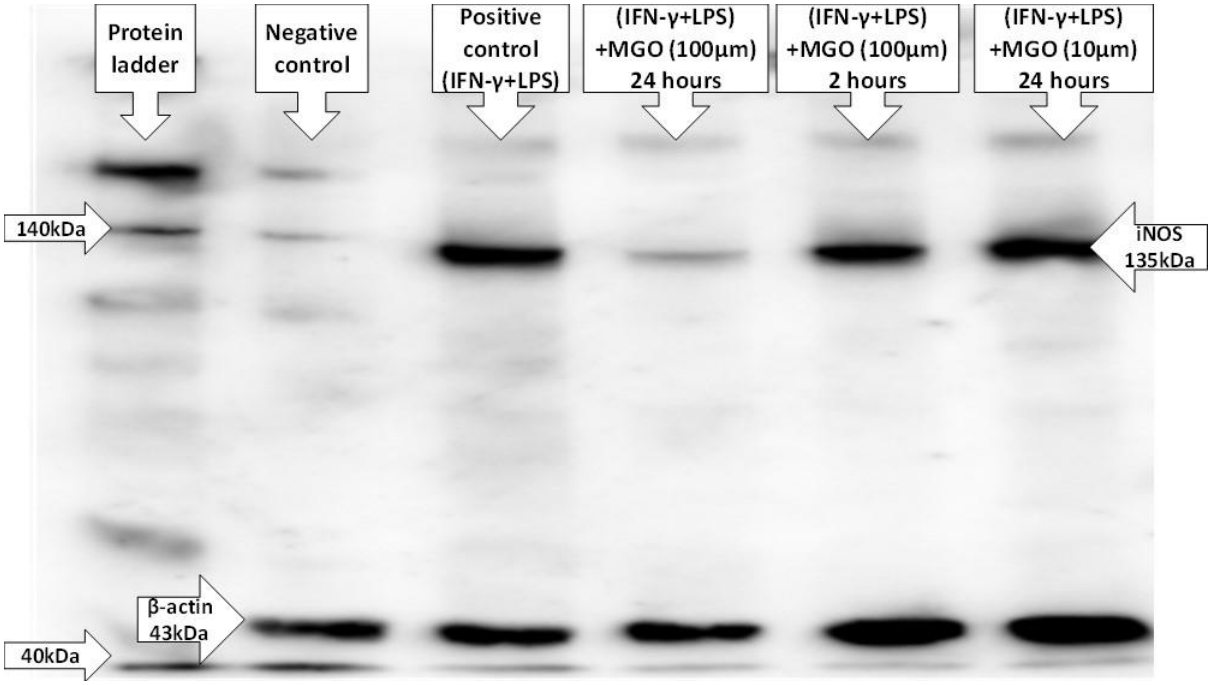

Figure 80. SDS-PAGE western blotting for iNOS expression in naïve ASMCs treated with MGO. Each lane was loaded with cells lysate that corresponds to 20μg. iNOS band was matched to approximately 135kDa through using the 140kDa band shown in protein ladder. β-actin protein was detected at approximately 43kDa just above the 40kDa band shown in protein ladder. The 1st lane was loaded with lysate of untreated ASMCs, the 2nd lane positive control of ASMCs incubated with IFN-γ (100IU/ml) and LPS (100μg/ml) for 24 hours. The 3rd lane of ASMCs incubated with IFN-γ (100IU/ml), LPS (100μg/ml) and MGO (100μM) for 24 hours. The 4th lane of ASMCs incubated with IFN-γ (100IU/ml), LPS (100μg/ml) and MGO (100μM) for 2 hours. The 5th lane of ASMCs incubated with IFN-γ (100IU/ml), LPS (100μg/ml) and MGO (10μM) for 24 hours.

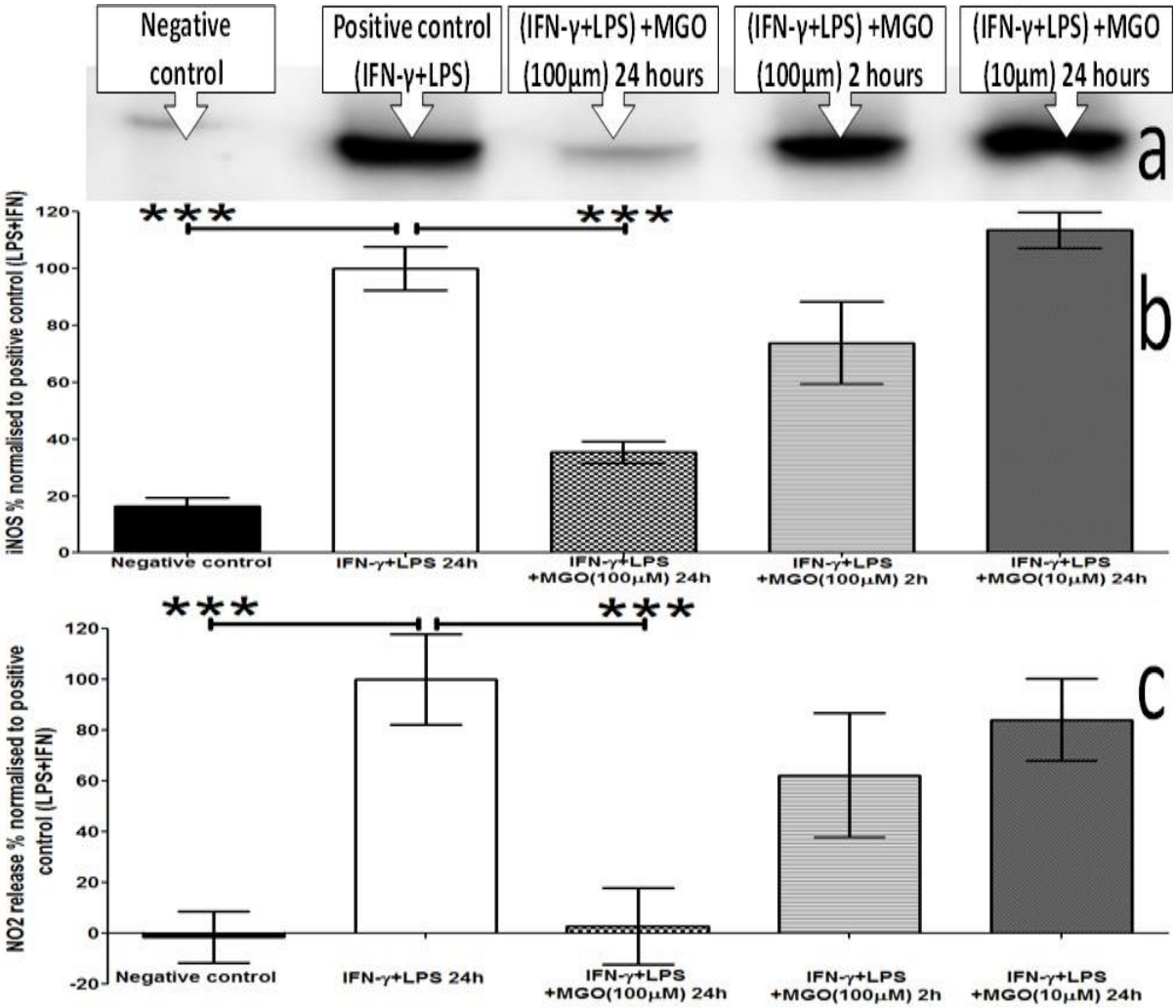

Figure 81. iNOS expression and NO_2 production in the presence of MGO physiological (10µM) and pathological (100µM) concentrations. SDS-PAGE western blotting showing iNOS bands expression (a). iNOS expression from ASMCs incubated with IFN-γ, LPS and MGO 10µM for 24 hours and 100µM for 24 hours and 2 hours compared with positive and negative controls ASMCs (b). Total NO_2 released from ASMCs incubated with IFN-γ, LPS and MGO 10µM for 24 hours and 100µM for 24 hours and 2 hours compared with positive and negative controls ASMCs (c). Data is presented as mean ± SEM. Significance is represented as *** $p < 0.001$ when compared with positive control by one-way ANOVA with Tukey post-hoc test.

- L-arginine restores MGO-suppressed iNOS inhibition

As shown in Figure 52, L-arginine (100μM) restored the endothelial function which was impaired through MGO (100μM). Moreover, L-arginine (100μM) restored the TRPV4 function which was suppressed through MGO (100μM) (Figure 68). Therefore, further confirmatory study was conducted to investigate the ability of L-arginine to restore the MGO-suppressed iNOS expression. L-arginine (100μM) was added to the ASMCs in addition to IFN-γ (100IU/ml), LPS (100μg/ml) and MGO (100μM) and the effect of L-arginine was analysed against untreated negative control, positive control (ASMCs treated with IFN-γ and LPS only) and positive control added with MGO (100μM) only. L-arginine was applied (100μM) at a concentration that is within the range of normal plasma L-arginine concentration (60-140μM) (Schwedhelm et al., 2008).

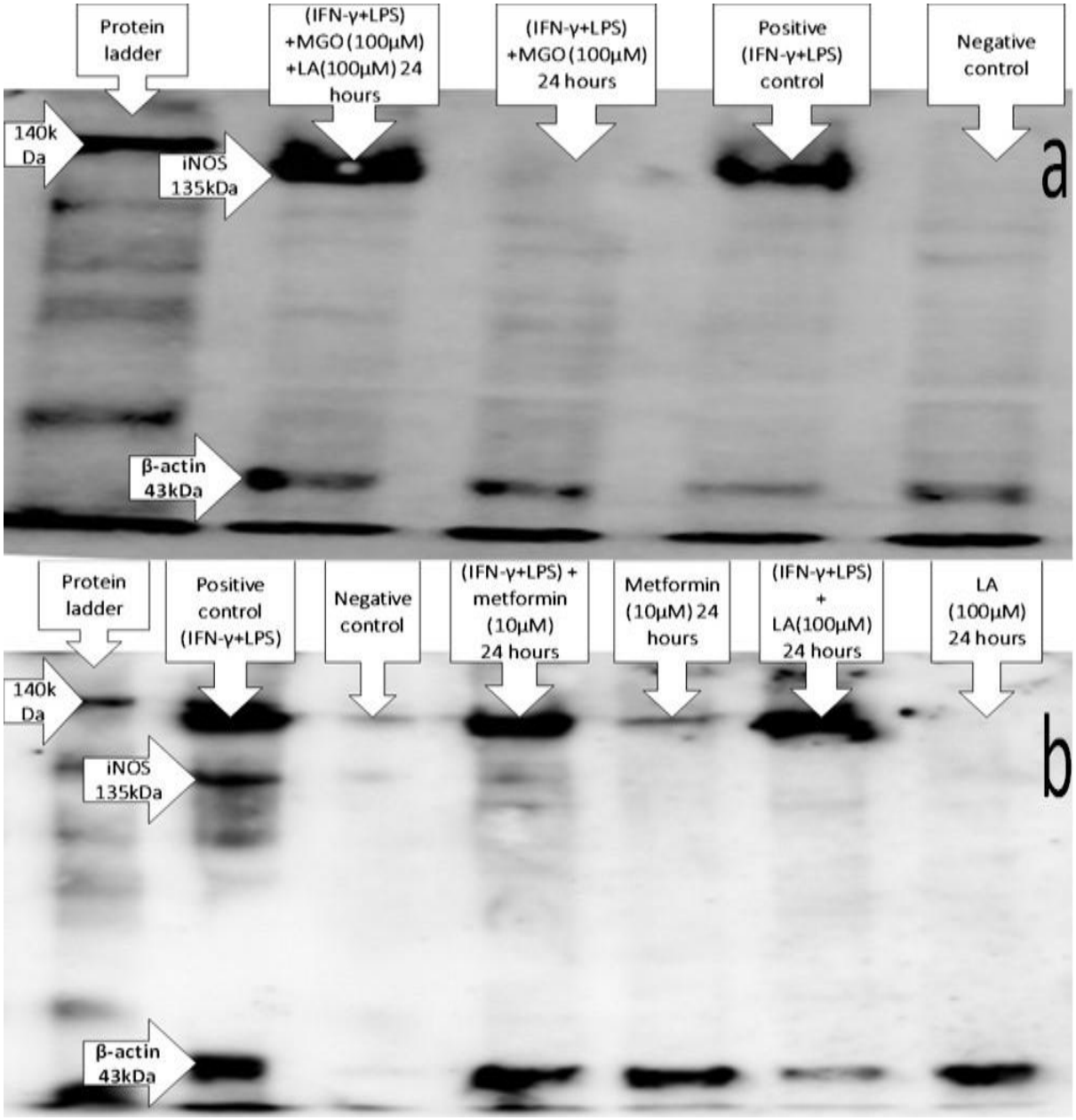

Figure 82. SDS-PAGE western blotting for iNOS expression in naïve ASMCs treated with MGO and L-arginine. Each lane was loaded with cells lysate that corresponds to 20μg. iNOS band was matched to approximately 135kDa through using the 140kDa band shown in protein ladder (the first lane on left). β-actin protein was detected at approximately 43kDa just above the 40kDa band shown in protein ladder. The 1st lane was loaded with lysate of ASMCs incubated with IFN-γ (100IU/ml), LPS (100μg/ml), MGO (100μM) and L-arginine (100μM) for 24 hours. The 2nd lane was loaded with ASMCs incubated with IFN-γ (100IU/ml), LPS (100μg/ml) and MGO (100μM) for 24 hours. The 3rd lane was loaded with ASMCs lysate of positive control of ASMCs incubated with IFN-γ (100IU/ml) and LPS (100μg/ml) for 24 hours. The 4th lane was loaded with lysate of untreated ASMCs (a). For the second membrane, the 1st lane was loaded with lysate of ASMCs lysate of positive control of ASMCs incubated with IFN-γ (100IU/ml) and LPS (100μg/ml) for 24 hours. The 2nd lane was loaded with untreated ASMCs lysate. The 3rd lane was loaded with cell lysate of ASMCs treated with IFN-γ (100IU/ml), LPS (100μg/ml) and metformin (10μM) whereas the 4th lane was loaded with ASMCs treated with metformin (10μM) only. The 5th lane was loaded with cell lysate of ASMCs treated with IFN-γ (100IU/ml), LPS (100μg/ml) and L-arginine (100μM) whereas the 6th lane was loaded with ASMCs treated with L-arginine (100μM) only (b).

iNOS expression and total NO_2 production were measured to evaluate the effect of L-arginine on MGO. ASMCs incubated with IFN-γ, LPS and MGO (100μM) for 24 hours showed significant iNOS suppression compared with L-arginine (100μM) co-treatment (N=4, *** $p < 0.001$, average iNOS expression= 33.9 ± 7.4% vs IFN-γ and LPS with MGO and L-arginine, average iNOS expression= 86.1 ± 7.7%). ASMCs treated with IFN-γ and LPS with MGO (100μM) and L-arginine (100μM), and ASMCs treated with IFN-γ, LPS and L-arginine (100μM) did not show significant difference in iNOS expression when compared with positive control ASMCs treated with IFN-γ and LPS only (N=4, ns $p \geq 0.05$, average iNOS expression= 86.1 ± 7.7%, ASMCs treated with IFN-γ, LPS and L-arginine , N=3, ns $p \geq 0.05$, average iNOS expression= 124.4 ± 6.7% vs positive control, average iNOS expression= 100.0 ± 3.5%). ASMCs treated with IFN-γ and LPS with MGO (100μM) and L-arginine (100μM) showed significantly iNOS downregulation compared with ASMCs treated with IFN-γ, LPS and L-arginine (100μM) (N=4, * $p < 0.05$, average iNOS expression= 86.1 ± 7.7% vs ASMCs treated with IFN-γ, LPS and L-arginine, N=3, average iNOS expression= 124.4 ± 6.7%) (Figure 83b).

Griess assay data showed significant reversal of total NO_2 release when ASMCs were incubated with L-arginine (100μM), IFN-γ, LPS with MGO (100μM) for 24 hours (IFN-γ and LPS with MGO, N=4, ** $p < 0.01$, total NO_2= 4.75±4.75% vs IFN-γ and LPS with MGO and L-arginine, total NO_2= 125.7 ± 34.4%). ASMCs treated with IFN-γ and LPS with MGO (100μM) and L-arginine (100μM), and ASMCs treated with IFN-γ, LPS and L-arginine (100μM) did not show significant difference in total NO_2 production when compared with positive control ASMCs treated with IFN-γ and LPS only (N=4, ns $p \geq 0.05$, total NO_2= 125.7 ± 34.4%, ASMCs treated with IFN-γ, LPS and L-arginine, N=3, ns $p \geq 0.05$, total NO_2= 146.0±7.6% vs positive control, total NO_2= 100.0 ± 26.5%). Co-incubating ASMCs with IFN-γ, LPS, MGO (100μM) and L-arginine (100μM) did not show significant difference in total NO_2 released compared with ASMCs treated with IFN-γ, LPS and L-arginine (N=4, ns $p \geq 0.05$, total NO_2= 125.7±34.4% vs ASMCs treated with IFN-γ, LPS and LA, N=3, ns $p \geq 0.05$, total NO_2= 146.0 ± 7.6%). L-arginine incubation did not induce iNOS expression (N= 3, average iNOS expression= 21.1 ± 9.7% and total NO_2= 12.6 ± 6.3%) (Figure 83c).

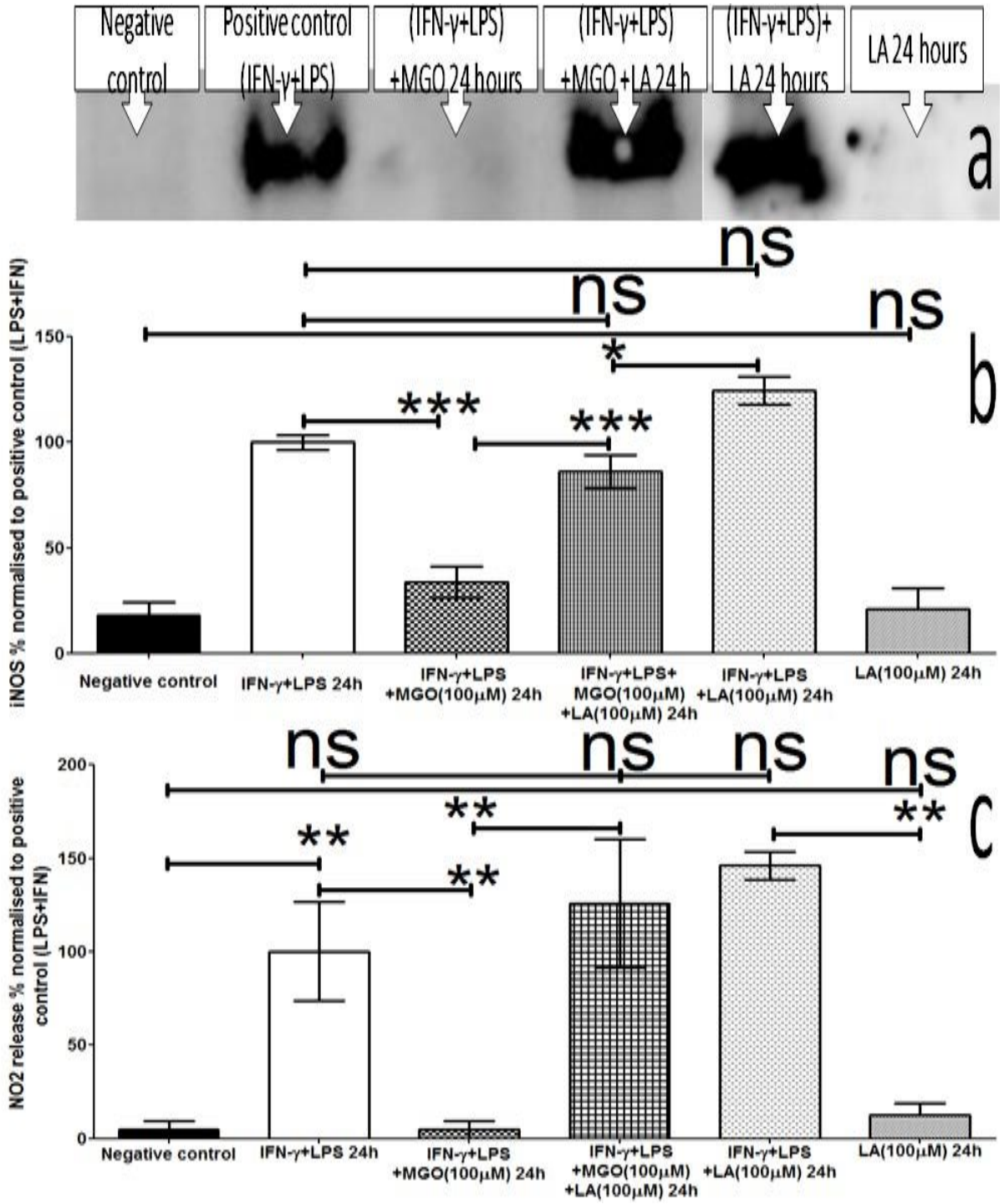

Figure 83. L-arginine effect on MGO in naïve ASMCs cultures. iNOS expression and NO_2 production induced by IFN-γ and LPS with L-arginine (LA) with/without MGO. SDS-PAGE western blotting showing iNOS bands expression (9a). iNOS expression from ASMCs incubated with IFN-γ, LPS and L-arginine (100μM) in the absence and presence of MGO (100μM) for 24 compared with negative and positive control ASMCs, and with L-arginine incubated ASMCs only (b). Griess assay of total NO_2 released from ASMCs incubated with IFN-γ, LPS and L-arginine (100μM) in the absence and presence of MGO 100μM for 24 compared with negative and positive control ASMCs, and L-arginine incubated ASMCs only (c). Data is presented as mean ± SEM. Significance is represented as *** $p < 0.001$ when compared with positive control (IFN-γ and LPS) or IFN-γ + LPS + MGO (100μM) treated ASMCs by one-way ANOVA with Tukey post-hoc test.

- MGO suppressed iNOS expression through inhibiting Akt phosphorylation

Previous studies found that protein kinase B (Akt) phosphorylation is essential for IFN-γ/LPS-induced iNOS expression in VSMCs (Hattori et al., 2003). Moreover, the phosphorylation of MAPK p38 is involved in insulin-induced iNOS expression in VSMCs (Begum & Ragolia, 2000). According to these studies, to decipher the mechanism through which iNOS expression was inhibited by MGO, levels of phospho-Akt (Ser473) and phospho-p38 (Thr180/Tyr182) were investigated to see whether they were affected by MGO (100µM) incubation. When ASMCs were incubated with IFN-γ, LPS and MGO (100µM) for 24 hours it showed a significant reduction in p-Akt (** $p < 0.01$) compared to the level of p-Akt induced by IFN-γ and LPS (N=3, ** $p < 0.01$, average p-Akt expression= 31.7±12.0% vs positive control, N=3, average p-Akt expression= 100±18.5%). When ASMCs were treated with IFN-γ and LPS, it showed significant increase in p-Akt (N=3, * $p < 0.05$, average p-Akt expression= 100 ± 18.5% vs negative untreated ASMCs, N=3, average p-Akt expression= 46.1 ± 13.2%) (Figure 84b).

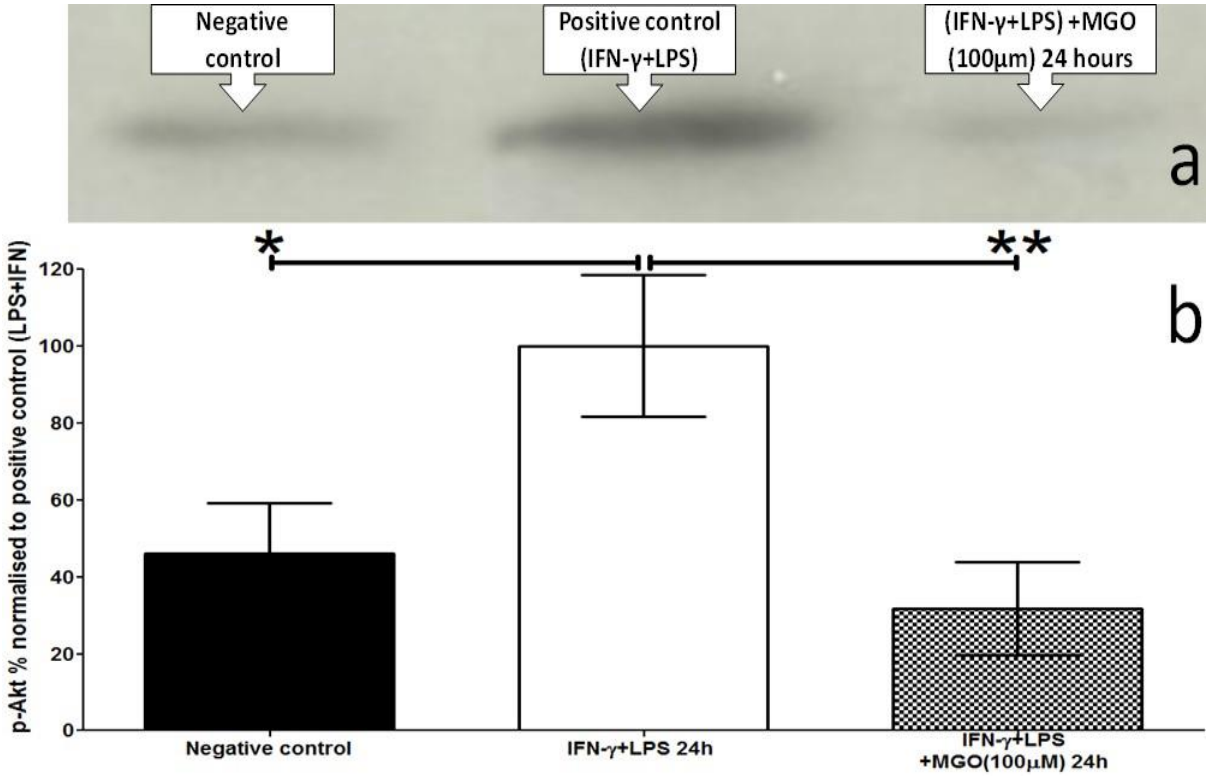

Figure 84. The effect of MGO (100µM) on IFN-γ and LPS-induced Akt phosphorylation (p-Akt). SDS-PAGE western blotting showing p-Akt expression bands (a). P-Akt expression from ASMCs incubated with IFN-γ, LPS and MGO (100µM) for 24 hours compared with positive and negative control ASMCs (b). Data is presented as mean ± SEM. Significance is represented as * $p < 0.05$ and ** $p < 0.01$ compared with positive control (IFN-γ + LPS) by repeated measures one-way ANOVA with Tukey post-hoc test.

However, when ASMCs were incubated with IFN-γ, LPS and MGO (100µM) for 24 hours, p-p38 levels were not changed (N= 3, ns $p \geq 0.05$, average p-p38 expression= 85.0 ± 28.3%

vs positive control, N= 3, average p-p38 expression= 100 ± 25.2%). When ASMCs were incubated with media only it did not show significant p-p38 suppression (N= 3, ns $p \geq 0.05$, average p-p38 expression= 90.6 ± 33.7% vs positive control, N= 3, average p-p38 expression= 100 ± 25.2%) (Figure 85b).

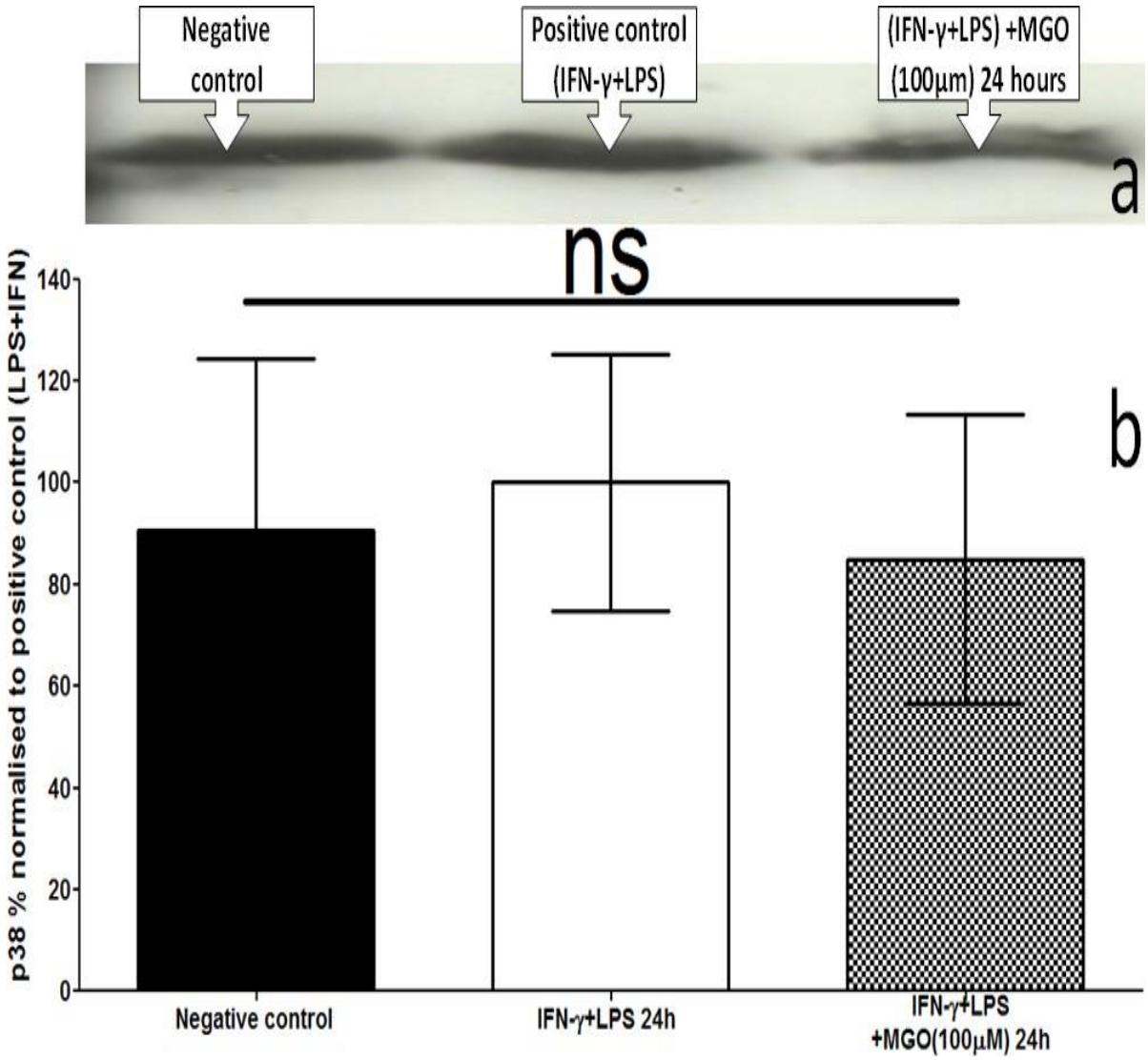

Figure 85. The effect of MGO (100µM) on IFN-γ and LPS-induced p38 phosphorylation (p-p38). SDS-PAGE western blotting showing p-p38 expression bands (a). P-p38 expression from ASMCs incubated with IFN-γ, LPS and MGO (100µM) for 24 hours compared with positive and negative control ASMCs. Data is presented as mean ± SEM. Non significance is represented as ns $p \geq 0.05$ compared with positive control (IFN-γ + LPS) by repeated measures one-way ANOVA with Tukey post-hoc test.

6.3.3. TRPV4 was significantly downregulated in STZ-diabetic ASMCs

ASMCs' TRPV4 expression was studied since TRPV4 showed partial endothelium-independent vasodilation (Figure 33) and aortic endothelial TRPV4 was significantly downregulated in STZ-diabetic rats (Figure 58 & 68). SDS-PAGE western blotting detected TRPV4 band at approximately 98kDa (Figure 86).

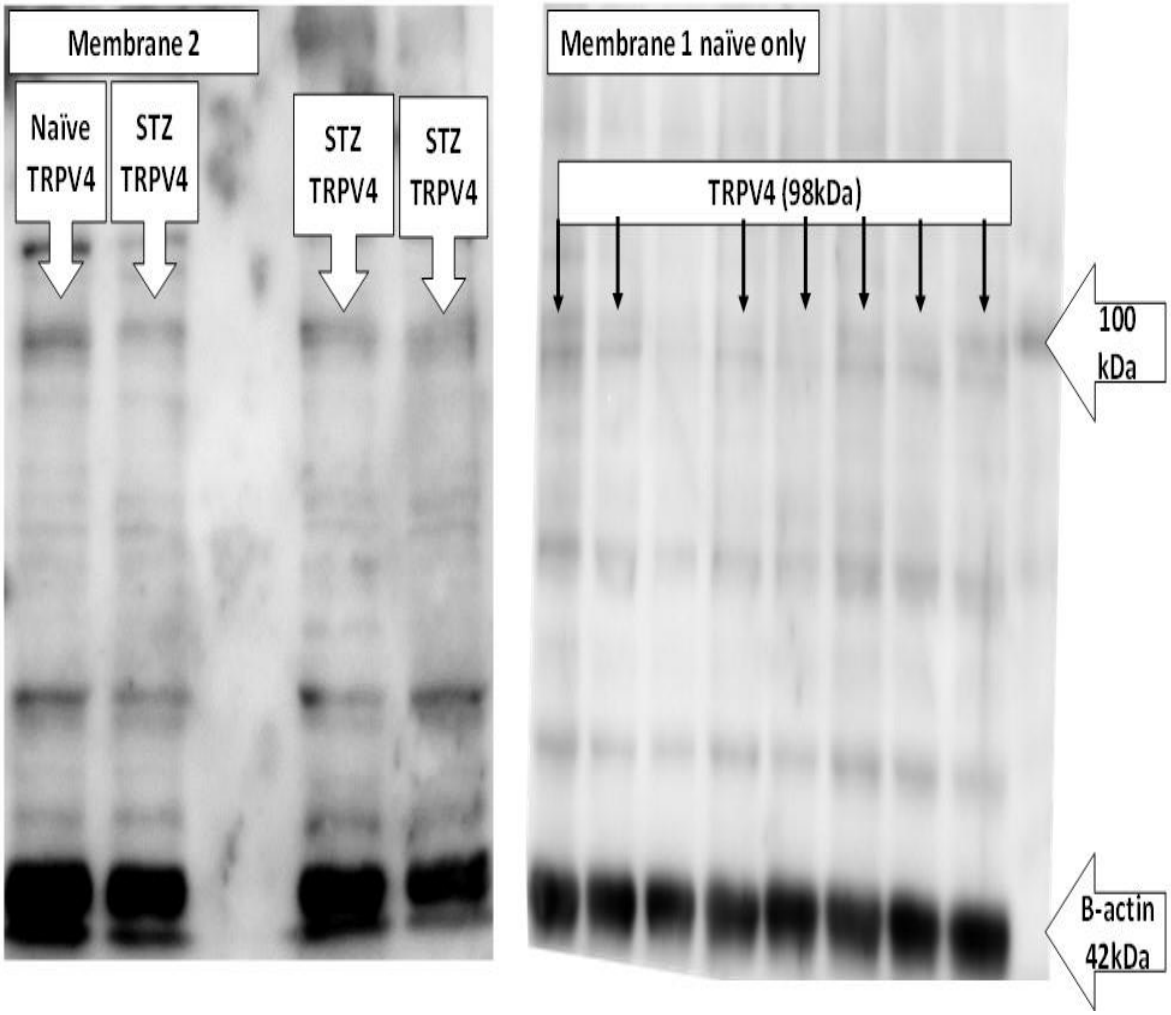

Figure 86. SDS-PAGE western blotting for TRPV4 expression in naïve and STZ-diabetic ASMCs. Each lane was loaded with cells lysate that corresponds to 20μg. TRPV4 band was matched to approximately 98kDa through using the 100kDa band shown in protein ladder. β-actin protein was detected at approximately 43kDa just above the 40kDa band shown in protein ladder. The 1st membrane was loaded with naïve cells lysate (membrane 1). The second membrane (left) was loaded with STZ-diabetic primary ASMCs lysate and 1 naïve primary ASMCs lysate (membrane 2).

When the Western blot gels were analysed through densitometric analysis as describe in section 2.7, TRPV4 expression in STZ-diabetic rats' ASMCs was significantly suppressed (N=5, ** $p < 0.01$, average TRPV4 expression= 56.2 ± 5.4% vs naïve ASMCs' average TRPV4 expression= 100 ± 8.8%) (Figure 87b).

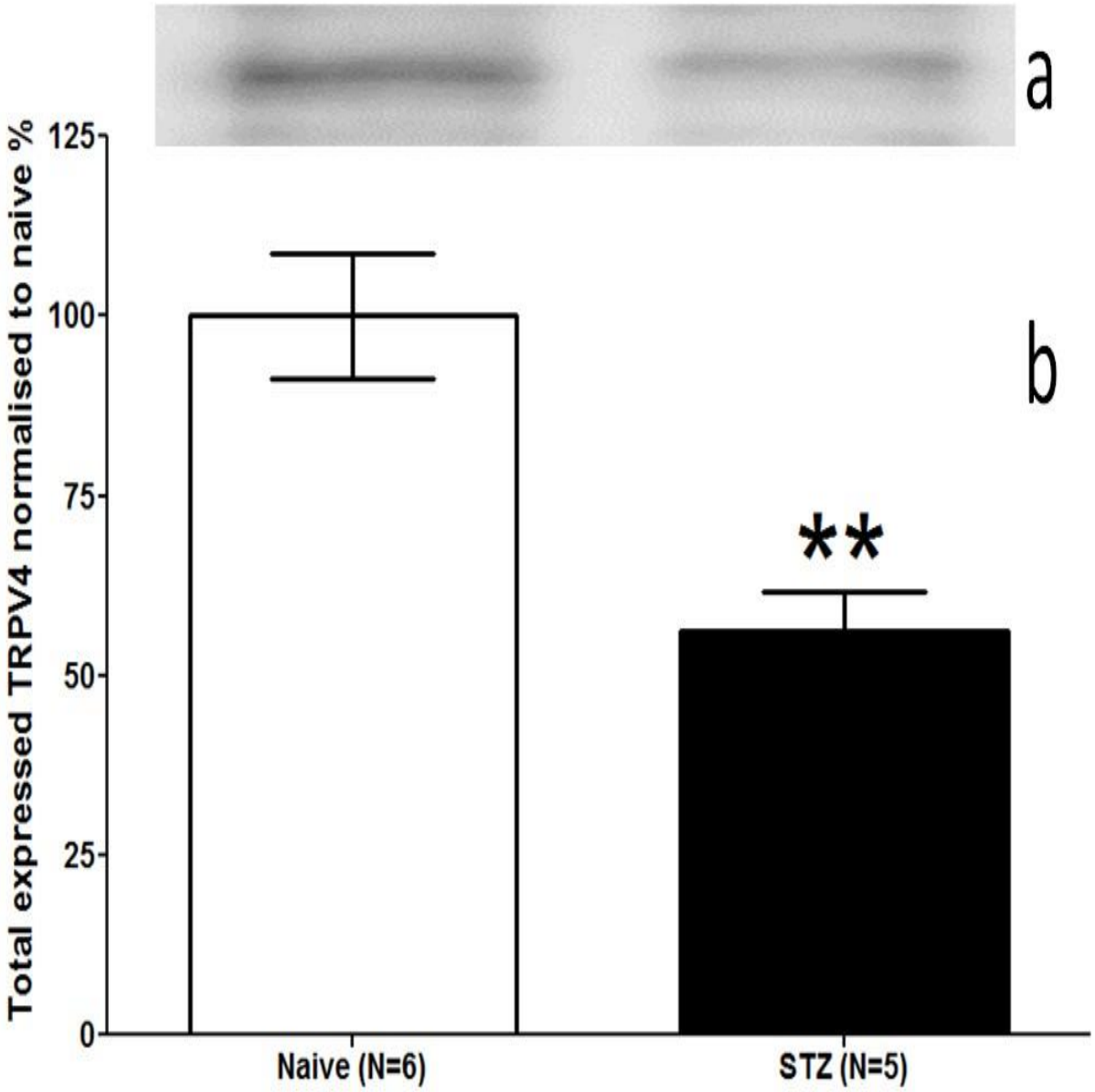

Figure 87. TRPV4 expression in naïve and STZ-diabetic ASMCs. Western blotting of rats' aortic smooth muscle cells' (ASMCs) TRPV4 (a). TRPV4 expression in streptozotocin (STZ)-diabetic rats' ASMCs was significantly suppressed (b). Data is presented as mean ± SEM. Significance is represented as ** $p < 0.01$ by unpaired two-tailed Student's t-test.

6.4. Discussion

In this chapter, the expression of both iNOS and TRPV4 in rat primary ASMCs was studied through SDS-PAGE Western blotting. Significant iNOS downregulation was shown in STZ-rats' ASMCs (Figure 77). According to this finding, and in addition to the previous findings of eNOS downregulation (Figures 62 & 63), it is suggested that both endothelium-dependent and endothelium-independent NOS function might be significantly compromised in diabetes.

A previous study showed that iNOS-derived NO plays a preventive role against increased vasospastic responses that is associated with arteriosclerosis (Fukumoto et al., 1997). Moreover, NOS blockade through L-NAME (100μM) showed significant increase in vasoconstriction tension in rat middle cerebral artery (McNeish, Altayo, & Garland, 2010). Such exaggerated vasoconstriction was reproduced in endothelial denuded control aortic rings incubated with L-NAME (100μM) that functionally inhibits NOS from releasing NO (Figure 79b). Additionally, since endothelium and adventitia were removed, therefore iNOS was supposed as the predominant NOS isoform in the endothelium denuded aortic rings (Figure 79b). Therefore, applying the available non-selective NOS inhibitor, L-NAME to the adventitia-cleaned and endothelium-denuded aortic rings was suggested to block the predominant NOS isoform, iNOS (Schott et al., 1993). STZ-diabetic rats' aortic rings showed significant increase in NA-induced vasoconstriction than vehicle control aortic rings (Figure 79a). Western blotting data showed significant reduction in iNOS expression from STZ-diabetic ASMCs stimulated with IFN-γ and LPS (Figure 77). These findings were supported by a previous study which revealed that endothelium denuding did not increase phenylephrine-induced vasoconstriction in rat small mesenteric arteries (Dora, Hinton, Walker, & Garland, 2000). Moreover, in endothelium intact rat mesenteric arteries, L-NAME (100μM) showed significant increase in phenylephrine-induced vasoconstriction (Dora et al., 2000). Therefore, the significant increase in STZ-diabetic aortic rings NA-induced vasoconstriction might be attributed to suppressed NOS activity.

Since MGO was significantly elevated in STZ-diabetic rats' serum (Figure 43), it was applied in both physiological (10μM) and diabetic (100μM) concentrations on naïve non-diabetic primary ASMCs which were treated with IFN-γ and LPS. Diabetic levels of MGO (100μM) suppressed iNOS expression in naïve non-diabetic primary ASMCs which was accompanied with abolished total NO_2 release (Figure 81). However, a physiological MGO concentration (10μM) did not suppress iNOS expression (Figure 81). Since iNOS is induced through bacterial inflammatory mediators such as LPS, therefore, MGO-suppressed iNOS might

explain the reason of diabetics being prone to infection with their immunity compromised. Moreover, in addition to MGO being an eNOS inhibitor, MGO impairs iNOS expression revealing that MGO impairs NO-mediated vasodilatory pathways.

These findings correlate the elevated serum MGO (Figure 43) with iNOS suppression (Figures 77 & 81), and increased vasoconstriction (Figure 79) since previous study revealed that LPS-induced iNOS causes NO release, that causes hyporeactivity to vasoconstrictors such as phenylephrine (Hall et al., 1996). Numerous researchers have shown that MGO induces iNOS and NO production together with superoxide anions to form $ONOO^-$, however, these studies were conducted on thoracic aortic smooth muscle cell line (A-10 cells) (Chang et al., 2005; Arti Dhar, Desai, Kazachmov, Yu, & Wu, 2008). By contrast, our study was conducted to primary ASMCs which would provide a robust evidence to the mechanism of MGO on iNOS which was proven through Akt and p38 studies. To the best of our knowledge this is the first study that shows MGO effect on primary ASMCs' iNOS suppression, and such effect was proven through further studies on the upstream factors involved in iNOS expression such as Akt.

Akt and p38 phosphorylation was investigated, since previous reports showed the essential role of these two second messengers in regulating iNOS expression (Begum & Ragolia, 2000; Hattori et al., 2003). As shown in Figure 84, Akt phosphorylation was significantly compromised in ASMCs incubated with IFN-γ (100IU/ml), LPS (100µg/ml) and MGO (100µM). However, p38 phosphorylation was not significantly influenced through MGO (100µM) co-incubation with IFN-γ (100IU/ml) and LPS (100µg/ml) (figure 85). These findings support the MGO mechanism of action through inhibiting iNOS. Akt is a protein kinase that is activated through PI3K activation. PI3K phosphorylates the membranous phosphoinositide lipids that provide docking sites for Akt. Akt binds to its phosphoinositide docking sites where it is phosphorylated at threonine 308 and serine 473 (Ser473) to further phosphorylate IκB (inhibitor nuclear factor of kappa light polypeptide gene enhancer in B-cells inhibitor) and hence tags it for ubiquitination and degradation. Once IκB is degraded, nuclear factor κB (NF κB) becomes active and translocates into the nucleus to induce iNOS expression (Hattori et al., 2003). Therefore, as shown in Figure 84, inhibiting Akt phosphorylation (Ser 473) contributed to the MGO-downregulated iNOS (Figure 81). Such effect might contribute to the exagerated vasospastic responses shown in Figure 79, since iNOS-derived NO plays a preventive role against increased vasospastic responses (Fukumoto et al., 1997). Moreover, since Akt plays a major role in glucose metabolism in addition to

being a cell survival factor (Franke, Kaplan, & Cantley, 1997), therefore, MGO elevation in diabetes might exacerbate the hyperglycaemia and might be attributed to accelerated aging (A. Dhar et al., 2011; Nicolay et al., 2006; Ramasamy et al., 2005).

L-arginine restored the MGO-inhibitory effect on iNOS expression (Figure 83). This finding was supported by a previous study which found that L-arginine serves as MGO scavenger (I. Dhar et al., 2012). Therefore, further analytical studies such as HPLC are required to prove the ability of L-arginine to scavenge MGO. Moreover, MGO effect on inhibiting iNOS expression was completely abolished in the presence of L-arginine revealing that both compounds were not free when they were in the same media and suggesting their capability to bind each other as shown in a previous HPLC study (I. Dhar et al., 2012). L-arginine (100μM) was applied within the normal plasma concentration (60-140μM) (Schwedhelm et al., 2008), which is less than the concentration applied in I. Dhar et al. (2012) study where it was applied at 300μM concentration. The applied L-arginine concentration did not induce iNOS expression (Figure 83) which supports the hypothesis of L-arginine acting as MGO scavenger (I. Dhar et al., 2012). Therefore, the applied L-arginine concentration is physiologically applicable. These findings suggest the importance of L-arginine as a therapeutic option for diabetics as previous studies revealed that L-arginine supplementation (3x2g/day) showed significant improvement in antioxidants and NO release (Jabłecka et al., 2012). Moreover, previous studies showed significant insulin sensitivity improvement in T2DM patients when they were given 8.3g/day L-arginine, such improvement was accompanied with improved glucose metabolism and antioxidants capacity (Lucotti et al., 2006). Therefore, L-arginine may play an essential role as a supplement for diabetes patients, especially with MGO impairing insulin pharmacokinetic and pharmacodynamic parameters that culminates in insulin resistance, endothelium dysfunction as well as neuropathic pain which are all common complications in diabetes (A. Dhar et al., 2011; Eberhardt et al., 2012; S. Jia et al., 2006; Van Eupen et al., 2013).

ASMCs' TRPV4 expression was also studied since TRPV4 showed partial endothelium-independent vasodilation (Figure 33) and aortic endothelial TRPV4 was downregulated in STZ-diabetic rats (Figures 58 & 59). Accordingly, significant reduction in TRPV4 expression was shown in primary ASMCs (Figure 87). A previous study conducted by Earley et al. (2005) revealed that TRPV4 forms a signalling complex with BKca to generate VSM hyperpolarisation and hence causes vasodilation. Moreover, Bagher and Garland (2014) revealed that TRPV4 mediates Ca^{2+} influx through cooperative gating in the MEPs that

activates Kca to exert VSM hyperpolarisation and vasodilation. These findings suggested that TRPV4 downregulation contributes to the impairment of both endothelium-dependent and endothelium-independent TRPV4-induced vasodilation.

To sum up, MGO was elevated in STZ-diabetic rats' serum to approximately 100µM. Incubating naïve non-diabetic ASMCs with MGO (100µM) for 24 hours inhibited Akt-phosphorylation and hence suppressed iNOS expression which might be attributed to increased diabetic aortic rings vasoconstriction. These findings suggest that MGO induces iNOS downregulation in addition to increasing vasoconstriction which are all culminate in compromised circulation in diabetes. L-arginine restored MGO-downregulated iNOS, this effect might be attributed to the L-arginine ability to scavenge MGO. According to these conclusions, MGO might be a pivotal therapeutic target to manage diabetes complications. L-arginine was shown to act as a scavenger for MGO and hence it might play a major therapeutic strategy for MGO-related diabetic complications such as vascular dysfunction (Bierhaus et al., 2012; A. Dhar et al., 2010). Moreover, TRPV4 downregulation in STZ-diabetic ASMCs might exaggerate the diabetic vascular dysfunction.

In the next chapter, the short-term effect of MGO will be discussed to investigate whether acute MGO treatment shows similar vascular effects to chronic MGO treatment.

Chapter 7: Acute effect of methylglyoxal on the vascular tone

7.1. Introduction

Chronic hyperglycaemia is the main DM complication where blood glucose concentration exceeds 7mmol/L (125mg/dl) (Sheader et al., 2001). Approximately 0.5% of glycolysis; glucose metabolism, elaborates electrophilic ROS such as MGO which is highly reactive with various cellular and interstitial molecules such as proteins and phospholipids to form stable adducts and AGE (Uchida, 2000). As shown in the previous two chapters, long-term incubation of non-diabetic aortic rings (for 12 hours) and primary ECs (for 5 days) and ASMCs (for 24 hours) with MGO (100μM) showed significant endothelial dysfunction, compromised TRPV4 function and NO_2 release, respectively. Numerous authors have correlated MGO elevation to vascular dysfunction and end organ damage such as nephropathy and neuropathy in diabetes (Chang et al., 2005; Shamsaldeen et al., 2016). In this chapter, the aim was to investigate the acute effect of MGO (100μM) on vascular function.

The main objectives of this chapter were to decipher the MGO targets in a whole aortic rings organ bath studies where aortic rings were incubated with a wide range of antagonists and blockers. Moreover, the second objective was to investigate the molecular mechanism of the acute effect of MGO on vasculature through FlexStation studies.

7.2. Materials and methods

7.2.1. MGO vascular contractility persistence studies

Contractility persistence was examined in separately different sets of naïve rats aortic rings through initial incubation with L-NAME (100µM) for 30 minutes or with TRPV4 antagonist: HC067047 (1µM) or RN-1734 (1µM), TRPM8 antagonist: AMTB (1µM), BKCa antagonist: iberiotoxin (1nM) for 30 minutes followed by the co-incubation of MGO (100nM) for 120 minutes. The aortic rings were then contracted with NA (300nM). Similar experiments were conducted on endothelium denuded aortic rings with MGO (100µM) alone for 120 minutes or in the presence of TRPV4 antagonist: HC067047 (1µM) or TRPM8 antagonist: AMTB (1µM). Additionally, MGO vascular effect was examined against high potassium Krebs-induced contraction.

7.2.2. FlexStation experiments on TRPM8 expressing CHO cells

FlexStation Ca^{2+} assay was conducted at King's College London, Wolfson centre for age related diseases with an invaluable supervision from Professor Stuart Bevan. Chinese hamster ovary cells transfected with rat TRPM8 channel (r-TRPM8) were grown in MEM AQmedia containing 10% of FBS, 1% of streptomycin-penicillin and 200µg/ml of hygromycin. However, the un-transfected Chinese hamster ovary (CHO) cells were grown in MEM AQmedia containing 10% FBS and 1% streptomycin-penicillin. When the cells became confluent, they were seeded in a black-wall 96 well plate (Costar 3603: tissue-culture plates) and incubated for 24 hours (CO_2 5%, 37°C). Thereafter, the cells were loaded with fura2-AM (2.5µM) and probenecid (1mM) in extracellular fluid (ECF) containing 130mM of NaCl, 5mM of KCl, 10mM of glucose, 10mM of HEPES, 2mM of $CaCl_2$, 1mM of $MgCl_2$ with a pH of 7.4. The loaded cells were then incubated for 1 hour (CO_2 5%, 37°C). Afterward, the cells were washed for once with ECF and loaded with 50µl ECF before being launched into the FlexStation. The CHO cells and r-TRPM8 cells were treated with icilin CRC (1nM-200nM) in the presence and absence of AMTB (5µM, 10µM and 50µM) to confirm the AMTB antagonistic efficiency on r-TRPM8 cells. Similarly, the r-TRPM8 cells and the un-transfected CHO cells were incubated with MGO (100µM-10mM) whilst in the FlexStation (28°C) for 1 hour. Moreover, r-TRPM8 cells-blocked with AMTB (5µM and 10µM) were treated with MGO (100µM-10mM). Sucrose (50mM) in ECF was applied as osmotic control since Quallo et al. (2015) concluded TRPM8 as a peripheral osmosensor. Therefore, applying an osmotic control was used to exclude any osmotic effect of MGO on rTRPM8 cells.

7.3. Results

7.3.1. Short-term effects of MGO on vascular tissue

In chapter 4-6, it was shown that 12 hour exposure of MGO (100μM) mimicked some of the change in vascular function seen in the STZ-induced diabetes model, consistent with the idea that chronic MGO elevation in the STZ model might be responsible for some of these changes. However, previous studies demonstrated acute effects of MGO on isolated tissues, so it was of interest to look at shorter exposure times. A study conducted by A. Dhar et al. (2010) found that incubating rat aortic ECs with MGO (30μM) for 3 hours showed significant reduction in acetylcholine mediated vascular vasodilation and in bradykinin-induced total NO_2 release. Therefore, pathological concentration of MGO (100μM) was investigated through incubating aortic rings with different time points, 15 minutes, 30 minutes, 1 hour and 2 hours followed by carbachol (100μM and 1mM).

As shown in Figures 88 and 89, incubating the aortic ring with MGO (100μM) for 15-60 minutes did not show significant difference compared to control aortic rings when carbachol was applied to induce vasodilation [N=6, ns $p \geq 0.05$, untreated control carbachol (1mM)= -73.1 ± 11.4%, N=4, MGO 15 minutes carbachol (1mM)= -53.3 ± 2.2%, N=3, MGO 30 minutes carbachol (1mM)= -67.4 ± 3.2% and N=5, MGO 60 minutes carbachol (1mM)= -75.1±10.6%) (Figure 88).

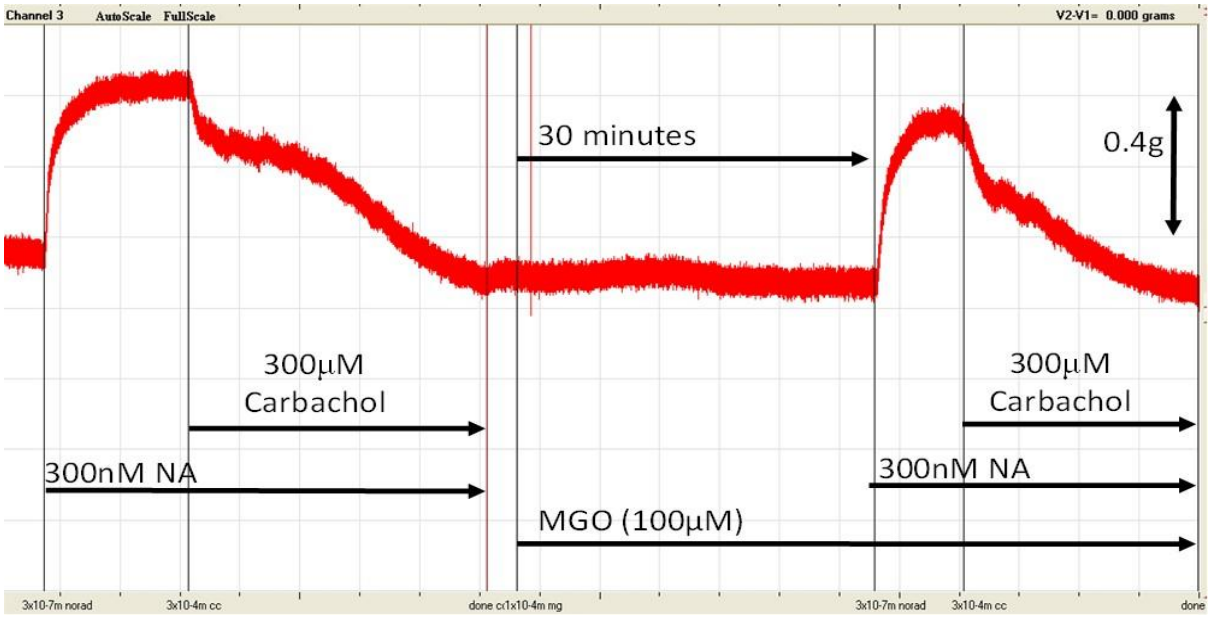

Figure 88. Representative trace of carbachol-induced vasodilation of pre-contracted rat's aortic rings after being incubated with MGO 100µM for 30 minutes. Aortic rings were incubated with MGO FBC 100µM for 30 minutes (right) which were pre-contracted with NA (300nM) followed by carbachol FBC 300µM, compared to non-MGO tissues. Both aortic rings showed full vasodilation, when recorded through iWORX LabScribe software.

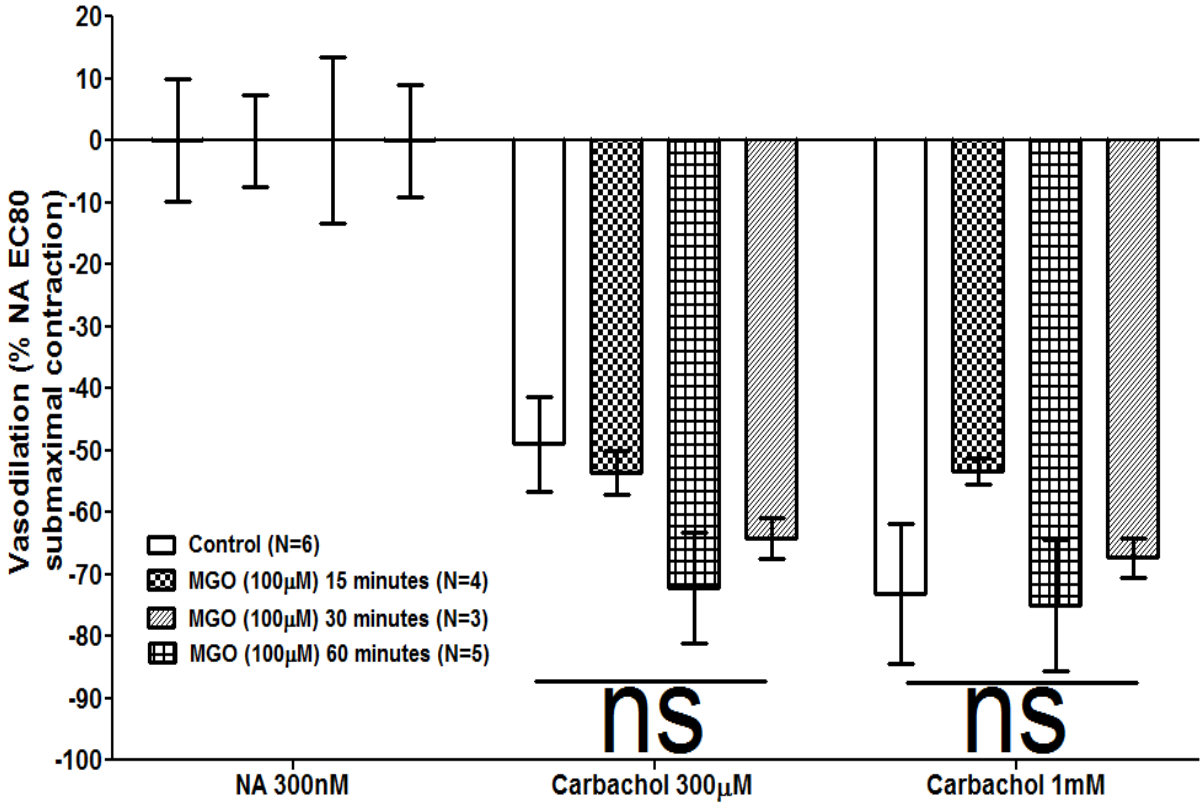

Figure 89. Aortic response to carbachol FBC 300µM and 1m3M normalised to noradrenaline (NA)-induced contraction through FBC 300nM. Control rat aortic rings were incubated with 100µM MGO at different time points (15, 30 and 60 minutes). Analysed through two-way ANOVA with Bonferroni post-hoc test. Data shown as percentage ± SEM [Control, N= 6, MGO (100µm) 15 minutes, N= 4, MGO (100µm) 30 minutes, N= 3 and MGO (100µm) 60 minutes, N= 5].

However, when aortic rings were incubated for 2 hours with MGO (100µM), spontaneous loss of vascular tone occurred after contracting the aortic rings with NA (300nM) instead of the normal sustained tension observed with NA as shown in Figure 90.

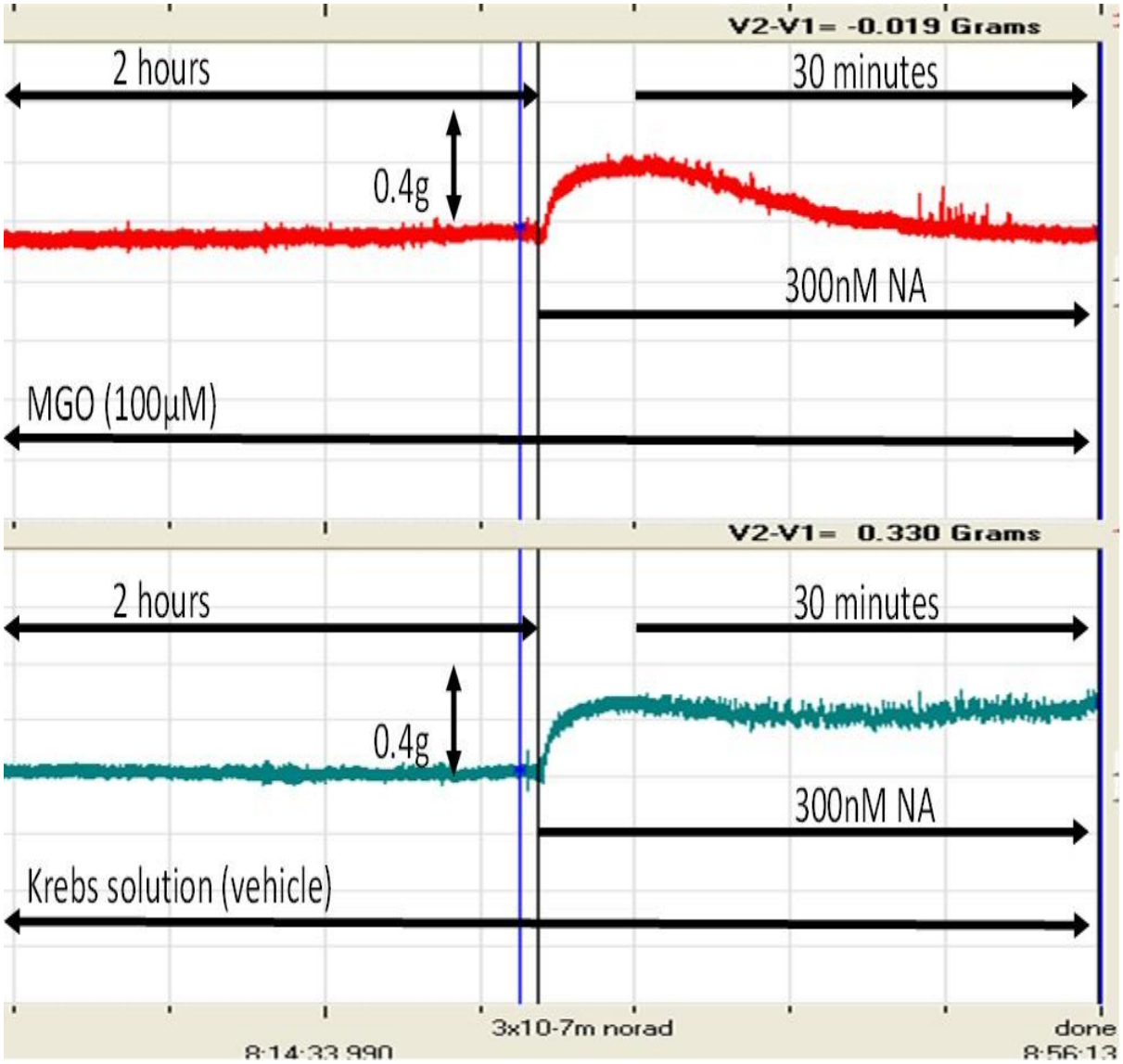

Figure 90. Representative trace of MGO-induced loss of contractility persistence (upper red) compared to control; non MGO. Aortic rings were incubated with MGO (100µM or 0 µM) for 2 hours before being contracted with NA 300nM to show loss of contractility persistence in MGO incubated aortic rings distinctively, when recorded through iWORX LabScribe.

7.3.2. MGO-induced loss of NA-induced contractility persistence

The loss of contractility persistence induced by MGO (100µM) incubation for 2 hours was unexpected, given the inhibition of vasodilation observed with longer MGO exposure (Figure 52). So, it was of interest to further explore the mechanism of this effect. L-NAME (100µM) and HC067047 (1µM), RN-1734 (1µM), AMTB (1µM), and high potassium Krebs solution were applied to examine their effect on the loss of contractility persistence induced by 120 minutes MGO (1µM & 100µM). In another experiment, different rat aortic rings were mechanically stripped of endothelium (denuded) to examine the endothelium dependence of MGO. All conditions were compared to MGO-induced loss of contractility persistence and non MGO-treated tissues (control). All antagonists were applied at approximately 30 minutes before adding MGO. HC067047 but not RN-1734 abolished MGO-induced loss of contractility persistence. Similar to HC067047, TRPM8 antagonist, AMTB showed significant suppression to MGO-induced loss of contractility persistence. Moreover, L-NAME, iberiotoxin and high potassium Krebs solution showed significant compromised MGO-induced loss of contractility persistence.

To ensure that the endothelium removal was effective in the denuded tissue we tested this by measuring the carbachol induced vasodilation of NA induced tension in control and denuded tissue (Figure 91). As expected, the carbachol induced vasodilation was almost completely abolished in the denuded rings consistent with endothelium removal. Endothelium denuding showed significant reduction in carbachol-induced vasodilation (N=5, *** $p < 0.001$, Emax= 16.6±4.8% vs intact endothelium carbachol induced-vasodilation Emax= 68.4±2.3%) (Figure 91). However, the EC_{50} was not significantly influenced (N=5, $p \geq 0.05$, EC_{50}= 3.8 ± 0.6μM and vs intact endothelium carbachol induced-vasodilation EC_{50}= 1.8 ± 1.1μM) (Figure 91).

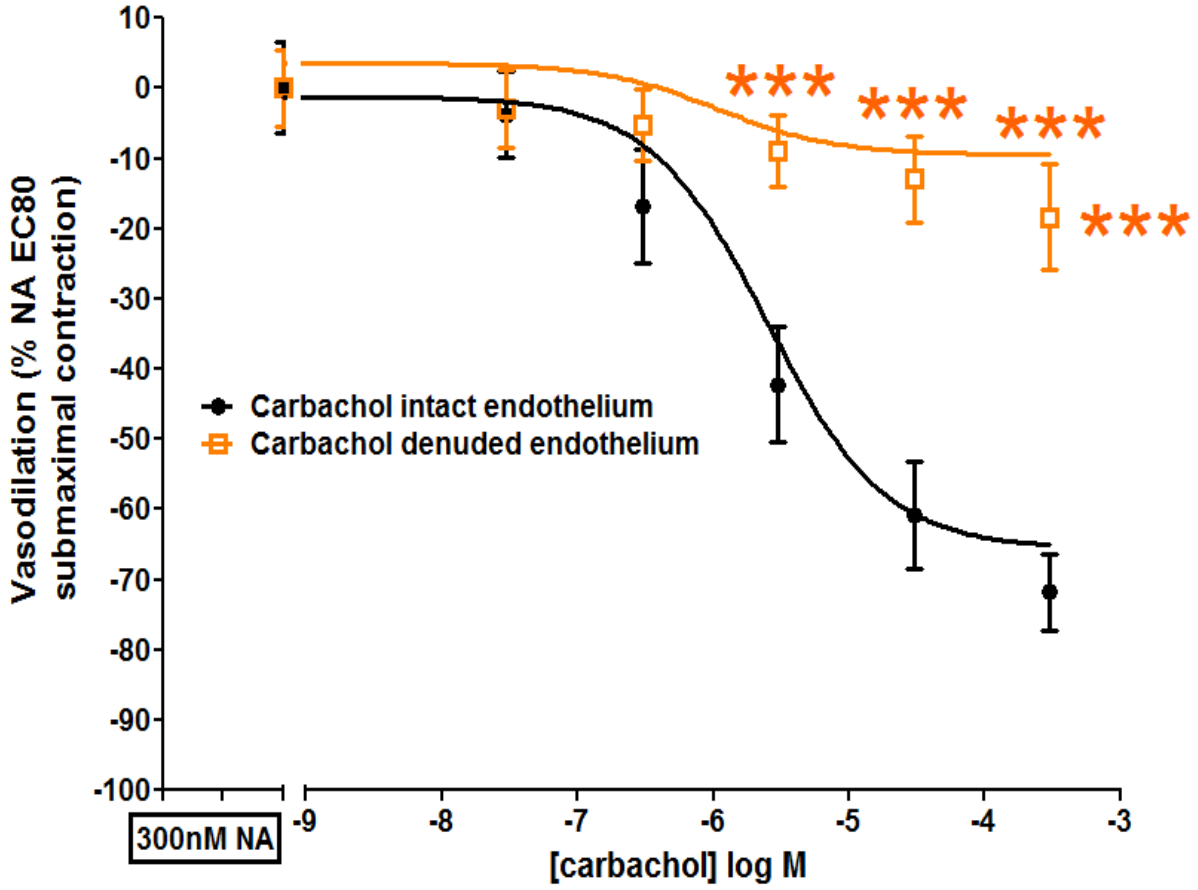

Figure 91. Carbachol cumulative concentration response curve when endothelium was denuded. Analysed through two-way ANOVA with Bonferroni post-hoc test. Significance is shown as *** $p < 0.001$ versus carbachol-induced vasodilation in intact endothelium aortic rings (N= 5).

- MGO induced significant loss of contractility persistence in intact aortic rings and in endothelium denuded aortic rings

MGO (1µM and 100µM) incubation for 2 hours showed significant spontaneous loss of contractility persistence (MGO 100µM: N= 5, *** $p < 0.001$, Emax: -90.4 ± 6.9%, tmax= 30 minutes, denuded endothelium MGO 100µM: N= 5, Emax: -103.2 ± 5.4%, tmax= 30 minutes, MGO 100µM: N= 6, Emax: -88.3 ± 7.1%, tmax= 30 minutes vs control, Emax: -12.7 ± 11.1%, tmax= 30 minutes) (Figure 92).

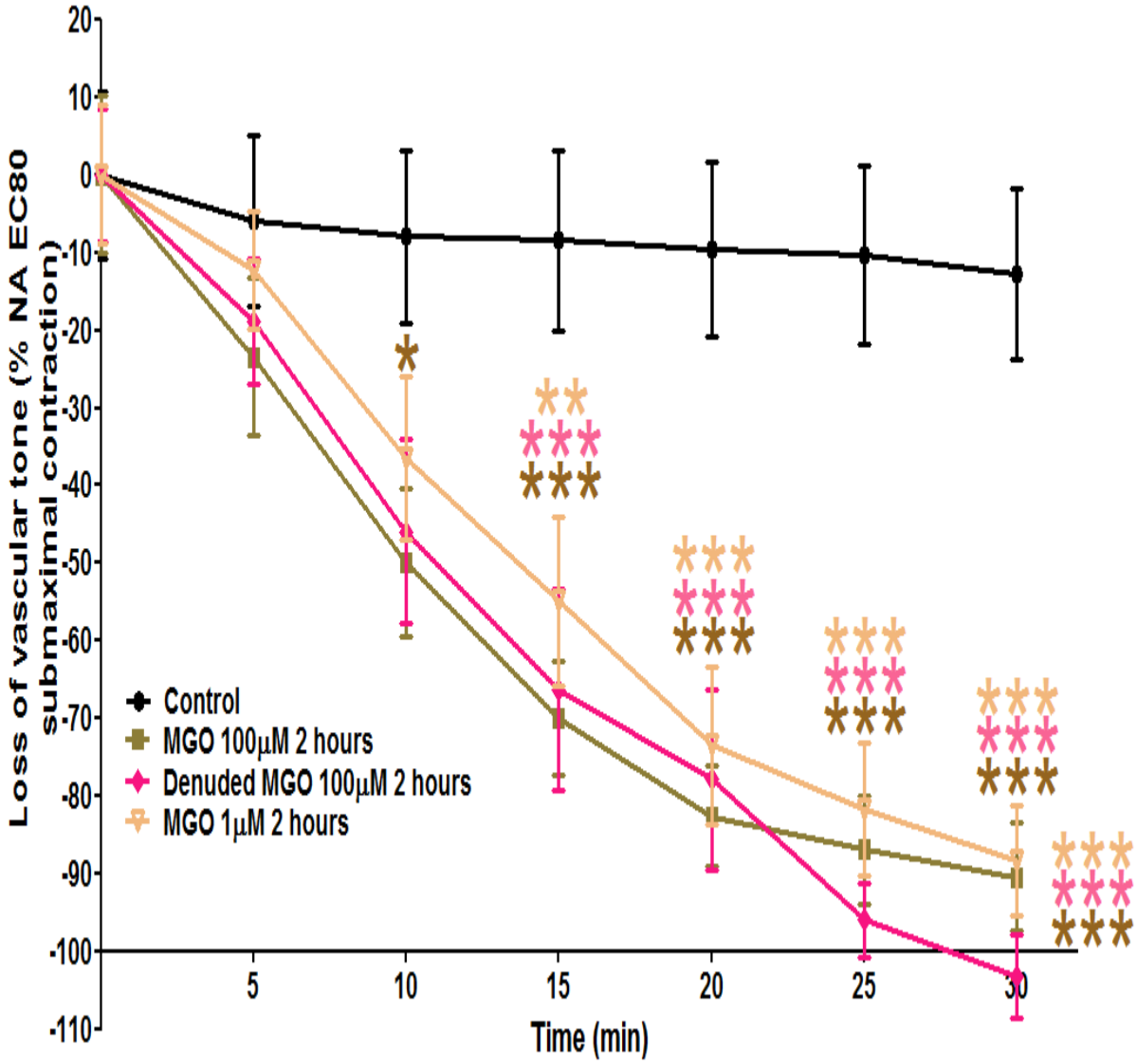

Figure 92. Methylglyoxal (MGO)-induced loss of vascular tone. MGO-induced significant loss of contractility persistence when aortic rings were incubated with MGO for 2 hours before being contracted with noradrenaline (300nM) even in the absence of endothelium analysed through Bonferroni's two-way ANOVA. Significance is represented as * $p < 0.05$, ** $p < 0.01$ and *** $p < 0.001$ when compared with untreated aortic rings (control). Data shown as percentage ± SEM (Control, N= 8, MGO 100µM 2 hours, N= 5, Denuded MGO 100µM 2 hours, N= 5 and MGO 1µM 2 hours, N= 6).

- MGO-induced loss of contractility persistence was significantly inhibited through incubating intact aortic rings with HC067047

Aortic rings were incubated for 30 minutes with either of two different TRPV4 blockers, HC067047 and RN1734. Afterward, MGO (100µM) was added for another 2 hours before adding NA (300nM). HC067047 showed significant reduction in the MGO-induced loss of contractility persistence [HC067047 (1µM) + MGO (100µM), N=4, *** $p < 0.001$, Emax= -13.2 ± 16.6%, tmax= 30 minutes, vs MGO (100µM), N= 5, Emax= -90.4 ± 6.9%, tmax= 30 minutes]. However, endothelium denuding significantly suppressed the effect of HC067047 [HC067047 (1µM) + MGO (100µM), N=4, $$$ $p < 0.001$, Emax: -13.2 ± 16.6%, tmax= 30 minutes vs endothelium denuded HC067047 (1µM) + MGO 100µM, N=4, Emax: -88.5 ± 12.3%, tmax= 30 minutes]. RN1734 showed significant inhibition to MGO-induced loss of contractility persistence [RN1734 (1µM) + MGO (100µM), N=5, && $p < 0.01$, Emax= -69.0 ± 11.3%, tmax= 30 minutes vs MGO (100µM), N=5, Emax= -90.4 ± 6.9%, tmax= 30 minutes] (Figure 93). The inconsistent effects of the two TRPV4 antagonists and the endothelium-dependent effect of HC067047 suggest that this might be acting as a functional antagonist by another mechanism.

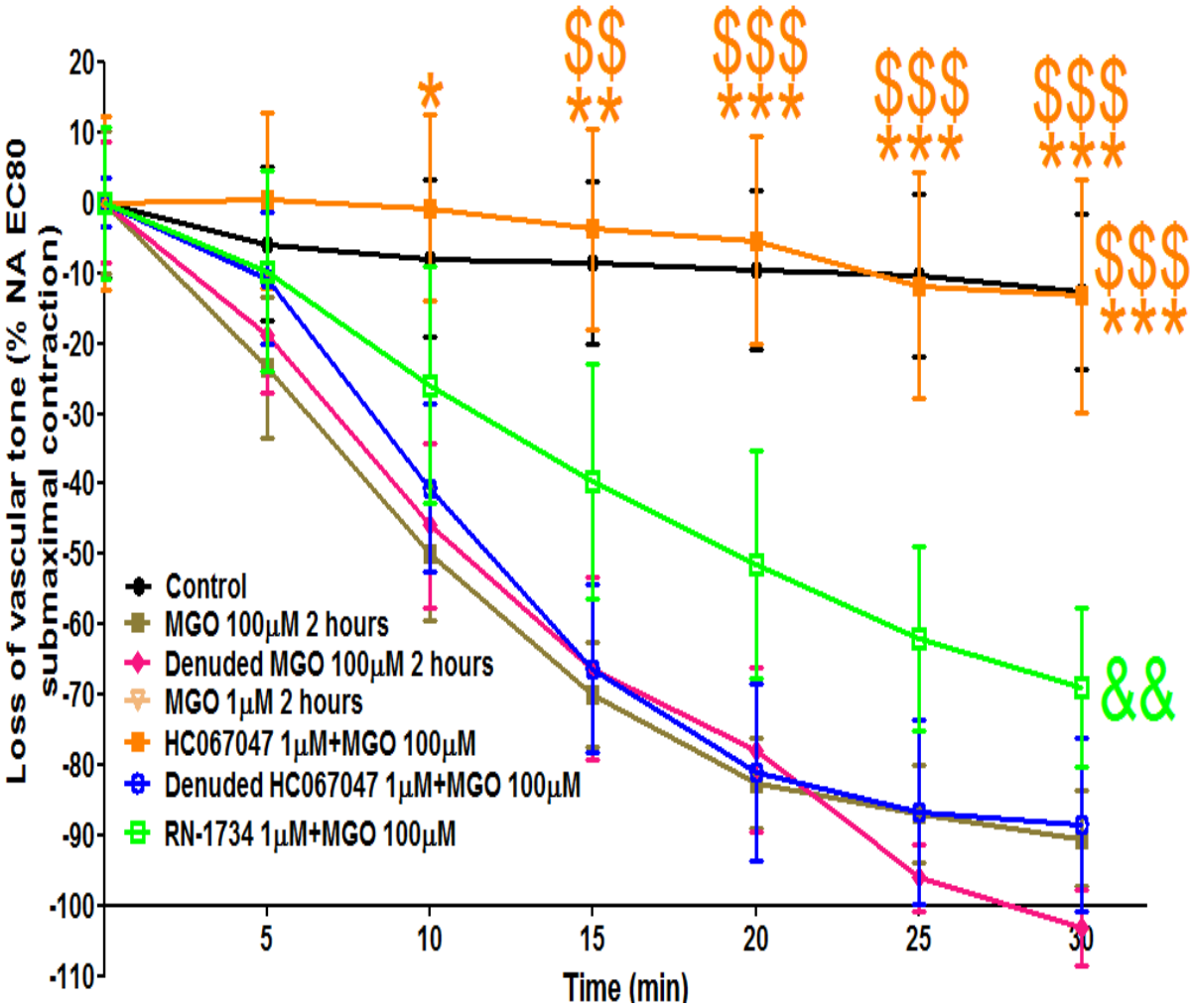

Figure 93. Methylglyoxal (MGO)-induced loss of contractility persistence against TRPV4 blockers (HC067047 and RN-1734). Intact and endothelium denuded aortic rings incubated with TRPV4 blocker and MGO were compared to intact and endothelium denuded aortic rings incubated with MGO only, all groups were compared to untreated aortic rings (control). Analysed through two-way ANOVA Bonferroni post-hoc test. Significance is represented as * $P<0.05$, ** $p < 0.01$ and *** $p < 0.001$ vs aortic rings treated with MGO (100µM). Significance is represented as $$ $p < 0.01$ and $$$ $p < 0.001$ vs endothelium denuded aortic rings treated with MGO (100µM). Data shown as percentage ± SEM (Control, N= 8, MGO 100µM 2 hours, N= 5, Denuded MGO 100µM 2 hours, N= 5, RN-1734 1µM+MGO 100µM, N= 5, HC067047 1µM+MGO 100µM, N= 4 and denuded HC067047 1µM+MGO 100µM, N= 4).

- MGO-induced loss of contractility persistence was significantly inhibited through incubating the intact and endothelium denuded aortic rings with AMTB

We next looked at the contribution of TRPM8 channels to the MGO-induced loss of contractility persistence. Aortic rings were incubated with TRPM8 blocker, AMTB (1μM) for 30 minutes. Afterward, the aortic ring was treated with MGO (100μM) for 2 hours, before adding NA (300nM). AMTB significantly reduced the MGO-induced loss of contractility persistence (*** $p < 0.001$) in intact rings and even when the endothelium was removed (denuded) ($$$ $p < 0.001$) as shown in Figure 94. This is consistent with the possibility that MGO is acting as a TRPM8 agonist in denuded rings. MGO-induced loss of contractility persistence was significantly blocked through AMTB (1μM) incubation [AMTB (1μM) + MGO (100μM), N= 4, *** $p < 0.001$, Emax= -38.2 ± 7.6% and tmax= 30 minutes vs MGO (100μM), N= 5, Emax: -90.4 ± 6.9% and tmax= 30 minutes). Endothelium denuding showed significant effect of AMTB to abolish MGO-induced loss of contractility persistence (endothelium denuded AMTB (1μM) + MGO (100μM), N= 4, $$$ $p < 0.001$, Emax= -23.8 ± 8.7% and tmax= 30 minutes vs denuded MGO 100μM, N= 5, Emax: -103.2 ± 5.4%, tmax= 30 minutes). AMTB effect on MGO-induced loss of contractility persistence was not significantly affected through endothelium denuding [AMTB (1μM) + MGO (100μM), N=4, $p \geq 0.05$, Emax= 38.2 ± 7.6% and tmax= 30 minutes vs denuded AMTB (1μM) + MGO (100μM), N=4, Emax: 23.8 ± 8.7% and tmax= 30 minutes] (Figure 94).

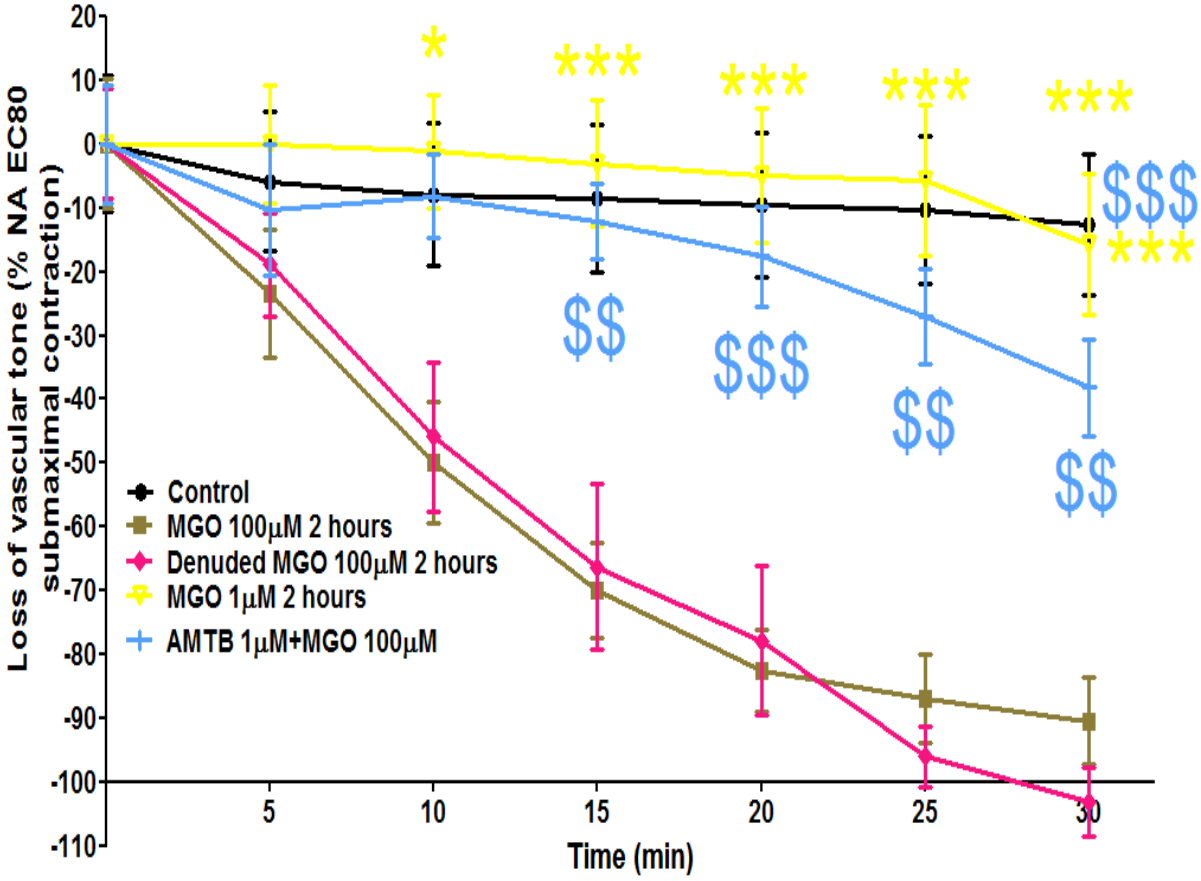

Figure 94. Methylglyoxal (MGO)-induced loss of contractility persistence against TRPM8 blocker (AMTB). Intact and endothelium denuded aortic rings incubated with AMTB and MGO were compared to intact and endothelium denuded aortic rings incubated with MGO only, all groups were compared to untreated aortic rings (control). Analysed through two-way ANOVA with Bonferroni post-hoc test. Significance is represented as * $p < 0.05$ and *** $p < 0.001$ vs intact aortic rings treated with MGO (100µM). Significance is represented as $ $p < 0.05$, $$ $p < 0.01$ and $$$ $p < 0.001$ vs endothelium denuded aortic rings treated with MGO (100µM). Data shown as percentage ± SEM (Control, N= 8, MGO 100µM 2 hours, N= 5, Denuded MGO 100µM 2 hours, N= 5, AMTB 1µM+MGO 100µM, N= 4 and denuded AMTB 1µM+MGO 100µM 2 hours, N= 4).

- MGO-induced loss of contractility persistence was significantly inhibited through incubating the intact aortic rings with iberiotoxin, L-NAME or contracting the aortic rings with high potassium Krebs solution

The involvement of intracellular signalling molecules in MGO-induced loss of contractility persistence was investigated next. Aortic rings were incubated with either NOS inhibitor (L-NAME) or BKCa blocker (iberiotoxin) in addition to MGO (100µM) incubation before being contracted with NA (300nM). In addition to these experiments, high potassium Krebs solution was applied to aortic rings incubated with MGO (100µM) to abolish the effect of potassium channels. L-NAME significantly reduced MGO-induced loss of contractility persistence [L-NAME (100µM) + MGO (100µM), N=4, *** $p < 0.001$, Emax= -37.1 ± 18.3% and tmax= 30 minutes vs MGO (100µM), N=5, Emax= -90.4±6.9% and tmax= 30 minutes). Iberiotoxin showed significant effect on MGO-induced loss of contractility persistence [iberiotoxin (1nM) + MGO (100µM), N=4, ££ $P<0.01$, Emax= -55.8 ± 5.5% and tmax= 30 minutes vs MGO (100µM), N=5, Emax= -90.4 ± 6.9% and tmax= 30 minutes). High potassium Krebs (123mM)-induced contraction showed significant resistance toward MGO-induced loss of contractility persistence [high potassium Krebs solution (123mM) + MGO (100µM), N=4, $$$ $p < 0.001$, Emax= -22.4 ± 10.5% and tmax= 30 minutes vs MGO (100µM), N=5, Emax: -90.4 ± 6.9% and tmax= 30 minutes) (Figure 95).

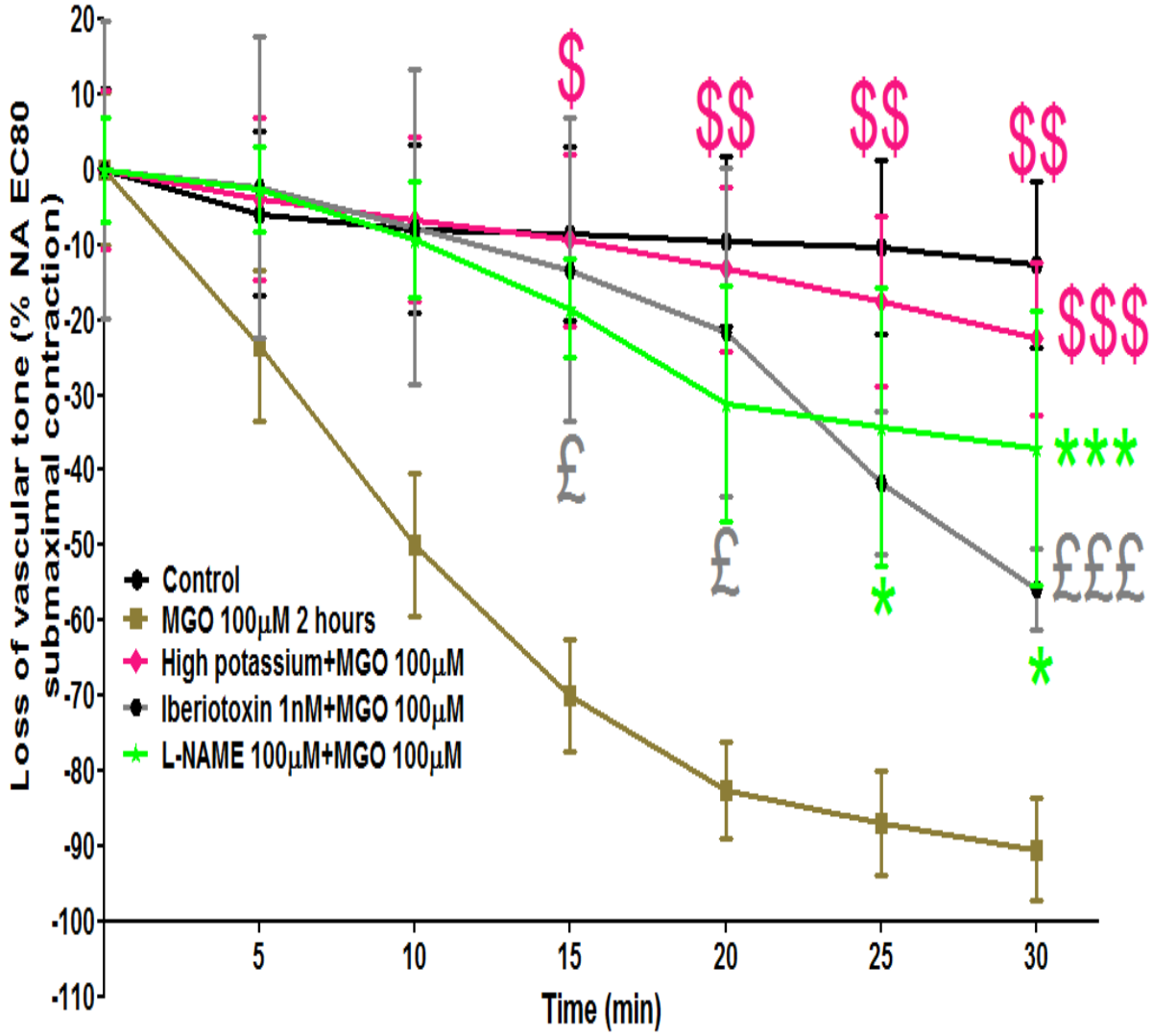

Figure 95. Methylglyoxal (MGO)-induced loss of contractility persistence against L-NAME, Iberiotoxin and high potassium Krebs solution. Analysed through two-way ANOVA with Bonferroni post-hoc test. Significance is represented as £ or $ or * $p < 0.05$ and $$ $p < 0.01$ when compared with intact aortic rings incubated with MGO (100µM). Data shown as percentage ± SEM (Control, N= 8 n= 8, MGO 100µM 2 hours, N= 5, L-NAME 100µM+MGO 100µM, N= 4, iberiotoxin 1nM+MGO 100µM, N= 4 n= 5 and high potassium Krebs + MGO 100µM, N= 4).

- Experiments visuals summary

The conducted experiments are summarised in the following figure.

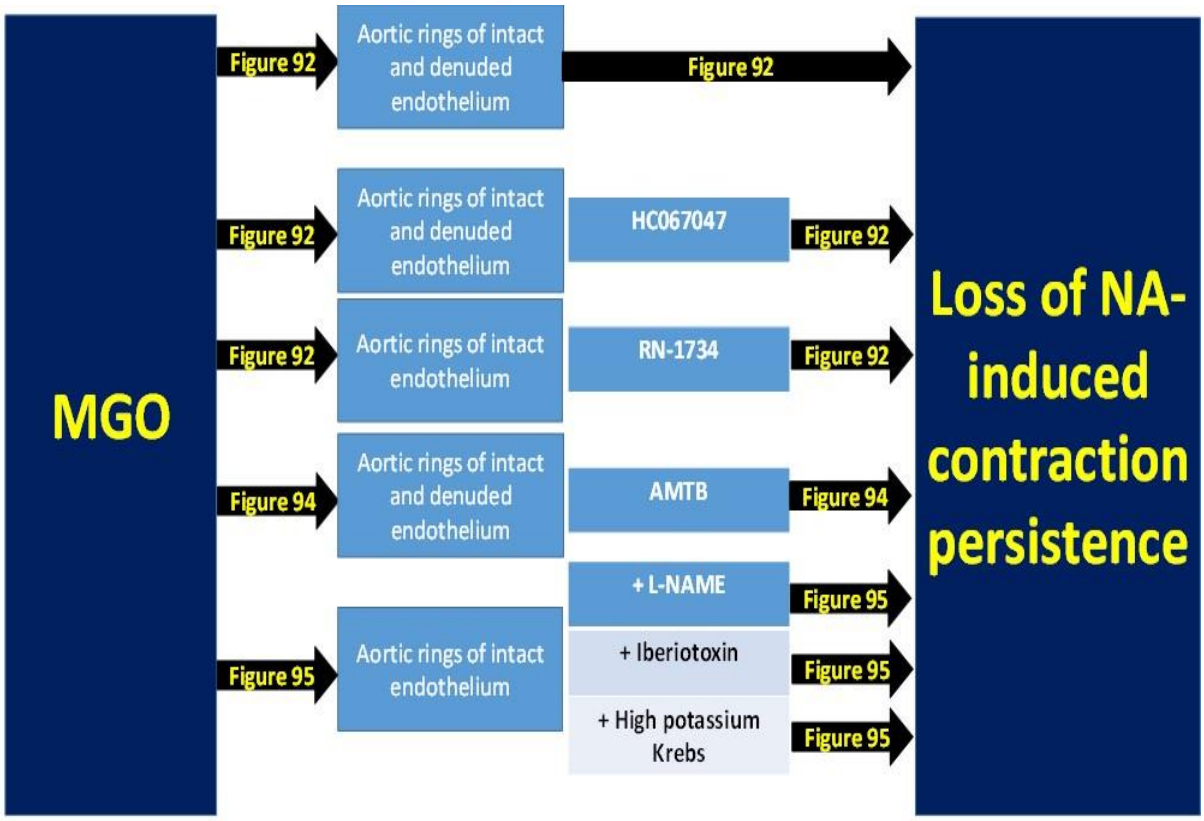

Figure 96. Methylglyoxal (MGO)-induced loss of contractility persistence in rat aortic rings experiments summary.

7.3.3. MGO and TRPM8 through FlexStation studies

MGO-induced loss of contractility persistence was abolished through TRPM8 antagonism with AMTB (Figure 94). This is consistent with the hypothesis that MGO is acting as a TRPM8 agonist. To test this idea we investigated the action of MGO on rTRPM8 cells.

A FlexStation Ca^{2+} assay was conducted to investigate whether MGO-induced $[Ca^{2+}]i$ through TRPM8 might explain the AMTB blocked MGO-induced loss of contractility persistence. R-TRPM8 cells showed significant increase in $[Ca^{2+}]i$ in response to icilin CRC (200nM-1nM) which was completely abolished by AMTB pre-incubation (5-50µM) for 30 minutes. Moreover, untransfected CHO cells showed no response to icilin CRC (200nM-1nM) ($p < 0.01$) consistent with the effect of icilin being due to TRPM8 activation, as shown in Figure 97. Pre-incubating r-TRPM8 with AMTB (5-50µM) showed significant reduction in icilin-induced $[Ca^{2+}]i$ [AMTB (5µM), * $p < 0.05$, Emax= 0.58 ± 0.0 fura-2 ratio change, AMTB (10µM), $ $p < 0.05$, Emax= 0.3 ± 0.0 fura-2 ratio change and AMTB (50µM), # $p < 0.05$, Emax= 0.2 ± 0.0 fura-2 ratio change vs icilin control, N=3, Emax= 2.4 ± 0.6 fura-2 ratio change). Moreover, untransfected CHO cells showed no significant icilin-induced $[Ca^{2+}]i$ (N=1, && $P<0.01$, Emax= 0.2 ± 0.0 fura-2 ratio change) (Figure 97).

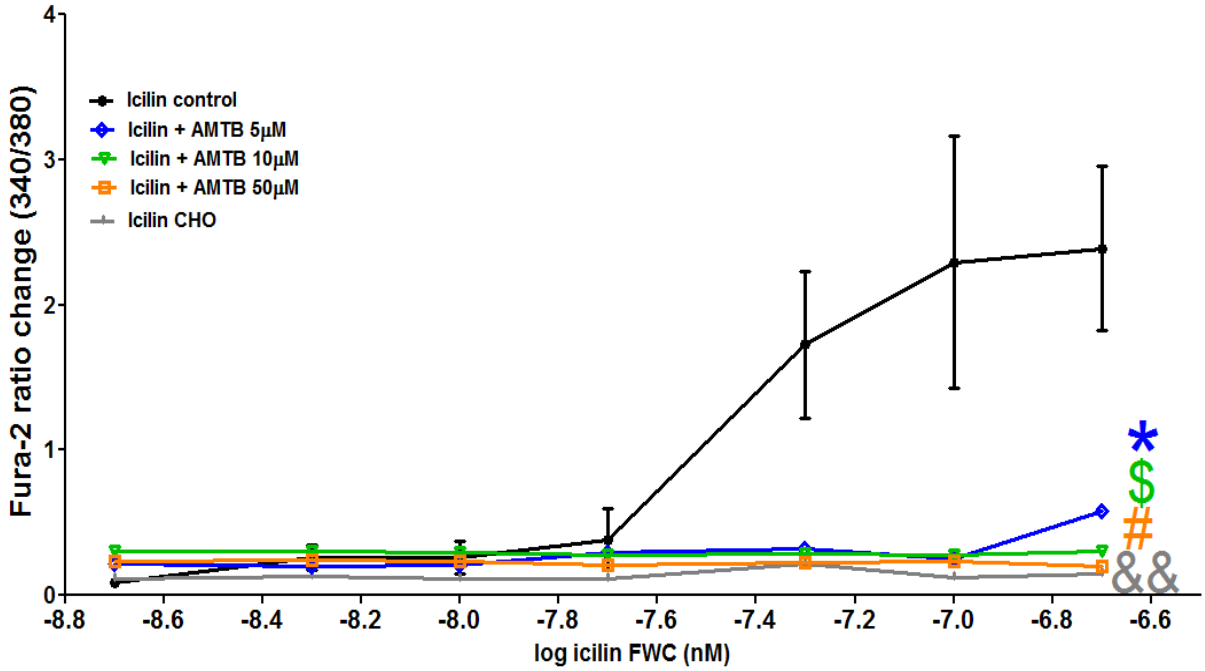

Figure 97. Icilin concentration response curve on r-TRPM8 and CHO cells. Pre-incubating r-TRPM8 with AMTB (5-50µM) before adding treating the cells with icilin CRC (1nM-200nM). Analysed through one-way ANOVA with Tuckey post-hoc test. Significance is represented as * or $ or # when $p < 0.05$ and && when $p < 0.01$ when compared against icilin control. Data is represented as fura-2 ratio. FWC: final well concentration.

- MGO induced intracellular calcium elevation in rTRPM8 cells

Afterward, r-TRPM8 cells were incubated with MGO (100µM-10mM) and an osmotic control well of sucrose (50mM) for 1 hour. MGO concentrations of 2mM and above showed a significant increase in $[Ca^{2+}]i$ level in time and dose-dependent manner as shown in Figure 98. MGO (10mM) showed significantly higher fura-2 ratio ($[Ca^{2+}]i$ elevation) (N=3, *** $p < 0.001$, Emax= 0.5 ± 0.2 fura-2 ratio change, vs the lower concentrations (5mM-100µM) and sucrose (50mM)]. MGO (5mM) showed significantly higher $[Ca^{2+}]i$ [N=3, && $p < 0.01$, Emax= 0.4 ± 0.15 fura-2 ratio change vs MGO (2mM) Emax= 0.35 ± 0.13 fura-2 ratio change, and $$$ $p < 0.01$ vs (1mM-100µM) and sucrose (50mM)]. MGO (2mM) showed significantly higher fura-2 ratio [N=3, £££ $p < 0.001$, Emax= 0.35 ± 0.13 fura-2 ratio change vs the lower concentrations (1mM-100µM) and sucrose (50mM)]. MGO (1mM-100µM) did not show significant difference ($p \geq 0.05$, N=3, Emax= 0.22 ± 0.07 fura-2 ratio change, Emax= 0.16 ± 0.05 fura-2 ratio change, Emax= 0.15 ± 0.05 fura-2 ratio change and Emax= 0.16 ± 0.06 fura-2 ratio change, respectively) when compared to sucrose (50mM) osmotic control (N=3, $p \geq 0.05$, Emax= 0.17 ± 0.05) (Figure 98).

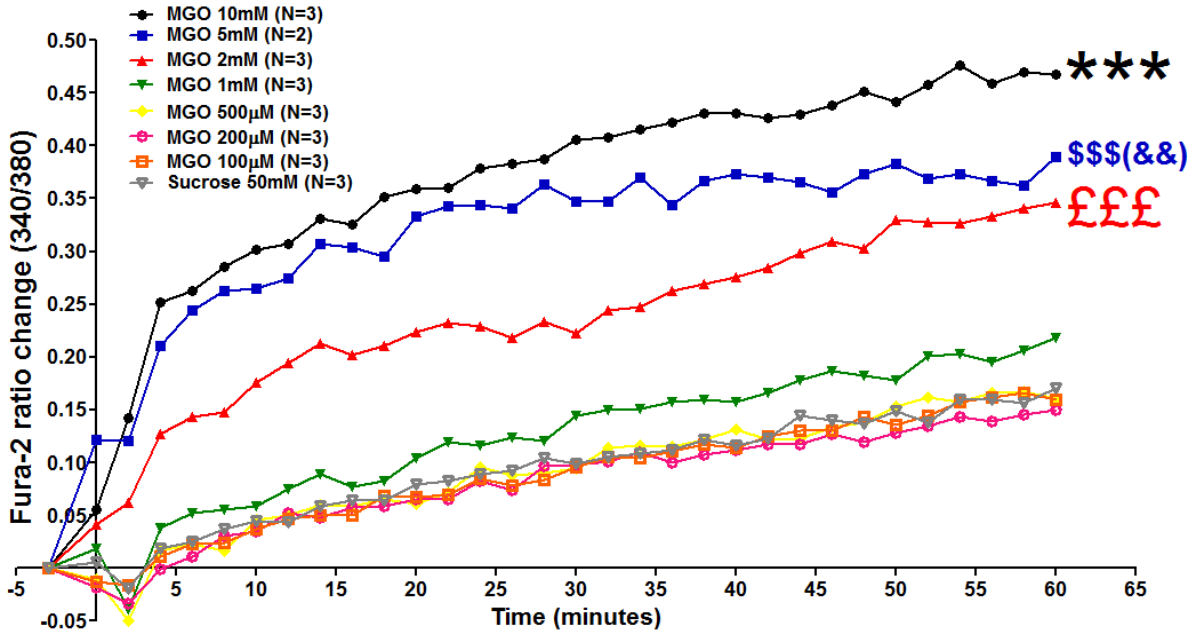

Figure 98. Methylglyoxal (MGO)-induced calcium influx in r-TRPM8 cells. R-TRPM8 cells incubated with MGO (1mM - 100µM) for 60 minutes compared to osmotic control of sucrose (50mM). Data analysed through one-way ANOVA with Tukey post-hoc test. Significance is represented as *** $p < 0.001$ vs MGO (5mM - 100µM) and sucrose (50mM). Significance is represented as && when $p < 0.01$ vs MGO (2mM). Significance is represented as $$$ or £££ $p < 0.001$ vs MGO (1mM -100µM) and sucrose (50mM). Data is represented as fura-2 ratio.

- MGO induced intracellular calcium elevation was significantly reduced in rTRPM8 cells and CHO cells pre-incubated with AMTB

Since AMTB (5µM) abolished icilin-induced Ca^{2+} influx in r-TRPM8 cells (Figure 97) we next investigate whether AMTB (5µM) could block the MGO-elevated $[Ca^{2+}]i$. Therefore, r-TRPM8 cells were incubated with AMTB (5µM) and (10µM) for 30 minutes before adding MGO (10 - 2mM). Each MGO concentration that showed significant increase in Ca^{2+} influx in Figure 97 was compared in a separate figure 99-111). As shown in Figure 99, MGO (10mM)-elevated $[Ca^{2+}]i$ was significantly reduced when rTRPM8 were pre-incubated with AMTB (5µM & 10µM) [AMTB (5µM), N=1, *** $p < 0.001$, t50= 18.4 minutes and Emax= 0.35 ± 0.0 fura-2 ratio change, AMTB (10µM), N=1, $$$ $p < 0.001$, t50= 16.7 minutes and Emax= 0.24 ± 0.0 fura-2 ratio change vs MGO (10mM) in r-TRPM8 without AMTB, N=3, t50= 3.7 minutes and Emax= 0.5±0.2 fura-2 ratio change) (Figure 99).

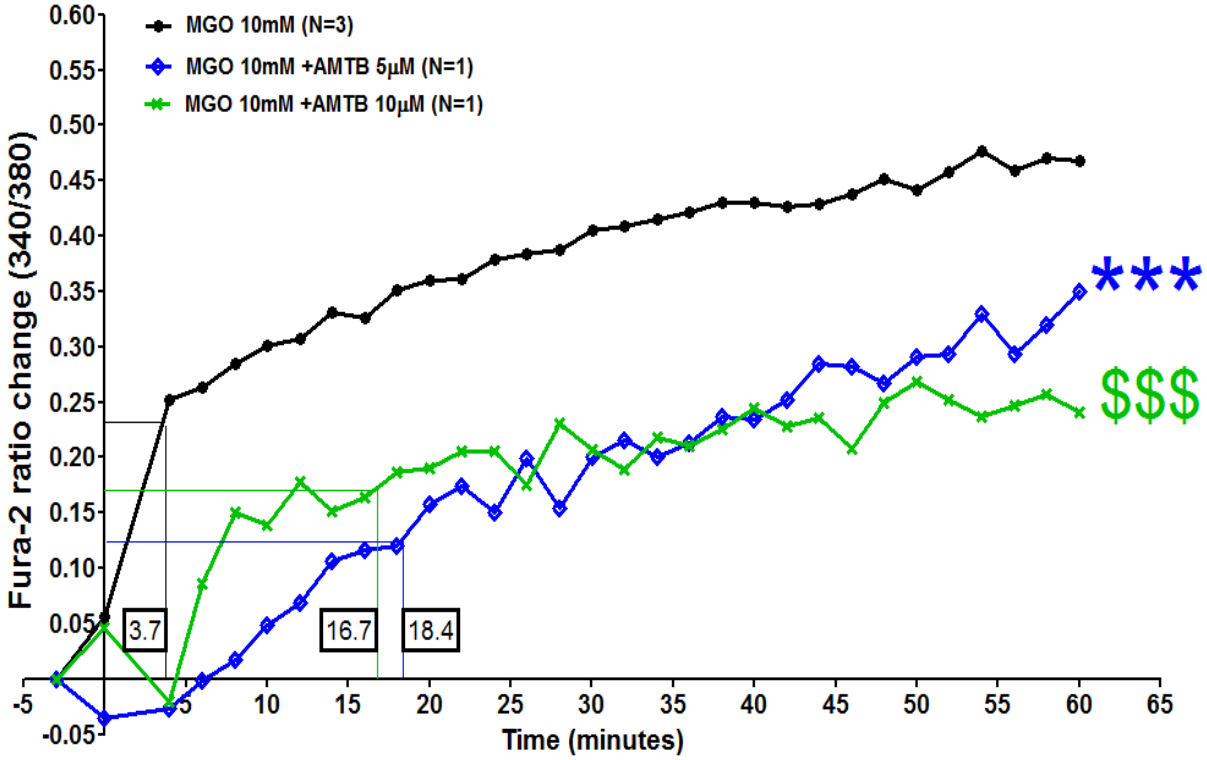

Figure 99. Methylglyoxal (MGO, 10mM)-induced intracellular calcium elevation in r-TRPM8 cells with AMTB (5µM and 10µM). Analysed through one-way ANOVA with Tukey post-hoc test. Significance is represented as £ when $p < 0.05$ and *** or $$$ when $p < 0.001$ vs r-TRPM8 treated with MGO (10mM). Data is represented as fura-2 ratio.

However, when applying MGO (10mM) to untransfected CHO cells, $[Ca^{2+}]i$ was significantly influenced with AMTB (5µM) pre-incubation [CHO cells, N=1, *** $p < 0.001$, t50= 16.7 minutes and Emax= 0.56 ± 0.0 fura-2 ratio change vs CHO cells with AMTB (5µM), N=1, t50= 30.7 minutes and Emax= 0.55 ± 0.0 fura-2 ratio change) (Figure 100).

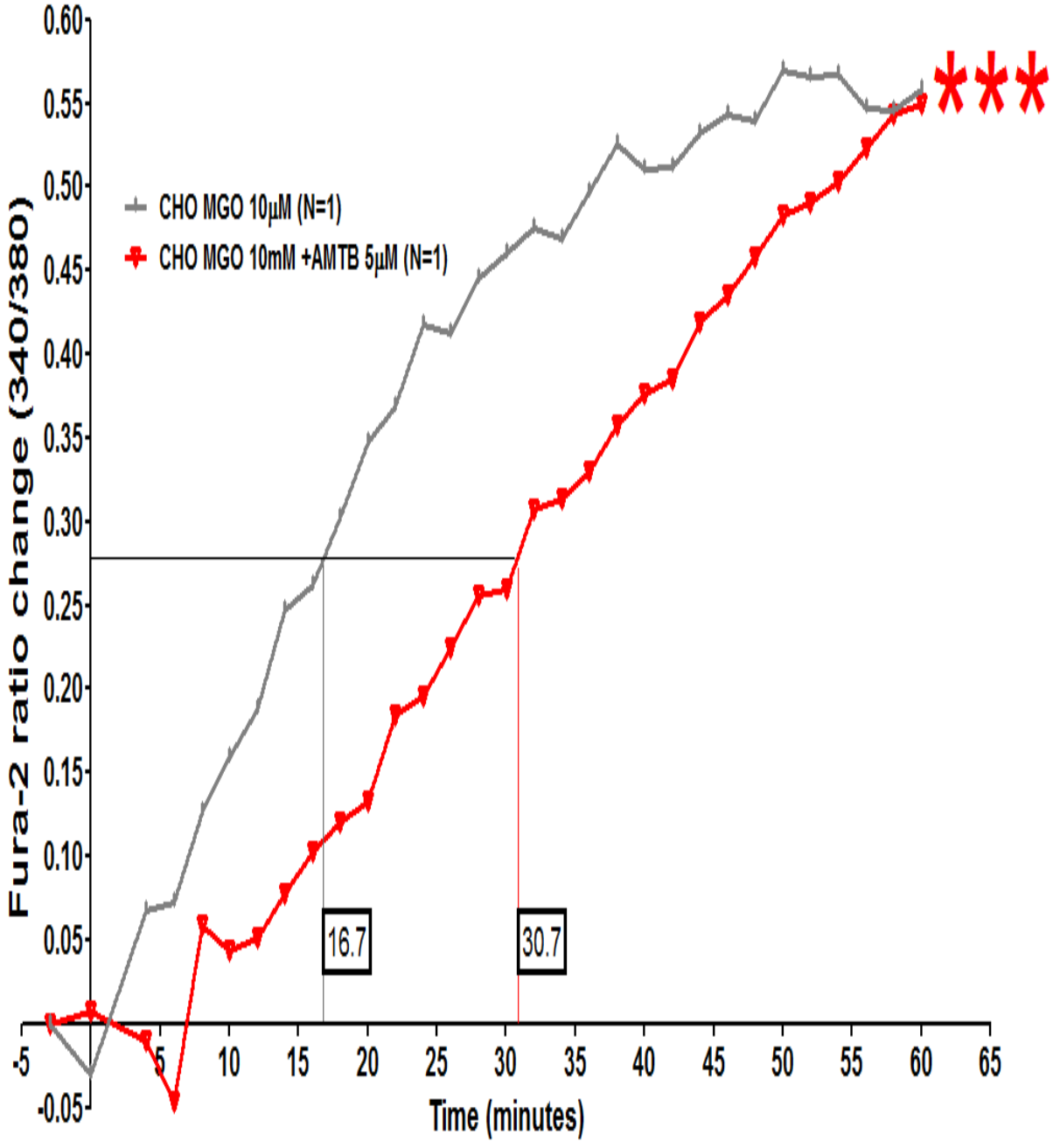

Figure 100. Methylglyoxal (MGO, 10mM)-increased intracellular calcium concentration with AMTB (5µM) in CHO cells. Analysed through paired two-tailed Student's t-test. Significance is represented as *** when $p<0.001$. Data is represented as fura-2 ratio.

MGO (5mM)-induced [Ca^{2+}]i elevation was significantly reduced in r-TRPM8 cells pre-incubated with AMTB (5µM & 10µM) [AMTB (5µM), N=1, *** $p < 0.001$, t50=6.3 minutes and Emax= 0.2 ± 0.0 fura-2 ratio change and $$$ $p < 0.001$, AMTB (10µM), N=1, t50= 4 minutes and Emax= 0.23 ± 0.0 fura-2 ratio change vs MGO (5mM) in r-TRPM8 without AMTB, N=2, t50= 3.4 minutes and Emax= 0.4 ± 0.15 fura-2 ratio change) (Figure 101).

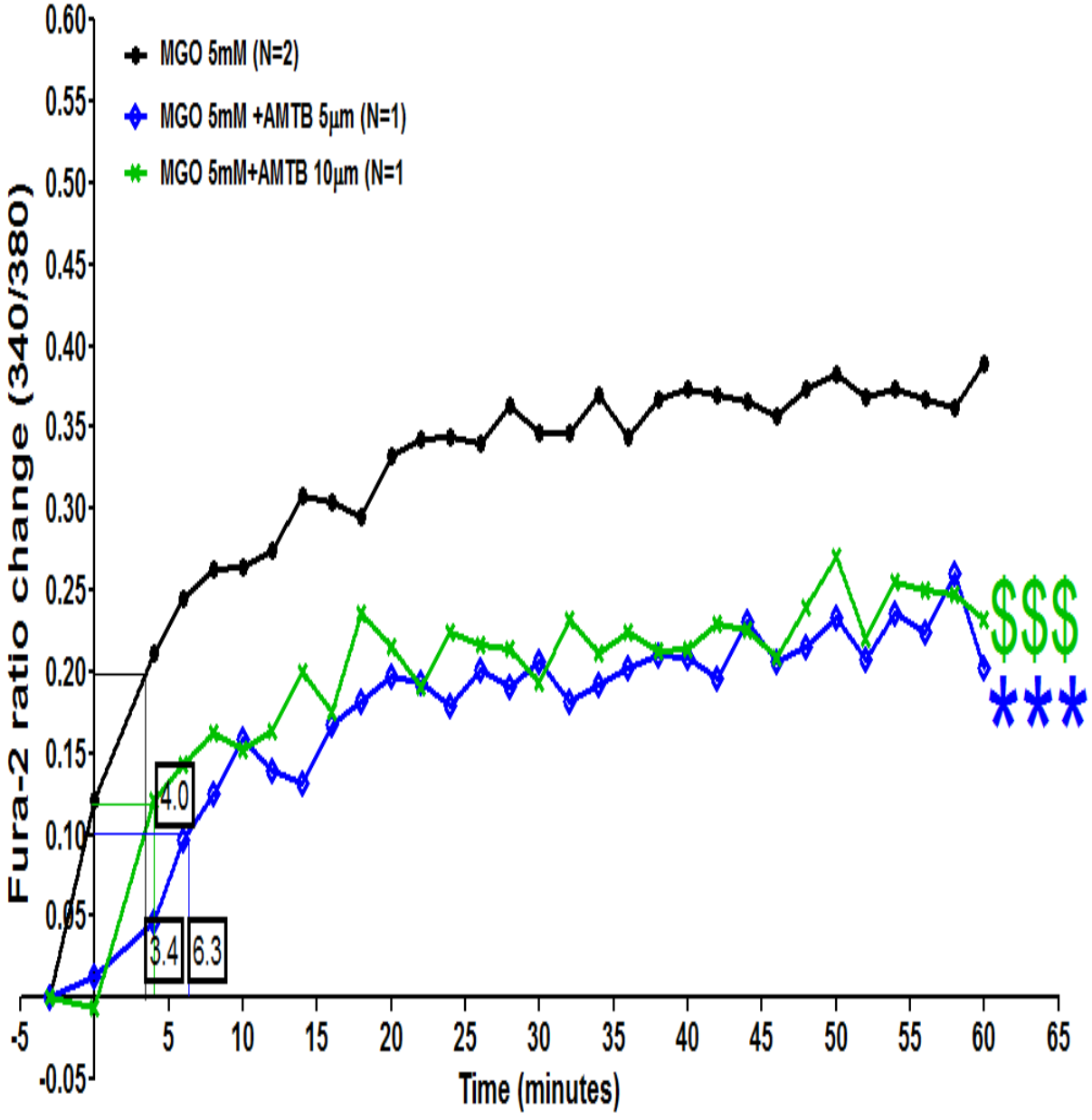

Figure 101. Methylglyoxal (MGO, 5mM)-induced calcium influx in r-TRPM8 cells with AMTB (5µM and 10µM). Analysed through one-way ANOVA with Tukey post-hoc test. Significance is represented as *** or $$$ when $p < 0.001$ vs r-TRPM8 treated with MGO (5mM). Data is represented as fura-2 ratio.

However, when applying MGO (5mM) to untransfected CHO cells, $[Ca^{2+}]i$ was significantly influenced with AMTB (5µM) pre-incubation [CHO cells, N=1, *** $p < 0.001$, t50= 7.1 minutes and Emax= 0.29 ± 0.0 fura-2 ratio change vs CHO cells with AMTB 5µM, N=1, t50= 32.0 minutes and Emax= 0.23 ± 0.0 fura-2 ratio change) (Figure 102).

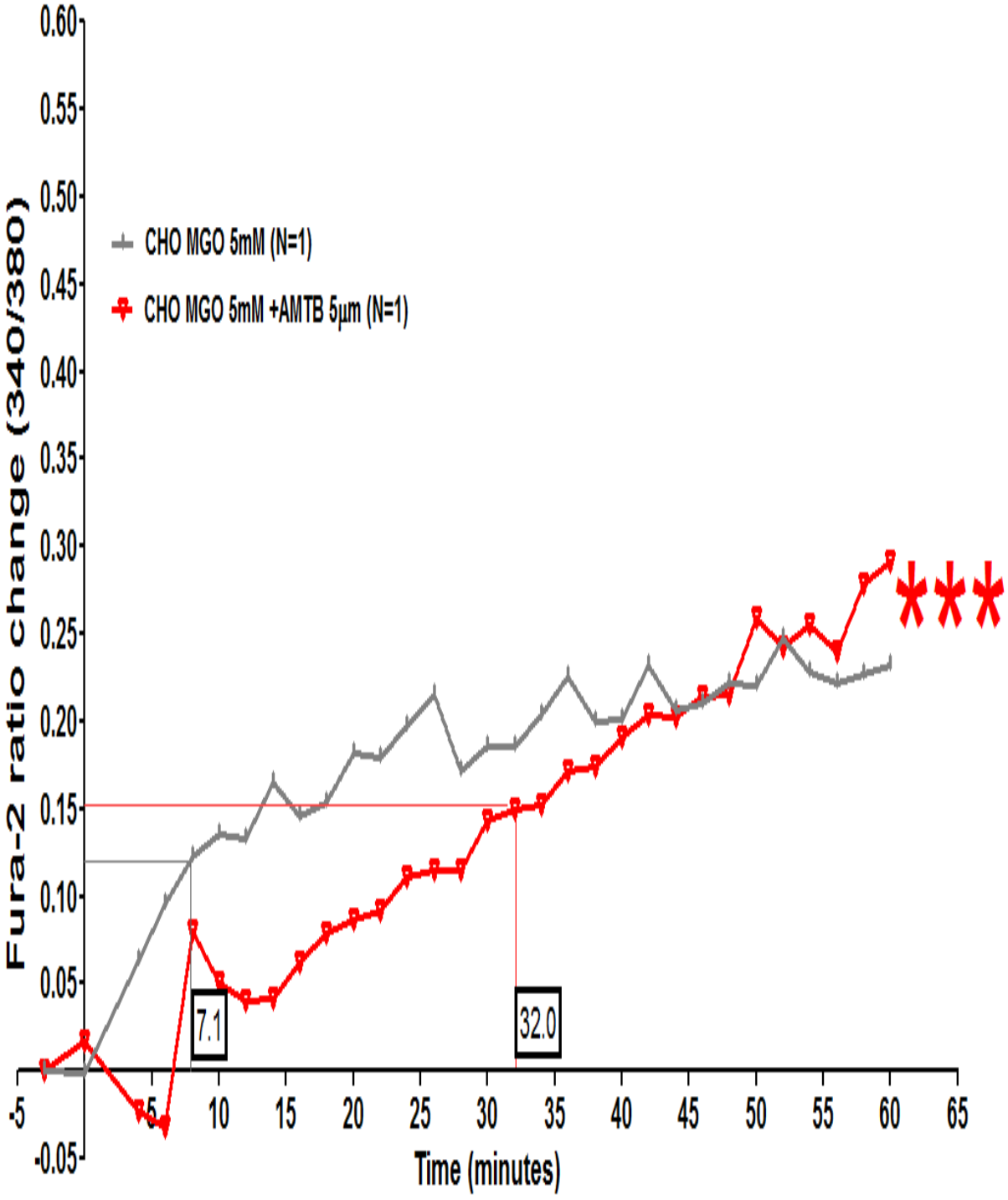

Figure 102. Methylglyoxal (MGO, 5mM)-increased intracellular calcium concentration with AMTB (5µM) in CHO cells. Analysed through paired two-tailed Student's t-test. Significance is represented as *** when $p < 0.001$. Data is represented as fura-2 ratio.

MGO (2mM)-elevated [Ca^{2+}]i was significantly compromised in r-TRPM8 cells were pre-incubated with AMTB (5µM & 10µM) [AMTB (5µM), N=1, *** $p < 0.001$, t50= 9.0 minutes and Emax= 0.2 ± 0.0 fura-2 ratio change and AMTB (10µM), N=1, $$$ $p < 0.001$, t50= 5.6 minutes and Emax= 0.27 ± 0.0 fura-2 ratio change vs MGO 5mM in r-TRPM8 without AMTB, t50= 9.8 minutes and Emax= 0.35 ± 0.13 fura-2 ratio change] (Figure 103).

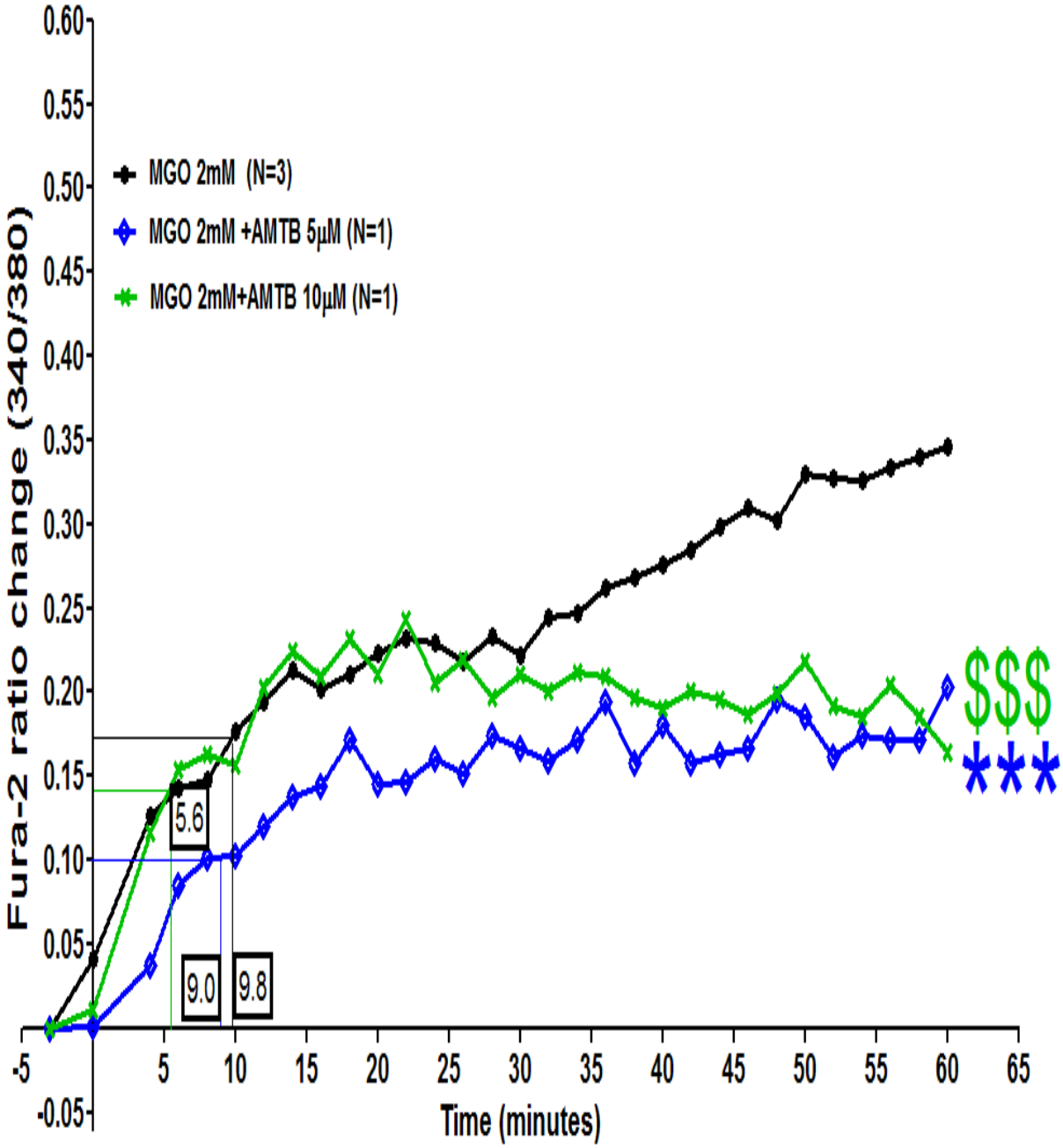

Figure 103. Methylglyoxal (MGO, 2mM)-induced calcium influx in r-TRPM8 cells with AMTB (5µM and 10µM). Analysed through Tukey's one-way ANOVA. Significance is represented as *** or $$$ when $p < 0.001$ vs r-TRPM8 treated with MGO (2mM). Data is represented as fura-2 ratio.

However, when applying MGO (2mM) to untransfected CHO cells, [Ca^{2+}]i was significantly influenced with AMTB (5µM) pre-incubation [CHO cells, N=1, *** $p < 0.001$, t50= 4.9 minutes and Emax= 0.17 ± 0.0 fura-2 ratio change vs CHO cells with AMTB (5µM), N=1, t50= 29.5 minutes and Emax= 0.15 ± 0.0 fura-2 ratio change] (Figure 104).

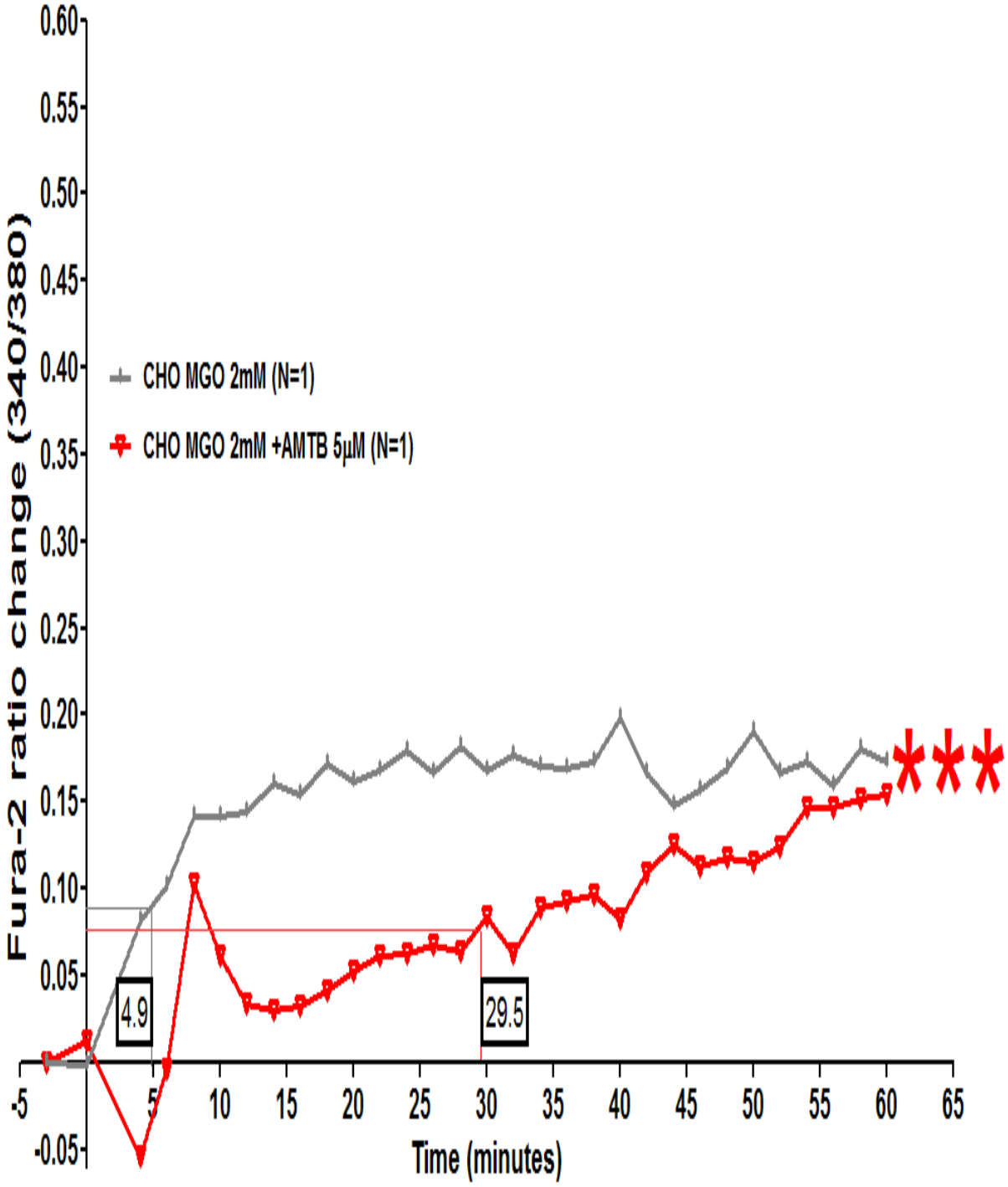

Figure 104. Methylglyoxal (MGO, 2mM)-increased intracellular calcium concentration with AMTB (5µM) in CHO cells. Analysed through paired two-tailed Student's t-test. Significance is represented as *** when $p < 0.001$. Data is represented as fura-2 ratio.

7.4. Discussion

In this chapter, the short-term effect of MGO was studied as the naïve rats' aortic rings were incubated with MGO (100µM) for 2 hours, 1 hour, 30 minutes and 15 minutes. However, NA-constricted aortic rings spontaneously relaxed when incubated with MGO (1µM or 100µM) for 2 hours (Figure 90 & 100) but not for 1 hour or less (Figure 88 & 97).

Aortic rings were pre-incubated with numerous blockers before being incubated with MGO (100µM) to decipher the mechanisms by which MGO induced vasodilation. TRPV4 antagonist, HC067047 but not RN-1734 showed significant inhibition to MGO-induced loss of contractility persistence (Figure 93). This finding suggests that HC067047 may act differently to RN-1734 as Vincent and Duncton (2011) revealed that HC067047 inhibits TRPM8 and voltage-gated K^+ channels (Kv1.1) at sub-micro molar concentrations while RN-1734 is a more selective TRPV4 antagonist. Moreover, as RN-1734 showed partial inhibition to MGO-induced loss of contractility persistence, it also showed significant difference to HC067047 effect on MGO-induced loss of contractility persistence revealing and confirming possible differences in the mechanism of TRPV4-antagonism (Figure 93). However, HC067047 did not inhibit MGO-induced loss of contractility persistence when endothelium was removed (Figure 93). Since HC067047 was reported to block TRPM8 (Vincent & Duncton, 2011), therefore, blocking TRPM8 with AMTB was examined against MGO-induced loss of contractility persistence.

As shown in Figure 94, AMTB counteracted MGO-induced loss of contractility persistence significantly and this effect was not influenced by the endothelium removal. This finding supports the previous finding that TRPM8-induced vasodilation is partially endothelium-independent (Figure 34). Moreover, as shown in Figure 31, BKCa blocking showed significant suppression to icilin-induced vasodilation. Therefore, iberiotoxin (1nM) was investigated against MGO-induced loss of contractility persistence.

As shown in Figure 95, MGO-induced loss of contractility persistence was significantly compromised through BKCa blocking with iberiotoxin (1nM). Moreover, MGO-induced loss of contractility persistence was significantly abolished when aortic rings were constricted with high potassium Krebs solution rather than NA (300nM) (Figure 95). In addition to these findings, Dragoni, Guida, and McIntyre (2006) revealed that TRPM8 activity is critically controlled through two cysteine residues located at positions 929 and 940 in the pore forming region, which might be preferentially targeted by MGO (Benemei et al., 2013). Moreover,

Eberhardt et al. (2012) concluded that TRPA1 is a pivotal mediator in MGO-induced nociception together with approximately 20% sequence homology among all TRP channels, including TRPM8 (Clapham, 2003). Therefore, TRPM8 was hypothesised as a possible target for MGO in the vascular tissue.

According to the stated hypothesis, r-TRPM8 cells were studied using FlexStation which showed significant $[Ca^{2+}]i$ elevation in a time and MGO dose-dependent manner (Figure 98). MGO-induced $[Ca^{2+}]i$ was significantly reduced by AMTB (5µM & 10µM) incubation (Figures 99, 101 & 103) revealing TRPM8 as a possible target for MGO. This finding was similar to Jan et al. (2005) who concluded that MGO higher than 0.5mM increases $[Ca^{2+}]i$ in Madin-Darby canine kidney (MDCK) renal tubular cells. Moreover, un-transfected CHO cells showed significant reduction in MGO-induced $[Ca^{2+}]i$ (Figures 100, 102 &104), however, the response was not abolished when compared to icilin-induced $[Ca^{2+}]i$ (Figure 97). This might be attributed to the effect of MGO on intracellular Ca^{2+} stores as a previous study showed that MGO increases $[Ca^{2+}]i$ as a product of both ER Ca^{2+} release and extracellular Ca^{2+} influx (Jan et al., 2005). Another previous study revealed that MGO-induced $[Ca^{2+}]i$ was significantly reduced but not abolished when MDCK cells were treated with Ca^{2+} free ECF containing MGO, suggesting that MGO induces ER Ca^{2+} release that contributes to the initial and the sustained $[Ca^{2+}]i$ elevation (Jan et al., 2005).

By contrast, when CHO cells incubated with AMTB (5µM), MGO-induced $[Ca^{2+}]i$ was significantly reduced as shown in Figures 100, 109 and 111. A previous study found that TRPM8 agonist; menthol induces Ca^{2+} release from intracellular ER Ca^{2+} stores which was concomitant with SOCs activation in human prostate cancer epithelial cells (LNCaP) and CHO cells (Mahieu et al., 2007; Thebault et al., 2005). These studies revealed that TRPM8 channels might contribute to Ca^{2+} release from ER cellular stores (Thebault et al., 2005). Therefore, in our studies, MGO might act on ER's TRPM8 channels in CHO cells. However, CHO cells incubated with AMTB (5 - 10µM) did not abolish MGO-induced Ca^{2+} elevation. As concluded by (Mahieu et al., 2007) study on un-transfected HEK293 and CHO cells, higher doses of TRPM8 agonist; menthol (1mM) can induce Ca^{2+} release independent of TRPM8. According to these findings, MGO is suggested to enhance $[Ca^{2+}]i$ elevation partly through three main sources; (i) membrane TRPM8 channels, (ii) intracellular TRPM8-dependent ER Ca^{2+} stores and (iii) intracellular TRPM8-independent ER Ca^{2+} stores which require further investigations.

Moreover, the increase in ECs cytoplasmic Ca^{2+} from ER stores (< 300ms) is called ECs Ca^{2+} pulsars. ECs Ca^{2+} pulsars are released from ER at spatially fixed sites proximal to MEPs (Bagher & Garland, 2014). Therefore, MGO might induce vasodilation through ECs Ca^{2+} pulsars that activate the MEPs' Kca (Bagher & Garland, 2014). Such non-selective MGO targeting might explain the 20-fold difference shown between the whole aortic rings (100μM) and the rTRPM8 cells (2mM). Therefore, in addition of showing its pathological role when elevated in diabetic serum, MGO might act as a redox-based cell signalling regulator (Chang et al., 2005; X. Jia & Wu, 2007).

To sum up, MGO was elevated in STZ-diabetic rats' serum to approximately 100μM. Incubating naïve non-diabetic aortic rings with MGO (100μM) for 2 hours induced spontaneous vasodilation which was partly mediated through TRPM8 as well as intracellular Ca^{2+} stores. These findings suggest that acute MGO might play an important physiological role in regulating cellular Ca^{2+} homeostasis and ER function. However, chronic MGO elevation might contribute to ER stress and hence causes protein misfolding as shown in chapter 6. Collectively these findings suggest that MGO might be a pivotal therapeutic target to manage diabetes vascular complications.

Chapter 8: General Discussion

Since the significant reduction in TRPV4-mediated vasodilation observed in aortic rings from STZ-induced diabetic rats in preliminary experiments, the aim of the present study was to investigate the effect of diabetes on the function of TRPV4 channels in the endothelium. The study examined primarily muscarinic, TRPV4, and TRPM8 function in the aortic endothelium of STZ-diabetic and control rats, with a conventional organ bath, myographic techniques, and a range of appropriate agonists and antagonists. Downstream functions of those pathways were investigated by using L-NAME and iberiotoxin, for example, and observations were extended to isolated primary aortic ECs and ASMCs using fura-2 Ca^{2+} imaging, LSCM, and SDS–PAGE Western blotting. These techniques enabled the discovery of whether the signalling pathways of TRP channels are altered. The course of diabetes's induction in relation to TRP channel function was studied in order to explain changes in the channels during the onset or development of the disease. The study also involved investigating circulating markers such as ox-LDL and MGO with ELISA, as well as the application of MGO to nondiabetic cells and tissues as a means to develop an in vitro diabetic model of endothelial and TRPV4 dysfunction. Ultimately, the study should expand understandings of endothelial dysfunction in diabetic patients and guide novel therapeutic strategies.

8.1. STZ-induced diabetes characterised with elevated blood glucose, serum MGO, and ox-LDL

The characterisation of the STZ model used in the studies highlighted numerous features consistent with human patients with diabetes. STZ-induced diabetes was characterised in terms of blood glucose elevation, and on that point, 95% of the STZ-injected rats were hyperglycaemic (blood glucose > 16mmol/L) by day 7, a condition which continued for 5 weeks (Figure 40), as consistent with other studies (Wei et al., 2003). By comparison, according to the most recent diagnostic criteria for diabetes, random plasma glucose should be ≥ 11.1mmol/L for a human patient with classic symptoms of hyperglycaemia (American Diabetes Association, 2016). This STZ-induced diabetes model thus provided an exceptional foundation for representing complications associated with diabetes and hyperglycaemia. An acute time point (i.e., Week 2) was used in most of the studies, since it showed the most significant endothelial dysfunction (Figure 49) and appeared to be less detrimental to animal health by the means of weight loss and neuropathic pain.

The fourfold increase in MGO levels in STZ-diabetic rats' serum samples (Figure 43) was accompanied by a fourfold increase in blood glucose concentration (Figure 40). As such, chronic hyperglycaemia might serve as a primary source of endogenous MGO (Kalapos, 2013; Shamsaldeen et al., 2016). A previous study revealed that MGO is four times greater in T2DM patients' plasma and can reach approximately 500nmol/g haemoglobin and thereby contributes to eryptosis (Nicolay et al., 2006). The MGO ratio in the STZ-induced diabetes model could therefore represent a robust translational marker for diabetic patients, since both showed a fourfold increase in the concentration of MGO, which is involved in common diabetes complications such as endothelial dysfunction (Figure 52) and neuropathic pain (A. Dhar et al., 2010; A. Dhar et al., 2011; Eberhardt et al., 2012).

Ox-LDL is increased by twofold in type 2 diabetic patients (L. Zhang, Guo, Zhang, Niu, & Wang, 2016), which corresponded with significant serum ox-LDL elevation observed in STZ-diabetic rats (Figure 44). The ox-LDL molecule is a cholesterol acceptor that binds to the CD36 endothelial scavenger receptor and competes with caveolae to deplete the caveolae from cholesterol, thereby causes caveolae disruption (Blair et al., 1999; Y. Zeng et al., 2003), which inhibits eNOS attachment to caveolin-1 (CAV-1) and prompts endothelial dysfunction, as detailed in Figures 60–63 (Blair et al., 1999). Previous studies have revealed a correlation between elevated serum ox-LDL and diabetic complications such as nephropathy and vascular dysfunction (Tsuzura et al., 2004). The consumption of tomato juice (500ml/day for 4 weeks) improved the concentration of the serum antioxidant lycopene by threefold. Such improvement was associated with decreased LDL susceptibility to oxidation and decreased c-reactive protein (CRP) that could reduce the risk of diabetes-associated myocardial infarction (Upritchard et al., 2000). Interestingly, as HMG-CoA reductase inhibitors, statins (i.e., simvastatin and lovastatin) protected eNOS activity from ox-LDL-induced downregulation (Laufs et al., 1998).

Ox-LDL is clearly higher in diabetes, and hyperglycaemia might be a principal contributor to its increased susceptibility to glycation and oxidation. LDL glycation and oxidation occurs simultaneously, since free radicals are generated through glycation from glucose and Amadori products, which enhances LDL susceptibility to further oxidation (H. Yoshida & Kisugi, 2010). Lipolysis is also accelerated in diabetes, and such accelerated lipid catabolism includes increased lipid peroxidation (Shamsaldeen et al., 2016), which begins with the production of lipid hydroperoxide, which undergoes metal-induced alkoxyl radical generation that forms a variety of aldehydes, including MGO (H. Yoshida & Kisugi, 2010).

Serum total protein measurements showed a significant time-dependent reduction in STZ-diabetic rats (Figure 45a). As a previous study has shown, proteinuria is a common complication of diabetes associated with plasma hypoproteinaemia (Bhonsle et al., 2012), a condition that is primarily attributed to nephropathy and has been associated with a significant (eight-fold) increase in urine protein in at least one study (Niwa et al., 1997). More recent research has shown that MGO increases by approximately twofold in patients with type 2 diabetes and nephropathy, as well as by twofold in similar patients without nephropathy, when compared to nondiabetic ones (Lu et al., 2011). Such data revealed that MGO might be implicated in diabetes prognosis by developing both nephropathy and endothelial dysfunction. Another recent study revealed that ox-LDL is significantly elevated (i.e., by twofold) in diabetic nephropathy (L. Zhang et al., 2016) and furthermore associated with the overexpression of lectin-like ox-LDL receptor (LOX-1) and the inactivation of p38, which might contribute to diabetic nephropathy (L. Zhang et al., 2016).

Altogether, chronic hyperglycaemia might increase MGO production, and by extension, hyperglycaemia and MGO elevation might contribute to LDL oxidation. As such, controlling blood glucose and reducing MGO production could limit ox-LDL formation, which could further provide an essential therapeutic strategy to limit the progression of complications in diabetes.

8.2. Increased vasoconstriction as a vascular complication in diabetes

STZ-diabetic aortic rings treated with NA (300nM) showed significantly higher vasoconstriction than naïve aortic rings (Figure 47). As a possible mechanism, the exaggerated TRP channels-mediated influx of Ca^{2+} might lead to vasoconstriction through agonist-induced membrane depolarisation-activated TRP channels—for instance, in α1-adrenergic receptor-stimulated TRPC6 commonly found in rat aortas and cerebral arteries (Inoue et al., 2009). Earlier studies have revealed that ox-LDL induces the expression of endothelin-1, a potent vasoconstrictor that might exacerbate vascular complications in diabetes (Galley & Webster, 2004). Therefore, along with being implicated in endothelial dysfunction, elevated serum ox-LDL (Figure 44) might also be related to the significant increase in STZ-vasoconstriction shown in Figure 47.

A previous study showed that NA infusion in type 2 diabetic patients' intrabrachial artery showed more vasoconstriction than in nondiabetic individuals (Hogikyan et al., 1999). However, plasma NA was not significantly different between the groups. Such an increase in

vascular tone was attributed to increased adrenergic responsiveness as a result of increased systemic sympathetic nervous system activity (Hogikyan et al., 1999).

MGO interacts with cellular proteins and nucleic acid and thereby accelerates AGE production and β-cell cytotoxicity (Sheader et al., 2001). AGE act as ligands for corresponding receptors, RAGE, which are upregulated in hyperglycaemia and normalised through GLO1 overexpression, which reveals the contribution of MGO in inducing RAGE expression (Schmidt et al., 1999; D. Yao & Brownlee, 2010). As other previous studies have showed, MGO induces RAGE expression and induces endothelial dysfunction (Sena et al., 2012), as well as $ONOO^-$ formation by inducing superoxide anion formation and NO in VSMCs (Chang et al., 2005). Superoxide anions quench NO to produce $ONOO^-$ that compromise NO bioavailability and hence cause endothelial dysfunction and exaggerated vasoconstriction (Alp et al., 2003; Hall et al., 1996; Milstien & Katusic, 1999). Moreover, superoxide anions inhibit SERCA pumps in VSMCs, thereby increasing $[Ca^{2+}]i$, impairing the vasodilation, and exaggerating vasoconstriction (Adachi et al., 2004; Cohen et al., 1999).

Earlier research has demonstrated that iNOS-derived NO plays a preventive role against increased vasospastic responses associated with arteriosclerosis (Fukumoto et al., 1997). Moreover, NOS blockade through L-NAME (100μM) significantly increased vasoconstriction tension force in the middle cerebral arteries of rats (McNeish et al., 2010). Such increased vasoconstriction was reproduced in endothelial denuded control aortic rings incubated with L-NAME (100μM), which functionally inhibits NOS from releasing NO (Figure 79b). Additionally, 3–5-week-old STZ-rats' aortic rings showed more significant increases in NA-induced vasoconstriction than vehicle control aortic rings (Figure 79a). Western blotting data moreover indicated significant reduction in iNOS expression from STZ ASMCs stimulated with IFN-γ and LPS (Figure 77). Therefore, the exaggerated NA-induced vasoconstriction in STZ-diabetic rats' aortic rings might be attributed to suppressed NOS activity (Figure 79a&b).

When non-diabetic ASMCs were treated with diabetic levels of MGO (100μM), iNOS expression was significantly suppressed which was accompanied with abolished NO release (Figure 81). Since iNOS is induced through bacterial inflammatory mediators such as LPS, MGO-suppressed iNOS might explain the reason of diabetics being prone to infection with their impaired immunity, and compromised circulation due to exaggerated vasoconstriction. Therefore, in addition to MGO inhibiting eNOS phosphorylation and hence impairing the

endothelium-dependent vasodilation, MGO impairs iNOS expression revealing that MGO might contribute to exaggerated vasoconstriction in diabetes.

As shown in Figure 84, since Akt phosphorylation was significantly compromised in ASMCs incubated with IFN-γ (100IU/ml), LPS (100 µg/ml), and MGO (100 µM), inhibiting Akt phosphorylation (Ser 473) contributed to MGO-downregulated iNOS (Figure 81). Such an effect might contribute to the increase in vasospastic responses shown in Figure 79, since iNOS-derived NO plays a preventive role against increased vasospastic responses (Fukumoto et al., 1997). Moreover, since Akt is vital to glucose metabolism and cell survival (Franke et al., 1997), MGO elevation in diabetes might exacerbate hyperglycaemia and be attributed to accelerated aging (A. Dhar et al., 2011; Nicolay et al., 2006; Ramasamy et al., 2005).

L-arginine restored the MGO-inhibitory effect on iNOS expression (Figure 82), which takes support from a previous study that found that L-arginine serves as an MGO scavenger (I. Dhar et al., 2012). However, further studies, including those with HPLC, are required to prove the ability of L-arginine to scavenge MGO. As Schwedhelm et al. (2008) showed earlier, L-arginine (100µM) applied as such is within the normal plasma concentration (60–140µM). Those findings thus suggest the importance of L-arginine as a therapeutic option for diabetics, particularly given earlier results that L-arginine supplementation (3 × 2g/day) significantly improved antioxidants and NO release (Jabłecka et al., 2012). Other previous research has observed significant improvement in insulin sensitivity in T2DM patients when given 8.3g/day L-arginine a day, an outcome accompanied by improved glucose metabolism and antioxidant capacity (Lucotti et al., 2006). Such findings suggest the importance of MGO scavenging via L-arginine for diabetes patients, especially when MGO impairs insulin pharmacokinetic and pharmacodynamic parameters culminating in insulin resistance, endothelium dysfunction, and neuropathic pain, all of which are common complications in diabetes (A. Dhar et al., 2011; Eberhardt et al., 2012; S. Jia et al., 2006; Van Eupen et al., 2013). Endothelial dysfunction (Figure 49) was moreover suggested to contribute to exaggerated vasoconstriction (Fukao et al., 1997).

A primary acyclic unsaturated terpene alcohol found in essential oils of ginger and citrus fruits, geraniol was shown to counteract the exaggerated vasoconstriction induced by phenylephrine in diabetic rats, possibly by inhibiting VGCCs and receptors-operated calcium channels (El-Bassossy, Elberry, & Ghareib, 2016). In an earlier study, when quercetin

(50mg/day) was administered orally to STZ-adult male albino diabetic rats, it reduced the exaggerated phenylephrine-induced vasoconstriction, putatively due to the inhibitory effect of quercetin on proinflammatory mediators such as CRP (Mahmoud, Hassan, El Bassossy, & Fahmy, 2013). Therefore, geraniol and quercetin could provide essential therapeutic benefits to prevent vasoconstriction exaggerated by diabetes.

8.3. Association of STZ-induced diabetes and endothelial dysfunction

Muscarinic-induced vasodilation was significantly compromised in aortic rings and mesenteric arteries, as illustrated in Figures 49 and 50. Those findings correspond with a previous study's conclusion that the vascular dysfunction of STZ-diabetic rats is attributed to impaired muscarinic-induced endothelium-dependent vasodilation (Fukao et al., 1997). STZ-diabetic endothelial dysfunction, shown in Figures 49 and 58, correlated with the significant increase in serum MGO (Figure 43). Therefore, when nondiabetic aortic rings were incubated with MGO (100 μM) for 12 hours, carbachol-induced vasodilation was significantly impaired (Figure 52). That finding takes support from a previous study that found that MGO inhibits the phosphorylation of serine-1177 of eNOS and thereby reduces endothelial NO release (A. Dhar et al., 2010). Accordingly, MGO might play a major role in diabetic endothelial dysfunction (Brownlee, 2001). At the same time, L-arginine (100μM) restored endothelial function in the presence of MGO (100μM), as shown in Figure 52, and such improved endothelial function could be attributed L-arginine's ability to scavenge MGO (I. Dhar et al., 2012) and increase the L-arginine concentration required to improve the endothelial function. Indeed, a study with Sprague–Dawley rats showed a significant reduction in plasma L-arginine in STZ-diabetic rats (65μM) compared to control rats (190μM), which was accompanied with endothelial dysfunction (Pieper & Dondlinger, 1997).

As a consequence of diabetes, endothelial dysfunction is a common complication in which endothelium-dependent vasodilation is impaired and results in peripheral artery disease, foot ischemia, and ulceration and can even require amputation (A. Dhar et al., 2010; Ruiter et al., 2012). Therefore, and as previously mentioned, L-arginine (3 × 2g/day or 8.3g/day) might allow significant benefits toward improving common diabetes complications such as endothelial dysfunction (Jabłecka et al., 2012; Lucotti et al., 2006).

8.4. Association of STZ-induced diabetes and TRPV4

The deterioration in endothelium-dependent vasodilation characterised by impaired muscarinic-induced vasodilation (Figures 49 and 58) was in parallel with impaired TRPV4-induced vasodilation in both STZ-diabetic aortic and mesenteric arteries (Figures 53–55). Therefore, the concomitant muscarinic and TRPV4 impaired vasodilation reveals a possible mechanistic collaboration of muscarinic receptors and TRPV4 channels (Figures 22 and 23). Muscarinic and TRPV4 cascades might be integrated through GPCR-activated PLC, which hydrolyses membranous PIP2 into DAG and IP3, the latter of which binds to its corresponding smooth ER receptors, IP3-R, to facilitate Ca^{2+} release from cellular stores, as observed in endothelial M3 receptors (Clapham, 2003; Ying et al., 2014). Moreover, TRPV4 was activated by the muscarinic downstream cascade component of DAG-activated PKC binding (Rohacs & Nilius, 2007). TRPV4 mice KO studies have also revealed TRPV4's essential role in muscarinic-mediated endothelium-dependent vasodilation by way of a novel mechanism that involves 11, 12 EET-activated TRPV4, which activates BKCa to induce membrane hyperpolarisation and vasodilation (Earley et al., 2005; M. Freichel et al., 2005).

Fura-2 studies illustrated that nondiabetic aortic ECs treated with MGO (100 μM/day for 5 days) significantly suppressed TRPV4-elevated $[Ca^{2+}]i$ (Figure 67). Such a reduction in TRPV4-mediated $[Ca^{2+}]i$ elevation was similar to the reduction in STZ-diabetic ECs and significantly less than in naïve control ECs (Figure 67). Moreover, LSCM images illustrated similar TRPV4 downregulation in STZ-diabetic ECs and naïve ECs treated with MGO (100 μM/day for 5 days) compared to naïve control ECs' TRPV4 (Figures 69 and 70). Accordingly, MGO-induced TRPV4 downregulation and dysfunction in naïve ECs might explain the STZ-diabetic TRPV4 downregulation in ECs. By extension, chronic MGO elevation might perturb ER Ca^{2+} stores and culminate in protein misfolding and ER stress and, in turn, significant decreases in TRPV4 expression with MGO-based treatment (Figures 69 and 70).

Antioxidants such as L-arginine buffer the increased ROS produced by ERO1α to maintain the redox status of ER (Marciniak & Ron, 2006). Therefore, L-arginine might not only act as a scavenger for MGO, but also facilitate the maintenance of ER redox status and hence relieve ER stress induced by MGO-induced OS (Figure 67). Therefore, TRPV4 function might be restored when ECs are incubated with L-arginine in the presence of MGO (Figure 67). A previous study with 26 individuals showed that an L-arginine oral supplement (9g/day

for 6 months) improved endothelial function in the coronary artery, thereby suggesting L-arginine as a potential therapeutic option for improved endothelial function (Lerman, Burnett, Higano, McKinley, & Holmes, 1998).

TRPV4 expression in STZ-diabetic primary aortic ECs was reduced by approximately 50% (Figure 58 and 68), which might reveal TRPV4 endothelial dysfunction in diabetes attributable to TRPV4 downregulation. Primary aortic ECs' TRPV4 downregulation matches the findings of a recent study by Monaghan et al. (2015) which reported TRPV4 downregulation in diabetic retinal microvascular ECs. Previous studies have also showed that CAV-1 is an essential component in modulating TRPV4-induced vasodilation by modulating TRPV4 membrane localisation (Saliez et al., 2008). Indeed, a recent study showed that TRPV4 is co-localised with CAV-1 and SK3 in human ECs (Fritz et al., 2015). As shown in Figures 60 and 70, CAV-1 was significantly compromised by approximately 30% in STZ-diabetic aortic ECs.

HDL binds mainly on scavenger SR-BI, where it delivers circulating cholesterol to caveolae and thereby maintains caveolae integrity and enhances eNOS activity (Malerød et al., 2002; Thomas & Smart, 2008; Yuhanna et al., 2001). Reconstituted HDL infusion (80mg/kg IV for 4 hours) improved HDL concentration by twofold and significantly improved the acetylcholine-induced vasodilation measure through the forearm blood flow in hypercholesteraemic individuals (Spieker et al., 2002). Endothelial function was also significantly improved in parallel with insulin sensitivity and HDL profile in type 2 diabetic patients treated with the PPAR-γ agonist pioglitazone (30mg/day for 12 weeks) when compared to the placebo (Sourij, Zweiker, & Wascher, 2006). The PPAR-α agonist fibrates enhances the HDL profile and therefore could also be involved in improving endothelial function in diabetic patients (Staels et al., 1998).

Diabetic kidneys showed significant reduction in CAV-1 and eNOS when compared to nondiabetic ones (Komers et al., 2006). CAV-1 is co-localised with eNOS in bovine aortic ECs (H. Wang et al., 2009), and eNOS showed a similar distribution as TRPV4 and CAV-1 in naïve aortic ECs (Figures 58a3, 60a3, and 62a3), thereby revealing the co-localisation of those three essential elements in the plasma membrane of ECs. eNOS furthermore showed significant downregulation in STZ-diabetic aortic ECs (Figure 62 and 72). Diabetic-induced eNOS and CAV-1 downregulation might thus be attributed to the inhibited PI3K-Akt pathway since the PI3K inhibitor wortmannin inhibited eNOS and CAV-1 translocation to the

plasma membrane (H. Wang et al., 2009). HMG-CoA reductase inhibitor cerivastatin (0.15mg/day for 3 days) improved endothelial function by enhancing flow-induced vasodilation in elderly diabetics (Tsunekawa et al., 2001). Such endothelial function enhancement might be attributed to improved eNOS expression, since human saphenous vein ECs treated with ox-LDL (50mg/ml) showed significant endothelial dysfunction associated with eNOS mRNA and protein levels. However, simvastatin (1mM) and lovastatin (10mM) significantly enhanced eNOS expression by approximately fourfold, which was associated with improved endothelial function (Laufs et al., 1998).

When STZ-diabetic ECs were treated with insulin for 5 days, TRPV4 expression, distribution, and function improved significantly (Figures 58 and 68). Such TRPV4-restored expression and distribution were in parallel with CAV-1 (Figure 60c&d) and eNOS-restored expression and distribution (Figure 62c&d). As explained by H. Wang et al. (2009), insulin induces the PI3K/Akt pathway to stimulate eNOS and CAV-1 translocation toward the plasma membrane. It also induces eNOS and CAV-1 palmitoylation and thus translocation toward the plasma membrane (Hernando et al., 2006). At the same time, eNOS palmitoylation increased CAV-1 coupling by tenfold, a process that is required to optimise eNOS activity (Shaul et al., 1996).

Previous researchers have explored the importance of CAV-1 and TRPV4 co-localisation to maintain the TRPV4 Ca^{2+} influx required for EDHF and NO generation and potassium channel activation (Rath, Dessy, & Feron, 2009; Saliez et al., 2008; Serban et al., 2010). Therefore, TRPV4–CAV-1–eNOS co-localisation might provide a cooperative functional complex. ECs constitutively secrete NO through L-arginine oxidation via eNOS, which can be induced by blood flow shear stress (Cines et al., 1998; Lüscher & Barton, 1997). Increased blood shear stress activates membrane-bound PLA2, which generates AA from the membrane cholesterol followed by a series of reactions that generate EET, a direct TRPV4 activator (Inoue et al., 2009). Therefore, TRPV4 plays a pivotal role in regulating vascular tone and function by sustaining endothelium Ca^{2+} entry that induces NO, PG, and EDHF generation (Inoue et al., 2009; Serban et al., 2010; Watanabe et al., 2008).

L-NAME partially inhibited TRPV4-induced vasodilation (Figure 27), thereby demonstrating that NO is not the only vasodilation contributor in the aorta and that EDHF might provide an additional vasodilation pathway (Garland et al., 1995; McCulloch et al., 1997). Furthermore, elevated $[Ca^{2+}]_i$ as a consequence of TRPV4 activation activates Kca channels, especially

BKca, which induces endothelium hyperpolarisation, which is in turn propagated through gap junctions into VSMCs and vasodilation (Edwards et al., 2010).

The BKca blocker iberiotoxin (10nM) significant suppressed 4-αPDD-induced vasodilation (Figure 30), which supports what was concluded by Earley et al. (2005): that TRPV4 forms a signalling complex with BKca to generate VSMCs hyperpolarisation and vasodilation. Moreover, TRPV4 mediates Ca^{2+} influx through cooperative gating in MEPs that activate the BKca to exert VSM hyperpolarisation and, in turn, vasodilation (Bagher & Garland, 2014).

Since the removal of endothelium showed a significant reduction in TRPV4-induced vasodilation (Figure 33), TRPV4 has been suggested to induce vasodilation in endothelium-dependent and -independent ways (Bagher & Garland, 2014). ASMCs' TRPV4 expression was also studied, since TRPV4 showed partial endothelium-independent vasodilation (Figure 33), and aortic endothelial TRPV4 was downregulated in STZ-diabetic rats (Figures 58 and 59). A significant reduction in TRPV4 expression was shown in primary ASMCs (Figure 87), which suggests that TRPV4 downregulation contributes to the impairment of both endothelium-dependent and -independent TRPV4-induced vasodilation.

8.5. Lack of association between STZ-induced diabetes and TRPM8 dysfunction

Pre-contracted diabetic aortic rings became relaxed through icilin CRC without any significant difference from nondiabetic aortic rings (Figure 54). Fura-2 Ca^{2+} imaging studies did not show any significant difference in TRPM8-mediated $[Ca^{2+}]i$ elevation in primary ECs isolated from either naïve control or STZ-rats' ECs (Figure 72). These findings of unaffected TRPM8-induced vasodilation in diabetes stress promise in managing diabetic endothelial dysfunction, since the TRPM8 vasodilatory pathway seems to be NO-independent (Figure 28). Alternatively, NO-dependent TRPV4 and muscarinic vasodilatory pathways were affected in diabetes.

The co-expression of TRPM8 and TRPV4 channels in the aortic vasculature was concluded as novel Ca^{2+} entry pathways that might control systemic circulation (X. R. Yang et al., 2006). EDHF provides another vasodilation system in addition to NO and prostacyclin (Garland et al., 1995).

TRPM8-induced vasodilation was significantly compromised when BKca was blocked with iberiotoxin (1nM), as shown in Figure 31. Previous studies have concluded that

lysophosphatidylinositol is an extracellular mediator and intracellular messenger that affects numerous ion channels, including BKCa and TRPM8 (D. A. Andersson et al., 2007; Bondarenko et al., 2011a; Bondarenko et al., 2011b). Therefore, BKca might form a signalling complex with TRPM8 via lysophosphatidylinositol, which suggests that TRPM8, TRPV4, and muscarinic pathways might share BKca as a common vasodilatory downstream target in the vasculature.

TRPM8 and TRPV4 might act along different pathways. Muscarinic receptors are known to stimulate PLC, an enzyme that hydrolyses the membranous PIP2 into IP3 and DAG, by which IP3 is capable of activating TRPV4 and binding to endoplasmic reticulum's IP3-R to induce stored Ca^{2+} release and depletion (Everaerts et al., 2010). However, TRPM8 was activated through TRP-domain-bound PIP2; therefore, upon the activation of muscarinic pathways and subsequently TRPV4, TRPM8 might be inhibited since its cytoplasmic activator, PIP2 level, is reduced by way of PLC activation (B. Liu & Qin, 2005; Rohács et al., 2005). Therefore, endothelial TRPM8 might act chiefly as an inducer of hyperpolarisation, since it showed BKca-dependent and NO-independent vasodilation.

Some diabetic patients with polyneuropathy experience Raynaud's disease-like symptoms of compromised peripheral circulation and cyanotic skin, especially in the fingers (Fries, Shariat, von Wilmowsky, & Böhm, 2005). A previous study showed that transcutaneous nerve stimulation enhances the peripheral blood flow with a significant temperature rise from 24°C to approximately 34°C in T2DM patients (Kaada, 1982). A more recent study concluded that topical menthol gel (0.04–8.0%) showed a dose-dependent increase in skin blood flow in cutaneous microvasculature that was mediated by EDHF (Craighead & Alexander, 2016). At the same time, menthol and icilin clearly activate TRPM8 channels (D. A. Andersson et al., 2007). Since icilin-induced vasodilation and icilin-induced $[Ca^{2+}]i$ elevation are not significantly affected in diabetes, applying the TRPM8 agonist (i.e., menthol) peripherally might provide a therapeutic option for mitigating compromised peripheral circulation associated with diabetes.

8.6. Short-term effects of MGO-induced TRPM8-mediated vasodilation

NA-constricted aortic rings spontaneously relaxed when incubated with MGO (1 or 100 µM), as Figures 90 and 100 show. Furthermore, as Figure 94 shows, AMTB significantly counteracted the MGO-induced loss of contractility persistence, but not due to the removal of the endothelium. In support, r-TRPM8 FlexStation studies showed significant $[Ca^{2+}]i$

elevation in a time- and MGO dose-dependent manner (Figure 98). MGO-induced $[Ca^{2+}]i$ became significantly reduced through AMTB (5 and 10 µM) incubation (Figures 99, 101, and 103), thereby revealing TRPM8 as a possible target for MGO. Moreover, untransfected CHO cells showed a far smaller MGO-induced $[Ca^{2+}]i$ rise (Figures 100, 102, and 104) and, when incubated with AMTB (5 µM), showed a significant reduction in MGO-induced $[Ca^{2+}]i$ (Figure 100, 109, & 111). Previous studies revealed that TRPM8 channels might contribute to Ca^{2+} release from ER cellular stores, even by way of intracellular TRPM8-independent ER Ca^{2+} stores, though the topic requires further investigation (Mahieu et al., 2007; Thebault et al., 2005). Nevertheless, MGO might induce vasodilation through ECs Ca^{2+} pulsars that activate the MEPs' Kca (Bagher & Garland, 2014). Accordingly, in addition to showing its pathological role when elevated in diabetic serum, MGO might act as a redox-based cell signalling regulator (Chang et al., 2005; X. Jia & Wu, 2007).

8.7. Conclusion

This research has demonstrated that the STZ-induced diabetes model mimics several key features of diabetes in humans and is therefore an experimentally applicable and useful model of diabetes. It moreover revealed for the first time the downregulation of TRPV4 in association with CAV-1 and eNOS downregulation in primary diabetic ECs, thereby revealing a possible functional complex of TRPV4 and CAV-1 with eNOS, which is significantly impaired at several levels in diabetes and restored through insulin treatment. By contrast, TRPM8 does not seem to be part of the TRPV4, CAV-1, and eNOS functional complex and was thus not affected by diabetes or chronic MGO treatment.

This study is also the first to link hyperglycaemia with both MGO and ox-LDL elevation and to correlate MGO elevation with TRPV4 downregulation via an STZ-induced diabetes model for treating primary nondiabetic ECs with MGO ex vivo. It moreover for the first time demonstrated an MGO-induced loss of contractility persistence in a whole tissue model, which highlighted that MGO is a TRPM8 agonist and could be an acute MGO signalling function.

8.8. Future work

8.8.1. Immunoprecipitation of TRPV4, CAV-1 and eNOS in intact human blood vessels to translate the downregulation of these three protein found in STZ-diabetic rats.

8.8.2. Using CAV-1 knockout model (CAV-$1^{-/-}$), to investigate whether CAV-$1^{-/-}$ would influence the integrity of TRPV4 and eNOS in the endothelium.

8.8.3. RT-PCR analysis for TRPV4 expression to examine whether the TRPV4 downregulation is due to transcription, translational or post-translational alteration in diabetes.

8.8.4. Semi-carbazide sensitive amino oxidase (SSAO) is elevated in diabetics plasma, which is the responsible enzyme for the bioconversion of aminoacetone into MGO and H_2O_2 (Kalapos, 2013). Moreover, Uribarri et al. (2007) detected significant reduction in eNOS expression and activity which was associated with increased VCAM-1 expression when healthy volunteers ingested AGE. Additionally, AGE ingestion was shown to induce non-alcoholic steatohepatitis after 39 weeks that is detected through elevated AST and ALT (Patel et al., 2012). Moreover, Kalapos (2013) stated that 11% of glucose is metabolised through sorbitol pathway that involves aldose reductase product, acetal which is converted into MGO through CYP2E1, an enzyme which is highly elevated in diabetic endothelium, and hence exacerbates OS through inhibiting NADPH due to elevated acetone and aminoacetone derived MGO. Therefore, human and rat STZ- diabetic serum MGO concentration should be measured and correlated with SSAO, endothelial CYP2E1, eNOS and VCAM-1 in addition to hepatic aminotransferases. Accordingly, if either hepatic enzymes or both with CYP2E1 are elevated in diabetic serum, disulfiram or resveratrol (reversible inhibitor) and other CYP2E1 inhibitors herbal or chemical might be applied (topically or systemically) for reversing vascular or neuronal function (Piver, Berthou, Dreano, & Lucas, 2001).

8.8.5. Since fructose is MGO precursor (H. Wang, Meng, Chang, & Wu, 2006), therefore, fructose might be responsible for AGE formation and accumulation, eNOS, VCAM-1, SSAO and CYP2E1 should be monitored for human volunteers (or rats) ingesting fructose or sucrose compared to other ingesting only glucose, since R. J. Johnson et al. (2009) stated that 1mM fructose concentration pc (After

meal) causes significant endothelial [ATP] decline that might be progressed to OS and ischemia.

8.8.6. S. Jia et al. (2006) concluded that insulin is structurally altered when incubated with MGO that is culminated with influence insulin pharmacodynamics and pharmacokinetic properties and hence yielding insulin resistance. Therefore, comparing insulin structure between T2D, obese and healthy individuals might be another good notion to investigate the possibility of freeing insulin from the MGO or other ROS that yields insulin molecular alteration.

8.8.7. Examine the effect of metformin on cell culture and tissues incubated with MGO or insulin (fat or muscular cells), in the presence of (high glucose concentration; mimicking diabetes) which should enhance the influx of glucose and possibly MGO formation. However, since TRPV4 was significantly reversed through insulin treatment, metformin-enhanced tissue insulin sensitivity might provide beneficial outcomes in diabetic vasculature.

References:

Aarts, M., Iihara, K., Wei, W.-L., Xiong, Z.-G., Arundine, M., Cerwinski, W., . . . Tymianski, M. (2003). A key role for TRPM7 channels in anoxic neuronal death. *Cell, 115*(7), 863-877.

AbouAlaiwi, W. A., Takahashi, M., Mell, B. R., Jones, T. J., Ratnam, S., Kolb, R. J., & Nauli, S. M. (2009). Ciliary polycystin-2 is a mechanosensitive calcium channel involved in nitric oxide signaling cascades. *Circulation Research, 104*(7), 860-869.

Adachi, T., Weisbrod, R. M., Pimentel, D. R., Ying, J., Sharov, V. S., Schöneich, C., & Cohen, R. A. (2004). S-Glutathiolation by peroxynitrite activates SERCA during arterial relaxation by nitric oxide. *Nature Medicine, 10*(11), 1200-1207.

Adak, S., Wang, Q., & Stuehr, D. J. (2000). Arginine Conversion to Nitroxide by Tetrahydrobiopterin-free Neuronal Nitric-oxide Synthase IMPLICATIONS FOR MECHANISM. *Journal of Biological Chemistry, 275*(43), 33554-33561.

Akbarzadeh, A., Norouzian, D., Mehrabi, M. R., Jamshidi, S., Farhangi, A., Verdi, A. A., . . . Rad, B. L. (2007). Induction of diabetes by Streptozotocin in rats. *Indian Journal of Clinical Biochemistry, 22*(2), 60-64. doi:10.1007/BF02913315

Alessandri-Haber, N., Yeh, J. J., Boyd, A. E., Parada, C. A., Chen, X., Reichling, D. B., & Levine, J. D. (2003). Hypotonicity Induces TRPV4-Mediated Nociception in Rat. *Neuron, 39*(3), 497–511. doi:10.1016/S0896-6273(03)00462-8

Alp, N. J., Mussa, S., Khoo, J., Cai, S., Guzik, T., Jefferson, A., . . . Channon, K. M. (2003). Tetrahydrobiopterin-dependent preservation of nitric oxide–mediated endothelial function in diabetes by targeted transgenic GTP–cyclohydrolase I overexpression. *The Journal of clinical investigation, 112*(5), 725-735.

American Diabetes Association. (2012). Diagnosis and Classification of Diabetes Mellitus. *Diabetes Care, 35*(1), S64-S71. doi:10.2337/dc12-s064

American Diabetes Association. (2016). Classification and Diagnosis of Diabetes. *Diabetes Care, 39*(1), S13-S22. doi:10.2337/dc16-S005

Andersson, D. A., Nash, M., & Bevan, S. (2007). Modulation of the Cold-Activated Channel TRPM8 by Lysophospholipids and Polyunsaturated Fatty Acids. *The Journal of Neuroscience, 27*(12), 3347-3355. doi:10.1523/JNEUROSCI.4846-06.2007

Andersson, M., Okeyo, G., Wilson, D., Keizer, H., Moe, P., Blount, P., . . . Duran, R. S. (2007). Voltage-induced gating of the mechanosensitive MscL ion channel reconstituted in a tethered lipid bilayer membrane. *Biosensors and Bioelectronics, 23*(6), 919-923. doi:10.1016/j.bios.2007.09.014

Arkhammar, P., Nilsson, T., Rorsman, P., & Berggren, P. (1987). Inhibition of ATP-regulated K+ channels precedes depolarization-induced increase in cytoplasmic free Ca2+ concentration in pancreatic beta-cells. *Journal of Biological Chemistry, 262*(12), 5448-5454.

Arnal, J. F., Dinh-Xuan, A. T., Pueyo, M., Darblade, B., & Rami, J. (1999). Endothelium-derived nitric oxide and vascular physiology and pathology. *Cell. Mol. Life Sci., 55*, 1078–1087.

Arner, P., & Langin, D. (2014). Lipolysis in lipid turnover, cancer, cachexia, and obesity-induced insulin resistance. *Trends in endocrinology and metabolism, 25*(5), 255-262. doi:10.1016/j.tem.2014.03.002

Ashcroft, F. M., Harrison, D. E., & Ashcroft, S. J. (1984). Glucose induces closure of single potassium channels in isolated rat pancreatic β-cells. *Nature, 312*(5993), 446-448.

Ashcroft, F. M., & Rorsman, P. (2012). Diabetes mellitus and β-cells: the last ten years. *Cell, 148*, 1160-1171. doi:10.1016/j.cell.2012.02.010

Bagher, P., Beleznai, T., Kansui, Y., Mitchell, R., Garland, C. J., & Dora, K. A. (2012). Low intravascular pressure activates endothelial cell TRPV4 channels, local Ca2+ events, and IKCa channels, reducing arteriolar tone. *PNAS, 109*(44), 18174–18179. doi:10.1073/pnas.1211946109

Bagher, P., & Garland, C. J. (2014). Scaffolding Builds to Reduce Blood Pressure. *Science Signaling, 7*(333), 1-3. doi:10.1126/scisignal.2005527

Bagri, P., Ali, M., Aeri, V., Bhowmik, M., & Sultana, S. (2009). Antidiabetic effect of Punica granatum flowers: Effect on hyperlipidemia, pancreatic cells lipid peroxidation and antioxidant enzymes in experimental diabetes. *Food and Chemical Toxicology, 47*(1), 50-54. doi:10.1016/j.fct.2008.09.058

Bainor, A., Chang, L., McQuade, T. J., Webb, B., & Gestwicki, J. E. (2011). Bicinchoninic acid (BCA) assay in low volume. *Analytical Biochemistry, 410*(2), 310-312. doi:10.1016/j.ab.2010.11.015

Bakker, W., Eringa, E. C., Sipkema, P., & van Hinsbergh, V. W. M. (2009). Endothelial dysfunction and diabetes: roles of hyperglycemia, impaired insulin signaling and obesitY. *Cell and Tissue Research, 335*(1), 165–189. doi:10.1007/s00441-008-0685-6

Banning, M. (2005). The carcinogenic and protective effects of food. *British Journal of Nursing, 14*(20), 1070-1074.

Battle, T., Arnal, J. F., Challah, M., & Michel, J. B. (1994). Selective isolation of rat aortic wall layers and their cell types in culture—Application to converting enzyme activity measurement. *Tissue and Cell, 26*(6), 943-955. doi:10.1016/0040-8166(94)90043-4

Baylie, R. L., & Brayden, J. E. (2011). TRPV channels and vascular function. *Acta Physiologica, 203*(1), 99-116. doi:10.1111/j.1748-1716.2010.02217.x

Begum, N., & Ragolia, L. (2000). High glucose and insulin inhibit VSMC MKP-1 expression by blocking iNOS via p38 MAPK activation. *American Journal of Physiology - Cell Physiology, 278*(1), C81-C91.

Benemei, S., De Cesaris, F., Fusi, C., Rossi, E., Lupi, C., & Geppetti, P. (2013). TRPA1 and other TRP channels is migraine. *The Journal of Headache and Pain, 14*(71), 1-8. doi:10.1186/1129-2377-14-71

Benham, C. D., Davis, J. B., & Randall, A. D. (2002). Vanilloid and TRP channels: a family of lipid-gated cation channels. *Neuropharmacology, 42*(7), 873-888. doi:10.1016/S0028-3908(02)00047-3

Bennett, B. L., Satoh, Y., & Lewis, A. J. (2003). JNK: a new therapeutic target for diabetes. *Current opinion in pharmacology, 3*(4), 420-425.

Bergdahl, A., Gomez, M. F., Dreja, K., Xu, S.-Z., Adner, M., Beech, D. J., . . . Swärd, K. (2003). Cholesterol depletion impairs vascular reactivity to endothelin-1 by reducing store-operated Ca2+ entry dependent on TRPC1. *Circulation Research, 93*(9), 839-847.

Bhonsle, H. S., Korwar, A. M., Kote, S. S., Golegaonkar, S. B., Chougale, A. D., Shaik, M. L., . . . Kulkarni, M. J. (2012). Low Plasma Albumin Levels Are Associated with Increased Plasma Protein Glycation and HbA1c in Diabetes. *J. Proteome Res., 11*(2), 1391–1396. doi:10.1021/pr201030m

Bierhaus, A., Flemin, T., Stoyanov, S., Leffler, A., Babes, A., Neacsu, C., . . . Nawroth, P. P. (2012). Methylglyoxal modification of Nav1.8 facilitates nociceptive neuron firing and causes hyperalgesia in diabetic neuropathy. *Nature Medicine*, 1-9. doi:10.1038/nm.2750

Blair, A., Shaul, P. W., Yuhanna, I. S., Conrad, P. A., & Smart, E. J. (1999). Oxidized Low Density Lipoprotein Displaces Endothelial Nitric-oxide Synthase (eNOS) from Plasmalemmal Caveolae and Impairs eNOS Activation. *The Journal of Biological Chemistry, 274*, 32512-32519. doi:10.1074/jbc.274.45.32512

Boese, M., Busse, R., Miilsch, A., & Kerth, V. S. (1996). Effect ofcyclic GMP-dependent vasodilators on the expression of inducible nitric oxide synthase in vascular smooth muscle cells: role of cyclic AMP. *British Journal of Pharmacology, 19*(4), 707-715. doi:10.1111/j.1476-5381.1996.tb15730.x

Böger, R. H. (2004). Asymmetric dimethylarginine, an endogenous inhibitor of nitric oxide synthase, explains the “L-arginine paradox” and acts as a novel cardiovascular risk factor. *The Journal of nutrition, 134*(10), 2842S-2847S.

Bondarenko, A. I., Malli, R., & Graier, W. F. (2011a). The GPR55 agonist lysophosphatidylinositol acts as an intracellular messenger and bidirectionally modulates Ca2+-activated large-conductance K+ channels in endothelial cells. *Eur J Physiol, 461*(1), 177-189. doi:10.1007/s00424-010-0898-x

Bondarenko, A. I., Malli, R., & Graier, W. F. (2011b). The GPR55 agonist lysophosphatidylinositol directly activates intermediate-conductance Ca2+-activated K+ channels. *Eur J Physiol, 462*(2), 245-255. doi:10.1007/s00424-011-0977-7

Boomsma, F., van den Meiracker, A. H., Winkel, S., Aanstoot, H. J., R., B. M., Man in 't Veld, A. J., & Bruining, G. J. (1999). Circulating semicarbazide-sensitive amine oxidase is raised both in Type I (insulin-dependent), in Type II (non-insulin-dependent) diabetes mellitus and even in childhood Type I diabetes at first clinical diagnosis. *Diabetologia, 42*(2), 233-237.

Bootman, M. D., Berridge, M. J., & Roderick, H. L. (2002). Calcium signalling: more messengers, more channels, more complexity. *Current Biology, 12*(16), R563–R565. doi:10.1016/S0960-9822(02)01055-2

Brownlee, M. (2001). Biochemistry and molecular cell biology of diabetic complications. *Nature, 414*(813-820). doi:10.1038/414813a

Bugrim, A. (1999). Regulation of Ca 2+ release by cAMP-dependent protein kinase A mechanism for agonist-specific calcium signaling? *Cell Calcium, 25*(3), 219-226.

Butler, A. E., Janson, J., Bonner-Weir, S., Ritzel, R., Rizza, R. A., & Butler, P. C. (2003). B-Cell Deficit and Increased B-Cell Apoptosis in Humans With Type 2 Diabetes. *Diabetes, 52*(1), 102-110. doi:10.2337/diabetes.52.1.102

Buxton, I. L., Cheek, D. J., Eckman, D., Westfall, D. P., Sanders, K. M., & Keef, K. D. (1993). NG-nitro L-arginine methyl ester and other alkyl esters of arginine are muscarinic receptor antagonists. *Circulation Research, 72*, 387-395. doi:10.1161/01.RES.72.2.387

Callera, G. E., He, Y., Yogi, A., Montezano, A. C., Paravicini, T., Yao, G., & Touyz, R. M. (2009). Regulation of the novel Mg2+ transporter transient receptor potential melastatin 7 (TRPM7) cation channel by bradykinin in vascular smooth muscle cells. *Journal of hypertension, 27*(1), 155-166.

Caterina, M. J., Rosen, T. A., Tominaga, M., Brake, A. J., & Julius, D. (1999). A capsaicin-receptor homologue with a high threshold for noxious heat. *Nature, 398*(6726), 436-441.

Cavusoglu, E., Ruwende, C., Chopr, V., Poludasu, S., Yanamadala, S., Frishman, W. H., . . . Marmur, J. D. (2010). Relation of baseline plasma ADMA levels to cardiovascular morbidity and mortality at two years in men with diabetes mellitus referred for coronary angiography. *Atherosclerosis, 210*(1), 226-231. doi:10.1016/j.atherosclerosis.2009.10.034

Chang, T., Wang, R., & Wu, L. (2005). Methylglyoxal-induced nitric oxide and peroxynitrite production in vascular smooth muscle cells. *Free Radical Biology and Medicine, 38*(2), 286-293. doi:10.1016/j.freeradbiomed.2004.10.034

Chao, E. C., & Henry, R. R. (2010). SGLT2 inhibition — a novel strategy for diabetes treatment. *Nature Reviews Drug Discovery, 9*, 551-559. doi:10.1038/nrd3180

Chataigneau, T., Félétou, M., Huang, P. L., Fishman, M. C., Duhault, J., & Vanhoutte, P. M. (1999). Acetylcholine-induced relaxation in blood vessels from endothelial nitric oxide synthase knockout mice. *British Journal of Pharmacology, 126*(1), 219-226.

Chen, C. W., Corselli, M., Peault, B., & Huard, J. (2012). Human Blood-Vessel-Derived Stem Cells for Tissue Repair and Regeneration. *Journal of Biomedicine and Biotechnology, 2012*, 1-9. doi:10.1155/2012/597439

Chen, G., Suzuki, H., & Weston, A. H. (1988). Acetylcholine releases endothelium-derived hyperpolarizing factor and EDRF from rat blood vessels. *British Journal of Pharmacology, 95*(4), 1165-1174.

Christensen, A. P., & Corey, D. P. (2007). TRP channels in mechanosensation: direct or indirect activation? *Nature, 8*, 510-521. doi:10.1038/nrn2149

Cines, D. B., Pollak, E. S., Buck, C. A., Loscalzo, J., Zimmerman, G. A., McEver, R. P., . . . Stern, D. M. (1998). Endothelial Cells in Physiology and in the Pathophysiology of Vascular Disorders. *The Journal of The American Society of Hematology, 91*(10), 3527-3561.

Clapham, D. E. (2003). TRP channels as cellular sensors. *Nature, 426*, 517-524. doi:10.1038/nature02196

Clapp, L. H., Turcato, S., Hall, S., & Baloch, M. (1998). Evidence that Ca 2+-activated K+ channels play a major role in mediating the vascular effects of iloprost and cicaprost. *European Journal of Pharmacology, 356*(2), 215-224.

Clark, K., Middelbeek, J., Morrice, N. A., Figdor, C. G., Lasonder, E., & van Leeuwen, F. N. (2008). Massive autophosphorylation of the Ser/Thr-rich domain controls protein kinase activity of TRPM6 and TRPM7. *PLoS ONE, 3*(3), e1876.

Cohen, R. A., Weisbrod, R. M., Gericke, M., Yaghoubi, M., Bierl, C., & Bolotina, V. M. (1999). Mechanism of nitric oxide–induced vasodilatation refilling of intracellular stores by sarcoplasmic reticulum Ca2+ ATPase and inhibition of store-operated Ca2+ influx. *Circulation Research, 84*(2), 210-219.

Coneski, P. N., & Schoenfisch, M. H. (2012). Nitric oxide release: Part III. Measurement and reporting. *Chem. Soc. Rev., 41*(10), 3753-3758. doi:10.1039/c2cs15271a

Craighead, D. H., & Alexander, L. M. (2016). Topical menthol increases cutaneous blood flow. *Microvascular Research*, 1-31. doi:10.1016/j.mvr.2016.04.010

Cuevas, S., Yang, Y., Upadhyay, K., Armando, I., & Jose, P. (2014). Dopamine D2 receptors regulate leptin and IL-6 in 3T3 L1 adipocytes (1107.5). *The FASEB Journal, 28*(1 Supplement), 1107.1105.

Davies, M., Brophy, S., Williams, R., & Taylor, A. (2006). The Prevalence, Severity, and Impact of Painful Diabetic Peripheral Neuropathy in Type 2 Diabetes. *Diabetes Care, 29*(7), 1518-1522. doi:10.2337/dc05-2228

Davies, M. G., & Hagen, P. O. (1993). The Vascular Endothelium. *Annals of Surgery, 218*(5), 593-609.

Davis, J. B., Gray, J., Gunthorpe, M. J., Hatcher, J. P., Davey, P. T., Overend, P., . . . Sheardown, S. A. (2000). Vanilloid receptor-1 is essential for infammatory thermal hyperalgesia. *Nature, 405*, 183-187. doi:10.1038/35012076

de la Garza-Rodea, A. S., Knaän-Shanzer, S., den Hartigh, J. D., Verhaegen, A. P. L., & van Bekkum, D. W. (2010). Anomer-Equilibrated Streptozotocin Solution for the Induction of Experimental Diabetes in Mice (Mus musculus). *J Am Assoc Lab Anim Sci., 49*(1), 40-44.

Del Guerra, S., Lupi, R., Marselli, L., Masini, M., Bugliani, M., Sbrana, S., . . . Marchetti, P. (2005). Functional and Molecular Defects of Pancreatic Islets in Human Type 2 Diabetes. *Diabetes, 54*(3), 727-735. doi:10.2337/diabetes.54.3.727

Delmas, P., Nauli, S. M., Li, X., Coste, B., Osorio, N., Crest, M., . . . Zhou, J. (2004). Gating of the polycystin ion channel signaling complex in neurons and kidney cells. *The FASEB Journal, 18*(6), 740-742.

Desai, B. N., & Clapham, D. E. (2005). TRP channels and mice deficient in TRP channels. *Eur J Physiol, 451*(1), 11-18. doi:10.1007/s00424-005-1429-z

Desbuquois, B., Tozzo, E., Collinet, M., Lopez, S., Bortoli, S., & Amessou, M. (1993). Regulation of insulin receptor expression and its gene. *Ann Endocrinol (Paris), 54*(6), 373-384.

Dhar, A., Desai, K., Kazachmov, M., Yu, P., & Wu, L. (2008). Methylglyoxal production in vascular smooth muscle cells from different metabolic precursors. *Metabolism, 57*(9), 1211-1220.

Dhar, A., Dhar, I., Desai, K. M., & Wu, L. (2010). Methylglyoxal scavengers attenuate endothelial dysfunction induced by methylglyoxal and high concentrations of glucose. *British Journal of Pharmacology, 161*, 1843–1856. doi:10.1111/j.1476-5381.2010.01017.x

Dhar, A., Dhar, I., Jiang, B., Desai, K. M., & Wu, L. (2011). Chronic methylglyoxal infusion by minipump causes pancreatic β-cell dysfunction and induces type 2 diabetes in Sprague-Dawley rats. *Diabetes, 60*, 899-908. doi:10.2337/db10-0627

Dhar, I., Dhar, A., Wu, L., & Desai, K. (2012). Arginine Attenuates Methylglyoxal- and High Glucose-Induced Endothelial Dysfunction and Oxidative Stress by an Endothelial Nitric-Oxide Synthase-Independent Mechanism. *The Journal of Pharmacology and Experimental Therapeutics, 342*(1), 196-204. doi:10.1124/jpet.112.192112

DiabetesUK. (2014). Diabetes: Facts and Stats. *Diabetes UK, 3*, 1-21.

Dietrich, A., y Schnitzler, M. M., Emmel, J., Kalwa, H., Hofmann, T., & Gudermann, T. (2003). N-linked protein glycosylation is a major determinant for basal TRPC3 and TRPC6 channel activity. *Journal of Biological Chemistry, 278*(48), 47842-47852.

Dietrich, A., y Schnitzler, M. M., Gollasch, M., Gross, V., Storch, U., Dubrovska, G., . . . Kalwa, H. (2005). Increased vascular smooth muscle contractility in TRPC6−/− mice. *Molecular and cellular biology, 25*(16), 6980-6989.

Ding, Y., Gonick, H. C., & Vaziri, N. D. (2000). Lead promotes hydroxyl radical generation and lipid peroxidation in cultured aortic endothelial cells. *Am J Hypertens, 13*(5), 552-555. doi:10.1016/S0895-7061(99)00226-5

Dolman, D., Drndarski, S., Abbott, N. J., & Rattray, M. (2004). Induction of aquaporin 1 but not aquaporin 4 messenger RNA in rat primary brain microvessel endothelial cells in culture. *Journal of Neurochemistry, 93*(4), 825-833. doi:10.1111/j.1471-4159.2005.03111.x

Dong, H., Waldron, G. J., Cole, W. C., & Triggle, C. R. (1998). Roles of calcium-activated and voltage-gated delayed rectifier potassium channels in endothelium-dependent vasorelaxation of the rabbit middle cerebral artery. *British Journal of Pharmacology, 123*(5), 821-832.

Dora, K. A., Hinton, J. M., Walker, S. D., & Garland, C. J. (2000). An indirect influence of phenylephrine on the release of endothelium-derived vasodilators in rat small mesenteric artery. *Br J Pharmacol., 129*(2), 381-387. doi:10.1038/sj.bjp.0703052

Dragoni, I., Guida, E., & McIntyre, P. (2006). The cold and menthol receptor TRPM8 contains a functionally important double cysteine motif. *The Journal of Biological Chemistry, 281*(49), 37353-37360. doi:10.1074/jbc.M607227200

Duncan, L. M., Deeds, J., Hunter, J., Shao, J., Holmgren, L. M., Woolf, E. A., . . . Shyjan, A. W. (1998). Down-regulation of the novel gene melastatin correlates with potential for melanoma metastasis. *Cancer Research, 58*(7), 1515-1520.

Dyer, D. G., Dunn, J. A., Thorpe, S. R., Bailie, K. E., Lyons, T. J., McCance, D. R., & Baynes, J. W. (1993). Accumulation of Maillard reaction products in skin collagen in diabetes and aging. *J Clin Invest, 91*(6), 2463-2469. doi:10.1172/JCI116481

Earley, S. (2010). Vanilloid and melastatin transient receptor potential channels in vascular smooth muscle. *Microcirculation, 17*(4), 237-249.

Earley, S., Gonzales, A. L., & Garcia, Z. I. (2010). A dietary agonist of transient receptor potential cation channel V3 elicits endothelium-dependent vasodilation. *Molecular pharmacology, 77*(4), 612-620.

Earley, S., Heppner, T. J., Nelson, M. T., & Brayden, J. E. (2005). TRPV4 forms a novel Ca2+ signaling complex with ryanodine receptors and BKCa channels. *Circulation Research, 97*, 1270-1279. doi:10.1161/01.RES.0000194321.60300.d6

Earley, S., Pauyo, T., Drapp, R., Tavares, M. J., Liedtke, W., & Brayden, J. E. (2009). TRPV4-dependent dilation of peripheral resistance arteries influences arterial pressure. *American Journal of Physiology, 297*(3), H1096-H1102. doi:10.1152/ajpheart.00241.2009

Earley, S., Waldron, B. J., & Brayden, J. E. (2004). Critical role for transient receptor potential channel TRPM4 in myogenic constriction of cerebral arteries. *Circulation Research, 95*(9), 922-929.

Eberhardt, M. J., Filipovic, M. R., Leffler, A., De la Roche, J., Kistner, K., Fischer, M. J., . . . Sauer, S. K. (2012). Methylglyoxal activates nociceptors through transient receptor potential A1 (TRPA1): a possible mechanism of metabolic neuropathies. *JBC, 287*(34), 28291-28306. doi:10.1074/jbc.M111.328674

Edwards, G., Félétou, M., & Weston, A. H. (2010). Endothelium-derived hyperpolarising factors and associated pathways: a synopsis. *Eur J Physiol, 459*(6), 863-879. doi:10.1007/s00424-010-0817-1

El-Bassossy, H. M., Elberry, A. A., & Ghareib, S. A. (2016). Geraniol improves the impaired vascular reactivity in diabetes and metabolic syndrome through calcium channel blocking effect. *Journal of Diabetes and Its Complications*, 1-9. doi:10.1016/j.jdiacomp.2016.04.006

Elsner, M., Guldbakke, B., Tiedge, M., Munday, R., & Lenzen, S. (2000). Relative importance of transport and alkylation for pancreatic beta-cell toxicity of streptozotocin. *Diabetologia, 43*(12), 1528-1533. doi:10.1007/s001250051564

Everaerts, W., Nilius, B., & Owsianik, G. (2010). The vanilloid transient receptor potential channel TRPV4: from structure to disease. *Progress in Biophysics and Molecular Biology, 103*(1), 2-17. doi:10.1016/j.pbiomolbio.2009.10.002

Federici, M., Pandolfi, A., De Filippis, E. A., Pellegrini, G., Menghini, R., Lauro, D., . . . Consoli, A. (2004). G972R IRS-1 Variant Impairs Insulin Regulation of Endothelial Nitric Oxide Synthase in Cultured Human Endothelial Cells. *Circulation, 109*(3), 399-405. doi:10.1161/01.CIR.0000109498.77895.6F

Ferguson, K. M., Lemmon, M. A., Schlessinger, J., & Sigler, P. B. (1995). Structure of the high affinity complex of inositol trisphosphate with a phospholipase C pleckstrin homology domain. *Cell, 83*(6), 1037-1046.

Fina, L., Molgaard, H. V., Robertson, D., Bradley, N. J., Monaghan, P., Delia, D., . . . Greaves, M. F. (1990). Expression of the CD34 gene in vascular endothelial cells. *Blood, 75*(12), 2417-2426.

Fleming, I., Rueben, A., Popp, R., Fisslthaler, B., Schrodt, S., Sander, A., . . . Hammock, B. D. (2007). Epoxyeicosatrienoic acids regulate Trp channel–dependent Ca2+ signaling and hyperpolarization in endothelial cells. *Arteriosclerosis, Thrombosis, and Vascular Biology, 27*(12), 2612-2618.

Föller, M., Huber, S. M., & Lang, F. (2008). Erythrocyte programmed cell death. *IUBMB Life, 60*(10), 661-668. doi:10.1002/iub.106

Frank, P. G., Woodman, S. E., Park, D. S., & Lisanti, M. P. (2003). Caveolin, Caveolae, and Endothelial Cell Function. *Arteriosclerosis, Thrombosis, and Vascular Biology, 23*, 1161-1168. doi:10.1161/01.ATV.0000070546.16946.3A

Franke, T. F., Kaplan, D. R., & Cantley, L. C. (1997). PI3K: Downstream AKTion Blocks Apoptosis. *Cell, 88*(4), 435–437. doi:10.1016/S0092-8674(00)81883-8

Freichel, M., Suh, S. H., Pfeifer, A., Schweig, U., Trost, C., Weißgerber, P., . . . Droogmans, G. (2001). Lack of an endothelial store-operated Ca2+ current impairs agonist-dependent vasorelaxation in TRP4−/− mice. *Nature cell biology, 3*(2), 121-127.

Freichel, M., Vennekens, R., Olausson, J., Stolz, S., Philipp, S. E., Weißgerber, P., & Flockerzi, V. (2005). Functional role of TRPC proteins in native systems: implications from knockout and knock-down studies. *tHe Journal of Physiology, 567*(1), 59-66. doi:10.1113/jphysiol.2005.092999

Fries, R., Shariat, K., von Wilmowsky, H., & Böhm, M. (2005). Sildenafil in the Treatment of Raynaud's Phenomenon Resistant to Vasodilatory Therapy. *Circulation, 112*, 2980-2985. doi:10.1161/CIRCULATIONAHA.104.523324

Fritz, S. G., Kaistha, A., Kacik, M., Markert, S., Hofmeister, A., Busch, C., . . . Hoyer, J. (2015). Evidence for functional and dynamic microcompartmentation of Cav-1/TRPV4/KCa in caveolae of endothelial cells. *European Journal of Cell Biology, 94*(7-9), 391-400. doi:10.1016/j.ejcb.2015.06.002

Fukao, M., Hattori, Y., Kanno, M., Sakuma, I., & Kitabatake, A. (1997). Alterations in endothelium-dependent hyperpolarization and relaxation in mesenteric arteries from streptozotocin-induced diabetic rats. *British Journal of Pharmacology, 121*(7), 1383-1391.

Fukumoto, Y., Shimokawa, H., Kozai, T., Kadokami, T., Kuwata, K., Yonemitsu, Y., . . . Takeshita, A. (1997). Vasculoprotective Role of Inducible Nitric Oxide Synthase at Inflammatory Coronary Lesions Induced by Chronic Treatment With Interleukin-1β in Pigs in Vivo. *Circulation, 96*, 3104-3111. doi:10.1161/01.CIR.96.9.3104

Furchgott, R. F., & Zawadzki, J. V. (1980). The obligatory role of endothelial cells in the relaxation of arterial smooth muscle by acetylcholine. *Nature, 288*(5789), 373-376.

Galley, H. F., & Webster, N. R. (2004). Physiology of the endothelium. *British Journal of Anaesthesia, 93*(1), 105-113. doi:10.1093/bja/aeh163

Garland, C. J., Hiley, C. R., & Dora, K. A. (2010). EDHF: spreading the influence of the endothelium. *Br J Pharmacol., 164*(3), 839–852. doi:10.1111/j.1476-5381.2010.01148.x

Garland, C. J., Plane, F., Kemp, B. K., & Cocks, T. M. (1995). Endothelium-dependent hyperpolarization: a role in the control of vascular tone. *TRENDS in Pharmacological Sciences, 16*(1), 23-30. doi:0.1016/S0165-6147(00)88969-5

Garland, C. J., & Weston, A. H. (2011). The vascular endothelium: still amazing us 30 years on. *Br J Pharmacol., 164*(3), 837-838. doi:10.1111/j.1476-5381.2011.01611.x

Goldberg, T., Cai, W., Peppa, M., Dardaine, V., Baliga, B. S., Uribarri, J., & Vlassara, H. (2004). Advanced Glycoxidation End Products in Commonly Consumed Foods. *Journal of the American Dietetic Association, 104*(8), 1287–1291. doi:10.1016/j.jada.2004.05.214

Gonzales, A. L., Garcia, Z. I., Amberg, G. C., & Earley, S. (2010). Pharmacological inhibition of TRPM4 hyperpolarizes vascular smooth muscle. *American Journal of Physiology-Cell Physiology, 299*(5), C1195-C1202.

Goy, A. S., & Psaltis, D. (2012). Digital confocal microscope. *Optics Express, 20*(20), 22720-22727. doi:10.1364/OE.20.022720

Gray, G. A., Schott, C., Julou-Schaeffer, G., Fleming, I., Parratt, J. R., & Stoclet, J. C. (1991). The effect of inhibitors of the l-arginine/nitric oxide pathway on endotoxin-induced loss of vascular responsiveness in anaesthetized rats. *British Journal of Pharmacology, 103*(1), 1218-1224.

Greka, A., Navarro, B., Oancea, E., Duggan, A., & Clapham, D. E. (2003). TRPC5 is a regulator of hippocampal neurite length and growth cone morphology. *Nature Neuroscience, 6*(8), 837-845.

Griffith, T. M., Chaytor, A. T., Taylor, H. J., Giddings, B. D., & Edwards, D. H. (2002). cAMP facilitates EDHF-type relaxations in conduit arteries by enhancing electrotonic conduction via gap junctions. *Proceedings of the National Academy of Sciences, 99*(9), 6392-6397.

Grimm, C., Kraft, R., Sauerbruch, S., Schultz, G., & Harteneck, C. (2003). Molecular and functional characterization of the melastatin-related cation channel TRPM3. *Journal of Biological Chemistry, 278*(24), 21493-21501.

Guzik, T. J., Mussa, S., Gastaldi, D., Sadowski, J., Ratnatunga, C., Pillai, R., & Channon, K. M. (2002). Mechanisms of increased vascular superoxide production in human diabetes mellitus Role of NAD (P) H oxidase and endothelial nitric oxide synthase. *Circulation, 105*(14), 1656-1662.

Hall, S., Turcato, S., & Clapp, L. (1996). Abnormal Activation of K+Channels Underlies Relaxation to Bacterial Lipopolysaccharide in Rat Aorta. *Biochemical and Biophysical Research Communications, 224*(1), 184-190. doi:10.1006/bbrc.1996.1005

Hammes, H. P., Du, X., Edelstein, D., Taguchi, T., Matsumura, T., Ju, Q., . . . Brownlee, M. (2003). Benfotiamine blocks three major pathways of hyperglycemic damage and prevents experimental diabetic retinopathy. *Nature Medicine, 9*(3), 294-299. doi:10.1038/nm834

Harden, N., & Cohen, M. (2003). Unmet Needs in the Management of Neuropathic Pain. *Journal of Pain and Symptom Management, 25*(5), S12–S17. doi:10.1016/S0885-3924(03)00065-4

Harja, E., Bu, D.-x., Hudson, B. I., Chang, J. S., Shen, X., Hallam, K., . . . Oruganti, S. (2008). Vascular and inflammatory stresses mediate atherosclerosis via RAGE and its ligands in apoE–/–mice. *The Journal of clinical investigation, 118*(1), 183-194.

Hattori, Y., Hattori, S., & Kasai, K. (2003). Lipopolysaccharide activates Akt in vascular smooth muscle cells resulting in induction of inducible nitric oxide synthase through nuclear factor-kappa B activation. *European Journal of Pharmacology, 481*(2-3), 153-158. doi:10.1016/j.ejphar.2003.09.034

Haworth, R. A., Goknur, A. B., Hunter, D. R., Hegge, J. O., & Berkoff, H. A. (1987). Inhibition of calcium influx in isolated adult rat heart cells by ATP depletion. *Circulation Research, 60*, 586-594. doi:10.1161/01.RES.60.4.586

Hecker, M., Bara, A. T., Bauersachs, J., & Busse, R. (1994). Characterization of endothelium-derived hyperpolarizing factor as a cytochrome P450-derived arachidonic acid metabolite in mammals. *tHe Journal of Physiology, 481*(Pt 2), 407.

Hecquet, C. M., Ahmmed, G. U., Vogel, S. M., & Malik, A. B. (2008). Role of TRPM2 channel in mediating H2O2-induced Ca2+ entry and endothelial hyperpermeability. *Circulation Research, 102*(3), 347-355.

Heitzer, T., Krohn, K., Albers, S., & Meinertz, T. (2000). Tetrahydrobiopterin improves endothelium-dependent vasodilation by increasing nitric oxide activity in patients with Type II diabetes mellitus. *Diabetologia, 43*(11), 1435-1438.

Hernando, C. F., Fukata, M., Bernatchez, P. N., Fukata, Y., Lin, M. I., Bredt, D. S., & Sessa, W. C. (2006). Identifi cation of Golgi-localized acyl transferases that palmitoylate and regulate endothelial nitric oxide synthase. *JCB, 174*(3), 369-377. doi:10.1083/jcb.200601051

Hex, N., Bartlett, C., Wright, D., Taylor, M., & Varley, D. (2012). Estimating the current and future costs of Type 1 and Type 2 diabetes in the UK, including direct health costs and indirect societal and productivity costs. *Diabetic Medicine, 29*(7), 855-862. doi:10.1111/j.1464-5491.2012.03698.x

Hisatsune, C., Kuroda, Y., Nakamura, K., Inoue, T., Nakamura, T., Michikawa, T., . . . Mikoshiba, K. (2004). Regulation of TRPC6 channel activity by tyrosine phosphorylation. *Journal of Biological Chemistry, 279*(18), 18887-18894.

Ho, L., Yemul, S., Knable, L., Katsel, P., Zhao, R., Haroutunian, V., & Pasinetti, G. M. (2012). Insulin Receptor Expression and Activity in the Brains of Nondiabetic Sporadic Alzheimer's Disease Cases. *International Journal of Alzheimer's Disease*, 1-13. doi:10.1155/2012/32128

Hoenderop, J., Voets, T., Hoefs, S., Weidema, F., Prenen, J., Nilius, B., & Bindels, R. (2003). Homo-and heterotetrameric architecture of the epithelial Ca2+ channels TRPV5 and TRPV6. *The EMBO journal, 22*(4), 776-785.

Hoenderop, J. G., Hartog, A., Stuiver, M., Doucet, A., Willems, P. H., & Bindels, R. J. (2000). Localization of the epithelial Ca2+ channel in rabbit kidney and intestine. *Journal of the American Society of Nephrology, 11*(7), 1171-1178.

Hogikyan, R. V., Galecki, A. T., Halter, J. B., & Supiano, M. A. (1999). Heightened norepinephrine-mediated vasoconstriction in type 2 diabetes. *Metabolism, 48*(12), 1536–1541. doi:10.1016/S0026-0495(99)90242-1

Huang, A., Sun, D., Smith, C. J., Connetta, J. A., Shesely, E. G., Koller, A., & Kaley, G. (2000). In eNOS knockout mice skeletal muscle arteriolar dilation to acetylcholine is mediated by EDHF. *American Journal of Physiology-Heart and Circulatory Physiology, 278*(3), H762-H768.

Huang, A. J., Manning, J. E., Bandak, T. M., Ratau, M. C., Hanser, K. R., & Silverstein, S. C. (1993). Endothelial cell cytosolic free calcium regulates neutrophil migration across monolayers of endothelial cells. *JCB, 120*(6), 1371-1380. doi:10.1083/jcb.120.6.1371

Huo, B., Lu, X. L., & Guo, X. E. (2010). Intercellular calcium wave propagation in linear and circuit-like bone cell networks. *Phil. Trans. R. Soc. A, 368*, 617-633. doi:10.1098/rsta.2009.0221

Inoue, R., Jian, Z., & Kawarabayashi, Y. (2009). Mechanosensitive TRP channels in cardiovascular pathophysiology. *Pharmacology & Therapeutics, 123*(3), 371-385. doi:10.1016/j.pharmthera.2009.05.009

Iredale, P. A., & Dickenson, J. M. (1995). *Signal Transduction Protocols*. In J. M. Walker (Series Ed.) Methods in Molecular Biology, Vol. 41. D. A. Kindall & S. J. Hill (Eds.), *Measurement of Intracellular free Calcium ion concentration in cell populations using Fura-2* (pp. 203-2013).

Jabłecka, A., Bogdański, P., Balcer, N., Cieślewicz, A., Skołuda, A., & Musialik, K. (2012). The effect of oral L-arginine supplementation on fasting glucose, HbA1c, nitric oxide and total antioxidant status in diabetic patients with atherosclerotic peripheral arterial disease of lower extremities. *European Review for Medical and Pharmacological Sciences, 16*, 342-350.

Jackson, W. F., Konig, A., Dambacher, T., & Busse, R. (1993). Prostacyclin-induced vasodilation in rabbit heart is mediated by ATP-sensitive potassium channels. *American Journal of Physiology-Heart and Circulatory Physiology, 264*(1), H238-H243.

Jadidi, R. B., Karachalias, N., Ahmed, N., Battah, S., & Thornalley, P. J. (2003). Prevention of incipient diabetic nephropathy by high dose thiamine and benfotiamine. *Diabetes, 52*, 2110-2120.

Jan, C. R., Chen, C. H., Wang, S. C., & Kuo, S. Y. (2005). Effect of methylglyoxal on intracellular calcium levels and viability in renal tubular cells. *Cellular Signalling, 17*(7), 847-855. doi:10.1016/j.cellsig.2004.11.007

Jia, S., H., O. D. J., Ross, A. R. S., & Wu, L. (2006). Structural and functional changes in human insulin induced by methylglyoxal. *FASEB, 20*, E871-E879. doi:10.1096/fj.05-5478fje

Jia, X., & Wu, L. (2007). Accumulation of endogenous methylglyoxal impaired insulin signaling in adipose tissue of fructose-fed rats. *Molecular and Cellular Biochemistry, 306*(1-2). doi:10.1007/s11010-007-9563-x

Jiang, F., Li, C. G., & Rand, M. J. (2000). Mechanisms of nitric oxide-independent relaxations induced by carbachol and acetylcholine in rat isolated renal arteries. *Br J Pharmacol., 130*(6), 1191-1200. doi:10.1038/sj.bjp.0703408

Jin, M., Berrout, J., Chen, L., & O'Neil, R. G. (2012). Hypotonicity-induced TRPV4 function in renal collecting duct cells: modulation by progressive cross-talk with Ca2+-activated K+ channels. *Cell Calcium, 51*(2), 131–139. doi:10.1016/j.ceca.2011.11.011

Johnson, C. D., Melanaphy, D., Purse, A., Stokesberry, S. A., Dickson, P., & Zholos, A. V. (2009). Transient receptor potential melastatin 8 channel involvement in the regulation of vascular tone. *American Journal of Physiology, 296*(6), H1868-H1877. doi:10.1152/ajpheart.01112.2008

Johnson, R. J., Perez-Pozo, S. E., Sautin, Y. Y., Manitius, J., Sanchez-Lozada, L. G., Feig, D. I., . . . Nakagawa, T. (2009). Hypothesis: could excessive fructose intake and uric acid cause type 2 diabetes. *Endocrine Reviews, 30*(1), 96-116. doi:http://dx.doi.org/10.1210/er.2008-0033

Jones, A. E., & Summers, R. L. (2000). Detection of isopropyl alcohol in a patient with diabetic ketoacidosis. *The Journal of Emergency Medicine, 19*(2), 165-168.

Jung, S., Mühle, A., Schaefer, M., Strotmann, R., Schultz, G., & Plant, T. D. (2003). Lanthanides potentiate TRPC5 currents by an action at extracellular sites close to the pore mouth. *Journal of Biological Chemistry, 278*(6), 3562-3571.

Kaada, B. (1982). Vasodilation induced by transcutaneous nerve stimulation in peripheral ischemia (Raynaud's phenomenon and diabetic polyneuropathy). *European Heart Journal, 3*(4), 303-314. doi:http://dx.doi.org/

Kalapos, M. K. (2013). Where does plasma methylglyoxal originate from? *Diabetes Research and Clinical Practice, 99*(3), 260-271. doi:10.1016/j.diabres.2012.11.003

Kashyap, S. R., Lara, A., Zhang, R., Park, Y. M., & DeFronzo, R. A. (2008). Insulin Reduces Plasma Arginase Activity in Type 2 Diabetic Patients. *Diabetes Care, 39*(2), 134-139. doi:10.2337/dc07-1198

Kenagy, R. D., Hart, C. E., Stetler-Stevenson, W. G., & Clowes, A. W. (1997). Primate Smooth Muscle Cell Migration From Aortic Explants Is Mediated by Endogenous Platelet-Derived Growth Factor and Basic Fibroblast Growth Factor Acting Through Matrix Metalloproteinases 2 and 9 *Circulation, 96*, 3555-3560. doi: 10.1161/01.CIR.96.10.3555

Kim, J. H., Bugaj, L. J., Oh, Y. J., Bivalacqua, T. J., Ryoo, S., Soucy, K. G., . . . Sikka, G. (2009). Arginase inhibition restores NOS coupling and reverses endothelial dysfunction and vascular stiffness in old rats. *Journal of applied physiology, 107*(4), 1249-1257.

Kleinert, H., Pautz, A., Linker, K., & Schwarz, P. M. (2004). Regulation of the expression of inducible nitric oxide synthase. *European Journal of Pharmacology, 500*(1), 255-266.

Köhler, R., Heyken, W. T., Heinau, P., Schubert, R., Si, H., Kacik, M., . . . Hoyer, J. (2006). Evidence for a Functional Role of Endothelial Transient Receptor Potential V4 in Shear Stress–Induced Vasodilatation. *Arteriosclerosis, Thrombosis, and Vascular Biology., 26*, 1495-1502. doi:10.1161/01.ATV.0000225698.36212.6a

Kolluru, G. K., Bir, S. C., & Kevil, C. G. (2012). Endothelial Dysfunction and Diabetes: Effects on Angiogenesis, Vascular Remodeling, and Wound Healing. *International Journal of Vascular Medicine, 119*(7), 1-30. doi:10.1155/2012/918267

Komers, R., Schutzer, W. E., Reed, J. F., Lindsley, J. N., Oyama, T. T., Buck, D. C., . . . Anderson, S. (2006). Altered Endothelial Nitric Oxide Synthase Targeting and Conformation and Caveolin-1 Expression in the Diabetic Kidney. *Diabetes, 55*(6), 1651-1659. doi:10.2337/db05-1595

Krüger, M., Kratchmarova, I., Blagoev, B., Tseng, Y. H., Kahn, C. R., & Mann, M. (2007). Dissection of the insulin signaling pathway via quantitative phosphoproteomics. *PNAS, 107*(7), 2451–2456. doi:10.1073/pnas.0711713105

Krzyzanowska, K., Mittermayer, F., Wolzt, M., & Schernthaner, G. (2007). Asymmetric Dimethylarginine Predicts Cardiovascular Events in Patients With Type 2 Diabetes. *Diabetes Care, 30*(7), 1834-1839. doi:10.2337/dc07-0019

Kurien, B. T., & Scofield, R. H. (2006). Western blotting. *Methods, 38*(4), 283-293. doi:10.1016/j.ymeth.2005.11.007

Kwan, H.-Y., Huang, Y., & Yao, X. (2004). Regulation of canonical transient receptor potential isoform 3 (TRPC3) channel by protein kinase G. *Proceedings of the National Academy of Sciences of the United States of America, 101*(8), 2625-2630.

Kwan, H.-Y., Shen, B., Ma, X., Kwok, Y.-C., Huang, Y., Man, Y.-B., . . . Yao, X. (2009). TRPC1 associates with BKCa channel to form a signal complex in vascular smooth muscle cells. *Circulation Research, 104*(5), 670-678.

Kwan, H. Y., Huang, Y., & Yao, X. (2007). TRP channels in endothelial function and dysfunction. *Biochimica et Biophysica Acta, 1772*(8), 907-914. doi:10.1016/j.bbadis.2007.02.013

Laffel, L. (1999). Ketone bodies: a review of physiology, pathophysiology and application of monitoring to diabetes. *Diabetes Metab Res Rev, 15*, 412-426.

Lambert, I., Pedersen, S., & Poulsen, K. (2006). Activation of PLA2 isoforms by cell swelling and ischaemia/hypoxia. *Acta Physiologica, 187*(1-2), 75-85.

LaPlante, J. M., Falardeau, J., Sun, M., Kanazirska, M., Brown, E. M., Slaugenhaupt, S. A., & Vassilev, P. M. (2002). Identification and characterization of the single channel function of human mucolipin-1 implicated in mucolipidosis type IV, a disorder affecting the lysosomal pathway. *FEBS Letters, 532*(1-2), 183-187.

LaPlante, J. M., Ye, C., Quinn, S. J., Goldin, E., Brown, E. M., Slaugenhaupt, S. A., & Vassilev, P. M. (2004). Functional links between mucolipin-1 and Ca 2+-dependent membrane trafficking in mucolipidosis IV. *Biochemical and Biophysical Research Communications, 322*(4), 1384-1391.

Lashinger, E. S. R., Steiginga, M. S., Hieble, J. P., Leon, L. A., Gardner, S. D., Nagilla, R., . . . Su, X. (2008). AMTB, a TRPM8 channel blocker: evidence in rats for activity in overactive bladder and painful bladder syndrome. *American Journal of Physiology - Renal Physiology, 295*(3), F803-F810. doi:10.1152/ajprenal.90269.2008

Laufs, U., Fata, V. L., Plutzky, J., & Liao, J. K. (1998). Upregulation of Endothelial Nitric Oxide Synthase by HMG CoA Reductase Inhibitors. *Circulation, 97*, 1129-1135. doi:doi: 10.1161/01.CIR.97.12.1129

Launay, P., Fleig, A., Perraud, A.-L., Scharenberg, A. M., Penner, R., & Kinet, J.-P. (2002). TRPM4 is a Ca 2+-activated nonselective cation channel mediating cell membrane depolarization. *Cell, 109*(3), 397-407.

Lawler, O. A., Miggin, S. M., & Kinsella, B. T. (2001). Protein kinase A-mediated phosphorylation of serine 357 of the mouse prostacyclin receptor regulates its coupling to Gs-, to Gi-, and to Gq-coupled effector signaling. *Journal of Biological Chemistry, 276*(36), 33596-33607.

Lefevre, E. (2016, 26/04/2016). [AMTB hydrochloride (Ref 3989)].

Leffler, A., Linte, R. M., Nau, C., Reeh, P., & Babes, A. (2007). A high-threshold heat-activated channel in cultured rat dorsal root ganglion neurons resembles TRPV2 and is blocked by gadolinium. *European Journal of Neuroscience, 26*(1), 12-22.

Lei, L., Cao, X., Yang, F., Shi, D. J., Tng, Y. Q., Zheng, J., & Wang, K. W. (2013). A TRPV4 Channel C-terminal Folding Recognition Domain Critical for Trafficking and Function. *The Journal of Biological Chemistry, 288*(15), 10427-10439. doi:10.1074/jbc.M113.457291

Lenzen, S. (2008). The Mechanisms of Alloxan and Streptozotocin-induced Diabetes. *Diabetologia, 52*(2), 216-226. doi:10.1007/s00125-007-0886-7

Lerman, A., Burnett, J. C., Higano, S. T., McKinley, L. J., & Holmes, D. R. (1998). Long-term L-Arginine Supplementation Improves Small-Vessel Coronary Endothelial Function in Humans. *Circulation, 79*, 2123-2128. doi:10.1161/01.CIR.97.21.2123

Lewis, C. J., Surprenant, A., & Evans, R. J. (1998). 2',3'-O-(2,4,6- trinitrophenyl) adenosine 5'-triphosphate (TNP-ATP)–a nanomolar affinity antagonist at rat mesenteric artery P2X receptor ion channels. *British Journal of Pharmacology, 124*(7), 1463–1466. doi:10.1038/sj.bjp.0702001

Liang, C., Ren, Y., Tan, H., He, Z., Jiang, Q., Wu, J., . . . Wu, Z. (2009). Rosiglitazone via upregulation of Akt/eNOS pathways attenuates dysfunction of endothelial progenitor cells, induced by advanced glycation end products. *Br J Pharmacol., 158*(8), 1865–1873. doi:10.1111/j.1476-5381.2009.00450.x

Liedtke, W., & Friedman, J. M. (2003). Abnormal osmotic regulation in trpv4-/-mice. *Proceedings of the National Academy of Sciences, 100*(23), 13698-13703.

Lim, E. L., Hollingsworth, K. G., Smith, F. E., Thelwall, P. E., & Taylor, R. (2011). Inhibition of lipolysis in type 2 diabetes normalizes glucose disposal without change in muscle glycogen synthesis rate. *Clinical Science, 121*, 169-177. doi:10.1042/CS20100611

Liman, E. R., Corey, D. P., & Dulac, C. (1999). TRP2: a candidate transduction channel for mammalian pheromone sensory signaling. *Proceedings of the National Academy of Sciences, 96*(10), 5791-5796.

Lin, K. Y., Ito, A., Asagami, T., Tsao, P. S., Adimoolam, S., Kimoto, M., . . . Cooke, J. P. (2002). Impaired Nitric Oxide Synthase Pathway in Diabetes Mellitus: Role of Asymmetric Dimethylarginine and Dimethylarginine Dimethylaminohydrolase. *Circulation, 106*(8), 987-992. doi:10.1161/01.CIR.0000027109.14149.67

Lin, M. I., Fulton, D., Babbitt, R., Fleming, I., Busse, R., Pritchard, K. A., & Sessa, W. C. (2003). Phosphorylation of threonine 497 in endothelial nitric-oxide synthase coordinates the coupling of L-arginine metabolism to efficient nitric oxide production. *Journal of Biological Chemistry, 278*(45), 44719-44726.

Lindsey, S., Tribe, R., & Songu-Mize, E. (2008). Cyclic stretch decreases TRPC4 protein and capacitative calcium entry in rat vascular smooth muscle cells. *Life Sciences, 83*(1), 29-34.

Liu, B., & Qin, F. (2005). Functional Control of Cold- and Menthol-Sensitive TRPM8 Ion Channels by Phosphatidylinositol 4,5-Bisphosphate. *Neuroscience, 25*(7), 1674-1681. doi:10.1523/JNEUROSCI.3632-04.2005

Liu, C.-l., Huang, Y., Nga, C.-y., Leung, Y.-k., & Yao, X.-q. (2006). TRPC3 is involved in flow-and bradykinin-induced vasodilation in rat small mesenteric arteries. *Acta pharmacologica Sinica, 27*(8).

Liu, X. R., Liu, Q., Chen, G. Y., Hu, Y., Sham, J. S. K., & Lin, M. J. (2013). Down-regulation of TRPM8 in pulmonary arteries of pulmonary hypertensive rats. *Cellular Physiology and Biochemistry, 31*(6), 892-904.

Lodish, H. F., & Kong, N. (1990). Perturbation of Cellular Calcium Blocks Exit of Secretory Proteins from the Rough Endoplasmic Reticulum. *The Journal of Biological Chemistry, 265*(19), 10893-10899.

Lodish, H. F., Kong, N., & Wikstrom, L. (1992). Calcium Is Required for Folding of Newly Made Subunits of the Asialoglycoprotein Receptor within the Endoplasmic Reticulum*. *The Journal of Biological Chemistry, 267*(18), 12753-12760.

Lopacinska, K. D., & Strosznajder, J. B. (2005). Cyclic gmp metabolism and its role in brain physiology. *Journal of physiology and pharmacology, 56*, 15-16.

Lu, J., Randell, E., Han, Y. C., Adeli, K., Krahn, J., & Meng, Q. H. (2011). Increased plasma methylglyoxal level, inflammation, and vascular endothelial dysfunction in diabetic nephropathy. *Clinincal Biochemistry, 44*(4), 307-311. doi:10.1016/j.clinbiochem.2010.11.004

Lucas, P., Ukhanov, K., Leinders-Zufall, T., & Zufall, F. (2003). A diacylglycerol-gated cation channel in vomeronasal neuron dendrites is impaired in TRPC2 mutant mice: mechanism of pheromone transduction. *Neuron, 40*(3), 551-561.

Lucotti, P., Setola, E., Monti, L. D., Galluccio, E., Costa, S., Sandoli, E. P., . . . Piatti, P. M. (2006). Beneficial effects of a long-term oral l-arginine treatment added to a hypocaloric diet and exercise training program in obese, insulin-resistant type 2 diabetic patients. *American Journal of Physiology - Endocrinology and Metabolism, 291*(5), E906-E912. doi:10.1152/ajpendo.00002.2006

Lüscher, T. F., & Barton, M. (1997). Biology of the Endothelium. *Clin. Cardiol., 20*(2), II-3–II-10.

Ma, X., Cheng, K. T., Wong, C. O., O'Neild, R. G., Birnbaumer, L., Ambudkar, I. S., & Yao, X. (2011). Heteromeric TRPV4-C1 channels contribute to store-operated Ca2+ entry in vascular endothelial cells. *Calcium Cell, 50*(6), 502-509. doi:10.1016/j.ceca.2011.08.006

Ma, X., Cheng, K. T., Wonga, C. O., O'Neild, R. G., Birnbaumer, L., Ambudkar, I. S., & Yao, X. (2011). Heteromeric TRPV4-C1 channels contribute to store-operated Ca2+ entry in vascular endothelial cells. *Calcium Cell, 50*(6), 502-509. doi:10.1016/j.ceca.2011.08.006

Ma, X., Du, J., Zhang, P., Deng, J., Liu, J., Lam, F. F. Y., . . . Yao, X. (2013). Functional role of TRPV4-KCa2.3 signaling in vascular endothelial cells in normal and streptozotocin-induced diabetic rats. *Hypertension, 62*, 134-139. doi:10.1161/HYPERTENSIONAHA.113.01500

Macpherson, L. J., Geierstanger, B. H., Viswanath, V., Bandell, M., Eid, S. R., Hwang, S., & Patapoutian, A. (2005). The pungency of garlic: activation of TRPA1 and TRPV1 in response to allicin. *Current Biology, 15*(10), 929-934.

Mahendran, Y., Vangipurapu, J., Cederberg, H., Stančáková, A., Pihlajamäki, J., Soininen, P., . . . Laakso, M. (2013). Association of ketone body levels with hyperglycemia and type 2 diabetes in 9,398 Finnish men. *Diabetes, 62*, 3618-3626.

Mahieu, F., Owsianik, G., Verbert, L., Janssens, A., De Smedt, H., Nilius, B., & Voets, T. (2007). TRPM8-independent Menthol-induced Ca2+ Release from Endoplasmic Reticulum and Golgi. *The Journal of Biological Chemistry, 82*(5), 3325-3336. doi:10.1074/jbc.M605213200

Mahmoud, M. F., Hassan, N. A., El Bassossy, H. M., & Fahmy, A. (2013). Quercetin Protects against Diabetes-Induced Exaggerated Vasoconstriction in Rats: Effect on Low Grade Inflammation. *PLoS ONE, 8*(5), 1-11. doi:http://dx.doi.org/10.1371/journal.pone.0063784

Malerød, L., Juvet, L. K., & Berg, T. G. T. (2002). The expression of scavenger receptor class B, type I (SR-BI) and caveolin-1 in parenchymal and nonparenchymal liver cells. *Cell and Tissue Research, 307*(2), 173-180. doi:10.1007/s00441-001-0476-9

Malhotra, J. D., & Kaufman, R. J. (2007). Endoplasmic Reticulum Stress and Oxidative Stress: A Vicious Cycle or a Double-Edged Sword? *Antioxidants & Redox Signaling, 9*(12), 2277-2294. doi:10.1089/ars.2007.1782

Marciniak, S. J., & Ron, D. (2006). Endoplasmic Reticulum Stress Signaling in Disease. *Physiological Reviews, 86*(4), 1133-1149. doi:10.1152/physrev.00015.2006

Martins, S. I. F. S., Jongen, W. M. F., & van Boekel, M. A. J. S. (2001). A review of Maillard reaction in food and implications to kinetic modelling. *Trends in Food Science & Technology, 11*(9-10), 364-373. doi:10.1016/S0924-2244(01)00022-X

Maruyama, Y., Nakanishi, Y., Walsh, E. J., Wilson, D. P., Welsh, D. G., & Cole, W. C. (2006). Heteromultimeric TRPC6-TRPC7 channels contribute to arginine vasopressin-induced cation current of A7r5 vascular smooth muscle cells. *Circulation Research, 98*(12), 1520-1527.

McCulloch, A. I., Bottrill, F. E., Randall, M. D., & Hiley, C. R. (1997). Characterization and modulation of EDHF-mediated relaxations in the rat isolated superior mesenteric arterial bed. *Br J Pharmacol., 120*(8), 1431–1438. doi:10.1038/sj.bjp.0701066

McNeish, A. J., Altayo, F. J., & Garland, C. J. (2010). Evidence both L-type and non-L-type voltage-dependent calcium channels contribute to cerebral artery vasospasm following loss of NO in the rat. *Vascular Pharmacology, 53*(3-4), 151-159. doi:10.1016/j.vph.2010.06.002

Miggin, S. M., & Kinsella, B. T. (2002). Investigation of the mechanisms of G protein: effector coupling by the human and mouse prostacyclin receptors Identification of critical species-dependent differences. *Journal of Biological Chemistry, 277*(30), 27053-27064.

Milstien, S., & Katusic, Z. (1999). Oxidation of tetrahydrobiopterin by peroxynitrite: implications for vascular endothelial function. *Biochemical and Biophysical Research Communications, 263*(3), 681-684.

Mio, K., Ogura, T., Kiyonaka, S., Hiroaki, Y., Tanimura, Y., Fujiyoshi, Y., . . . Sato, C. (2007). The TRPC3 channel has a large internal chamber surrounded by signal sensing antennas. *Journal of molecular biology, 367*(2), 373-383.

Mitch, W. E., Bailey, J. L., Wang, X., Jurkovitz, C., Newby, D., & Price, S. R. (1999). Evaluation of signals activating ubiquitin-proteasome proteolysis in a model of muscle wasting. *American Journal of Physiology, 25*(5), C1132-C1138.

Mitchell, J. A., Ali, F., Bailey, L., Moreno, L., & Harrington, L. S. (2008). Role of nitric oxide and prostacyclin as vasoactive hormones released by the endothelium. *Experimental physiology, 93*(1), 141-147.

Mizuno, A., Matsumoto, N., Imai, M., & Suzuki, M. (2003). Impaired osmotic sensation in mice lacking TRPV4. *American Journal of Physiology-Cell Physiology, 285*(1), C96-C101.

Mochizuki, T., Wu, G., Hayashi, T., & Xenophontos, S. (1996). PKD2, a gene for polycystic kidney disease that encodes an integral membrane protein. *Science, 272*(5266), 1339.

Monaghan, K., McNaughten, J., McGahon, M. K., Kelly, C., Kyle, D., Yong, P. H., . . . Curtis, T. M. (2015). Hyperglycemia and Diabetes Downregulate the Functional Expression of TRPV4 Channels in Retinal Microvascular Endothelium. *PLoS ONE, 10*(6), 1-16. doi:10.1371/journal.pone.0128359

Moqrich, A., Hwang, S. W., Earley, T. J., Petrus, M. J., Murray, A. N., Spencer, K. S., . . . Patapoutian, A. (2005). Impaired thermosensation in mice lacking TRPV3, a heat and camphor sensor in the skin. *Science, 307*(5714), 1468-1472.

Morgan, A. J., & Thomas, A. P. (1999). *Calcium Signaling Protocols*. In J. M. Walker (Series Ed.) Methods in Molecular Biology, Vol. 114. D. G. Lambert (Ed.) *Single cell and subcellular measurement of intracellular Ca2+ concentration ([Ca2+]i* (pp. 93-123).

Muraki, K., Iwata, Y., Katanosaka, Y., Ito, T., Ohya, S., Shigekawa, M., & Imaizumi, Y. (2003). TRPV2 is a component of osmotically sensitive cation channels in murine aortic myocytes. *Circulation Research, 93*(9), 829-838.

Murata, T., Lin, M. I., Stan, R. V., Bauer, P. M., Yu, J., & Sessa, W. C. (2007). Genetic evidence supporting caveolae microdomain regulation of calcium entry in endothelial cells. *The Journal of Biological Chemistry, 282*, 16631-16643. doi:10.1074/jbc.M607948200

Murphy, M. E., & Brayden, J. E. (1995a). Apamin-sensitive K+ channels mediate an endothelium-dependent hyperpolarization in rabbit mesenteric arteries. *tHe Journal of Physiology, 489*(3), 723-734.

Murphy, M. E., & Brayden, J. E. (1995b). Nitric oxide hyperpolarizes rabbit mesenteric arteries via ATP-sensitive potassium channels. *tHe Journal of Physiology, 486*(1), 47-58.

Mustafa, S., Sharma, V., & McNeill, J. H. (2009). Insulin resistance and endothelial dysfunction: are epoxyeicosatrienoic acids the link? *Exp Clin Cardiol., 14*(2), e41-e50.

Naeini, R. S., Witty, M.-F., Séguéla, P., & Bourque, C. W. (2006). An N-terminal variant of Trpv1 channel is required for osmosensory transduction. *Nature Neuroscience, 9*(1), 93-98.

Nauli, S. M., Kawanabe, Y., Kaminski, J. J., Pearce, W. J., Ingber, D. E., & Zhou, J. (2008). Endothelial cilia are fluid shear sensors that regulate calcium signaling and nitric oxide production through polycystin-1. *Circulation, 117*(9), 1161-1171.

Naylor, J., Li, J., Milligan, C. J., Zeng, F., Sukumar, P., Hou, B., . . . Beri, D. (2010). Pregnenolone sulphate- and cholesterol-regulated TRPM3 channels coupled to vascular smooth muscle secretion and contraction. *Circulation Research, 106*(9), 1507-1515.

Nicolay, J. P., Schneider, J., Niemoeller, O. M., Artunc, F., Otin, M. P., Haik Jr., G., . . . Lang, F. (2006). Stimulation of suicidal erythrocyte death by methylglyoxal. *Cell Physiol Biochem, 18*, 223-232.

Nigro, C., Raciti, G. A., Leone, A., Flemin, T. H., Longo, M., Prevenzano, I., . . . Miele, C. (2014). Methylglyoxal impairs endothelial insulin sensitivity in both in vitro and in vivo. *Diabetologia, 57*, 1485–1494. doi:10.1007/s00125-014-3243-7

Nijenhuis, T., Hoenderop, J. G., Nilius, B., & Bindels, R. J. (2003). (Patho) physiological implications of the novel epithelial Ca2+ channels TRPV5 and TRPV6. *Pflügers Archiv, 446*(4), 401-409.

Nilius, B., Mahieu, F., Karashima, Y., & Voets, T. (2007). Regulation of TRP channels: a voltage–lipid connection. *Biochemical Society Transactions, 35*(1), 105-108.

Nilius, B., Prenen, J., Droogmans, G., Voets, T., Vennekens, R., Freichel, M., . . . Flockerzi, V. (2003). Voltage dependence of the Ca2+-activated cation channel TRPM4. *Journal of Biological Chemistry, 278*(33), 30813-30820.

Niwa, T., Katsuzaki, T., Ishizaki, Y., Hayase, F., Miyazaki, T., Uematsu, T., . . . Takei, Y. (1997). Imidazolone, a novel advanced glycation end product, is present at high levels in kidneys of rats with streptozotocin-induced diabetes. *FEBS Letters, 407*(3), 297-302. doi:10.1016/S0014-5793(97)00362-1

Oberwinkler, J., Lis, A., Giehl, K. M., Flockerzi, V., & Philipp, S. E. (2005). Alternative splicing switches the divalent cation selectivity of TRPM3 channels. *Journal of Biological Chemistry, 280*(23), 22540-22548.

Olson, B. J. S. C., & Markwell, J. (2007). Assays for determination of protein concentration. *Current Protocols in Protein Science, 48*(3.4), 3.4.1-3.4.29. doi:10.1002/0471140864.ps0304s48

Oya, T., Hattori, N., Mizuno, Y., Miyata, S., Maeda, S., Osawa, T., & Uchida, K. (1999). Methylglyoxal Modification of Protein CHEMICAL AND IMMUNOCHEMICAL CHARACTERIZATION OF METHYLGLYOXAL-ARGININE ADDUCTS. *JBC, 274*, 18492-18502. doi:10.1074/jbc.274.26.18492

Paravicini, T. M., Yogi, A., Mazur, A., & Touyz, R. M. (2009). Dysregulation of vascular TRPM7 and annexin-1 is associated with endothelial dysfunction in inherited hypomagnesemia. *Hypertension, 53*(2), 423-429.

Patel, R., Baker, S. S., Liu, W., Desai, S., Alkhouri, R., Kozielski, R., . . . Zhu, L. (2012). Effect of Dietary Advanced Glycation End Products on Mouse Liver. *PLoS ONE, 7*(4). doi:10.1371/journal.pone.0035143

Pedersen, S. F., Owsianik, G., & Nilius, B. (2005). TRP channels: an overview. *Cell Calcium, 38*(3-4), 233-252. doi:10.1016/j.ceca.2005.06.028

Peier, A. M., Reeve, A. J., Andersson, D. A., Moqrich, A., Earley, T. J., Hergarden, A. C., . . . McIntyre, P. (2002). A heat-sensitive TRP channel expressed in keratinocytes. *Science, 296*(5575), 2046-2049.

Peppiatt-Wildman, C., Albert, A., Saleh, S., & Large, W. (2007). Endothelin-1 activates a Ca2+-permeable cation channel with TRPC3 and TRPC7 properties in rabbit coronary artery myocytes. *tHe Journal of Physiology, 580*(3), 755-764.

Perraud, A.-L., Takanishi, C. L., Shen, B., Kang, S., Smith, M. K., Schmitz, C., . . . Zhang, J. (2005). Accumulation of free ADP-ribose from mitochondria mediates oxidative stress-induced gating of TRPM2 cation channels. *Journal of Biological Chemistry, 280*(7), 6138-6148.

Philips, S. A., & Thornalley, P. J. (1993). The formation of methylglyoxal from triose phosphates Investigation using a specific assay for methylglyoxal. *European Journal of Biochemistry, 212*(1), 101-105.

Pieper, G. M., & Dondlinger, L. A. (1997). Plasma and vascular tissue arginine are decreased in diabetes: acute arginine supplementation restores endothelium-dependent relaxation by augmenting cGMP production. *Journal of Pharmacology and Experimental Therapeutics, 283*(2), 684-691.

Piver, B., Berthou, F., Dreano, Y., & Lucas, D. (2001). Inhibition of CYP3A, CYP1A and CYP2E1 activities by resveratrol and other non volatile red wine components. *Toxicology Letters, 125*(1-3), 83-91. doi:10.1016/S0378-4274(01)00418-0

Popp, R., Bauersachs, J., Hecker, M., Fleming, I., & Busse, R. (1996). A transferable, beta-naphthoflavone-inducible, hyperpolarizing factor is synthesized by native and cultured porcine coronary endothelial cells. *tHe Journal of Physiology, 497*(Pt 3), 699.

Poulos, T. L. (2006). Soluble guanylate cyclase. *Current Opinion in Structural Biology, 16*(6), 736–743. doi:10.1016/j.sbi.2006.09.006

Quallo, T., Vastani, N., Horridge, E., Gentry, C., Parra, A., Moss, S., . . . Bevan, S. (2015). TRPM8 is a neuronal osmosensor that regulates eye blinking in mice. *Nature communications, 6*.

Ramasamy, R., Vannucci, S. J., Yan, S. S. D., Herold, K., Yan, S. F., & Schmidt, A. M. (2005). Advanced glycation end products and RAGE: a common thread in aging, diabetes, neurodegeneration, and inflammation. *Glycobiology, 15*(7), 16R-28R. doi:10.1093/glycob/cwi053

Ramsey, I. S., Delling, M., & Clapham, D. E. (2006). An introduction to TRP channels. *Annual Review of Physiology, 68*, 619-647. doi:10.1146/annurev.physiol.68.040204.100431

Rath, G., Dessy, C., & Feron, O. (2009). CAVEOLAE, CAVEOLIN AND CONTROLOF VASCULAR TONE: NITRIC OXIDE (NO) AND ENDOTHELIUM DERIVED HYPERPOLARIZING FACTOR (EDHF) REGULATION. *Journal of physiology and pharmacology, 60*(4), 105-109.

Reading, S. A., & Brayden, J. E. (2007). Central role of TRPM4 channels in cerebral blood flow regulation. *Stroke, 38*(8), 2322-2328.

Reading, S. A., Earley, S., Waldron, B., Welsh, D., & Brayden, J. (2005). TRPC3 mediates pyrimidine receptor-induced depolarization of cerebral arteries. *American Journal of Physiology-Heart and Circulatory Physiology, 288*(5), H2055-H2061.

Rohács, T., Lopes, C. M. B., Michailidis, I., & Logothetis, D. E. (2005). PI(4,5)P2 regulates the activation and desensitization of TRPM8 channels through the TRP domain. *Nature Neuroscience, 8*(5), 626-634. doi:10.1038/nn1451

Rohacs, T., & Nilius, B. (2007). Regulation of transient receptor potential channels by phosphoinositides. *Eur J Physiol, 455*(1), 157-168. doi:10.1007/s00424-007-0275-6

Romero, M. J., Platt, D. H., Tawfik, H. E., Labazi, M., El-Remessy, A. B., Bartoli, M., . . . Caldwell, R. W. (2008). Diabetes-induced Coronary Vascular Dysfunction Involves Increased Arginase Activity. *Circulation Research, 102*(1), 95-102. doi:10.1161/CIRCRESAHA.107.155028

Rosenbaum, T., Gordon-Shaag, A., Munari, M., & Gordon, S. E. (2004). Ca2+/calmodulin modulates TRPV1 activation by capsaicin. *The Journal of general physiology, 123*(1), 53-62.

Rosolowsky, M., & Campbell, W. B. (1993). Role of PGI2 and epoxyeicosatrienoic acids in relaxation of bovine coronary arteries to arachidonic acid. *American Journal of Physiology-Heart and Circulatory Physiology, 264*(2), H327-H335.

Ruiter, M. S., Van Golde, J. M., Schaper, N. C., Stehouwer, C. D., & Huijberts, M. S. (2012). The role of methylglyoxal in hyperglycemia-induced impairments of vasoreactivity in rat saphenous artery. In M. S. Ruiter (Ed.), Reactivity, recruitment and remodeling of collateral arteries in diabetes (pp. 83-98). Amsterdam: Gildeprint Drukkerijen.

Saliez, J., Bouzin, C., Rath, G., Ghisdal, P., Desjardins, F., Rezzani, R., . . . Dessy, C. (2008). Role of Caveolar Compartmentation in Endothelium-Derived Hyperpolarizing Factor–Mediated Relaxation. *Circulation, 117*, 1065-1074. doi:10.1161/CIRCULATIONAHA.107.731679

Sandow, S. L., & Hill, C. E. (2000). Incidence of myoendothelial gap junctions in the proximal and distal mesenteric arteries of the rat is suggestive of a role in endothelium-derived hyperpolarizing factor–mediated responses. *Circulation Research, 86*(3), 341-346.

Schmidt, A. M., Du Yan, S., Wautier, J.-L., & Stern, D. (1999). Activation of receptor for advanced glycation end products a mechanism for chronic vascular dysfunction in diabetic vasculopathy and atherosclerosis. *Circulation Research, 84*(5), 489-497.

Schnedl, W. J., Ferber, S., Johnson, J. H., & Newgard, C. B. (1994). STZ transport and cytotoxicity: specific enhancement in GLUT2-expressing cells. *Diabetes, 43*(11), 1326-1333. doi:10.2337/diab.43.11.1326

Schott, C. A., Gray, G. A., & Stoclet, J. C. (1993). Dependence of endotoxin-induced vascular hyporeactivity on extracellular l-arginine. *British Journal of Pharmacology, 108*(1), 38-43.

Schröder, M. (2008). Endoplasmic reticulum stress responses. *Cellular and Molecular Life Sciences, 65*(6), 862-894. doi:10.1007/s00018-007-7383-5

Schwedhelm, E., Maas, R., Freese, R., Jung, D., Lukacs, Z., Jambrecina, A., . . . Böger, R. H. (2008). Pharmacokinetic and pharmacodynamic properties of oral L-citrulline and L-arginine: impact on nitric oxide metabolism. *BJCP, 65*(1), 51-59. doi:10.1111/j.1365-2125.2007.02990.x

Scotland, R. S., Chauhan, S., Davis, C., De Felipe, C., Hunt, S., Kabir, J., . . . Ahluwalia, A. (2004). Vanilloid receptor TRPV1, sensory C-fibers, and vascular autoregulation a novel mechanism involved in myogenic constriction. *Circulation Research, 95*(10), 1027-1034.

Sena, C. M., Matafome, P., Crisóstomo, J., Rodrigues, L., Fernandes, R., Pereira, P., & Seic¸a, R. M. (2012). Methylglyoxal promotes oxidative stress and endothelial dysfunction. *Pharmacological Research, 65*, 497-506. doi:10.1016/j.phrs.2012.03.004

Sena, C. M., Pereira, A. M., & Seiça, R. (2013). Endothelial dysfunction — A major mediator of diabetic vascular disease. *Biochimica et Biophysica Acta (BBA) - Molecular Basis of Disease, 1832*(12), 2216–2231. doi:10.1016/j.bbadis.2013.08.006

Serban, D. N., Nilius, B., & Vanhoutte, P. M. (2010). The endothelial saga: the past, the present, the future. *Eur J Physiol, 459*(6), 787-792. doi:10.1007/s00424-010-0805-5

Shamsaldeen, Y. A., Mackenzie, L. S., Lione, L. A., & Benham, C. D. (2016). Methylglyoxal, A Metabolite Increased in Diabetes is Associated with Insulin Resistance, Vascular Dysfunction and Neuropathies. *Current Druge Metabolism, 17*(4), 359-367.

Shaul, P. W., Smart, E. J., Robinsoni, L. J., German, Z., Yuhanna, I. S., Ying, Y., . . . Micheli, T. (1996). Acylation Targets Endothelial Nitric-oxide Synthase to Plasmalemmal Caveola. *The Journal of Biological Chemistry, 271*(11), 6518-6522. doi:10.1074/jbc.271.11.6518

Sheader, E. A., Benson, R. S. P., & Best, L. (2001). Cytotoxic action of methylglyoxal on insulin-secreting cells. *Biochemical Pharmacology, 61*, 1381-1386.

Sherkheli, M. A., Gisselmann, G., Vogt-Eisele, A. K., Doerner, J. F., & Hatt, H. (2008). Menthol Derivative WS-12 Selectively Activates Transient Receptor Potential Melastatin-8 (TRPM8) Ion Channels. *Pak. J. Pharm. Sci., 21*(4), 370-378.

Sherkheli, M. A., Vogt-Eisele, A. K., Bura, D., Márques, L. R. B., Gisselmann, G., & Hatt, H. (2010). Characterization of Selective TRPM8 Ligands and their Structure Activity Response (S.A.R) Relationship. *Journal of Pharmacy & Pharmaceutical Sciences, 13*(2), 242-253. doi:http://dx.doi.org/10.18433/J3N88N

Shi, J., Ju, M., Saleh, S., Albert, A., & Large, W. (2010). TRPC6 channels stimulated by angiotensin II are inhibited by TRPC1/C5 channel activity through a Ca2+-and PKC-dependent mechanism in native vascular myocytes. *tHe Journal of Physiology, 588*(19), 3671-3682.

Shi, J., Mori, E., Mori, Y., Mori, M., Li, J., Ito, Y., & Inoue, R. (2004). Multiple regulation by calcium of murine homologues of transient receptor potential proteins TRPC6 and TRPC7 expressed in HEK293 cells. *tHe Journal of Physiology, 561*(2), 415-432.

Shimokawa, H., Yasutake, H., Fujii, K., Owada, M. K., Nakaike, R., Fukumoto, Y., . . . Fujishima, M. (1996). The importance of the hyperpolarizing mechanism increases as the vessel size decreases in endothelium-dependent relaxations in rat mesenteric circulation. *Journal of cardiovascular pharmacology, 28*(5), 703-711.

Silva, D. F., de Almeida, M. M., Chaves, C. G., Braz, A. L., Gomes, M. A., Pinho-da-Silva, L., . . . de Albuquerque, J. G. F. (2015). TRPM8 Channel Activation Induced by Monoterpenoid Rotundifolone Underlies Mesenteric Artery Relaxation. *PLoS ONE, 10*(11).

Sinha, S. (2013). *Role of TRPA1 and TRPV1 in Propofol Induced Vasodilation.* Kent State University.

Sitterley, G. (2008a). Collagen attachment protocols, solubility, and stability. *Biofiles, 3*(8), 3-5.

Sitterley, G. (2008b). Poly-L-Lysine cell attachment protocol. *Biofiles, 3*(8), 12.

Smith, P. A., Proks, P., & Moorhouse, A. (1999). Direct effects of tolbutamide on mitochondrial function, intracellular Ca2+ and exocytosis in pancreatic b-cells. *Eur J Physiol, 437*(4), 577-588.

Sonkusare, S. K., Dalsgaard, T., Bonev, A. D., Hill-Eubanks, D. C., Kotlikoff, M. I., Scott, J. D., . . . Nelson, M. T. (2014). AKAP150-dependent cooperative TRPV4 channel gating is central to

endothelium-dependent vasodilation and is disrupted in hypertension. *Science Signaling, 7*(333), ra66.

Sourij, H., Zweiker, R., & Wascher, T. C. (2006). Effects of Pioglitazone on Endothelial Function, Insulin Sensitivity, and Glucose Control in Subjects With Coronary Artery Disease and New-Onset Type 2 Diabetes. *Diabetes Care, 29*(5), 1039-1045. doi:10.2337/dc05-2226

Spassova, M. A., Hewavitharana, T., Xu, W., Soboloff, J., & Gill, D. L. (2006). A common mechanism underlies stretch activation and receptor activation of TRPC6 channels. *Proceedings of the National Academy of Sciences, 103*(44), 16586-16591.

Spieker, L. E., Sudano, I., Hürlimann, D., Lerch, P. G., Lang, M. G., Binggeli, C., . . . Noll, G. (2002). High-Density Lipoprotein Restores Endothelial Function in Hypercholesterolemic Men. *Circulation, 105*, 1399-1402. doi: 10.1161/01.CIR.0000013424.28206.8F

Staels, B., Dallongeville, J., Auwerx, J., Schoonjans, K., Leitersdorf, E., & Fruchart, J. C. (1998). Mechanism of Action of Fibrates on Lipid and Lipoprotein Metabolism. *Circulation, 98*, 2088-2093. doi:10.1161/01.CIR.98.19.2088

Story, G. M., Peier, A. M., Reeve, A. J., Eid, S. R., Mosbacher, J., Hricik, T. R., . . . Hwang, S. W. (2003). ANKTM1, a TRP-like channel expressed in nociceptive neurons, is activated by cold temperatures. *Cell, 112*(6), 819-829.

Strübing, C., Krapivinsky, G., Krapivinsky, L., & Clapham, D. E. (2001). TRPC1 and TRPC5 form a novel cation channel in mammalian brain. *Neuron, 29*(3), 645-655.

Suchyna, T. M., Tape, S. E., Koeppe, R. E., Andersen, O. S., Sachs, F., & Gottlieb, P. A. (2004). Bilayer-dependent inhibition of mechanosensitive channels by neuroactive peptide enantiomers. *Nature, 430*(6996), 235-240.

Sukumaran, S. V., Singh, T. U., Parida, S., Reddy, C. E. N., Thangamalai, R., Kandasamy, K., . . . Mishra, S. K. (2013). TRPV4 channel activation leads to endothelium-dependent relaxation mediated by nitric oxide and endothelium-derived hyperpolarizing factor in rat pulmonary artery. *Pharmacological Research, 78*, 18-27. doi:10.1016/j.phrs.2013.09.005

Sun, M., Goldin, E., Stahl, S., Falardeau, J. L., Kennedy, J. C., Acierno Jr, J. S., . . . Bromley, M. C. (2000). Mucolipidosis type IV is caused by mutations in a gene encoding a novel transient receptor potential channel. *Human molecular genetics, 9*(17), 2471-2478.

Szkudelski, T. (2001). The Mechanism of Alloxan and Streptozotocin Action in B Cells of the Rat Pancreas. *Physiological research, 50*(6), 536-546. doi:10.1037/0003-066X.59.1.29

Tabit, C. E., Chung, W. B., Hamburg, N. M., & Vita, J. A. (2010). Endothelial dysfunction in diabetes mellitus: Molecular mechanisms and clinical implications. *Rev Endocr Metab Disord, 11*(1), 61-74. doi:10.1007/s11154-010-9134-4

Takezawa, R., Schmitz, C., Demeuse, P., Scharenberg, A. M., Penner, R., & Fleig, A. (2004). Receptor-mediated regulation of the TRPM7 channel through its endogenous protein kinase domain. *Proceedings of the National Academy of Sciences of the United States of America, 101*(16), 6009-6014.

Tallarida, R. J., Cowan, A., & Adler, M. W. (1979). pA2 and receptor differentiation: a statistical analysis of competitive antagonism. *Life Sciences, 25*(8), 637-654.

Tallarida, R. J., & Murray, R. B. (1987). pA2 analysis I: schild plot *Manual of Pharmacologic Calculations* (pp. 53-56): Springer.

Taniguchi, C. M., Emanuelli, B., & Kahn, C. R. (2006). Critical nodes in signalling pathways: insights into insulin action. *Nature Reviews Molecular Cell Biology, 7*. doi:10.1038/nrm1837

Thebault, S., Lemonnier, L., Bidaux, G., Flourakis, M., Bavencoffe, A., Gordienko, D., . . . Prevarskaya, N. (2005). Novel Role ofCold/Menthol-sensitive Transient Receptor Potential Melastatine Family Member 8 (TRPM8) in the Activation of Store-operated Channels in LNCaP Human Prostate Cancer Epithelial Cells. *The Journal of Biological Chemistry, 280*(47), 39423–39435. doi:10.1074/jbc.M503544200

Thomas, C. M., & Smart, E. J. (2008). Caveolae structure and function. *J. Cell. Mol. Med., 12*(3), 796-809. doi:10.1111/j.1582-4934.2008.00295.

Tian, W., Salanova, M., Xu, H., Lindsley, J. N., Oyama, T. T., Anderson, S., . . . Cohen, D. M. (2004). Renal expression of osmotically responsive cation channel TRPV4 is restricted to water-impermeant nephron segments. *American Journal of Physiology - Renal Physiology, 287*(1), F17-F24. doi:10.1152/ajprenal.00397.2003

Touyz, R. M., He, Y., Montezano, A. C., Yao, G., Chubanov, V., Gudermann, T., & Callera, G. E. (2006). Differential regulation of transient receptor potential melastatin 6 and 7 cation channels by ANG II in vascular smooth muscle cells from spontaneously hypertensive rats. *American Journal of Physiology-Regulatory, Integrative and Comparative Physiology, 290*(1), R73-R78.

Tseng, P.-H., Lin, H.-P., Hu, H., Wang, C., Zhu, M. X., & Chen, C.-S. (2004). The canonical transient receptor potential 6 channel as a putative phosphatidylinositol 3, 4, 5-trisphosphate-sensitive calcium entry system. *Biochemistry, 43*(37), 11701-11708.

Tsunekawa, T., Hayashi, T., Kano, H., Sumi, D., Matsui-Hirai, H., Thakur, N. K., . . . Iguchi, A. (2001). Cerivastatin, a Hydroxymethylglutaryl Coenzyme A Reductase Inhibitor, Improves Endothelial Function in Elderly Diabetic Patients Within 3 Days. *Circulation, 104*, 376-379. doi:10.1161/hc2901.094094

Tsuzura, S., Ikeda, Y., Suehiro, T., Ota, K., Osaki, F., Arii, K., . . . Hashimoto, K. (2004). Correlation of plasma oxidized low-density lipoprotein levels to vascular complications and human serum paraoxonase in patients with type 2 diabetes. *Metabolism, 53*(3), 297–302. doi:10.1016/j.metabol.2003.10.009

Uchida, K. (2000). Role of reactive aldehyde in cardiovascular diseases. *Free Radical Biology & Medicine, 28*(12), 1685–1696. doi:10.1016/S0891-5849(00)00226-4

Uemura, S., Rothbard, J. B., Matsushita, H., Tsao, P. S., Fathman, C. G., & Cooke, J. P. (2002). Short Polymers of Arginine Rapidly Translocate Into Vascular Cells Effects on Nitric Oxide Synthesis. *Circulation Journal, 66*(12), 1155-1160. doi:10.1253/circj.66.1155

UK Prospective Diabetes Study Group. (1991). UK prospective diabetes study. *Diabetologia, 34*(12), 877-890. doi:10.1007/BF00400195

Ullrich, N. D., Voets, T., Prenen, J., Vennekens, R., Talavera, K., Droogmans, G., & Nilius, B. (2005). Comparison of functional properties of the Ca 2+-activated cation channels TRPM4 and TRPM5 from mice. *Cell Calcium, 37*(3), 267-278.

Upritchard, J. E., Sutherland, W. H., & Mann, J. I. (2000). Effect of supplementation with tomato juice, vitamin E, and vitamin C on LDL oxidation and products of inflammatory activity in type 2 diabetes. *Diabetes Care, 23*(6), 733-738. doi:10.2337/diacare.23.6.733

Uribarri, J., Negrean, M., Stirban, A., Buenting, C. E., Sander, D., Koschinsky, T., . . . Vlassara, H. (2007). Single Oral Challenge by Advanced Glycation End Products Acutely Impairs Endothelial Function in Diabetic and Nondiabetic Subjects. *Diabetes Care, 30*(10), 2579-2582. doi:10.2337/dc07-0320

Vaidya, H., Goyal, R. K., & Cheema, S. K. (2012). Anti-diabetic activity of swertiamarin is due to an active metabolite, gentianine, that upregulates PPAR-g gene expression in 3T3-L1 cells. *Cell, 40*, 60.

van den Oever, I., A. M., Raterman, H. G., Nurmohamed, M. T., & Simsek, S. (2010). EndothelialDysfunction,Inflammation,andApoptosisin DiabetesMellitus. *Mediators of inflammation, 2010*(7), 1-15. doi:10.1155/2010/792393

Van Eupen, M. G. A., Scharm, M. T., Colhoun, H. M., Hansen, N. M. J., Niessen, H. W. M., Tarnow, L., . . . Schalkwijk, C. G. (2013). The methylglyoxal-derived AGE tetrahydropyrimidineis increased in plasma of individuals with type 1 diabetes mellitus and in atherosclerotic lesions and is associated with sVCAM-1. *Diabetologia, 56*, 1845-1855. doi:10.1007/s00125-013-2919-8

Vannier, B., Peyton, M., Boulay, G., Brown, D., Qin, N., Jiang, M., . . . Birnbaumer, L. (1999). Mouse trp2, the homologue of the human trpc2 pseudogene, encodes mTrp2, a store depletion-activated capacitative Ca2+ entry channel. *Proceedings of the National Academy of Sciences, 96*(5), 2060-2064.

Vazquez, G., Wedel, B. J., Kawasaki, B. T., Bird, G. S. J., & Putney, J. W. (2004). Obligatory role of Src kinase in the signaling mechanism for TRPC3 cation channels. *Journal of Biological Chemistry, 279*(39), 40521-40528.

Venkatachalam, K., Zheng, F., & Gill, D. L. (2003). Regulation of canonical transient receptor potential (TRPC) channel function by diacylglycerol and protein kinase C. *Journal of Biological Chemistry, 278*(31), 29031-29040.

Verbeuren, T. J., Jordaens, F. H., Zonnekeyn, L. L., Van Hove, C. E., Coene, M. C., & Herman, A. G. (1986). Effect of hypercholesterolemia on vascular reactivity in the rabbit. *Circulation Research, 58*, 552-564. doi:10.1161/01.RES.58.4.552

Vilsbøll, T., Brock, B., Perrild, H., Levin, K., Lervang, H. H., Kølendorf, K., . . . Le-Thi, T. (2008). Liraglutide, a once-daily human GLP-1 analogue, improves pancreatic B-cell function and arginine-stimulated insulin secretion during hyperglycaemia in patients with Type 2 diabetes mellitus. *Diabetic Medicine, 25*(2), 152-156.

Vincent, F., & Duncton, M. A. J. (2011). TRPV4 Agonists and Antagonists. *Current Topics in Medicinal Chemistry, 11*(17), 2216-2226. doi:http://dx.doi.org/10.2174/156802611796904861

Virally, M., Blicklé, J.-F., Girard, J., Halimi, S., Simon, D., & Guillausseau, P.-J. (2007). Type 2 diabetes mellitus: epidemiology, pathophysiology, unmet needs and therapeutical perspectives. *Diabetes & Metabolism, 33*(4), 231–244. doi:10.1016/j.diabet.2007.07.001

Voets, T., Nilius, B., Hoefs, S., van der Kemp, A. W., Droogmans, G., Bindels, R., & Hoenderop, J. G. (2004). TRPM6 forms the Mg2+ influx channel involved in intestinal and renal Mg2+ absorption. *Journal of Biological Chemistry, 279*(1), 19-25.

Voets, T., Prenen, J., Fleig, A., Vennekens, R., Watanabe, H., Hoenderop, J., . . . Nilius, B. (2001). CaT1 and the calcium release-activated calcium channel manifest distinct pore properties. *Journal of Biological Chemistry, 276*(51), 47767-47770.

Voets, T., Talavera, K., Owsianik, G., & Nilius, B. (2005). Sensing with TRP channels. *Nature Chemical Biology, 1*(2), 85-92. doi:10.1038/nchembio0705-85

Vriens, J., Owsianik, G., Fisslthaler, B., Suzuki, M., Janssens, A., Voets, T., . . . Busse, R. (2005). Modulation of the Ca2 permeable cation channel TRPV4 by cytochrome P450 epoxygenases in vascular endothelium. *Circulation Research, 97*(9), 908-915.

Wang, H., Meng, Q. H., Chang, T., & Wu, L. (2006). Fructose-fed peroxynitrite production is mediated by methylglyoxal in vascular smooth muscle cells. *Life Sciences, 79*(26), 2448-2454. doi:10.1016/j.lfs.2006.08.009

Wang, H., Wang, A. X., Liu, Z., Chai, W., & Barrett, E. J. (2009). The Trafficking/Interaction of eNOS and Caveolin-1 Induced by Insulin Modulates Endothelial Nitric Oxide Production. *Molecular Endocrinology, 23*(10), 1613–1623. doi:http://dx.doi.org/10.1210/me.2009-0115

Wang, X., Miyares, R. L., & Ahern, G. P. (2005). Oleoylethanolamide excites vagal sensory neurones, induces visceral pain and reduces short-term food intake in mice via capsaicin receptor TRPV1. *tHe Journal of Physiology, 564*(2), 541-547.

Watanabe, H., Murakami, M., Ohba, T., Takahashi, Y., & Ito, I. (2008). TRP channel and cardiovascular disease. *Pharmacology & Therapeutics, 118*(3), 337–351. doi:10.1016/j.pharmthera.2008.03.008

Wei, M., Ong, L., Smith, M. T., Ross, F. B., Schmid, K., Hoey, A. J., . . . Brown, L. (2003). The Streptozotocin-Diabetic Rat as a Model of the Chronic Complications of Human Diabetes. *Heart Lung & Circulation, 12*(1), 44-50. doi:10.1046/j.1444-2892.2003.00160.x

Wes, P. D., Chevesich, J., Jeromin, A., Rosenberg, C., Stetten, G., & Montell, C. (1995). TRPC1, a human homolog of a Drosophila store-operated channel. *Proceedings of the National Academy of Sciences, 92*(21), 9652-9656.

Widmann, M. D., Weintraub, N. L., Fudge, J. L., Brooks, L. A., & Dellsperger, K. C. (1998). Cytochrome P-450 pathway in acetylcholine-induced canine coronary microvascular vasodilation in vivo. *American Journal of Physiology-Heart and Circulatory Physiology, 274*(1), H283-H289.

Winston, J., Toma, H., Shenoy, M., & Pasricha, P. J. (2001). Nerve growth factor regulates VR-1 mRNA levels in cultures of adult dorsal root ganglion neurons. *Pain, 89*(2), 181-186.

World Health Organization. (2015). http://www.who.int/mediacentre/factsheets/fs317/en/ Retrieved from http://www.who.int/mediacentre/factsheets/fs317/en/

Wu, C.-C., Szabo, C., Chen, S.-J., Thiemermann, C., & Vane, J. R. (1994). Activation of soluble guanylyl cyclase by a factor other than nitric oxide or carbon monoxide contributes to the vascular hyporeactivity to vasoconstrictor agents in the aorta of rats treated with endotoxin. *Biochemical and Biophysical Research Communications, 201*(1), 436-442.

Wu, S. N., Wu, P. Y., & Tsai, M. L. (2011). Characterization of TRPM8-Like Channels Activated by the Cooling Agent Icilin in the Macrophage Cell Line RAW 264.7. *The Journal of Membrane Biology, 241*(1), 11-20. doi:10.1007/s00232-011-9358-6

Xu, H., Delling, M., Li, L., Dong, X., & Clapham, D. E. (2007). Activating mutation in a mucolipin transient receptor potential channel leads to melanocyte loss in varitint–waddler mice. *PNAS, 104*(46), 18321-18326. doi:10.1073/pnas.0709096104

Xu, J., Wu, Y., Song, P., Zhang, M., Wang, S., & Zou, M. H. (2007). Proteasome-Dependent Degradation of Guanosine 5'-Triphosphate Cyclohydrolase I Causes Tetrahydrobiopterin Deficiency in Diabetes Mellitus. *Circulation, 116*(8), 944-953. doi:10.1161/CIRCULATIONAHA.106.684795

Xu, S.-Z., Boulay, G., Flemming, R., & Beech, D. J. (2006). E3-targeted anti-TRPC5 antibody inhibits store-operated calcium entry in freshly isolated pial arterioles. *American Journal of Physiology-Heart and Circulatory Physiology, 291*(6), H2653-H2659.

Xue, J., Ray, R., Singer, D., Böhme, D., Burz, D. S., Rai, V., . . . Shekhtman, A. (2014). The receptor for advanced glycation end products (RAGE) specifically recognizes methylglyoxal-derived AGEs. *Biochemistry, 53*(20), 3327-3335.

Yang, D., Luo, Z., Ma, S., Wong, W. T., Ma, L., Zhong, J., . . . Yan, Z. (2010). Activation of TRPV1 by dietary capsaicin improves endothelium-dependent vasorelaxation and prevents hypertension. *Cell metabolism, 12*(2), 130-141.

Yang, X. R., Lin, M. J., McIntosh, L. S., & Sham, J. S. K. (2006). Functional expression of transient receptor potential melastatin- and vanilloid-related channels in pulmonary arterial and aortic smooth muscle. *American Journal of Physiology - Lung Cellular and Molecular Physiology, 290*(6), L1267-L1276. doi:10.1152/ajplung.00515.2005

Yao, D., & Brownlee, M. (2010). Hyperglycemia-induced reactive oxygen species increase expression of the receptor for advanced glycation end products (RAGE) and RAGE ligands. *Diabetes, 59*(1), 249-255.

Yao, X., & Garland, C. J. (2005). Recent Developments in Vascular Endothelial Cell Transient Receptor Potential Channels. *Circulation Research, 97*(9), 853-863. doi:10.1161/01.RES.0000187473.85419.3e

Ying, W. Z., Aaron, K. J., & Sanders, P. W. (2014). Sodium and potassium regulate endothelial phospholipase C- and Bmx. *American Journal of Physiology - Renal Physiology, 307*(1), F58-F63. doi:10.1152/ajprenal.00615.2013

Yip, H., Chan, W.-Y., Leung, P.-C., Kwan, H.-Y., Liu, C., Huang, Y., . . . Yao, X. (2004). Expression of TRPC homologs in endothelial cells and smooth muscle layers of human arteries. *Histochemistry and cell biology, 122*(6), 553-561.

Yoshida, H., & Kisugi, R. (2010). Mechanisms of LDL oxidation. *Clinica Chimica Acta, 411*(23-24), 1875-1882. doi:10.1016/j.cca.2010.08.038

Yoshida, T., Inoue, R., Morii, T., Takahashi, N., Yamamoto, S., Hara, Y., . . . Mori, Y. (2006). Nitric oxide activates TRP channels by cysteine S-nitrosylation. *Nature Chemical Biology, 2*(11), 596-607.

Yuhanna, I. S., Zhu, Y., Cox, B. E., Hahner, L. D., Lawrence, S. O., Lu, P., . . . Shaul, P. W. (2001). High-density lipoprotein binding to scavenger receptor-BI activates endothelial nitric oxide synthase. *Nature Medicine, 7*, 853-857. doi:10.1038/89986

Zeng, F., Xu, S. Z., Jackson, P. K., McHugh, D., Kumar, B., Fountain, S. J., & Beech, D. J. (2004). Human TRPC5 channel activated by a multiplicity of signals in a single cell. *tHe Journal of Physiology, 559*(3), 739-750.

Zeng, Y., Tao, N., Chung, K. N., Heuser, J. E., & Lublin, D. M. (2003). Endocytosis of Oxidized Low Density Lipoprotein through Scavenger Receptor CD36 Utilizes a Lipid Raft Pathway That Does Not Require Caveolin-1. *The Journal of Biological Chemistry, 278*(46), 45931–45936.

Zhang, D. X., Mendoza, S. A., Bubolz, A. H., Mizuno, A., Ge, Z. D., Li, R., . . . Gutterman, D. D. (2009). Transient receptor potential vanilloid type 4–deficient mice exhibit impaired endothelium-dependent relaxation induced by acetylcholine in vitro and in vivo. *Hypertension, 53*, 532-538. doi:10.1161/HYPERTENSIONAHA.108.127100

Zhang, L., & Barritt, G. J. (2004). Evidence that TRPM8 is an androgen-dependent Ca2+ channel required for the survival of prostate cancer cells. *Cancer Research, 64*(22), 8365-8373.

Zhang, L., Guo, L., Zhang, M., Niu, N., & Wang, L. (2016). The involvement of lectin-like oxidized low density lipoprotein receptor-1 and p38MAPK in early diabetic nephropathy. *Int J Clin Exp Med, 9*(2), 2391-2398.

Zhang, L., Papadopoulos, P., & Hamel, E. (2013). Endothelial TRPV4 channels mediate dilation of cerebral arteries: impairment and recovery in cerebrovascular pathologies related to Alzheimer's disease. *British Journal of Pharmacology, 170*(3), 661-670. doi:10.1111/bph.12315

Zhang, W., Chu, X., Tong, Q., Cheung, J. Y., Conrad, K., Masker, K., & Miller, B. A. (2003). A novel TRPM2 isoform inhibits calcium influx and susceptibility to cell death. *Journal of Biological Chemistry, 278*(18), 16222-16229.

Zhang, Y., Hoon, M. A., Chandrashekar, J., Mueller, K. L., Cook, B., Wu, D., . . . Ryba, N. J. (2003). Coding of sweet, bitter, and umami tastes: different receptor cells sharing similar signaling pathways. *Cell, 112*(3), 293-301.

Zurborg, S., Yurgionas, B., Jira, J. A., Caspani, O., & Heppenstall, P. A. (2007). Direct activation of the ion channel TRPA1 by Ca2+. *Nature Neuroscience, 10*(3), 277-279.

Zygmunt, P. M., & Högestätt, E. D. (1996). Role of potassium channels in endothelium-dependent relaxation resistant to nitroarginine in the rat hepatic artery. *British Journal of Pharmacology, 117*(7), 1600-1606.